

**Isotopic and elemental distribution of copper between
Cu-bearing minerals and aqueous fluids: implications
of an experimental study**

Von der Naturwissenschaftlichen Fakultät der

Gottfried Wilhelm Leibniz Universität Hannover

zur Erlangung des Grades

Doktorin der Naturwissenschaften (Dr. rer. nat.)

genehmigte Dissertation

von

Dongmei Qi, Master of Science (China)

2019

Referent: Prof. Dr. Harald Behrens (Leibniz Universität Hannover)

Korreferent: Prof. Dr. Roman Botcharnikov (Johannes Gutenberg Universität Mainz)

Tag der Promotion: 18.12.2018

Acknowledgments

I would like to express the deepest appreciation to my primary supervisor Prof. Harald Behrens, who has the attitude to treat science as a piece of art: always be patient, serious, open-minded and perfect. Without his guidance, persistent help, stimulating discussion this dissertation would not have been possible. Besides my advisor, I would like to thank my other co-supervisors: Prof. Roman Botcharnikov, Prof. Stefan Weyer and Prof. Francois Holtz for their great support and invaluable advice. I am thankful to Prof. Roman Botcharnikov, an expert in experimental petrology, for his crucial inspirations that help to fulfill the tasks of this PhD project. I am quite grateful to Prof. Stefan Weyer for sharing with me his knowledge about isotope geochemistry. I am appreciative of Prof. Francois Holtz for his insightful ideas and extensive discussions about the project.

I would like to thank Dr. Marina Lazarov for teaching me with fluid sample preparation in clean lab, providing me with necessary materials, and accommodating my schedule with regard to the use of the (LA)MC-ICPMS. Insa Cassens (birth name of Derrey) is specially thanked for her kind support with capsule preparation and her thorough instruction with experimental vessels. The technical assistance provided by Dr. Moritz Albrecht, Dr. Martin Oeser-Rabe and Dr. Ingo Horn (LA-ICPMS), Dr. Chao Zhang (EMP analyses), Dr. Valeriy Petrov and Dr. Lars Schomborg (XRD and SEM analyses), Alexandra Tangen (OES measurements), Julian Feige (sample preparation), Ulrich Kroll and Adreas Reimer (hydrothermal vessel maintenance) are greatly appreciated. Thanks also go to Dr. Christian Ostertag-Henning (BGR) for his creative suggestions and generous help with gas determination. Additionally, I would like to express my gratitude toward Dr. Sören Wilke for his help with abstract translation. I would like to thank my other lab mates that include Dr. Xiaoyan Li, Dr. André Stechern, Dr. Tong Hou, Dr. Adriana Currin, Mahender Rajpurohit, Asiye Shabestari, Annika Neddermeyer (birth name of Brüske), Lining Cheng, Dachuan Wang, Marcel Dietrich for making my experience in the hydrothermal lab and department exciting and fun.

My great appreciation goes to my mother, Yunong Li, who taught me how to cope with the adversity and provided me with the confidence to challenge difficulties in my life. Finally, but by no means least, thanks go to Yanjiang Qi for almost unbelievable support and continued patience, who is always there for me.

Thanks are also due to the (DAAD) German Academic Exchange Service (under grant 57076462), Leibniz Universität Hannover and Graduate School GeoFluxes for their financial support that I otherwise would not have been able to develop my scientific discoveries.

Abstract

Transport and deposition of copper in the Earth's crust are mainly controlled by the speciation of Cu and solubility of Cu-bearing phases in magmatic-hydrothermal fluids. In order to improve our understanding of mobilization of copper by hydrothermal fluids, we conducted experiments with Cu-bearing phases (metallic copper, Cu₂O, CuCl) and aqueous solutions (H₂O, NaCl_{aq}, KCl_{aq}, HCl, acetate solutions with/without pH buffer) at 25°C-800°C and 0.1 -200 MPa.

The high temperature and high pressure (i.e., 800°C and 200 MPa) experiments were conducted in rapid heat/rapid quench argon cold seal pressure vessel using the synthetic fluid inclusion technique. The experimental charges Cu₂O_s ± CuCl_s + H₂O ± NaCl_{aq} ± HCl_{aq} (chloride concentration: 0 to 4.3 mol/kg) were loaded in either Cu or Au capsules. Two types of quartz cylinders were used to trap in-situ hydrothermal fluids: (i) pre-cracked and (ii) intact prior to experiment. Fluid composition was subsequently determined by analyzing individual fluid inclusions using laser ablation inductively coupled plasma mass spectrometry. Two types of inclusions, i.e., fluid inclusion and Na-bearing silicate melt inclusion, have been formed exclusively in metallic Cu-NaCl system. Moreover, micron- to submicron-sized cuprite has been observed in both types of inclusions. In HCl±CuCl-bearing systems, fluid inclusion trapping potential nantokite (CuCl) is observed. The Cu content is strongly enhanced by initial chloride content, and can reach up to 4.3 wt% and 11 wt% in 4.3 m NaCl and 1.9 m HCl solutions, respectively. Fast cooling which is avoided by most researchers shows advantages of preservation of ample inclusions in Cu-NaCl system. In addition, the fluid inclusions after rapid quench (25 K/s) yields much smaller variation of Cu content in comparison to the usually favored slow quench process (0.5 K/s). The H-D exchange experiment demonstrates that only H₂O is present in isolated, isometric inclusions whereas D₂O has been measured in necking-down inclusions, implying isolated (and isometric) inclusions are well sealed and are representative of fluid present at run conditions. This study confirms that synthetic fluid inclusion is an effective method to preserve in situ hydrothermal fluid at high P-T conditions. Two coexisting phases, i.e. hydrothermal brine and silica-rich melt phases, may be responsible for Cu transport and enrichment.

The moderate temperature and pressure (100-250°C, 5-30 MPa) experiments were conducted in a Parr autoclave allowing for in-situ sampling of liquid phase. The partitioning of Cu between cuprite and hydrothermal fluids (KCl_{aq}, H₂O, pH buffered KCl_{aq} and H₂O, where pH buffer refers to 0.2 m HAc/KAc) has been investigated from two aspects: Cu concentration and isotope fractionation. Experimental products are native copper and tenorite. Native copper is formed at 250°C and occurs in H₂O and KCl-bearing runs and short-termed (≤24 hours) acetate-bearing runs. Tenorite formed in 150°C and 250°C long-termed (72 hours) acetate-bearing runs. Four competing reactions control the Cu partitioning, i.e., cuprite dissolution, Cu(I) disproportionation into Cu(II) and native Cu, decomposition of acetate into methane and carbon dioxide and oxidation of dissolved Cu(I) to Cu(II). It is worth noting that the last reaction exclusively occurs in Cu₂O-acetate systems. During the cuprite dissolution stage (<~6 hours), Cu content in pH buffered solution is by an order of magnitude higher than that without. In pH buffered solutions: (i) Cu content in KCl solutions is up to two orders magnitude higher than that of acetate solutions; (ii) temperature and salinity can significantly affect Cu content, whereas the effect of pressure is insignificant. The

subsequent coupled Cu(I) disproportionation and acetate decarboxylation processes result in a reduction of dissolved Cu. Conjointly, the resulting isotope fractionation is $0.10 \pm 0.10\text{‰}$ ($\Delta^{65}\text{Cu}_{[\text{Cu}(0)-\text{Cu}(I)]}$). The oxidation substantially increases $\Delta^{65}\text{Cu}_{\text{Cu(II)O}-\text{Cu(I)}}$ to $0.35 \pm 0.05\text{‰}$.

The low temperature-pressure (5-80°C, 0.1 MPa) experiments were conducted to get insights into the mechanisms of isotope fractionations induced by reduction processes ($\text{Cu}^{2+} + 2\text{e}^- = \text{Cu}^0$). All experiments have been conducted in aqueous CuSO_4 solutions using Cu electroplating method. In all cases, the plated Cu metal is enriched in the light isotope (^{63}Cu) with respect to the solution. At room temperature the Cu isotopic fractionation between the electroplated Cu and electrolyte is found to increase with electrolyte concentration and stirring speed, and to decrease with current and run duration. These trends can be explained by three competing processes: copper transport in the solution, the kinetics of electrochemical reduction of copper ions and the surface diffusion at the electrode, i.e., transport becomes important at low copper concentration, low stirring speed, high currents and large amount of copper precipitation. Copper isotope fractionation has a maximum ($\Delta^{65}\text{Cu} = -2.66 \pm 0.02\text{‰}$) near 35°C, decreasing both towards higher and lower temperatures. Our findings in comparison to other studies imply that transformation of fivefold to sixfold coordinated aquacomplexes of Cu^{2+} to linear Cu^+ complexes is a key step during reduction of copper in aqueous solutions, inducing large negative copper isotope fractionation. These findings support that copper isotopes can be used as effective tracers of redox processes. This may have implications to various hydrothermal ore deposits, such as supergene processes, black smokers and volcanic-hosted massive sulfide.

Keywords: Native Cu, cuprite, tenorite, nantokite, synthetic fluid inclusions, silicate melt inclusions, Cu solubility in aqueous fluids, Cu isotopes, disproportionation, decarboxylation, oxidation, electrochemical reduction, thermodynamic equilibrium, kinetics

Kurzzusammenfassung

Der Transport und die Ablagerung von Kupfer in der Erdkruste wird hauptsächlich durch die Speziation des Cu und die Löslichkeit von Cu-haltigen Phasen in magmatisch-hydrothermalen Flüssigkeiten gesteuert. Um unser Verständnis der Mobilisierung von Kupfer durch hydrothermale Flüssigkeiten zu verbessern, haben wir Experimente mit Cu-haltigen Phasen (metallisches Kupfer, Cu_2O , CuCl) und wässrigen Lösungen (H_2O , NaCl_{aq} , KCl_{aq} , HCl , Acetatlösungen mit/ohne pH-Puffer) bei 25°C - 800°C und 0,1-200 MPa durchgeführt.

Die Hochtemperatur- und Hochdruckversuche (d.h. 800°C und 200 MPa) wurden in einem Argon-cold seal pressure vessel (CSPV) mit rapid-heat/rapid-quench-Funktion unter Verwendung der künstliche-Fluideinschluss-Technik durchgeführt. Die experimentellen Bestandteile $\text{Cu}_2\text{O}_s \pm \text{CuCl}_s + \text{H}_2\text{O} \pm \text{NaCl}_{\text{aq}} \pm \text{HCl}_{\text{aq}}$ (Chloridkonzentration: 0 bis 4,3 mol/kg) wurden entweder in Cu- oder Au-Kapseln geladen. Zwei Arten von Quarzzylindern wurden in den Versuchen verwendet, um in-situ hydrothermale Flüssigkeiten einzufangen: (i) zur Rissbildung vorbehandelt und (ii) intakt. Die Fluidzusammensetzungen wurde anschließend durch die Analyse einzelner Flüssigkeitseinschlüsse mittels Laserablation und induktiv gekoppelter Plasma-Massenspektrometrie bestimmt. Zwei Arten von Einschlüssen, nämlich der Flüssigkeitseinschluss und der Na-haltige Silikatschmelzeinschluss, wurden ausschließlich im metallischen Cu-NaCl-System gebildet. Darüber hinaus wurde bei beiden Arten von Einschlüssen mikron- bis submikrongroße Cuprit-Kristalle beobachtet. In $\text{HCl} \pm \text{CuCl}$ -haltigen Systemen wird das Einfangen von sich potentiell bildenden Nantokite (CuCl ; wahrscheinlich eine Quenchphase) in Flüssigkeitseinschlüssen beobachtet. Der Cu-Gehalt wird durch den initialen Chloridgehalt stark erhöht und kann bis zu 4,3 Gew.-% bzw. 11 Gew.-% in 4,3 m NaCl- und 1,9 m HCl-Lösungen erreichen. Die von den meisten Forschern vermiedene schnelle Abkühlung der Experimente zeigt Vorteile bei der Erhaltung einer Vielzahl von Einschlüssen im Cu-NaCl-System. Darüber hinaus ergeben sich für die Flüssigkeitseinschlüsse nach dem Schnellabschrecken (25 K/s) eine wesentlich geringere Variation des Cu-Gehalts im Vergleich zum normalerweise bevorzugten langsamen Abschreckverfahren (0,5 K/s). Das H-D-Austausch-Experiment zeigt, dass nur H_2O in den isolierten, isometrischen Einschlüssen vorhanden ist, was bedeutet, dass diese Einschlüsse gut versiegelt sind und für das unter Experimentalbedingungen vorhandene Fluid repräsentativ sind. Diese Studie bestätigt, dass die Herstellung synthetischer Fluideinschlüsse eine effektive Methode ist, um in situ hydrothermale Fluide unter hohen P-T-Bedingungen zu erhalten. Zwei koexistierende Phasen, nämlich hydrothermale Sole und siliziumhaltige Schmelzphasen, können für den Cu-Transport und die Anreicherung verantwortlich sein.

Die Experimente mit moderaten Temperaturen und Drücken (100 - 250°C , 5-30 MPa) wurden in einem Parr-Autoklaven durchgeführt, der eine in-situ-Probenahme der flüssigen Phase ermöglicht. Die Verteilung des Cu zwischen Cuprit und hydrothermalen Flüssigkeiten (KCl_{aq} , H_2O , pH-gepuffertes KCl_{aq} und H_2O , mit pH-Puffer 0,2 m HAc/KAc) wurde unter zwei Aspekten untersucht: Cu-Konzentration und Isotopenfraktionierung. Experimentelle Produkte sind gediegenes Kupfer und Tenorit. Gediegenes Kupfer wurde bei 250°C gebildet und trat in H_2O - und KCl-Experimenten und kurzfristigen (≤ 24 Stunden) acetathaltigen Experimenten auf. Tenorit bildete sich in den Experimenten bei 150°C und 250°C sowie in lang anhaltenden (72 Stunden) acetathaltigen Experimenten. Vier

konkurrierende Reaktionen steuern die Cu-Aufteilung, als da wären Cupritauflösung, Cu(I)-Disproportionierung in Cu(II) und gediegenes Cu, Abbau von Acetat in Methan und Kohlendioxid und die Oxidation von gelöstem Cu(I) zu Cu(II). Dabei ist festzuhalten, dass die letzte Reaktion ausschließlich in Cu₂O-Acetatssystemen stattfindet. Während der Stufe der Cupritauflösung (<~6 Stunden) ist der Cu-Gehalt in pH-gepufferter Lösung um eine Größenordnung höher als ohne. In pH-gepufferten Lösungen: (i) Der Cu-Gehalt in KCl-Lösungen ist um bis zu zwei Größenordnungen höher als bei Acetatlösungen; (ii) Temperatur und Salzgehalt können den Cu-Gehalt signifikant beeinflussen, während der Einfluss des Drucks unbedeutend ist. Die nachfolgenden gekoppelten Cu(I)-Disproportionierungs- und Acetatdecarboxylierungsprozesse führen zu einer Reduktion von gelöstem Cu. Die resultierende Isotopenfraktionierung beträgt insgesamt bis zu 0,10±0,10‰ ($\Delta^{65}\text{Cu}_{[\text{Cu}(0)\text{-Cu}(I)]}$). Die Oxidation erhöht $\Delta^{65}\text{Cu}_{\text{Cu(II)-Cu(I)}}$ erheblich auf 0,35±0,05‰.

Die Experimenten bei Tiefen Drücken und Temperaturen (5-80°C, 0.1 MPa) wurden durchgeführt, um Einblicke in die Mechanismen der Isotopenfraktionierung durch Reduktionsprozesse ($\text{Cu}^{2+} + 2\text{e}^- = \text{Cu}^0$) zu erhalten. Alle Experimente wurden mit wässrigen CuSO₄-Lösungen unter Verwendung der Cu-Galvanisierungsmethode durchgeführt. In allen Fällen wird das galvanisierte Cu-Metall gegenüber der Lösung mit dem leichten Isotop (⁶³Cu) angereichert. Bei Raumtemperatur nimmt die Cu-Isotopenfraktionierung zwischen dem galvanisierten Cu und dem Elektrolyten mit der Elektrolytkonzentration und der Rührgeschwindigkeit zu und mit Strom und Betriebsdauer ab. Diese Trends lassen sich durch drei konkurrierende Prozesse erklären: den Kupfertransport in der Lösung, die Kinetik der elektrochemischen Reduktion von Kupferionen und die Oberflächendiffusion an der Elektrode, d.h. der Transport wird bei niedriger Kupferkonzentration, niedriger Rührgeschwindigkeit, hohen Strömen und großer Menge an Kupferfällung zunehmend wichtig. Die Kupferisotopenfraktionierung hat ein Maximum ($\Delta^{65}\text{Cu} = -2,66\pm 0,02\%$) bei 35°C und sinkt sowohl zu höheren als auch zu niedrigeren Temperaturen hin ab. Die Kombination unserer Ergebnisse mit den Befunden anderer Studien deutet darauf hin, dass die Transformation von fünffach bis sechsfach koordinierten Aquakomplexen von Cu²⁺ zu linearen Cu⁺-Komplexen ein wichtiger Schritt bei der Reduktion von Kupfer in wässrigen Lösungen ist und zu einer großen negativen Kupferisotopenfraktionierung führt. Diese Ergebnisse belegen, dass Kupferisotope als effektive Tracer für Redoxprozesse eingesetzt werden können. Dies birgt Implikationen für verschiedene hydrothermale Erzvorkommen, wie z.B. supergene Prozesse, black smoker und vulkanische Massivsulfide.

Schlüsselwörter: Gediegenes Cu, Cuprit, Tenorit, Nantokite, synthetische Fluideinschlüsse, silikatische Schmelzeinschlüsse, Kupfer Löslichkeit in wässrigen Lösungen, Kupferisotope, Disproportionierung, Decarboxylierung, Oxidation, elektrochemische Reduktion, thermodynamisches Equilibrium, Kinetik

Contents

Contents

Introduction	8
Chapter I Reaction between Cu-bearing minerals and hydrothermal fluids at 800°C and 200 MPa: constraints from synthetic fluid inclusions	17
Abstract	18
1. Introduction	19
2. Experimental and analytical procedure	20
2.1 Starting materials and fluid inclusion synthesis	20
2.2 Additional supportive runs for inclusion study	23
2.3 Microthermometry and chemical analyses	23
3. Results	25
3.1 Fluid inclusion microscopy	25
3.2 Chemical and spectroscopic analyses	30
3.3 Quench fluid analyses	31
3.4 LA-ICP-MS data standardization	32
3.5 Effect of run duration and intermediate Quench on FI	35
3.6 Effect of silica gel	36
3.7 Cu content VS. Cl content in fluid inclusions	37
4. Discussion	38
4.1 Silicate melt inclusions and quartz solubility	38
4.2 Redox state and stable phase	40
4.3 Influence of cooling rate on nucleation of cuprite	40
4.4 Proper sealing of synthetic fluid inclusions	42
4.5 Copper diffusion	43
4.6 Copper speciation in fluids	44
4.7 Implications	45
5. Conclusions	46
Supplementary data	47
Chapter IIA An experimental study of the elemental and Cu isotopic fractionation between cuprite and water/acetate hydrothermal fluids to 250°C and 30 MPa	54
Abstract	55
1. Introduction	56

Contents

2. Experimental and analytical procedures.....	57
2.1 Reagents and material	57
2.2 Fluid sampling procedure.....	58
3. Analytical procedures.....	60
3.1 Solid sample analyses	60
3.2 Copper isotope microanalysis	60
3.3 Fluids treatment and analysis.....	61
4. Results	63
4.1 Formation of new minerals	63
4.2 Raman spectra of tenorite	65
4.3 Calculation of Cu isotope composition of initial cuprite pellets.....	66
4.4 Pressure medium dilution effect on elements concentration.....	71
4.5 Cu concentration and isotope signature of fluids in Cu ₂ O-HAc/KAc system at 20 MPa	72
4.6 T, P, pH effects on cuprite dissolution.....	74
4.7 Cu(I) disproportionation effect on Cu isotope fractionation.....	76
4.8 Oxidation of Cu(I) to Cu(II).....	78
5. Discussion	79
5.1 Cu speciation in hydrothermal fluids	79
5.2 Acetate effect on metal transport and deposition.....	81
5.3 Fractionation mechanism	83
5.4 Implications	83
6. Conclusion.....	84
Chapter IIB Partitioning behavior of Cu and its isotopes between cuprite and K(Na)Cl-bearing hydrothermal fluids to 250°C and 30 MPa: constraints from in situ hydrothermal fluid.....	86
Abstract	87
1. Introduction	88
2. Experimental and analytical procedures.....	90
2.1 Experiments setup.....	90
2.2 Chromatographic purification	90
3. Results.....	92
3.1 Formation of new minerals	92
3.2 Elements concentration and Cu isotope fractionation as a function of run duration.....	96
3.3 T, P, Cl and pH effects on cuprite dissolution process.....	98
3.4 The influence of the disproportionation of Cu(I) on Cu concentration and isotope fractionation	101
4. Discussion	103
4.1 Cu speciation in fluids	103

Contents

4.2 Thermal decarboxylation of acetate.....	104
4.3 Fractionation mechanism.....	106
4.4 Implications.....	110
5. Conclusion.....	111
Appendix:.....	113
Chapter III Cu isotope fractionation during reduction processes in aqueous systems: evidences from electrochemical deposition.....	123
Abstract.....	124
1. Introduction.....	125
2. Experimental setup.....	127
3. Analytical methodology.....	127
4. Results.....	128
5. Discussion.....	134
5.1 Mechanisms of Cu electrodeposition.....	135
5.2 Equilibrium effects on isotope fractionation.....	137
5.3 Kinetic effects on isotope fractionation.....	138
5.4 Temperature dependence in comparison to other studies.....	141
6. Conclusions and implications.....	143
Summary and conclusions.....	149
Curriculum Vitae.....	152
List of publications.....	154

Introduction

World copper consumption grew from ~ 50 000 metric tons per year to approximately 8.5 million metric tons per year over a century (Mikesell, 2013). Among the Cu-bearing deposits, porphyry copper deposits are of great importance as they supply 75% of the world's copper (Sillitoe, 2010). In addition, there is significant production from volcanogenic massive sulfide, sediment-hosted copper ores, and skarn deposits, with sedimentary-exhalative, epithermal and polymetallic vein deposits as further sources (e.g., Brown, 1992; Hitzman et al., 2005). Thus, many attentions have been aroused to understand Cu transport, enrichment and precipitation, and to trace the metal source. Fortunately, these questions can be answered equivocally by detailed experimental and analytical investigations.

Magmatic and hydrothermal fluids play an essential role in the sequestration and transport of economically important metals. For example, Blundy et al. (2015) proposed that copper enrichment and transport in porphyry copper deposits is strongly associated with metalliferous, magmatic-hydrothermal fluids stemmed from the underlying mafic intrusions. In addition, Cu shows stronger affinity to fluid phase than the melt phase (e.g., Keppler and Wyllie, 1991; Williams et al., 1995; Bai and Koster van Groos, 1999; Simon et al., 2006). Preservation of hydrothermal fluids in miniscule inclusions yields the most direct evidence about the physical and chemical characteristics of these hydrothermal fluids. Furthermore, synthetic fluid inclusions, produced at controlled experimental conditions (favored at high temperatures), provide a quantitative link between the laboratory studies and the natural observations demonstrating a high potential in exploration of ore deposits (Nash, 1976). The application of synthetic fluid inclusion provides metal solubility, speciation and partitioning data for high T-P fluids and sheds light on the earliest stages of the hydrothermal ore formation process. At low temperatures, fluid inclusion synthesis is no longer appropriate due to less formation of inclusions and sluggish crack healing. Cu-bearing mineral and hydrothermal fluid interaction has been studied by silica tube technique (e.g., Xiao et al., 1998; Liu et al., 2001), titanium autoclave (Archibald et al., 2001), and heated flow-through apparatus (Mountain and Seward, 1999, 2003). These methods have certain limitations that they can be either operated at vapor-saturated pressure or very low temperature (<100°C).

In hydrothermal fluids, complexing ligands such as Cl^- , HS^- , Ac^- and OH^- are described as the main agents for mobilization, transport and concentration of copper at ore forming conditions (e.g., Barnes, 1967; Seward and Barnes, 1997; Liu et al., 2001; Mountain and Seward, 2003; Zajacz et al., 2011). Cuprous bisulfide complexes are stable under reduced, near neutral to alkaline conditions with high total S concentrations (Crerar and Barnes, 1976; Thompson and Helz, 1994; Mountain and Seward, 1999, 2003). At higher temperatures (>300°C), chloride will be the dominant ligand (Mountain and Seward, 2003). The solubility of aqueous copper complexes has been focused on Cl^- and HS^- at both low and high temperatures (e.g., Xiao et al., 1998; Mountain and Seward, 1999; Zajacz et al., 2011). Less emphasis has been put on the acetate and very little investigations have been conducted on Cu-acetate complexes (Liu et al., 2001; Lai et al., 2018). However, acetate can be a major component of oil field waters and

Introduction

sedimentary brines (e.g., Willey et al., 1975; Fisher, 1987) and subduction zone fluids (Sverjensky et al., 2014). Indeed, up to 5000 ppm acetate has been reported in oil field water (Carothers and Kharaka, 1978). Acetate in sedimentary brines can play a vital role in metal complexation in sediment-hosted ores (e.g., Barnes, 1979; Giordano and Barnes, 1981; Giordano, 1985). Thus, acetate has been considered in this study. In addition, ore-forming fluids cover wide ranges in temperature (25 to > 600°C), pressure (0.1 to > 500 MPa) and compositions ranging from nearly pure water to highly saline fluids (> 50 mol% NaCl, KCl, CaCl₂ and FeCl₂) (Brugger et al., 2016). Therefore, the investigation of Cu transport process in this study has been conducted at both high T-P (800°C and 200 MPa) and low T-P conditions (5 -250°C and 0.1-30 MPa).

Deciphering metal transport and enrichment during hydrothermal and other geological processes is difficult due to a variety of pressure-temperature conditions and variable compositions of fluids interacting with the lithosphere. The precise transition metal isotope ratios (e.g., for Fe, Cu and Zn) can help to answer the longstanding questions on the source of the metals and mineralization processes in ore-forming systems. Among the transition metals, copper has received the greatest attention among researchers interested in applying metal stable isotope to mineral deposits. Cu isotopes are often used as a geological tracer due to its significance in a variety of natural processes, such as liquid-vapor separation (Pokrovski et al., 2008; Rempel et al., 2012), multi-step equilibrium processes (Zhu et al., 2002), fluid-rock chemical interaction (Rouxel et al., 2004; Markl et al., 2006; Asael et al., 2012b; Gregory and Mathur, 2017), ore forming supergene process (Larson et al., 2003; Mathur et al., 2005; Haest et al., 2009; Mathur and Fantle, 2015), and the formation of the solar system (Luck et al., 2005; Barrat et al., 2012). Such processes generate pronounced variation in copper isotope composition in natural samples (expressed as $\delta^{65}\text{Cu}$ (‰) = $[(^{65}\text{Cu}/^{63}\text{Cu})_{\text{sample}} / (^{65}\text{Cu}/^{63}\text{Cu})_{\text{NIST-SRM 976}}] - 1] \times 1000$) that ranges from -17‰ to +10‰ with respect to the NIST-SRM 976 standard (e.g., Mathur et al., 2009; Asael et al., 2012a; Mathur and Fantle, 2015). Among various geological processes, oxidation-reduction (redox) process related Cu isotope fractionation induces largest fractionation, which is frequently observed in various systems (such as oceanic sea floor, weathering process) and is particularly pronounced at low temperatures. Although the redox reactions induced isotope fractionation has been widely studied between Cu(I) and Cu(II) phases at low temperature (<100°C), the reduced Cu (native Cu/metallic Cu) may also affect isotope fractionation during redox state change and the related data is rare.

Although numerous experimental studies have been carried out to obtain Cu solubility, speciation, partitioning behavior and isotope fractionation (e.g., Ehrlich et al., 2004; Hack and Mavrogenes, 2006a; Righter et al., 2010), there are still open questions. Firstly, it is generally agreed that copper is transported as Cu(I) both in melt and fluid phases at temperature >100°C (e.g., Ripley and Brophy, 1995; Fulton et al., 2000b), the stability of multivalent Cu species (Cu^0 , Cu^+ and Cu^{2+}) at high temperature and their interactions with hydrothermal fluids are not well understood. Secondly, the previous experiments may have potential limitations regarding to: attainment of equilibrium, alloying problems with capsule materials, overprint by retrograde exchange processes, and precision of chemical analysis of the fluid phase. Thirdly, the knowledge of Cu transport and speciation in hydrothermal fluids at low temperature are restricted to vapor saturated conditions due to limitation of experimental vessels, which cannot represent the general condition that liquid is likely the dominant phase in metal transport at ore forming conditions.

Introduction

The main objectives of this study are addressed as follows:

(1) To provide a detailed study of native copper in addition to cuprite and copper(I) chloride dissolution mechanism in hydrothermal fluids (H₂O/NaCl/HCl) at elevated temperature and pressure (800°C and 200 MPa). In addition, this study tries to shed some lights about the properties of fluid inclusion, such as the sealing issue of inclusion, the effect of silica gel on inclusions, and cooling rate effect on inclusion.

(2) A thermodynamic stable mineral (i.e., cuprite, >100°C; Fulton et al., 2000b) is selected to study the partitioning behavior of Cu between crystalline phase and fluid phases (H₂O/KCl/NaCl/HAc-KAc) via Cu concentration and isotope determination at low P-T conditions (100-250°C, 5-30 MPa). The additional aim is to understand the dominant complexation ligands (Cl⁻, Ac⁻, OH⁻) in hydrothermal fluids and their ability to transport and precipitate Cu. Furthermore, the data allow us to deduce the reaction mechanisms (simple cuprite dissolution reaction or coupled with other competing reactions) and their influences on Cu partitioning. The result of this part can be used to unravel Cu transport process in sediment-hosted Cu ores.

(3) To explore the reduction ($\text{Cu}^{2+} + 2\text{e}^{-} = \text{Cu}^0$) effect on Cu isotope fractionation by using the Cu electroplating technique. The isotopic variability of Cu(II) and Cu(0) species facilitate the understanding of the influence of each factor (electrolyte concentration, stirring speed, current, time and temperature), and the resulting fractionation data can unravel the controlling mechanisms. More knowledge can be gained about the possible bonding environments by linking the theoretical predicted data and the results in this study.

Introduction

References:

- Archibald, S., Migdisov, A.A. and Williams-Jones, A. (2001) The stability of Au-chloride complexes in water vapor at elevated temperatures and pressures. *Geochimica et cosmochimica acta* 65, 4413-4423.
- Asael, D., Matthews, A., Bar-Matthews, M., Harlavan, Y. and Segal, I. (2012a) Tracking redox controls and sources of sedimentary mineralization using copper and lead isotopes. *Chemical Geology* 310-311, 23-35.
- Asael, D., Matthews, A., Bar-Matthews, M., Harlavan, Y. and Segal, I. (2012b) Tracking redox controls and sources of sedimentary mineralization using copper and lead isotopes. *Chemical Geology* 310, 23-35.
- Bai, T.B. and Koster van Groos, A.F. (1999) The distribution of Na, K, Rb, Sr, Al, Ge, Cu, W, Mo, La, and Ce between granitic melts and coexisting aqueous fluids. *Geochimica et Cosmochimica Acta* 63, 1117-1131.
- Barnes, H. (1979) Solubilities of ore minerals. *Geochemistry of hydrothermal ore deposits*, 404-460.
- Barnes, H.L. (1967) *Geochemistry of hydrothermal ore deposits*. Holt, Rinehart and Winston. Inc., New York.
- Barrat, J.-A., Zanda, B., Moynier, F., Bollinger, C., Liorzou, C. and Bayon, G. (2012) Geochemistry of CI chondrites: Major and trace elements, and Cu and Zn isotopes. *Geochimica et Cosmochimica Acta* 83, 79-92.
- Blundy, J., Mavrogenes, J., Tattitch, B., Sparks, S. and Gilmer, A. (2015) Generation of porphyry copper deposits by gas-brine reaction in volcanic arcs. *Nature Geoscience* 8, ngeo2351.
- Brown, A.C. (1992) Sediment-hosted stratiform copper deposits. *Geoscience Canada* 19.
- Brugger, J., Liu, W., Etschmann, B., Mei, Y., Sherman, D.M. and Testemale, D. (2016) A review of the coordination chemistry of hydrothermal systems, or do coordination changes make ore deposits? *Chemical Geology* 447, 219-253.
- Carothers, W.W. and Kharaka, Y.K. (1978) Aliphatic acid anions in oil-field waters--implications for origin of natural gas. *AAPG Bulletin* 62, 2441-2453.
- Crerar, D.A. and Barnes, H. (1976) Ore solution chemistry; V, Solubilities of chalcopyrite and chalcocite assemblages in hydrothermal solution at 200 degrees to 350 degrees C. *Economic Geology* 71, 772-794.
- Ehrlich, S., Butler, I., Halicz, L., Rickard, D., Oldroyd, A. and Matthews, A. (2004) Experimental study of the copper isotope fractionation between aqueous Cu (II) and covellite, CuS. *Chemical Geology* 209, 259-269.
- Fisher, J.B. (1987) Distribution and occurrence of aliphatic acid anions in deep subsurface waters. *Geochimica et Cosmochimica Acta* 51, 2459-2468.
- Fulton, J.L., Hoffmann, M.M., Darab, J.G., Palmer, B.J. and Stern, E.A. (2000) Copper (I) and copper (II) coordination structure under hydrothermal conditions at 325 C: an X-ray absorption fine structure and molecular dynamics study. *The Journal of Physical Chemistry A* 104, 11651-11663.
- Giordano, T. (1985) A preliminary evaluation of organic ligands and metal-organic complexing in Mississippi Valley-type ore solutions. *Economic Geology* 80, 96-106.
- Giordano, T. and Barnes, H. (1981) Lead transport in Mississippi Valley-type ore solutions. *Economic Geology* 76, 2200-2211.
- Gregory, M.J. and Mathur, R. (2017) Understanding Copper Isotope Behavior in the High Temperature Magmatic - Hydrothermal Porphyry Environment. *Geochemistry, Geophysics, Geosystems* 18, 4000-4015.
- Hack, A.C. and Mavrogenes, J.A. (2006) A cold-sealing capsule design for synthesis of fluid inclusions and other hydrothermal experiments in a piston-cylinder apparatus. *American Mineralogist* 91, 203-210.
- Haest, M., Muechez, P., Petit, J.C. and Vanhaecke, F. (2009) Cu isotope ratio variations in the Dikulushi Cu-Ag deposit, DRC: of primary origin or induced by supergene reworking? *Economic Geology* 104, 1055-1064.
- Hitzman, M., Kirkham, R., Broughton, D., Thorson, J. and Selley, D. (2005) The sediment-hosted stratiform copper ore system. *Economic geology* 100.
- Kepler, H. and Wyllie, P.J. (1991) Partitioning of Cu, Sn, Mo, W, U, and Th between melt and aqueous fluid in the systems haplogranite-H₂O- HCl and haplogranite-H₂O- HF. *Contributions to Mineralogy and Petrology* 109, 139-150.
- Lai, F., Liu, L. and Cao, W. (2018) Complexation of copper in acetate-rich low-temperature hydrothermal fluids: Evidence from ab initio molecular dynamics simulations. *Chemical Geology* 476, 100-118.
- Larson, P.B., Maher, K., Ramos, F.C., Chang, Z., Gaspar, M. and Meinert, L.D. (2003) Copper isotope ratios in magmatic and hydrothermal ore-forming environments. *Chemical Geology* 201, 337-350.
- Liu, W., McPhail, D. and Brugger, J. (2001) An experimental study of copper (I)-chloride and copper (I)-acetate complexing in hydrothermal solutions between 50 C and 250 C and vapor-saturated pressure. *Geochimica et Cosmochimica Acta* 65, 2937-2948.
- Luck, J.M., Ben Othman, D. and Albarede, F. (2005) Zn and Cu isotopic variations in chondrites and iron meteorites: Early solar nebula reservoirs and parent-body processes. *Geochimica Et Cosmochimica Acta* 69, 5351-5363.
- Markl, G., Lahaye, Y. and Schwinn, G. (2006) Copper isotopes as monitors of redox processes in hydrothermal mineralization. *Geochimica et cosmochimica acta* 70, 4215-4228.
- Mathur, R. and Fantle, M.S. (2015) Copper Isotopic Perspectives on Supergene Processes: Implications for the Global Cu Cycle. *Elements* 11, 323-329.
- Mathur, R., Ruiz, J., Tittley, S., Liermann, L., Buss, H. and Brantley, S. (2005) Cu isotopic fractionation in the supergene environment with and without bacteria. *Geochimica et Cosmochimica Acta* 69, 5233-5246.
- Mathur, R., Tittley, S., Barra, F., Brantley, S., Wilson, M., Phillips, A., Munizaga, F., MaksaeV, V., Vervoort, J. and Hart, G. (2009) Exploration potential of Cu isotope fractionation in porphyry copper deposits. *Journal of Geochemical exploration* 102, 1-6.
- Mikesell, R.F. (2013) *The world copper industry: structure and economic analysis*. RFF Press.

Introduction

- Mountain, B. and Seward, T. (1999) The hydrosulphide/sulphide complexes of copper (I): Experimental determination of stoichiometry and stability at 22 C and reassessment of high temperature data. *Geochimica et Cosmochimica Acta* 63, 11-29.
- Mountain, B. and Seward, T. (2003) Hydrosulfide/sulfide complexes of copper (I): experimental confirmation of the stoichiometry and stability of Cu (HS) 2- to elevated temperatures. *Geochimica et cosmochimica acta* 67, 3005-3014.
- Nash, J.T. (1976) Fluid-inclusion petrology--data from porphyry copper deposits and applications to exploration: a summary of new and published descriptions of fluid inclusions from 36 porphyry copper deposits and discussion of possible applications to exploration for copper deposits. US Govt. Print. Off.
- Pokrovski, G.S., Borisova, A.Y. and Harrichoury, J.-C. (2008) The effect of sulfur on vapor-liquid fractionation of metals in hydrothermal systems. *Earth and Planetary Science Letters* 266, 345-362.
- Rempel, K.U., Liebscher, A., Meixner, A., Romer, R.L. and Heinrich, W. (2012) An experimental study of the elemental and isotopic fractionation of copper between aqueous vapour and liquid to 450° C and 400bar in the CuCl-NaCl-H 2 O and CuCl-NaHS-NaCl-H 2 O systems. *Geochimica et Cosmochimica Acta* 94, 199-216.
- Righter, K., Pando, K., Danielson, L. and Lee, C.-T. (2010) Partitioning of Mo, P and other siderophile elements (Cu, Ga, Sn, Ni, Co, Cr, Mn, V, and W) between metal and silicate melt as a function of temperature and silicate melt composition. *Earth and Planetary Science Letters* 291, 1-9.
- Ripley, E.M. and Brophy, J.G. (1995) Solubility of copper in a sulfur-free mafic melt. *Geochimica et Cosmochimica Acta* 59, 5027-5030.
- Rouxel, O., Fouquet, Y. and Ludden, J.N. (2004) Copper isotope systematics of the Lucky Strike, Rainbow, and Logatchev seafloor hydrothermal fields on the Mid-Atlantic Ridge. *economic geology* 99, 585-600.
- Seward, T. and Barnes, H. (1997) Metal transport by hydrothermal ore fluids. *Geochemistry of hydrothermal ore deposits*, 435-486.
- Sillitoe, R.H. (2010) Porphyry copper systems. *Economic Geology* 105, 3-41.
- Simon, A.C., Pettke, T., Candela, P.A., Piccoli, P.M. and Heinrich, C.A. (2006) Copper partitioning in a melt-vapor-brine-magnetite-pyrrhotite assemblage. *Geochimica et cosmochimica acta* 70, 5583-5600.
- Sverjensky, D.A., Stagno, V. and Huang, F. (2014) Important role for organic carbon in subduction-zone fluids in the deep carbon cycle. *Nature Geoscience* 7, 909.
- Thompson, R.A. and Helz, G.R. (1994) Copper speciation in sulfidic solutions at low sulfur activity: Further evidence for cluster complexes? *Geochimica et Cosmochimica Acta* 58, 2971-2983.
- Willey, L.M., Kharaka, Y.K., Presser, T.S., Rapp, J.B. and Barnes, I. (1975) Short chain aliphatic acid anions in oil field waters and their contribution to the measured alkalinity. *Geochimica et Cosmochimica Acta* 39, 1707-1711.
- Williams, T.J., Candela, P.A. and Piccoli, P.M. (1995) The partitioning of copper between silicate melts and two-phase aqueous fluids: an experimental investigation at 1 kbar, 800 C and 0.5 kbar, 850 C. *Contributions to Mineralogy and Petrology* 121, 388-399.
- Xiao, Z., Gammons, C. and Williams-Jones, A. (1998) Experimental study of copper (I) chloride complexing in hydrothermal solutions at 40 to 300 C and saturated water vapor pressure. *Geochimica et cosmochimica acta* 62, 2949-2964.
- Zajacz, Z., Seo, J.H., Candela, P.A., Piccoli, P.M. and Tossell, J.A. (2011) The solubility of copper in high-temperature magmatic vapors: a quest for the significance of various chloride and sulfide complexes. *Geochimica et cosmochimica acta* 75, 2811-2827.
- Zhu, X., Guo, Y., Williams, R., O'nions, R., Matthews, A., Belshaw, N., Canters, G., De Waal, E., Weser, U. and Burgess, B. (2002) Mass fractionation processes of transition metal isotopes. *Earth and Planetary Science Letters* 200, 47-62.

Chapter I

Reaction between Cu-bearing minerals and hydrothermal fluids at 800°C and 200 MPa: constraints from synthetic fluid inclusions

Dongmei Qi^{a*}, Harald Behrens^a, Roman Botcharnikov^b, Insa Derrey^a,
Francois Holtz^a, Chao Zhang^a, Xiaoyan Li^a, Ingo Horn^a

^aInstitute of Mineralogy, Leibniz Universität Hannover, Callinstraße 3, Hannover, D-30167, Germany

^bInstitute of Geosciences, Johannes Gutenberg Universität Mainz, J.-J.-Becher-Weg 21, Mainz, D-55128, Germany

(*d.qi@mineralogie.uni-hannover.de)

(Submitted to *Geochimica et Cosmochimica Acta*)

Abstract

Transport and deposition of copper in the Earth's crust are mainly controlled by the speciation of Cu and solubility of Cu-bearing phases in magmatic-hydrothermal fluids. In order to improve our understanding of mobilization of copper by hydrothermal fluids, we conducted experiments with Cu-bearing phases (metallic copper, Cu₂O, CuCl) and aqueous chloride solutions (H₂O ± NaCl ± HCl; 0 to 4.3 mol/kg) in rapid heat/rapid quench argon-cold seal pressure vessels at 800°C, 200 MPa and log_fO₂ = NNO + 2.3. The addition of silica gel (as a crack healing agent) is favored in most runs to generate more and larger fluid inclusions. Either Cu capsules or Au capsules were used as container. The run products were sampled in-situ by the entrapment of synthetic fluid inclusions in two types of quartz cylinders: 1) pre-cracked and 2) intact prior to experiment. Fluid composition was subsequently determined by analyzing individual fluid inclusions using laser ablation inductively coupled plasma mass spectrometry. Na-bearing silicate melt inclusions have been observed exclusively in metallic Cu-NaCl system in addition to fluid inclusions. Moreover, micron- to submicron-sized cuprite has been observed in fluid inclusions and in Na-bearing silicate melt inclusions. In HCl/CuCl bearing systems, potential nantokite (CuCl) is observed by optical microscopy and Raman spectroscopy. The Cu content is strongly enhanced by initial chloride content with Cu/Cl molal ratios of 1:7 and 1:1 in native Cu-NaCl_{aq} and native Cu-HCl systems, respectively. Thus, Cu content can reach up to 4.3 wt% and 11 wt% in 4.3 m NaCl and 1.9 m HCl solutions, respectively. However, a Cu/Cl molal ratio of 1:3 has been found in native Cu-CuCl-H₂O and Cu₂O-NaCl_{aq} systems, which is caused by a back reaction with the production of native Cu (i.e., Cu⁺ + ½ H₂ = Cu + H⁺). Thus, the stability of Cu-bearing phases is strongly affected by oxygen fugacity and the dissolved Cu⁺ content.

The influence of silica gel (crack healing agent) on elements content in fluid inclusions has been tested in some runs. It is evident that the fluid inclusions formed in runs with additional silica gel show much smaller variation of Cs content and relatively higher Cu content than those without silica gel. Different quench techniques were compared to clarify whether formation of fluid inclusions is affected by the way of cooling. Interestingly, fast cooling which is avoided by most researchers shows advantages of preservation of ample inclusions in Cu-NaCl system. In addition, the fluid inclusions after rapid quench (25 K/s) yields much smaller variation of Cu content in comparison to the usually favored slow quench process (0.5 K/s). In NaCl-bearing system, rapid quench can be an optimum experimental procedure to preserve ample fluid inclusion at high P-T conditions and to avoid overprint from late stage modifications. The exchange experiment between H₂O-bearing inclusion and outer D₂O solution demonstrates that only H₂O is present in the isolated, isometric inclusions, implying these inclusions are properly sealed and are representative of fluid present at experimental conditions. This study confirms that synthetic fluid inclusion is an effective method to preserve in situ hydrothermal fluid at high temperature and high pressure conditions. Two coexisting phases, i.e. hydrothermal brine and silica-rich melt, may be responsible for Cu transport and enrichment.

Keywords

Synthetic fluid inclusions, silicate melt inclusions, native copper, nantokite

1. Introduction

Formation of hydrothermal ore deposits requires a fluid with the capability to transport and deposit metals. Sources as well as physical and chemical characteristics of these hydrothermal fluids may vary widely (Bodnar et al., 2014). Fluid inclusions trapped in minerals yield the most direct evidence about the composition of hydrothermal fluids responsible for mineralization and deposition of metals. Furthermore, synthetic fluid inclusions, produced at controlled experimental conditions, provide a quantitative link between the laboratory studies and the natural observations demonstrating a high potential in exploration of ore deposits (Nash, 1976). For more than a century, data obtained from fluid inclusion studies have provided important information to better understand ore-forming processes in hydrothermal deposits (see reviews in Sorby, 1858; Hedenquist and Richards, 1998; Bodnar et al., 2014).

Compilation of experimental and thermodynamic data show that ligands, mostly Cl^- and HS^- , are important for solution of Cu in magmatic hydrothermal fluids (e.g. Seward and Barnes, 1997; Liu and McPhail, 2005). Cuprous bisulfide complexes are stable under reduced, near neutral to alkaline conditions with high total S concentrations (Crerar and Barnes, 1976; Thompson and Helz, 1994; Mountain and Seward, 1999, 2003). At higher temperatures ($>300^\circ\text{C}$), chloride will be the dominant ligand (Mountain and Seward, 2003). Experimental investigations of Cu speciation in fluids at lower temperatures ($<500^\circ\text{C}$; Crerar and Barnes, 1976; Var'yash, 1992; Xiao et al., 1998; Fulton et al., 2000a; Archibald et al., 2001; Brugger et al., 2001; Liu et al., 2001; Liu et al., 2002; Berry et al., 2006; Sherman, 2007; Rempel et al., 2012) indicate that $[\text{CuCl}]^0$ and $[\text{CuCl}_2]^-$ complexes dominate in a wide range of Cl concentrations. Higher order complexes with the stoichiometry of CuCl_n^{n-1} (where $n>2$) and $\text{Cu}_3\text{Cl}_3 \cdot (\text{H}_2\text{O})_n^{\text{gas}}$ are also considered to be possible complexes in vapor phase (Xiao et al., 1998; Archibald et al., 2002; Williams-Jones et al., 2002; Liu et al., 2008). The application of synthetic fluid inclusion provides metal solubility and speciation data for high T-P fluids and sheds light on the earliest stages of the hydrothermal ore formation process.

The available synthetic fluid inclusion studies of Cu solubility in hydrothermal brines in the single fluid phase region are generally focused on cuprous (e.g., Cu_2O) and/or cupric (e.g., CuCl_2) phases (Berry et al., 2006; Hack and Mavrogenes, 2006). Based on the analysis of synthetic fluid inclusions, Hack and Mavrogenes (2006) studied the influence of Cl concentration, temperature, and pressure on copper solubility at oxygen fugacity and pH buffered conditions. The experimental charges of their study were composed of native copper + cuprite + talc + quartz + $\text{CuCl}_{2(\text{aq})}$. The experiments were conducted in a piston cylinder apparatus with a cooling rate of $50^\circ\text{C}/\text{min}$ in a temperature range from 525°C to 725°C and pressure range from 300 MPa to 1750 MPa. They analyzed fluid inclusion with laser ablation inductively coupled plasma mass spectrometry (LA-ICP-MS) and measured up to 15 wt% Cu at 630°C and 340 MPa. They inferred high order complexes with general stoichiometry $\text{CuCl}(\text{HCl})_{n-1}^0$ (where n is up to 4), preferring $n \leq 2$ at geological conditions. Berry et al. (2006) used XANES spectroscopy to extend the synthetic fluid inclusion study of Hack and Mavrogenes (2006) using native copper + magnetite + hematite + orthoclase + quartz + sillimanite + $\text{KCl}_{(\text{aq})}$ as starting materials. Their LA-ICP-MS and PIXE analyses indicated that ~10 wt% Cu were dissolved in the fluid (700°C and 341 MPa; 4 - 8 m $\text{KCl}_{(\text{aq})}$) which was equilibrated with native

copper and mineral buffers. Berry et al. (2006) concluded that Cu^+ occurs as linear species $[\text{CuCl}_2]^-$ in the presence of K^+ and as $[\text{CuCl}_4]^{3-}$ species in the absence of K^+ . Zajacz et al. (2011) conducted experiments in $\text{Au}_{97}\text{Cu}_3$ alloy capsules ($a_{\text{Cu}}=0.01$) with various chemical components at 1000°C and 150 MPa. A maximum Cu content of 0.025wt% was reached in 0.75 m NaCl_{aq} solution. This study proposed the presence of NaCuCl_2 and KCuCl_2 complexes. There is a general agreement that Cu(I) remains stable at high temperature regime, however, the redox state change between native Cu and cuprous Cu at near magmatic-hydrothermal conditions has not been well understood.

Native copper is known to precipitate from hydrothermal fluids in ancient oceanic spilitic pillow basalts (Nagle et al., 1973) or in continental flood basalt (e.g., Stoiber and Davidson, 1959; Pinto et al., 2011; Zhang et al., 2013; Ikehata et al., 2016). In several localities hydrothermal processes have resulted in concentration of native copper to economic or near economic levels, such as the world's largest and most significant Keweenaw Peninsula native copper ore district in USA, and Emeishan large igneous province in China, (e.g. Butler and Burbank, 1929; Zhu et al., 2003; Wang et al., 2006; Bornhorst and Mathur, 2017). However, the transport process of native copper in hydrothermal fluids has not been systematically studied at elevated temperature and pressure. Thus, we conducted a detailed study of the behavior of copper in water and chlorine-bearing fluids at magmatic-hydrothermal conditions. Experiments were performed to equilibrate native Cu with aqueous hydrothermal fluids at 800°C and 200 MPa over a range of Cl (namely NaCl, HCl and CuCl) contents from 0 to 4 m ($\text{mol kg}^{-1} \text{H}_2\text{O}$). The resulting fluids were trapped in quartz seed crystals and the fluid inclusions were analyzed by LA-ICP-MS. In comparison to previous studies ($a_{\text{Cu}}=1$ (Hack and Mavrogenes, 2006; Berry et al., 2006) and $a_{\text{Cu}}=0.01$ (Zajacz et al., 2011)), we provide a systematic study to investigate the behavior of copper in different systems (both in NaCl-absent system (similar to Hack and Mavrogenes (2006)) and in NaCl-present systems (similar to Zajacz et al. (2011))) at copper saturated condition ($a_{\text{Cu}}=1$).

2. Experimental and analytical procedure

2.1 Starting materials and fluid inclusion synthesis

Quartz samples used in this study were prepared from a large, inclusion-free synthetic single crystal. Quartz cylinders, 2.0 mm in diameter, ca. 3 mm in length, ca.0.025 g in weight, were drilled parallel to c-axis of the crystal. These cylinders were first cleaned with acetone and distilled water in an ultrasonic bath. Some cylinders were fractured by heating them at 350°C for 10 min in an atmospheric oven and quenching them in distilled water. After drying, these cylinders were immersed in 40% hydrofluoric acid for 10 min to leach quartz along the cracks and to produce larger and more abundant fluid inclusions, as suggested by Derrey et al. (2017). After leaching the pre-fractured quartz cylinders (hereafter denoted as pref. Qz), acetone and distilled water were used to remove acid and further clean the cylinders. Both pref. Qz and intact quartz cylinders (denoted as *in-situ* fractured quartz or i.s. Qz) were placed in an oven at 110°C overnight to remove rests of water from the surface and cracks.

Copper tubing was purchased from *Sürth Stahl-Metalle und Schrauben*. Metallic copper contains 99.97 wt% Cu and 0.03 wt% P as determined by electron microprobe analyses. Copper(I) oxide powder (purity of 97%, purchased

Chapter I

from *Sigma Aldrich*) was directly used as a starting material or it was transformed into pellets by sintering. In doing so, cuprite (Cu_2O) powder (~1g) was pressed into pellet of 13 mm in diameter and 2 mm in thickness by uniaxial pressing method at 140 MPa. Afterwards, these pellets were sintered at 1030°C for 30 h at atmospheric condition, i.e. in the stability field of cuprite (Neumann et al., 1984). NaCl solutions were prepared using distilled water and NaCl powder (purity of 99.99%, purchased from *Alfa Aesar*). HCl solutions were diluted from a 6 mol l^{-1} stock solution. All solutions were doped with 400 - 600 $\mu\text{g/g}$ RbCl and CsCl for internal standardization during LA-ICP-MS measurements (Duc-Tin et al., 2007; Derrey et al., 2017). Silica gel (purity of 99.99%) and Cu(I)Cl powder (purity of 99.999%) were purchased from *Alfa Aesar*. Further details about each proportion of the starting materials are provided in supplementary Table A1.

A schematic drawing of the assemblage in the capsule is shown in Fig.1a. Two types of capsule material were used in this study, namely Cu capsules (2.45 mm I.D., 2.55 mm O.D. and 30 mm length) and Au capsules (2.80 mm I.D., 3.20 mm O.D. and 30 mm length). Solutions ($\text{H}_2\text{O} \pm \text{NaCl} \pm \text{HCl}$; doped with internal standards) and solid reactants (fine silica gel / quartz powder / CuCl powder / Cu_2O powder / sintered Cu_2O pellet) were placed at the bottom of the capsule which was welded shut on one end prior to loading (Table 1). The total volume of liquid in the capsule was calculated to be lower than the free volume in the capsule under experimental P,T condition using the equation from Pitzer and Sterner (1994) for pure H_2O . The capsules were crimped at the center, and then two quartz cylinders were loaded in the upper part of the capsule. The intact quartz cylinder was always placed beneath the pre-factured quartz cylinder (Fig. 1a). Capsules were squeezed on top, weighed, cut and then welded shut under Ar flow. During welding, the capsule was cooled with a wrapped tissue soaked with distilled water and then frozen by liquid nitrogen to avoid loss of volatile components during welding. The capsule was weighed again to check for volatile loss during welding, stored in an oven at 110°C overnight, and weighed a third time to test for possible leakage.

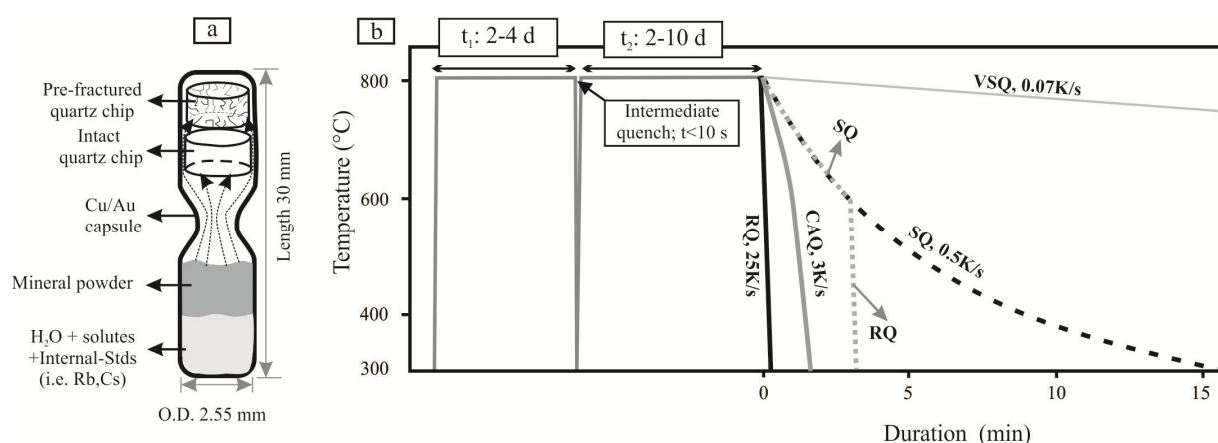


Figure 1 Schematic drawing of the experiment conducted in RH/RQ Ar-CSPV. (a) The design of capsule which is modified after Derrey et al. (2017); (b) Thermal history of the experiment. The cooling rates were calculated based on the total time needed for the temperature dropping from 800°C to 300°C at the external thermocouple. SQ - slow quench (applied in most cases); CAQ - compressed air quench; RQ - rapid quench; VSQ- very slow quench.

Chapter I

A rapid heat/rapid quench argon cold seal pressure vessel (RH/RQ Ar-CSPV, similar to Matthews et al. (2003)) was used for the experiments. All experiments were conducted at 800°C and 200 MPa. Based on calibration, the uncertainties of temperature and pressure measurements are $\leq \pm 5^\circ\text{C}$ and $\leq \pm 5$ MPa, respectively. The oxygen fugacity imposed by the vessel was ca. $\text{NNO} + 2.3$ (i.e., 2.3 log units above the Ni-NiO buffer; Berndt et al. (2001)). Loaded capsules were firstly pressurized to 200 MPa at room temperature and rapidly moved to the preheated hot zone of the vessel by an externally moving magnet. The temperature distribution in the hot zone was previously calibrated using a calibration inset with three shielded type-K thermocouples. The heating of the capsules to 800°C occurred within few minutes at isobaric conditions.

Almost all experiments included an “intermediate quench” step by descending the sample to the water-cooled region to initiate cracks within the intact quartz cylinder as a result of thermal stress (e.g., Li and Audétat, 2009). After intermediate quench the capsules were rapidly placed back to their previous position in the hot zone (see Fig. 1b). The technique to trap fluid at run conditions in synthetic fluid inclusions in quartz follows the procedure of Bodnar and Sterner (1987) and Derrey et al. (2017). Five types of quench technique were tested to optimize quantity and quality of trapped fluid inclusions (Fig. 1b):

[1] *Slow quench* (SQ) was used to avoid further cracking of the quartz cylinders after experiment due to thermal shock. The autoclave was pulled out of the hot furnace and slowly cooled to ambient conditions. The initial cooling rate of SQ is about 0.5 K/s (heavy dashed line in Fig. 1b) as estimated by the temperature evolution of the inner calibration unit and the outer thermocouple from target temperature down to 300°C. It must be noted that this strategy was applied in most of the synthetic fluid inclusion studies.

[2] *Slow quench + rapid quench* (SQ+RQ) were conducted to avoid any formation of fluid inclusions at low temperature. This technique was conducted in two steps: firstly, the autoclave was removed out of the hot furnace (as in case [1]); secondly, the sample was rapidly cooled at temperature $\leq 600^\circ\text{C}$. The cooling rates for these two stages were estimated to be 2 K/s (800°C - 600°C) and ~ 25 K/s (600°C - 300°C; light gray dashed line in Fig. 1b), respectively.

[3] *Very slow quench + rapid quench* (VSQ+RQ) were only performed in HCl-bearing system to test whether it can produce more inclusions. The sample was cooled slowly from 800°C to 600°C at constant pressure by setting a cooling rate of the furnace to 0.07 K/s (thin gray line in Fig. 1b). After cooling to 600°C the sample was quenched rapidly (RQ, see below). In this case the rapid quench was within the stability field of α -quartz ($< 630^\circ\text{C}$ at 200 MPa; Swamy et al. (1994)).

[4] *Compressed air quench* (CAQ) was applied to adjust an intermediate cooling rate as high as 3 K/s (gray line in Fig. 1b). The autoclave was pulled out of the furnace and immediately cooled down by compressed air at the hot end.

[5] *Rapid quench* (RQ) revealed the highest cooling rate of 25 K/s (thick black line in Fig. 1b), initiated by dropping the external magnet rapidly to place the sample at water-cooled zone.

After the experiment, the capsules were cleaned and weighed to verify that they had no leaks. The capsules were then carefully opened at one side, and the two quartz cylinders were taken out. When the capsule was inflated and the weight of the capsule had not changed, it was possible to collect the quench fluids by a metal syringe and

Chapter I

transfer the fluid into Teflon vials. Otherwise, only the acidity of the fluid was tested with pH paper. Both sides polished slices with a thickness of ca.300 μm were prepared along the axis of the quartz cylinders.

2.2 Additional supportive runs for inclusion study

In order to investigate the cooling path of the rapid quench process, ~30 mg synthesized rhyolitic glass (~ 5 wt % H_2O) was added to a Au capsule according to the method of Zhang et al. (1997). The samples were pre-equilibrated for few minutes at 800°C and 200 MPa and then quenched rapidly. Then the sample was doubly polished to remove the diffusive layer and analyzed by Fourier transform infrared spectroscopy (FTIR). The final quenched speciation of molecular H_2O_m and OH groups in the quenched glass can provide a geospeedometer to estimate the cooling rate of certain process (Zhang et al., 2000; Xu and Zhang, 2002). A cooling rate of 25 K/s was calculated from the water speciation in a rhyolitic glass

With the purpose to find out whether synthetic fluid inclusions remain a closed system at our run conditions, we conducted a two-step experiment. Fluid inclusions were firstly synthesized using a 1.5 m NaCl solution in Cu capsule for 6 days at 800°C and 200 MPa (DQ-121 in Table 1). Then the retrieved quartz cylinders were transferred to a new Au capsule which was only loaded with pure D_2O prior to run (DQ-124 in Table 1). This experiment was conducted at the same condition for an hour. After this run, synthetic fluid inclusions were analyzed with Raman spectrometry and Fourier transform infrared spectroscopy to characterize qualitatively the abundance of H_2O and D_2O .

In order to understand the kinetics of Cu mobility in water and to compare the results of both fluid inclusion analysis and quench fluid measurement, two experiments were conducted in Cu capsule with deionized H_2O (~30 mg) at the same P-T condition for 19 and 26 hrs, respectively. These runs were quenched rapidly. The crimped capsules were firstly expanded at 200°C for 15 min in atmospheric furnace. Then, the Cu capsules were frozen by liquid nitrogen and pierced to extract the quench fluids which were later diluted with certain amount of water for pH test and ICP-OES determination.

2.3 Microthermometry and chemical analyses

Microthermometry was carried out on a *Linkam THMSG 600* heating ($T < 600^\circ\text{C}$) and freezing stage. The in-house synthesized standard fluid inclusions (pure water-bearing and CO_2 -bearing inclusions) were used to calibrate the stage and is accurate to $\pm 0.1^\circ\text{C}$ in the range of -56.6°C to 0.0°C , and $\pm 1^\circ\text{C}$ up to 347°C . Typically five fluid inclusions were analyzed on each quartz chip. Final ice melting temperatures (T_m) were determined to obtain bulk salinity (i.e. NaCl_{eq}) of the fluids. Homogenization temperatures (T_h) were acquired by heating up the inclusions until a uniform phase is observed. Heating and cooling were repeated again to obtain a duplicate analysis to check for reproducibility. The computer program BULK (Bakker, 2003) was used to estimate the bulk salinity of the fluid inclusion.

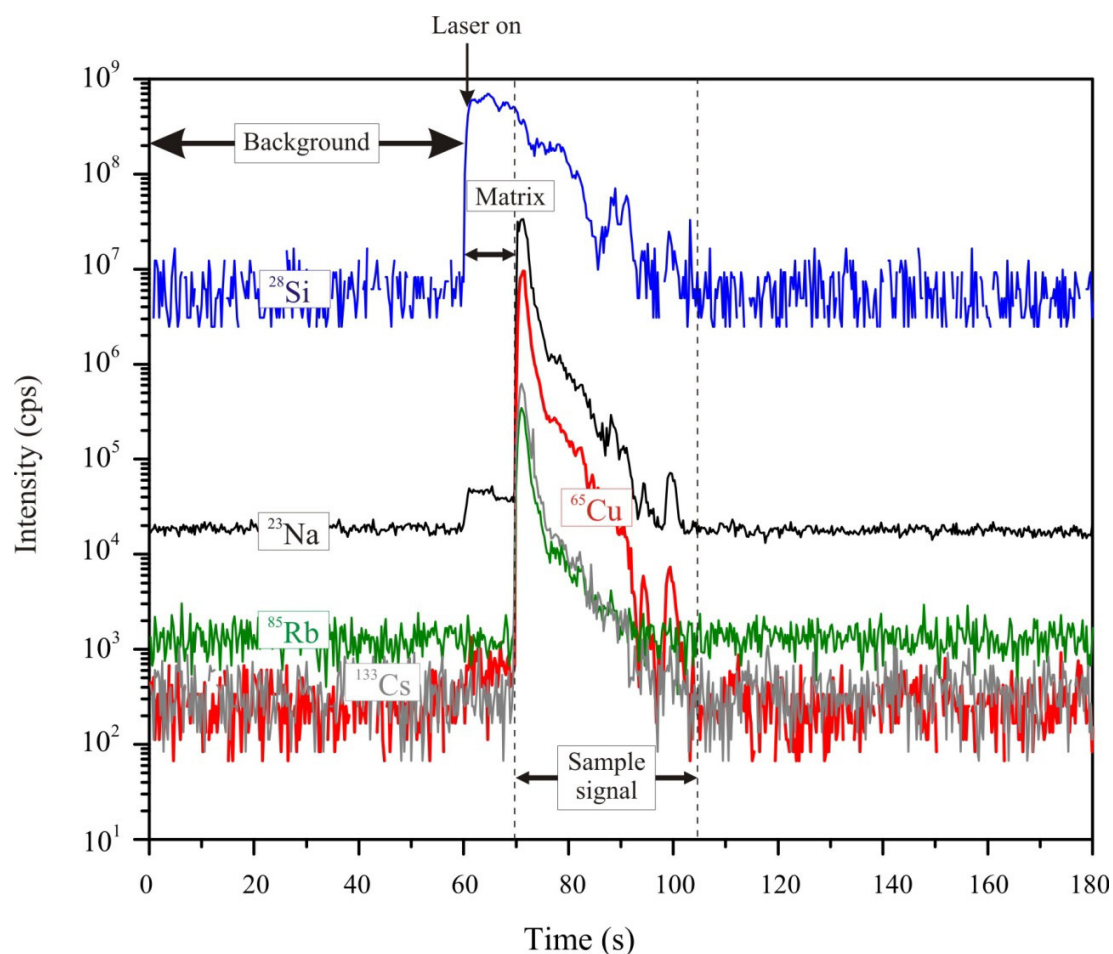


Figure 2 Typical LA-ICP-MS signal from a frozen fluid inclusion (DQ-21, $\text{Cu}+\text{SiO}_{2(\text{gel})}+8\text{wt}\% \text{NaCl}$, formed at 800°C , 200 MPa) using a UV-fs-laser, heating-freezing cell and *Element XR* ICP-MS.

The inclusions were analyzed for their major and minor element contents by LA-ICP-MS. An in-house build laser ablation system based on a UV-femtosecond-laser (*Spectra Physics*) was combined with a heating-freezing cell and a fast scanning sector field inductively coupled plasma mass spectrometer (*Element XR*, *Thermo Scientific*) (for more details see Albrecht et al. (2014)). The laser system is operating in the deep UV at 194 nm and spot size was set to ca. $25\mu\text{m}$. The ablation cell was a modified INSTECTM heating-freezing stage with an adjusted volume of 3 cm^3 . Helium mixed with 2 vol% hydrogen (to adjust the hydrogen flow rate to ca. 5-6 ml/min as suggested by Guillong and Heinrich (2007)) was used as sample-chamber gas. After leaving the sample chamber it was mixed with argon as a carrier gas. Analyses were performed at a temperature of -40°C , guaranteeing completely frozen fluid inclusions prior to the ablation, which resulted in an excellent control on the opening of the inclusions and considerably longer signal analysis time compared to the analysis of liquid fluid inclusions. The analytical uncertainty of the method is estimated to be 10-30% for most elements as discussed in Albrecht et al. (2014). NIST SRM 610 glass was used as external standard (using reference values of the GeoReM database; Jochum et al. (2005)) and measured with a repetition rate of 10 Hz. Laser repetition rates for fluid inclusions analyses have been adjusted

Chapter I

from 5 to 10 Hz, depending on the depth of the inclusion, with higher rates for deeper (down to 40 μm) and lower rates for shallower (down to 20 μm) ones. To evaluate the acquired data, the SILLs data reduction software designed by Guillong et al. (2008) was applied, which is particularly suitable for the interpretation of fluid inclusion signals. The known initial Rb content was used for internal standardization of Cu-H₂O \pm HCl \pm CuCl \pm Cu₂O and Cu₂O-NaCl systems, and the microthermometrically determined Na content was used for Cu-NaCl system (reasons are given below). Figure 2 shows a representative example of a fluid inclusion analysis.

The elemental contents of quench fluids were analyzed by inductively coupled plasma optical emission spectrometry (ICP-OES) on a Varian Vista Pro system (Varian GmbH, Germany).

Raman spectroscopy was used to identify trapped minerals and the presence of H₂O and D₂O in inclusions. The measurements were performed using a confocal Bruker Senterra micro-Raman spectrometer equipped with an Olympus BX 51 microscope and an Andor DU420-OE CCD camera. Unpolarized spectra were collected under ambient conditions, using the 532 nm laser excitation line with 20 mW power, under a long distance Olympus 50 \times magnification objective for 10s with 2 times acquisition repetitions. Instrumental precision was within $\pm 3 \text{ cm}^{-1}$.

Fourier transform infrared spectroscopy (FTIR) was used for geospeedometry as well as to estimate the relative abundance of H₂O and D₂O in synthetic fluid inclusions. The spectra were collected with a Bruker IFS88 FTIR spectrometer equipped with a Bruker IRscope II microscope (operation conditions: global light source and MCT detector). Absorption spectra were collected both in the mid-infrared region (MIR) for quantification of H₂O and D₂O in synthetic fluid inclusions and in the near-infrared region (NIR) for geospeedometry. The spectral resolution was 2 cm^{-1} and 100 scans were collected for each spectrum. A flexi-curve baseline and the calibration of Withers and Behrens (1999) were employed to determine the concentration of water species in the rhyolitic glass used as geospeedometer (Zhang et al., 1997).

The composition of silicate melt inclusion was determined with an electron probe micro-analyzer (EMP) CAMECA SX100. The reference materials for calibration included jadeite (Na), kyanite (Al), wollastonite (Si, Ca), orthoclase (K), NaCl (Cl) and Cu(Cu). Raw analytical data were corrected using the standard PAP procedure (Pouchou and Pichoir, 1991). The acceleration voltage was set as 15 kV. Focused beam and 15 nA were used for cuprite analysis, and defocused beam (2 μm) and 5 nA were used for Na-bearing silicate glass determination.

3. Results

3.1 Fluid inclusion microscopy

Results are presented and discussed in terms of three systems: 1) native Cu + NaCl_{aq}; 2) native Cu \pm Cu₂O \pm CuCl + H₂O \pm HCl; and 3) cuprite (Cu₂O) + NaCl_{aq}. The inclusion description follows the order of increasing quench rate as described in *Experimental and analytical procedure*. It must be noted that silica gel is generally added to the starting material unless otherwise mentioned. All experimental details are tabulated in Table 1.

Chapter I

Table 1 Details of synthetic fluid inclusion experiments

SNO	Capsule material	System (+ Qz cylinders)	NaCl _{eq.} wt%	t ₁ (d)	t ₂ (d)	Quench Technique	Cooling rate (K/s)	Type
DQ-22	Cu	1 wt% NaCl+SiO _{2(gel)}	1.1	2	3	SQ	0.5	FI+SMI
DQ-36	Cu	8 wt% NaCl	8.9	3	2	SQ	0.5	FI+SMI
DQ-21	Cu	8 wt% NaCl+SiO _{2(gel)}	8.7	2	3	SQ	0.5	FI+SMI
DQ-145	Cu	8 wt% NaCl+SiO _{2(gel)}	8.5	3	3	SQ+RQ	0.5;25	FI+SMI
DQ-146	Cu	8 wt% NaCl+SiO _{2(gel)}	8.3	3	3	CAQ	3	FI+SMI
DQ-154	Cu	8 wt% NaCl+SiO _{2(gel)}	8.7	4	4	RQ	25	FI+SMI
DQ-183	Cu	8 wt% NaCl+SiO _{2(gel)}	8.5	/	2	RQ	25	FI+SMI
DQ-165	Cu	8 wt% NaCl+SiO _{2(gel)}	8.5	2	10	RQ	25	FI+SMI
DQ-23	Cu	8 wt% NaCl+SiO _{2(gel)}	20.2	2	3	SQ	0.5	FI+SMI
DQ-121	Cu	8 wt% NaCl+SiO _{2(gel)}		2	7	SQ	0.5	FI+SMI
DQ-124	Au	D ₂ O (Qz from DQ121)				SQ	0.5	FI+SMI
DQ-99	Au	8 wt% NaCl	8.0	3	3	SQ	0.5	FI
DQ-100	Au	8 wt% NaCl +SiO _{2(gel)}	8.1	3	3	SQ	0.5	FI
DQ-101	Au	8 wt% NaCl +Qz powder	8.0	2	4	SQ	0.5	FI
DQ-187	Au	8 wt% NaCl+ Cu ₂ O _(s) + SiO _{2(gel)}	6.8	2	5	SQ	0.5	FI
DQ-188	Au	8 wt% NaCl+ Cu ₂ O _(s) + SiO _{2(gel)}	6.8	/	10	SQ	0.5	FI
DQ-37	Cu	H ₂ O		3	2	SQ	0.5	FI
DQ-123	Cu	0.5 m HCl+SiO _{2(gel)}		2	4	VSQ+RQ	0.07;25	FI
DQ-42	Cu	1.5 m HCl		3	3	SQ	0.5	FI
DQ-43	Cu	1.5 m HCl		3	3	SQ	0.5	FI
DQ-169	Cu	1.5 m HCl + Cu ₂ O _(powder) + SiO _{2(gel)}		3	3	RQ	25	FI
DQ-102	Cu	1.5 m HCl +H ₂ O+ CuCl _(s) + SiO _{2(gel)}		3	3	RQ	25	FI
DQ-47	Cu	H ₂ O+CuCl _(s) + SiO _{2(gel)}		3	3	SQ	0.5	FI

Notes:

All experiments were conducted with two types of quartz cylinders (excluding DQ-188 with only pref. Qz) at 800°C, 200 MPa.

m denotes the molality of the solution, mol/kg.

Cu₂O_(powder) and *Cu₂O_(s)* denote the powder form of cuprite and the sintered cuprite pellet, respectively.

All batch solutions in each run are taken from the same stock solutions.

In order to compare the bulk salinity after microthermometry measurements (NaCl_{eq.}) and initial solution, we used wt% instead of molality of NaCl solutions. The conversion between wt% and molality is : 1wt% = 0.17 m NaCl_{aq}, 8 wt% = 1.49 m NaCl_{aq}, 20 wt% = 4.30 m NaCl_{aq}.

t₁ denotes experiment duration before intermediate quench, *t₂* means the run duration after intermediate quench. The runs DQ-183 and DQ-188 were not conducted with intermediate quench.

Quench techniques: *CAQ* - compressed air quench; *RQ* - rapid quench; *SQ* - slow quench; *VSQ+RQ* - very slow quench and rapid quench (for more details see *Experimental and analytical procedure*).

FI represents fluid inclusion, *SMI* represents silicate melt inclusion.

Chapter I

3.1.1 Native Cu-NaCl system

[1] *SQ (Slow Quench, 0.5 K/s)*: There were two types of inclusions formed in this system: fluid inclusion and silicate melt inclusion. Fluid inclusion (FI) contained condensed liquid phase and a vapor shrinkage bubble (Fig. 3a). The size of most fluid inclusions varied from 20 μm to 30 μm . Silicate melt inclusion (SMI; Fig. 3b) usually consisted of a vapor bubble, a liquid phase, sodium-bearing silicate glass and one or several reddish to dark opaque minerals (Raman has been used to identify these phases, more information has been given below). The relative abundance of the silicate melt inclusions was dependent on the initial NaCl content in the system. SMIs accounted for <5 vol. %, 10-15 vol. % and 30-40 vol. % of inclusions in 0.17 m, 1.49 m and 4.28 m NaCl-bearing runs. Note that vol. % was estimated from 50 inclusions. The shape of these inclusions changed from small single isolated inclusion to large connected channels with increasing salinity. The microthermometry measurements indicated that the measured NaCl_{eq} values of fluid inclusions of the run products in Cu-NaCl systems were similar to their initial NaCl values (Table 1), which may be due to a coexistence of Na^+ and Cu^+ in fluid inclusion in which CuCl_2^- may be dominant (Hack and Marvogenes, 2006). The silicate melt inclusions was not subject to any visible change upon heating (<600°C) and freezing (>-100°C).

In *SQ experiment without SiO₂ (gel)*: Inclusions tended to be less abundant and smaller than those in the run with the presence of SiO_2 (gel). Nevertheless, both fluid inclusions and silicate melt inclusions were detected in the two quartz chips. The sizes of inclusions were < 20 μm (FI) and 20-30 μm (SMI) in pref. Qz, whereas the i.s. Qz cylinder contained very few and tiny inclusions, which made the interpretation of LA-ICP-MS data difficult.

[2] *SQ+RQ (slow quench, 0.5 K/s for 800-600°C, and rapid quench, ~25 K/s for 600-300°C)*: Inclusions in pref. Qz were less abundant than the SQ run. The size of fluid inclusions and silicate melt inclusions were less than 20 μm and 25 μm , respectively. Silicate melt inclusions usually contained more micron- to submicron-sized cuprite crystals especially in necking down channels (similar to Fig. 10d). In contrast, few tiny inclusions were preserved in the i.s. Qz.

[4] *CAQ (compressed air quench, 3 K/s)*: In pref. Qz, the amount of preserved fluid inclusions was the least among all experiments with NaCl. The inclusions were smaller than 25 μm . Silicate melt inclusions were smaller than 10 μm and often appeared as connected channels containing submicron-sized cuprite crystals (e.g. Fig.10d). Very few inclusions could be found in i.s. Qz of this run.

[5] *RQ (rapid quench 25 K/s)*: Three runs (DQ-183, DQ-154 and DQ-165) with the same starting materials and cooling rate but various run durations (2-14 d) were conducted and compared. Even though the run (DQ-183) was conducted only for two days and was later quenched rapidly, there were still ample inclusions preserved in the pref. Qz (Fig.3c, d) while few inclusions (<10 μm) could be preserved in the i.s. Qz without conducting intermediate quench. In addition, inclusions of these runs were very abundant, the size of which varied mostly from 15 to 30 μm . Most fluid inclusions contained cuprite (identified by Raman; see below), while silicate melt inclusions contained no discernible minerals and appeared to be rather homogeneous (Fig.3d). Moreover, larger fluid inclusions containing more cuprite crystals were observed in the longest run (14 d, DQ-165), whereas smaller inclusions with less cuprite crystals were produced in the shorter run (2 days, DQ-183).

Chapter I

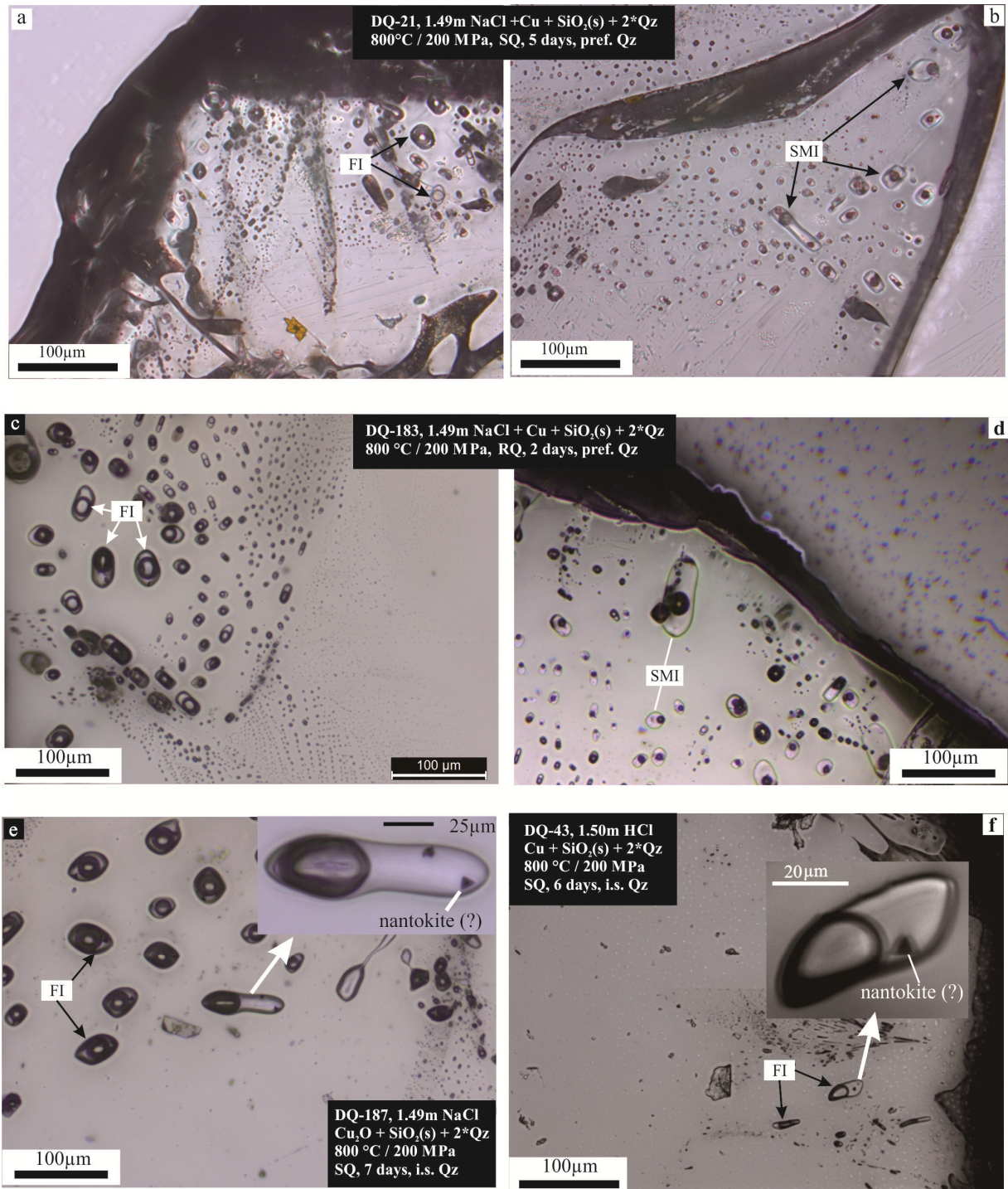


Figure 3 Photomicrographs of typical quartz-hosted inclusions at 25°C. (a, b) Photos are taken from different area of the pref. Qz of DQ-21 in which both FI (marked in (a)) and SMI (marked in (b)) coexist. Discernible cuprite crystals are observed in SMI in despite of FI. (c, d) Both FI (Fig. 3c) and SMI (Fig. 3d) coexist in the pref. Qz of DQ-183, no intermediate quench was adopted. FI often contains cuprite aggregates. (e) Possible nantokite was observed in fluid inclusions of the run with cuprite (Cu_2O) + NaCl_{aq} (DQ-187); (f) Potential nantokite was precipitated in fluid inclusions of the run with native Cu + HCl_{aq} (DQ-43); pref. Qz- prefractured quartz cylinder; i.s. Qz-in situ fractured quartz cylinder; FI-fluid inclusion; SMI-silicate melt inclusion.

3.1.2 Native Cu- $H_2O \pm HCl \pm CuCl \pm Cu_2O$ system

[1] SQ (slow quench, 0.5K/s): It is worth noting that fewer inclusions were observed in HCl/CuCl systems than the pure water system. Only one type of fluid inclusions was observed in these systems ($H_2O \pm HCl \pm CuCl$ solutions), consisting of condensed liquid, a vapor bubble and/or a colorless to dark tetrahedral crystal, possibly nantokite (CuCl; Fig.3f). The nantokite crystal was absent in the run with pure water. Fluid inclusions were generally smaller than 25 μ m, with elongated oval to irregular shape. The nantokite crystal tended to decompose with exposure to incident Raman beam. Berry et al. (2006) undertook experiments with similar starting materials (native Cu and KCl_{aq}) as our study, and used XANES spectroscopy to identify a similar tetrahedral mineral as nantokite (CuCl). They suggested that this mineral was not stable at room temperature as well as under laser beam.

In SQ experiment without $SiO_{2(gel)}$: Fluid inclusions were less abundant than the runs with the presence of $SiO_{2(gel)}$, often smaller than 10 μ m in size. Fluid inclusions mostly appeared as necking-down inclusions. Opaque minerals (i.e., possible nantokite) could be only observed in larger inclusions than 30 μ m.

[3] VSO+RO (very slow quench, 0.07 K/s, 800-600°C, and rapid quench, 25 K/s, 600-300°C): Fluid inclusions were the most abundant in comparison to the rest runs. The size of these inclusions was smaller than 20 μ m.

[5] RQ (rapid quench 25 K/s): This run contained the smallest amount of inclusions, generally smaller than 20 μ m. Nantokite could be only observed in large inclusions. The inclusions retrieved from i.s. Qz were too small to be measured with LA-ICP-MS.

3.1.3 Cu_2O - NaCl system

[1] SQ (slow quench, 0.5K/s): The fluid inclusions were similar to those of the previous series (native Cu + $Cu_2O_{(s)}$ $H_2O/HCl/CuCl_{(s)}+H_2O$), which consisted of condensed liquid, a vapor bubble and/or a colorless to dark tetrahedral daughter crystal (nantokite; Figure 3e). Inclusions mostly ranged from 15 to 40 μ m, with a round to oval shape. The measured $NaCl_{eq}$ value of the fluid inclusions was lower than the initial NaCl content, i.e., 6.8 ± 0.1 wt% and 8 wt%, respectively.

To sum up, the most abundant fluid inclusions were observed in the run with NaCl aqueous solutions with a cooling rate of 0.5 K/s and 25 K/s. Two types of inclusions, namely fluid inclusion and silicate melt inclusion, were only observed in native Cu-NaCl system. Cuprite (Cu_2O) was observed as quench products in both fluid inclusions and silicate melt inclusions. Microthermometric measurements demonstrated that the homogenization temperatures of fluid inclusions and silicate melt inclusions are 440-480°C and a higher temperature than the limit of the current thermal stage (600°C), respectively, resulting in a coexistence of two immiscible fluids at run conditions. In contrast, only one type of fluid inclusion was observed in Cu- Cu_2O -CuCl- H_2O -HCl systems and Cu_2O - $NaCl_{aq}$ system, which usually contained a tetrahedral mineral, potentially nantokite (CuCl).

3.2 Chemical and spectroscopic analyses

Thin sections of quartz cylinders were polished to expose silicate melt inclusions for the EMP analysis. Fig 4 shows a typical backscattered electron (BSE) image of the silicate melt inclusion. The rounded bright dots marked in Fig.4 were possible cuprite which was later identified by Raman spectra (Fig. 5a). The total oxide amount of the silicate melt inclusions varies from 71 wt% to 91wt% (given in Supplementary Table A2). The atomic ratios of Na/Si and Cu/Si are ~ 0.1 and $0.01 - 0.2$, respectively. These qualitative data can be used to interpret the composition of silicate melt (mainly SiO_2 , less Na and Cu).

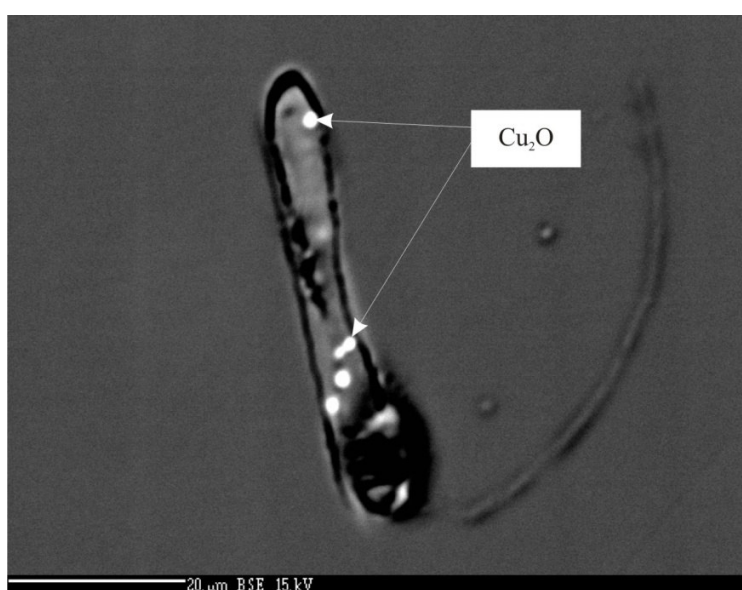


Figure 4 A BSE image of a silicate melt inclusion of the pref. Qz of DQ-21. The run was conducted with Cu +1.49 m NaCl_{aq} + SiO_2 (gel) + Qz at 800°C and 200 MPa for 5 days.

Fig 5a depicts the Raman measurements of the opaque minerals trapped in fluid inclusions and silicate melt inclusions from both SQ and RQ runs with native Cu + NaCl_{aq} . The Raman spectrum of fibrous minerals (Fig.3c) trapped in fluid inclusions of RQ series exhibits five complex bands, centered at 146 cm^{-1} , 218 cm^{-1} , 308 cm^{-1} , 412 cm^{-1} and 625 cm^{-1} (Fig.5a), which is analogous to natural cuprite (RRUF database, ID: R050374). The Raman spectra of the red minerals (Fig.3b) trapped in silicate melt inclusions of SQ series are in good agreement with these spectra. Therefore, the mineral phase trapped in fluid inclusions with rapid quench and in silicate melt inclusion with slow quench is identified as cuprite, i.e. Cu_2O .

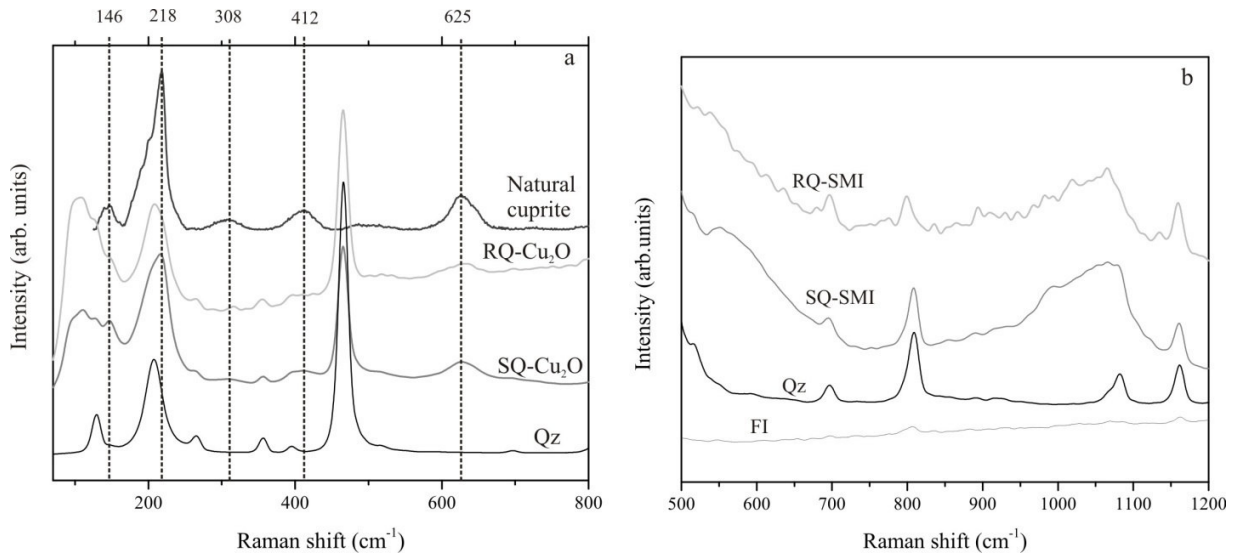


Figure 5 Raman spectra of different phases in inclusions after *SQ* (DQ-21) and *RQ* (DQ-183) runs. (a) Raman analyses of crystals trapped in fluid inclusions (DQ-183) and silicate melt inclusions (DQ-21) in comparison with natural cuprite and quartz host. The vertical dashed lines are assigned to typical cuprite Raman bands (for more details in text). (b) Raman analyses of silicate melt phase in comparison to quartz and fluid inclusion. Broad bands at $550\text{-}600\text{ cm}^{-1}$ and $1000\text{-}1100\text{ cm}^{-1}$ may be assigned to amorphous silica (see text). *SQ* (DQ-21): $\text{Cu} + \text{SiO}_2(\text{gel}) + \text{Qz} + 1.49\text{m NaCl}$, 800°C , 200 MPa , *SQ*, 5 d; *RQ* (DQ-183): $\text{Cu} + \text{SiO}_2(\text{gel}) + \text{Qz} + 1.49\text{m NaCl}$, 800°C , 200 MPa , 2 d.

Fig.5b shows the Raman spectra of the silicate melt phase from these runs. The distinctive broad band at $992\text{ - }1076\text{ cm}^{-1}$ is found to be similar to silicon Q^n vibrational modes (e.g. $950\text{-}1050\text{ cm}^{-1}$ for Q^2 species; ca. 1000 cm^{-1} for Q^3 species (Colomban and Schreiber, 2005)). Unlike a crystalline phase, there are no well defined and intense peaks of the spectra in these silicate melt inclusions. Halasz et al. (2007) have reported the Raman spectra of crystalline Na_2SiO_3 , $\text{Na}_2\text{SiO}_3 \cdot 9\text{H}_2\text{O}$ and aqueous Na_2SiO_3 solutions. They assign the 931 and 997 cm^{-1} bands to $(\text{Na}/\text{H})\text{O-Si-O}(\text{Na}/\text{H})$ vibration, likely $\text{Na}_2\text{H}_2\text{SiO}_4$, and the band at 1018 cm^{-1} to $(\text{X})\text{O-Si-O}(\text{X})$ vibration, where X is Na, H or - charge, likely $\text{NaH}_2\text{SiO}_4^-$. There are Raman peaks at 3500 cm^{-1} (not shown here, but similar to Fig.11a), indicating the presence of H_2O in these silicate melt inclusions. Moreover, the absence of Raman bands below 300 cm^{-1} confirms that this phase could be amorphous (Handke and Mozgawa, 1993) and a broad band in the range of $500\text{-}600\text{ cm}^{-1}$ also indicate an amorphous structure. The broad region ($992\text{ - }1076\text{ cm}^{-1}$) in this case may be assigned to sodium-bearing silicate glass, e.g. $\text{Na}_2\text{SiO}_3 \cdot n\text{H}_2\text{O}$. Therefore, low Na/Si ratio, high wavenumber of these bands as well as broad bands, support polymerized units of silicon.

3.3 Quench fluid analyses

Quench fluids were collected only from two runs after inclusion synthesis, i.e., DQ-165 and DQ-169. The visual inspection shows no precipitates at the bottom of the capsule. In the quench fluid of the run with native $\text{Cu} + \text{NaCl}_{\text{aq}}$ (DQ-165) 1.56 m Na (8.4 wt% NaCl) and 0.002 m Cu have been measured by ICP-OES. This analysis confirms that Na content after run is in a good agreement with the initial Na content, implying that less Na is incorporated in the

melt phase. Quench fluid collected from a Na⁺-free run (Cu+Cu₂O+HCl; DQ-169) contained 0.09 m Cu (570 ppm Cu). The visual inspection and the OES result indicate that the added Cu₂O powder and HCl solution have been consumed, resulting in a less acidic fluids (pH= 4.06) than the initial solution (pH= ~0). These evidences are consistent with the initial loading in which the ratio of Cu⁺/Cl⁻ is nearly 1:1.

Quench fluids collected from Cu capsule loaded with pure water yield 0.02 m and 0.04 m Cu after 19 and 26 hours, respectively. The content data indicate that reaction kinetics may prevent reaching equilibrium within one day, but the measured values can be treated as the minimum solubility of Cu in hydrothermal fluids of the run with native Cu and H₂O. After re-calculation the pH value based on the dilution factor, it is likely that acidic fluids are responsible for Cu enrichment in pure water system, i.e., pH values of ~3.

3.4 LA-ICP-MS data standardization

In this study we analyzed the content of five isotopes with masses of ²³Na, ²⁸Si, ⁶⁵Cu, ⁸⁵Rb and ¹³³Cs in fluid inclusions with LA-ICP-MS (a typical example is shown in Fig. 2), and the results are tabulated in Table 2. Using experimental assemblages initially doped with Rb or Cs to normalize LA-ICP-MS data of synthetic fluid inclusions is widely accepted in previous studies (e.g., Duc-Tin et al., 2007; Lerchbaumer and Audetat, 2012; Derrey et al., 2017). By applying this method to quantify Na content, the evaluated Na content (Na_(std=Rb)) is in a good agreement with the Na_{eq.} value of the microthermometry analysis for the runs with Cu₂O+NaCl_{aq} and pure NaCl_{aq} (note that Au capsule was used in both cases; Fig.6). In contrast, it can be noted that the evaluated Na_(std=Rb) content of fluid inclusions is several times higher than that of the Na_{eq.} in the runs with native Cu + NaCl_{aq} (Fig.6). Thus, using Rb or Cs content to evaluate the LA-ICP-MS data is inappropriate for the system of native Cu + NaCl_{aq} due to the formation of silicate melt phase which can adsorb certain amount of Rb and Cs into the system.

Microthermometry data can help to interpret multicomponent fluid inclusion compositions. However, the bulk salinity obtained from the microthermometry represents the overall salt content, i.e., NaCl_{aq} and possibly CuCl_{aq}. On the one hand, it is evident that NaCl is the dominant dissolved component in the fluid regardless of the partitioning of some Na into silicate melt phase. As mentioned above the Na content in quench fluid matches well with Na_{initial}. Moreover, in NaCl-bearing aqueous fluids, Na strongly partitions toward the fluid in comparison to melt (e.g., granitic melt and NaCl; Bai and Koster van Groos, 1999). On the other hand, submicron-sized cuprite is probably the dominant metal phase (Fig.3b, 3c, 10), which controls the total amount of Cu and these minerals cannot be dissolved along heating during microthermometry measurements. Furthermore, Na content evaluated from microthermometry data can provide a reliable proxy for data standardization, as suggested by Günther et al. (1998). An example given by Steele-MacInnis et al. (2016) demonstrates that ca. 5% of error can be introduced using NaCl_{eq.} (determined by T_{m, ice}; similar method used in our case) instead of a corrected (predicted) NaCl value based on the generic H₂O-(Na,K)Cl-ΣXⁿ⁺Cl_n phase stability relations in a multi-salt system (NaCl-KCl-FeCl₂). Thus, the uncertainty of using Na_{eq.} (evaluated from NaCl_{eq.}) to standardize the LA-ICP-MS data can probably be limited to few percents.

Chapter I

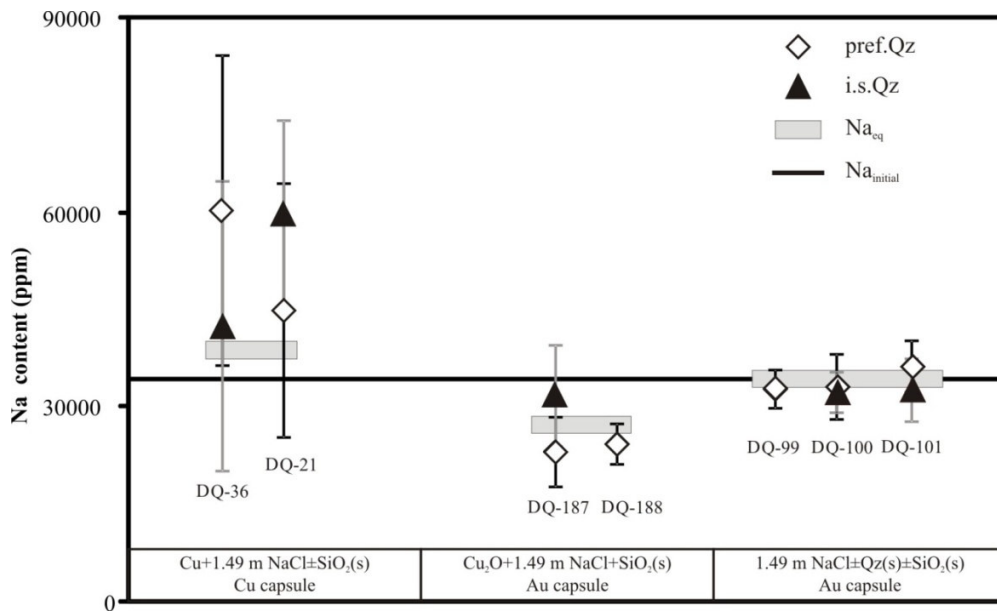


Figure 6 Examples of Na contents in fluid inclusions based on the internal standardization using Rb (400 ppm). The gray bar represents Na_{eq} , which is calculated by the $NaCl_{eq}$, from the microthermometric data; $Na_{initial}$ denotes the initial loading of $NaCl_{aq}$. Apparently, using Rb content is inappropriate for evaluation the LA-ICP-MS data of native $Cu+NaCl_{aq}$ series, more details are given in text.

Chapter I

Table 2 Experimental details and measured Cu concentration from LA-ICP-MS analyses

SNO	pH	Cl _{tot.}	Quench fluid	Cu (pref. Qz)	n flinc	Cu (i.s. Qz)	n flinc	Note
		m	m	m		m		
<i>Native Cu + NaCl</i>								
DQ-22	7	0.17		0.05 ±0.02	13	0.08±0.03	11	Na std.
DQ-36	13	1.49		0.21±0.16	11	0.11±0.09	11	Na std.
DQ-21	7	1.49		0.23±0.11	20	0.23±0.14	15	Na std.
DQ-145	n.m.	1.49		0.20±0.09	16	Small		Na std.
DQ-146	13	1.49		0.19±0.08	16	Small		Na std.
DQ-154	n.m.	1.49		0.20±0.07	15	0.23±0.05	15	Na std.
DQ-183	8	1.49		0.22±0.19	14	Small		Na std.
DQ-165	5.61 ^b	1.49	1.56(Na)/0.002(Cu)	0.22±0.14	13	0.27±0.11	14	Na std.
DQ-23	8	4.28		0.66±0.29	22	0.64±0.25	18	Na std.
<i>Native Cu ± Cu₂O + H₂O ± HCl ± CuCl</i>								
DQ-37	4	0	0.02-0.04*(Cu)	0.04±0.08	15	0.003±0.002	10	Rb std.
DQ-123	3	0.5		0.44±0.21	15	0.62±0.21	9	Rb std.
DQ-42	1	1.5		0.82±0.36	12	1.23±0.37	16	Rb std.
DQ-43	1	1.5		1.28±0.56	16	1.29±0.58	13	Rb std.
DQ-169	4.06 ^b	1.5	0.09(Cu)	1.01±0.38	12	Small		Rb std.
DQ-102	3	1.88		1.63±0.30	11	Small		Rb std.
DQ-47	1	1.45		0.54±0.19	13	0.57±0.21	15	Rb std.
<i>Cuprite + NaCl</i>								
DQ-187	7.00	1.49		0.54±0.14	15	0.53±0.12	14	Rb std.
DQ-188	7.00	1.49		0.43±0.17	15	N		Rb std.

Notes:

All experiments were conducted at 800°C/200 MPa.

pH^b of quench fluids is measured by an Inlab microelectrode, the final data presented in this table are justified based on the dilution factor; *n.m.* denotes pH of the quench fluids was not measured.

Cl_{tot.} represents the initial Cl added to the experiment.

Quench fluids are measured by ICP-OES which yields a precision less than 10% (2SD). Na and Cu represent the elements concentration of Na and Cu.

Note that 0.02 - 0.04 m Cu in quench fluids are not collected from the run DQ-37, which are directly collected from the Cu capsule after comparable runs with pure H₂O after 19 and 26 hrs, respectively (for more details see text).

Cu concentration is the mean Cu concentration obtained from *n* individual fluid inclusion measurements by LA-ICP-MS. Concentration uncertainties are 95% confidence limits about the mean.

n_{flinc} denotes the number of fluid inclusions which have been measured by LA-ICP-MS.

Na std. is calculated based on NaCl_{eq.} of microthermometric data; *Rb std.* is calculated by the initial RbCl_(s).

Inclusions of i.s. Qz of DQ-145,146,183,169 and 102 are too small to be analyzed; DQ-188 was not loaded with i.s. Qz.

Chapter I

3.5 Effect of run duration and intermediate Quench on FI

To understand the formation of fluid inclusions, three experiments with same starting materials (native Cu+1.5 m NaCl_{aq}) but different run durations, were performed using rapid quench for cooling (Table 1). As it is shown in Fig.1b, there are two stages in fluid inclusion synthesis: (i) the first stage is prior to intermediate quench (DQ-183) and (ii) the second stage is after intermediate quench (i.s. Qz cylinders of DQ-154 and DQ-165).

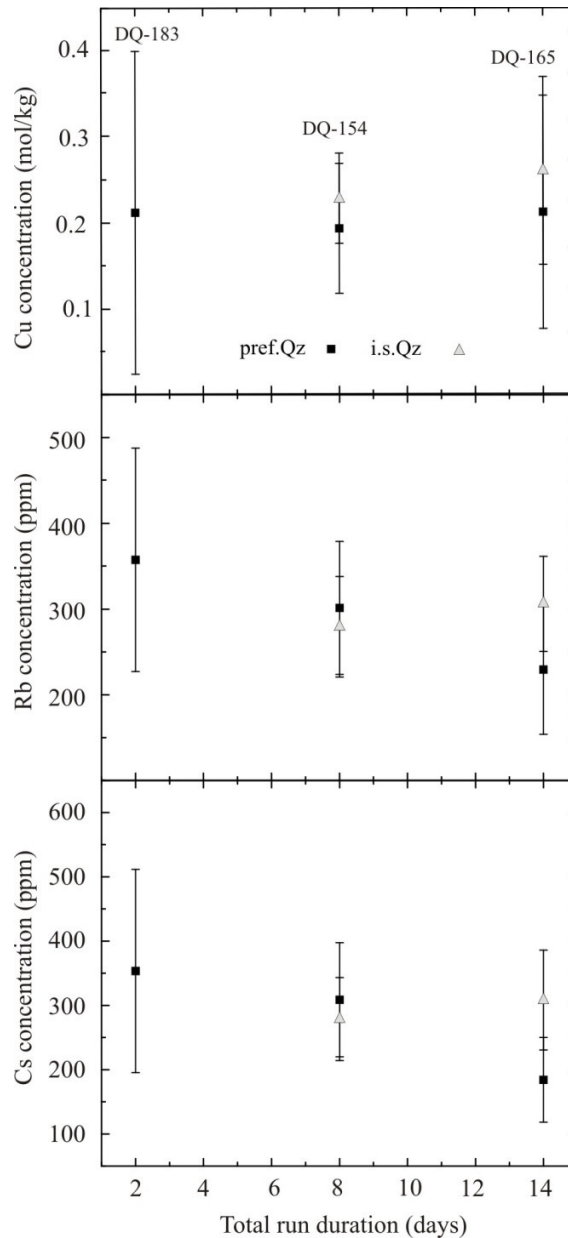


Figure 7 Average Cu, Rb and Cs concentrations of fluid inclusions (error bar is given by the standard deviation of the data). All runs were conducted with native Cu + 8wt% NaCl + SiO_{2(gel)} + Qz at 800°C and 200 MPa, using rapid quench technique. DQ-183- no intermediate quench was performed; DQ-154- intermediate quench after 4 days; DQ-165- intermediate quench after 2 days.

Chapter I

Fig.7 depicts the variations of Cu, Rb and Cs as a function of run duration. The mean Cu contents of short term run (DQ-183) is in a good agreement with long term runs (8 d and 14 d for DQ-154 and DQ-165, respectively), i.e., ~ 0.2 m Cu. In general, Rb and Cs contents of these runs range from 100 to 500 $\mu\text{g/g}$. The i.s. Qz of the run (DQ-154) with longer equilibration time (4 d) prior to intermediate quench yields smaller Cu, Rb, Cs content variations than those with short equilibration durations (2 d for DQ183 and DQ-165). This may imply that fluid-metal equilibration needs longer time than expected, in addition, the potential equilibrated fluids can be trapped in unfractured quartz cylinders after the in situ cracking (i.s. Qz; Derrey et al. (2017)).

3.6 Effect of silica gel

Figure 8 describes Cu variation with respect to Cs content in the presence or absence of silica gel in the Na^+ bearing and Na^+ free systems. Obviously, Cu content of the system Cu-HCl is at least twice higher than that of the system Cu + NaCl_{aq} . In the presence of silica gel, rather constant Rb and Cu contents are achieved for both pref. Qz and i.s. Qz in both systems. In addition, the evaluated Cs content (using Rb as the internal standard) in Cu-HCl system is consistent with the initial Cs content, whereas the Cs content in Cu-NaCl system is lower than the initial value due to Cs partitioning into melt phase. In the absence of silica gel, the variation of Cs content is several times larger than that of the runs with silica gel. Moreover, Cu content is lower than the runs with the addition of silica gel. The content variation can be caused by a low silica supply which hinders crack healing as well as entrapment of more equilibrated fluids.

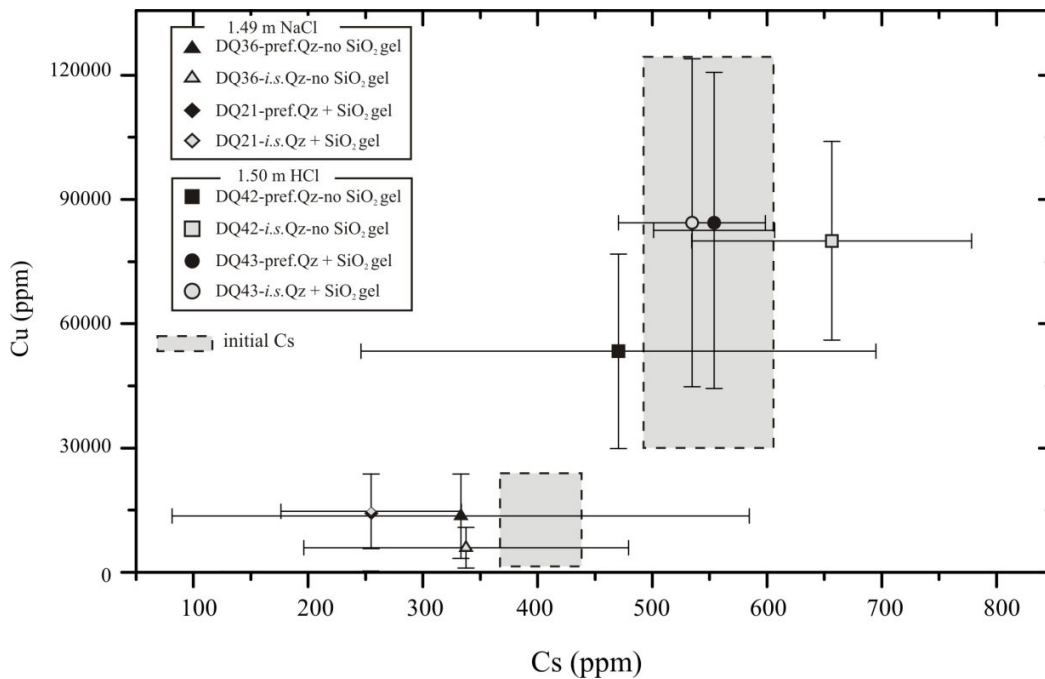


Figure 8 Cu content versus Cs content in Na^+ bearing and Na^+ free systems. Elemental concentrations of the runs with 1.49 m NaCl are standardized based on Na_{eq} ; Elemental concentrations of the runs with 1.50 m HCl are standardized based on $\text{Rb}_{\text{initial}}$.

Chapter I

3.7 Cu content VS. Cl content in fluid inclusions

In systems containing Na^+ , the pH measurements show that the quench fluids tend to be neutral to basic up to a pH of ~ 13 (e.g. DQ-36 and DQ-146 in Table 2). Cu contents in native Cu-NaCl series increase from 0.08 ± 0.03 m to 0.23 ± 0.14 m and 0.63 ± 0.30 m as the salinity (NaCl) increases from 0.17 m to 1.49 m and 4.28 m, respectively (Fig.9). A positive correlation derived from Fig.9 shows a Cu/Cl ratio of $\sim 1:6$. Results of the comparable runs (Cu+1.49 NaCl_{aq}) quenched at different cooling rates (Table 2) demonstrate a similar mean Cu content, ca. 0.23 m. Cu content of the run applied with rapid quench (25 K/s) indicates smaller data variation than the others, i.e., 0.20 ± 0.07 m vs. 0.20 ± 0.14 m (Table 2). When native Cu is replaced by Cu_2O (relic Cu_2O can be found after run), the content of Cu in NaCl solution is increased by a factor of ~ 2 , i.e., to 0.54 ± 0.14 m. In addition, the Cu content in Cu_2O -NaCl_{aq} system without conducting intermediate quench (DQ-188) slightly lower than the value of the run applied with intermediate quench, i.e., 0.43 ± 0.17 m and 0.54 ± 0.14 m, respectively.

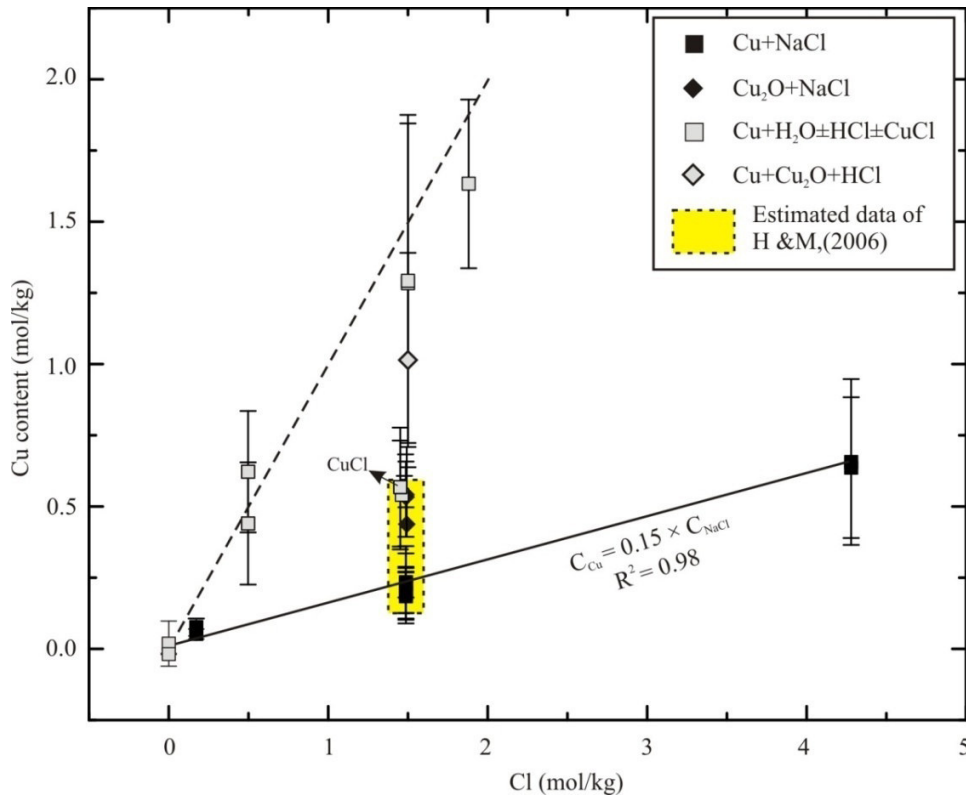


Figure 9 Cu concentrations as a function of initial chloride concentration in fluid inclusions. All runs were performed in Cu capsules, except for the run with $\text{Cu}_2\text{O} + \text{NaCl}_{\text{aq}}$ (Au capsule). Most runs were quenched with slow cooling rates (0.5 K/s). Runs with different cooling rates in the Cu-NaCl (1.49 m) system were also plotted, however, the average Cu content remains constant (ca. 0.23 m) and the difference of Cu contents is within the error. Solid symbols represent the runs with NaCl solution, whereas the gray symbols stand for the runs without NaCl solution. Solid line is a regression relation between the average Cu concentration (native Cu + NaCl_{aq}) and initial chloride concentration. Dashed line represents Cu/Cl ratio of 1. The arrow represents the run with Cu + CuCl + H₂O. Experiments of Hack and Mavrogenes (2006) (H&M) were conducted in the system of Cu + Cu₂O + CuCl₂ + H₂O (fluid acidity was buffered by talc and quartz) at temperature range of 525-725°C and pressure range of 300-1700 MPa.

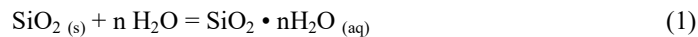
Chapter I

In H₂O-HCl-CuCl systems, the quenched fluids are acidic in the pH range of 1-4. After inspection of capsules, white precipitates (possibly CuCl powder) were observed after the runs with HCl solution, excluding the run with Cu₂O (DQ-169) due to consumption. Note that the initial composition of each component is given in *Supplementary Table A1*. The Cu contents increase with increasing acid contents (Fig.9). In pure water, the Cu content of the pref. Qz is 0.04±0.08 m, which is comparable to the value of quench fluid (Table 2). The i.s. Qz of pure water system yields much lower Cu content (0.003±0.002) than that of pref. Qz due to weak healing in absence of silica gel. Cu enrichment in pure water in this study is ca. 4 times higher than that of Zajacz et al. (2011) who have conducted the experiment in Au₉₇Cu₃ capsule (a_{Cu}=0.01). A nearly 1:1 ratio of Cu/HCl can be derived from Cu content and initial acid content (dashed line in Fig.9). When Cu₂O is added to 1.5 m HCl solution, the Cu content (1.01±0.38 m) of Cu-Cu₂O-HCl system is lower than its value (1.28±0.56 m) in Cu-HCl system, yet twice higher than its value (0.54±0.14 m) when NaCl is present (Cu₂O+NaCl in Au capsule). When CuCl is added to the system (Cu-CuCl-HCl, with an initial Cu⁺ / Cl⁻ = 1/2; Table A2), Cu content is three times higher than that in pure CuCl system (Cu-CuCl-H₂O, initial Cu⁺ / Cl⁻ = 1), i.e., 1.63±0.30 m and 0.54±0.19 m, respectively. The lower Cu content in pure CuCl system than that in pure HCl/CuCl-HCl system may be due to a reduction of Cu⁺ to native Cu (more details are given below). The Cu content of Cu-CuCl-H₂O system is in a good agreement with its content in Cu₂O-NaCl_{aq} system (in Au capsule) at the same chloride content (1.5 m), ca. 0.5 m. It is worth noting that Cu contents in systems such as Cu-NaCl_{aq}, Cu₂O-NaCl_{aq}, Cu-CuCl-H₂O are in a good agreement with the estimated data of Hack and Mavrogenes (2006) who investigated Cu solubility in Cu-Cu₂O-CuCl₂-H₂O system at lower temperature and higher pressure ranges than this study, i.e., 525-725°C and 300-1700 MPa.

4. Discussion

4.1 Silicate melt inclusions and quartz solubility

Knowledge of the silica solubility in aqueous fluids is fundamental for the quantitative understanding of hydrothermal processes. The strong partitioning of SiO₂ into a concentrated salt solution (or even diluted salt solutions, Xie and Walther (1993)) is called a ‘salting in’ effect, or quartz solubility enhancement. The dissolution of quartz into the surrounding fluid is described formally by the reaction:



The solute species is thought to be dominantly a neutral complex represented by the formulas Si(OH)₄ or H₂SiO₄, thus *n* is generally considered to be 4 (Walther and Orville, 1983; Shmulovich et al., 2001).

Shmulovich et al. (2006) proposed a modified Setchenow-type equation (2) to estimate the quartz solubility in fluids at crustal conditions,

$$\log S_{\text{Qz}} = \log S_{\text{Qz}}^0 + 3.5 \cdot \log X_{\text{H}_2\text{O}} + a \cdot (m \text{ NaCl}_{\text{aq}})^b \quad (2)$$

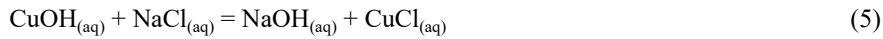
Chapter I

where S_{Qz} is the overall quartz solubility, S_{Qz}^0 is the quartz solubility in pure water at certain run condition, X_{H_2O} is mole fraction of H_2O , $m NaCl_{aq}$ is the molality of sodium chloride in the aqueous solution, a and b are constants dependent on specific P and T. Given the fact that the run conditions are fixed at $800^\circ C$ and $200 MPa$, SiO_2 solubility increases with increasing salinity ($NaCl_{aq}$), i.e., increasing from $\sim 0.2 m$ to $0.26 m$, $0.33 m$ and $0.37 m$ when $NaCl_{aq}$ ranges from 0 to 0.2 , 1.5 and $4.3 m$ (Anderson and Burnham, 1965; Shmulovich et al., 2006; Dolejš and Manning, 2010). Therefore, up to $\sim 0.7 mg$ of SiO_2 is expected to be dissolved in the fluid at run conditions.

Silicate melt inclusions were absent in experiments conducted with pure water (no $NaCl$ and no HCl), which can be expected considering the results of Shmulovich et al. (2006) showing a drastic change in quartz solubility behavior between pure H_2O and $NaCl$ bearing fluids. On the other hand, the solubility of Qz in H_2O is about 50% lower than that in $1.5 m NaCl$ at $800^\circ C$ and $200 MPa$ (Eq.(2); Shmulovich et al. (2006)). However, the presence of a melt phase has only been observed in native $Cu-NaCl$ series (Fig.3b, d), but not in experiments conducted with $Cu-HCl/CuCl$, which may be due to a pH effect or the dissolution mechanism. Table 2 shows that the pH of quench fluids from native $Cu + NaCl$ runs may be more basic than those in other systems (native $Cu \pm Cu_2O \pm HCl \pm CuCl$ and $Cu_2O + NaCl_{aq}$). The pH values of 13 indicates that the OH^- concentration in quench fluids is $\sim 0.1 m$. Quartz is found to be much more soluble in alkali hydroxide solutions than in alkali chloride solutions (Anderson and Burham, 1967). Anderson and Burham (1967) have invoked the following reaction (3):



The production of sodium hydroxide in this case is probably triggered by the following reactions (4)-(6):



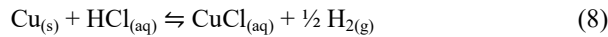
An overall reaction is comparable to what has been proposed by Zajacz et al. (2011) :



Unfortunately, Zajacz et al. (2011) did not find any evidence of the presence of NaH_3SiO_4 in their experiments. The likelihood of NaH_3SiO_4 has been confirmed in this study by the Raman spectroscopic determination. The Raman spectra of the melt phase indicate that the silicate melt phase is dominantly composed of silicon Q^2 and Q^3 units, meaning that a silicate network is formed by condensation reactions of $NaOH$ with quartz and silica gel (reaction (3)). Furthermore, the formation of the amorphous silicate phase which occurs in 2 -14 days experiments with/without additional silica gel is likely a kinetic controlled process, suggesting that the system at run condition reaches an immiscibility gap, i.e., a fluid phase coexists with a melt phase.

4.2 Redox state and stable phase

It is necessary to understand the oxygen and hydrogen fugacity at run conditions in presence of native Cu and/or Cu(I) minerals (i.e., Cu₂O, CuCl) in some runs. At the initial stage, the log f_{O_2} of the inner capsule is probably buffered at Cu-Cu₂O, which is expected to be 3 log units higher in oxygen fugacity than the autoclave (log f_{O_2} : ca. NNO+2.3). During this stage the reactions (4 and 8) can explain the oxidation of native Cu in Cu-NaCl_{aq} and Cu-HCl systems.



In a subsequent stage, hydrogen that is present in the pressure medium can diffuse through the capsule wall and the conditions become more reducing, i.e., Cu₂O (or Cu⁺) is not stable. At experimental condition, the bulk production of hydrogen in all runs is less than 4.5 × 10⁻⁵ g, the time needed for hydrogen migration through the Cu capsule wall is far less than an hour at 800°C and 200 MPa. The permeation rate of hydrogen through copper capsule is 1.18 × 10⁻¹⁰ g/cm·sec·bar^{1/2} (Reiter et al., 1993). The external hydrogen fugacity imposed by the vessel may control or disturb the internal reactions in Cu capsule. It is noteworthy that hydrogen fugacity within the Cu capsule is dependent on the aqueous Cu⁺ content according to Eq.(8). In addition, the oxygen fugacity is given by



It is evident that native Cu maintains its stability at the late stage. This is corroborated by the following evidences: (i) the fluid acidity of the run with Cu + CuCl (DQ-47) turns from neutral into very acidic (pH=1), additionally, Cu content in this system is three times lower than that in pure HCl solutions (Fig. 9), both implying that the reaction (8) is shifted to the left side. (ii) A microscopic observation of Au foil after the run with Cu₂O + NaCl_{aq} (DQ-187, 188) confirms the deposition of thin native Cu layer on Au.

4.3 Influence of cooling rate on nucleation of cuprite

A slow quench rate was adopted to terminate the experiment by most researchers to avoid inclusion decrepitation and to preserve more inclusions, e.g. cooling rate of ~0.5 K/s (Zhang et al., 2012; Derrey et al., 2017), ~0.8 K/s (Hack and Mavrogenes, 2006). We applied various quenching techniques to investigate their effects on Cu content of fluids trapped in inclusions with the same starting materials (Table 1).

An interesting observation is that the appearance of cuprite in both FI and SMI depends on the cooling rate (Fig. 10). In FIs, the presence of cuprite is mainly observed at fast cooling rate (Fig.10 c, e), but cuprite phases could not be discerned at slow cooling rate (Fig.10a), which is surprising. This may be due to different nucleation behavior of cuprite. During rapid cooling process cuprite is likely formed within the fluid (homogeneous nucleation) while in the case of slow quench cuprite favors depositing on the inner surface of inclusions (heterogeneous nucleation) or being adsorbed on the bubble surface or locating in its interior. However, the average copper contents in FI remain constant independent on cooling rates, i.e., ca. 0.2 m, implying that cuprite as a quench phases may also have been formed at slow quench rates. The most probable explanation is that the nucleation and growth of the cuprite differs

Chapter I

strongly depending on quench rate. In SMIs, the presence of cuprite is mainly observed at slow-intermediate cooling rates (Fig. 10b, d), but not observed at fast cooling rate (Fig.10a). However the presence of micron-sized cuprite can't be excluded in rapid quench runs. The different behavior of cuprite in SMIs and FIs might be due to the higher viscosity of silicate melt than fluid phase.

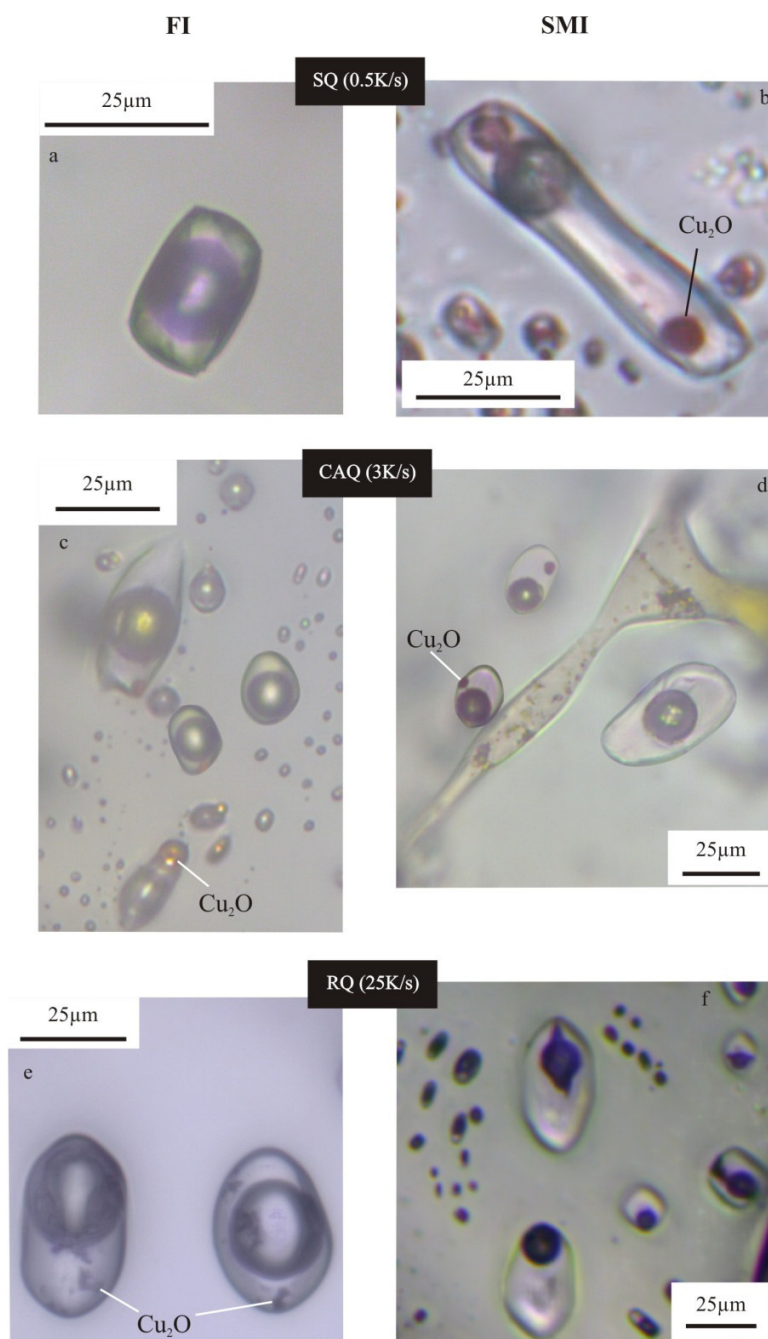


Figure 10 Presence of cuprite in fluid inclusions (FIs) and silicate melt inclusions (SMIs) with respect to cooling rate. All runs were conducted in the system of Cu-NaCl (1.49 m) at 800°C and 200 MPa for 5-8 d. (a, b) Inclusions of DQ-21 which was cooled with a rate of 0.5 K/s; (c, d) Inclusions of DQ-146 adopted with a moderate cooling rate (3 K/s); (e, f) Inclusions of DQ-183 quenched rapidly (25K/s).

Although the mean copper contents of the inclusions after different cooling rates are the same (ca. 0.2 m), the variations of Cu content in each run are somehow related to cooling rates. When the cooling rate decreases from 25 K/s to 0.5 K/s, this variation increases by a factor of 2 (Table 1). The larger Cu variation of the runs with slow cooling rate (e.g. 0.5 K/s) may be related to the formation of late inclusions during cooling. Hence, the rapid quench is an effective technique to preserve reliable information of synthetic fluid inclusions at high T-P conditions in NaCl bearing system and to eliminate formation of post-quench inclusions. However, rapid quench technique is not suitable to Na⁺ free systems in which very little inclusions are formed.

4.4 Proper sealing of synthetic fluid inclusions

One of the important assumptions in fluid inclusion studies is that nothing is added to, or removed from, the inclusion following trapping (Roedder, 1984). Several studies illustrate that elements in inclusions can be re-equilibrated in relatively short experimental run times at elevated temperature and pressures (Mavrogenes and Bodnar, 1994; Audetat and Gunther, 1999; Li et al., 2009b; Audétat et al., 2018). Previous findings of Doppler et al. (2013) show that hydrogen isotope in inclusions can be fully exchanged with outer deuterium isotope after 19 days at 650°C and 337 MPa.

The minimum area of the analyzed volume of inclusions with FTIR in this study is 30 μm × 30 μm, the results are strongly biased especially when there are more than one inclusion and/or cracks adjacent to the analyzed area. The results of FTIR analyses show that single and isometric inclusions contain only H₂O, however, larger fluid inclusions (>50 μm), e.g. necking-down inclusions and inclusions of irregular shape, contain D₂O as well as H₂O (Fig.11b). The confocal Raman spectroscopy allows precise single inclusion measurement due to its high spatial resolution. Both H₂O and D₂O have well defined Raman spectra, with discrete bands in the range of 2900 - 3800 cm⁻¹ and 2100 - 2800 cm⁻¹, respectively. The Raman analyses indicate that isometric, isolated inclusions contain only H₂O (Fig. 11a). Whether these findings can be generalized needs further investigation since we have conducted only one experiment.

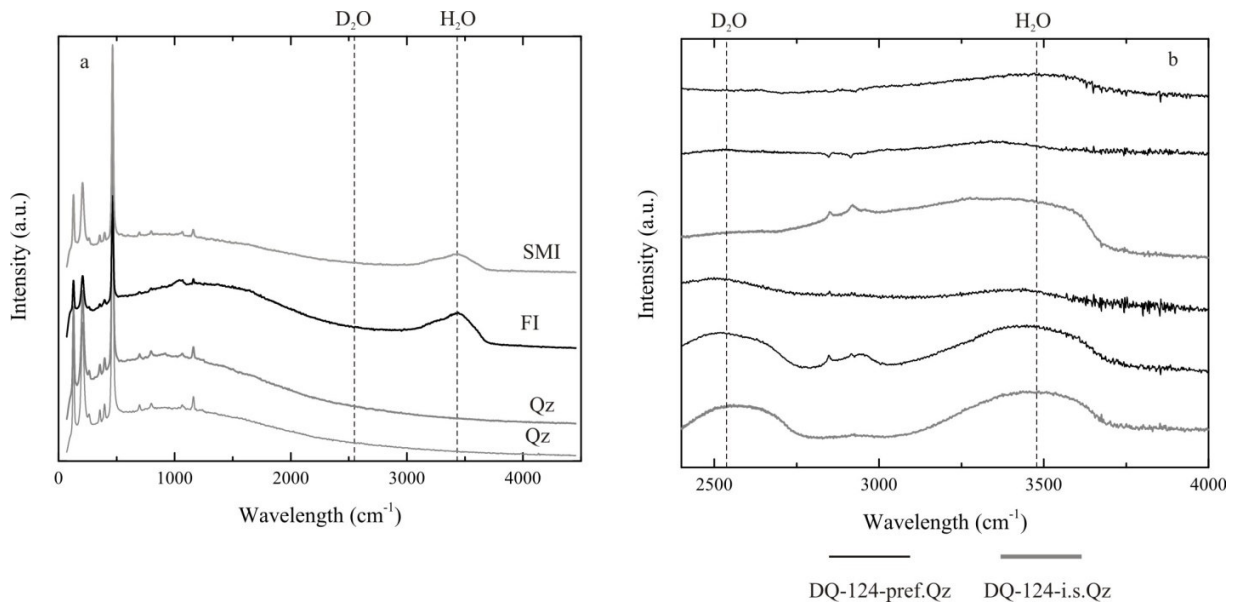


Figure 11 Spectra are shown to discuss possible hydrogen-deuterium isotope exchange between fluid and inclusions. The Raman spectra (a) clearly show no contamination of the inclusion by D_2O . The FTIR spectra (b) in most cases show bands of H_2O as well as of D_2O due to possible incorporation of poor quality inclusions, e.g., necking-down inclusions (more details are given in text). Bands at $2800 - 3000\text{ cm}^{-1}$ are due to hydrocarbon from contamination during sample preparation.

Crack healing is a process where an open micro-crack is filled with locally redistributed quartz through pore-fluid diffusion (Brantley, 1992). The enhancement of micro-crack healing in quartz is a function of fluid chemistry in the order: $CO_2-H_2O < H_2O < NaCl$ bearing fluids, and the healing is more effective with increasing temperature and pressure (Brantley et al., 1990; Brantley, 1992). Even in short duration experiments (~ 15 min) significant healing occurs at $600^\circ C$ and 200 MPa, and micro-cracks such as $\sim 100\ \mu m$ in length and $< \sim 10\ \mu m$ in width are healed in 4 hours at this condition (Brantley et al., 1990). Brantley (1992) reported that quartz micro-fractures underwent at least 50% self-healing on a time scale of 5 hours at $600^\circ C$ and 200 MPa in the presence of $NaCl-H_2O$ fluids. Simon et al. (2007) showed that crack healing would not be promoted prior to aqueous fluid equilibration even if brine salinities approaching 60 wt% $NaCl_{eq}$ at $800^\circ C$ and 100-110 MPa. Although crack healing might be fast at our run condition, the formation of silicate melt inclusions and enhanced quartz solubility (dissolution of up to 2 wt% of total SiO_2) can speed up the crack healing rate. As a result, the faster rates of crack healing, perhaps prior to fluid-solid equilibration, will lead to entrapment of fluids from different stages and large content variations even in a single run are possible.

4.5 Copper diffusion

At elevated temperature ($\geq 100^\circ C$) the valence state of copper has been widely accepted as monovalent Cu^+ in magmatic hydrothermal fluids (e.g., Fulton et al., 2000a; Brugger et al., 2007; Schmidt et al., 2018), and in silicate

melt (e.g., Ripley and Brophy, 1995; Holzheid and Lodders, 2001). Our observations in this study are consistent with Cu(I) being the predominant oxidation state.

Kats (1961) and Götze (2009) suggest that monovalent cations, including H^+ , Li^+ , Na^+ , Cu^+ , and Ag^+ , can be located within channels parallel to the quartz c-axis to compensate the charge deficit of Al^{3+} replacing Si^{4+} in quartz. Many experimental results have revealed that interstitial ions (mainly H^+ , Li^+ , and Na^+) diffused quickly along the quartz channel (c-axis) by applying an electric field (Verhoogen, 1952; White, 1970; Kronenberg and Kirby, 1987; Girardet et al., 1988). Li et al. (2009b) performed Na, Cu exchange experiments between synthetic fluid inclusions and external aqueous solutions and measured up to 0.5 wt% Cu gained during the re-equilibration experiments at 600-800°C, 70-140MPa and 6-8 days. They suggested that the increment of Cu content was likely controlled by processes other than Na-Cu interdiffusion. Lerchbaumer and Audetat (2012) measured ~6 wt% Cu gained within three days in vapor inclusions of re-equilibrated experiments at 800°C and 70 MPa. The copper diffusion coefficient in quartz reported from this study was $2.9 \times 10^{-10} \text{ m}^2/\text{s}$ at temperature of 800°C. Rottier et al. (2017) studied trace element diffusion in quartz during heating experiments with a Linkam TS 1500 stage. Their results show that Cu content of melt inclusions increase 10 folds and Cu content of hydrothermal quartz crystals are two orders of magnitude higher than its starting content from 0°C to 900°C. Since we synthesized fluid inclusions from an inclusion-free synthetic single quartz crystal, we can rule out any elemental contributions from the pre-existing inclusions. Cu diffusional gain over a period of 15 min during cooling process (800°C-300°C) is $< 1 \mu\text{g/g}$ based on the diffusivity of Cu at 400°C, i.e. $1.5 \times 10^{-12} \text{ m}^2/\text{s}$ (Lerchbaumer and Audetat, 2012). This process is highly dependent on the cation (e.g., Na^+ , Cu^+) concentration in quartz. However, the diffusion exchange upon intermediate quench and cooling has rather weak influence on Cu content in the fluid inclusions. Cu contents in fluid inclusions span a large range even in a single run (Fig.9), which cannot be simply attributed to diffusion coefficient. Furthermore, it is the transport rate not the diffusion coefficient of Cu that determines how much Cu can be transferred from or into the inclusions. Fluid inclusions of various Cu contents may be caused by transport process.

4.6 Copper speciation in fluids

Cu solubility in the single phase region by synthetic fluid inclusion technique has been investigated in the temperature range from 525°C to 1000°C, at pressure from 300 MPa to 1700 MPa (Berry et al., 2006; Hack and Mavrogenes, 2006; Zajacz et al., 2011). Both XANES spectroscopy investigation (Berry et al., 2006; 2009) and theoretical calculations (Zajacz et al., 2011; Mei et al., 2014) agree that Cu(I) is found to occur exclusively as linear species $CuCl_2^-$ in solutions. The dominant Cu(I) species is $Na(K)CuCl_2$ in NaCl/KCl solutions (Berry et al., 2006; Zajacz et al., 2011). Whereas higher order copper chloride complexes, stoichiometrically $CuCl(HCl)_{n-1}^0$ (where n is up to 4), have been characterized in Na^+/K^+ -free solutions by the solubility study (Hack and Mavrogenes, 2006) and spectroscopic investigation (Berry et al., 2006).

It is evident from Fig.9 that Cu:Cl ratio reaches ~1:6 in Na^+ -bearing system, which is similar to the ratios (up to 1:6) determined by Berry et al. (2006) in the pH and oxygen buffered native Cu- KCl_{aq} system. This consistency may indicate that $NaCuCl_2$ predominates in the native Cu-NaCl system. Interestingly, none of these studies have reported

the presence of Na-bearing silicate melt phase even when native copper was added as the metal source (Berry et al., 2006; Zajacz et al., 2011). The possible reasons can be related to different experimental conditions and starting materials. In Cu-HCl systems, the Cu:Cl ratios of nearly 1:1 ratio (in HCl solutions) and very acidic fluid with pH values of ~ 1 corroborate the likely form of $\text{CuCl}(\text{HCl})_{n-1}^0$ (the coefficient n describes the average stoichiometry of copper(I)-chloride species present). The unlikelihood of HCuCl_2 (where $n = 2$) is also due to rather low dielectric constant of water in 'supercritical' fluids (Uematsu and Frank, 1980).

4.7 Implications

The finding of coexisting silicate melt and fluid inclusion in this study may shed some lights on the understanding of Cu enrichment in porphyry copper deposit (PCD). PCDs supplying 75% of the world's copper are associated with hydrothermal fluids and magmatic processes which play a key role in the enrichment of copper and its precipitation as sulphide (Blundy et al., 2015). Cu enrichment and transport are favored by oxidized, chlorine-rich fluids. Copper enrichment is attributed to fractional crystallization of volatile-rich, mafic parent magmas under oxidizing conditions to form silicic magmas that are rich in chlorine and potentially copper but poor in sulphur (Lee et al., 2012; Blundy et al., 2015). Magmatic brines which are derived from the silicic magmas play a vital role in Cu transport. For example, weight per cent levels of dissolved copper are found in high-salinity fluid inclusions (Bodnar et al., 2014). Although as proposed that brines are exsolved from silicic magma due to low-pressure degassing or condensation of supercritical gas (Blundy et al., 2015), it is not clear whether these two phase can coexist. Here we draw on observations of synthetic fluid inclusion to propose an alternation explanation for Cu enrichment in PCD. The coexisting high-silica rich melt phase containing cuprite and hydrothermal brines containing 0.5-4 wt% Cu (1-20 wt% NaCl) may support that Cu can be enriched in sulphur-poor high silica melt and in chlorine-rich fluids, and may ultimately provide favorable sites for PCD formation. The silicate melt has a limited influence on Cu transport due to its high viscosity and solidification at rather high temperature. The hydrothermal brine can be no longer stable at low pressure (e.g., it separates into low-salinity vapor and high-density brine at 800°C and 130 MPa), thus the presence of different types of inclusion and silicate melt inclusion is not surprising. For example, the contemporaneous trapping of K-feldspar-rich melt inclusions, hypersaline and vapor-rich inclusions are observed in Grasberg porphyry Cu-Au deposit (Mernagh and Mavrogenes, 2018). Coeval silicate melt and fluid inclusions have also been documented elsewhere, such as Pantleria, Italy (Lowenstern, 1994), Erzgebirge, Germany (Thomas, 1994) and synthetic fluid inclusion (Student and Bodnar, 1999).

The data obtained in this study may help to qualitatively estimate the transport of Cu in a native Cu ore in Keweenaw peninsula, Michigan, USA. The ore deposits of the Keweenaw Peninsula are unique, where native copper accounts for more than 99% of the district production (ca. 5 billion kg of refined copper) in the period of 1845-1968 (Weege and Pollack, 1971). This native copper ore deposit is hosted by the source rock, Keweenaw basalt. It is evident that under reduced and sulfide-absent conditions, magmatic native copper (Cu^0) can be the stable species coexisting with silicate minerals such as olivine and plagioclase in mantle derived peridotite (Zhang et al., 2006; Ikehata and Hirata, 2012). Native copper blebs were also found in Keweenaw basalt (Scofield, 1980; Hofmeister and Rossman, 1985). Larson et al. (2003) and Bornhorst and Mathur (2017) provide a Cu isotopic study

to constrain the genesis of the Keweenaw native copper ore. Bornhorst and Mathur (2017) proposed that Keweenaw basalt was enriched in native copper and underwent later burial metamorphism; the progressive batches of metamorphogenic ore-forming fluids with similar copper isotopic composition of source rock were transporting Cu as Cu^+ (e.g. CuCl_2^-); the final reductive precipitation of native copper from the metamorphogenic ore-forming fluids was facilitated by the mixing with meteoric waters. Cu contents in Keweenaw basalt range from 20 to 200 $\mu\text{g/g}$, averaging at 70 $\mu\text{g/g}$ (Jolly, 1974), the dimension of which is ca. 4 km wide, 40 km long and 25 km thick (Weege and Pollack, 1971; Bornhorst, 1997; Bornhorst and Mathur, 2017). Given the fact that the average density of the basalt is 2.55 g cm^{-3} (Moore, 2001). Based on these parameters, the estimated Cu content in Keweenaw basalt is $7 \times 10^{11} \text{ kg}$, indicating that the basalt has a potential to form an ore deposit. Fig.9 shows that the dissolution of native copper by 13 wt% NaCl_{aq} (Audetat et al., 2008) can uptake 2.5 wt% dissolved Cu in magmatic-hydrothermal fluids. Provided that flow rates range from 1 to 5 m/yr and total discharge rate is $5 \times 10^6 \text{ m}^3/\text{yr}$ (Garven, 1985), we estimated that $\sim 30 \text{ km}^3$ of fluid would be required to form the deposits, and the ore forming event would last ~ 6000 years, rather than tens of millions of years (Woodruff et al., 1995).

5. Conclusions

This study has shown that chloride-bearing aqueous fluids have the potential to increase Cu content appreciably at magmatic-hydrothermal conditions (800°C , 200 MPa), e.g., 1.5 wt% and 5.4 wt% of Cu dissolved in 1.5 m NaCl and 1.5 m HCl solutions, respectively. In native Cu- NaCl_{aq} systems, two types of inclusions were formed, namely fluid inclusions and Na-bearing silicate melt inclusion, indicating that hydrothermal brine and silicate melt phase can coexist. Cuprite trapped in fluid inclusions and Na-bearing silicate melt inclusions is precipitated as quench product due to different cooling rates. In HCl-bearing systems, nantokite has been a common daughter mineral throughout all experiments. Quench fluids of native Cu + NaCl and $\text{Cu}_2\text{O} + \text{NaCl}$ systems are neutral to basic whereas the fluids collected from native Cu \pm Cu_2O + HCl + CuCl systems are generally acidic. A linear correlation between Cu content and initial chloride content has been derived, with Cu/Cl ratios of 1:7 in native Cu- NaCl_{aq} system and 1:1 to 1:3 in native Cu \pm Cu_2O + HCl + CuCl and $\text{Cu}_2\text{O} + \text{NaCl}_{\text{aq}}$ runs.

Although there are few inclusions already formed in the intact quartz cylinder prior to intermediate quench, this will have minor effect on Cu content in in situ cracked quartz, and the two types of quartz cylinders, i.e. prefractured and in situ fractured quartz, is a reliable technique to acquire information of hydrothermal fluids. Rapid quench is an optimum quench technique to rule out fluid inclusions formed at late stage, which can be applied to NaCl-bearing system. The addition of silica gel is of great importance not only for cracks healing but also for improvement of fluid inclusion quality. Caution should be taken when using Rb and Cs as internal standards in native Cu- NaCl_{aq} system to evaluate LA-ICP-MS data, if two phases (fluid and melt) are present, which will lead to trace elements partitioning between both phases.

Acknowledgments

This research was supported by the German Academic Exchange Service (DAAD-57076462) and Graduate School GeoFluxes. We thank Dr. M. Albrecht, U. Kroll and J. Feige for their technical supports.

Chapter I

Supplementary data

Table A1 Initial loading of all runs

SNO	SiO ₂ (gel) 10 ⁻³ g	Cu ₂ O _(s) 10 ⁻³ g	CuCl _(s) 10 ⁻³ g	NaCl _(aq) 10 ⁻³ g	HCl _(l) 10 ⁻³ g	H ₂ O _(l) 10 ⁻³ g	Cu ⁺ / Cl ⁻ Initial ratio
<i>Native Cu + NaCl</i>							
DQ-22	2.41			25.07			
DQ-36				26.52			
DQ-21	1.73			24.49			
DQ-145	3.70			30.72			
DQ-146	2.38			30.16			
DQ-154	1.63			29.96			
DQ-183	2.34			31.21			
DQ-165	2.05			30.96			
DQ-23	2.22			27.56			
<i>Native Cu ± Cu₂O + H₂O ± HCl ± CuCl</i>							
DQ-37						25.92	
DQ-123	3.91				9.94	20.15	
DQ-42					24.10		
DQ-43	3.41				24.25		
DQ-169	3.25	3.67			28.51		1.2
DQ-102	2.20		3.13		15.50	14.59	0.6
DQ-47	2.58		4.37			30.43	1.0
<i>Cuprite + NaCl</i>							
DQ-187	2.13	22.89		22.89			10.2
DQ-188	2.36	22.29		35.18			6.5

Note:

Stock solutions, such as NaCl_(aq), HCl_(aq), are prepared prior to loading. Unless otherwise mentioned, H₂O has not added in each capsule.

The ratio of Cu⁺/Cl⁻ denotes a mole ratio between the initial Cu(I) minerals (CuCl, Cu₂O) and chloride content.

Chapter I

Table A2 EMP analyses of quartz and silicate melt inclusions in run DQ21 (% *m/m*)

Sample	Na ₂ O	SiO ₂	Cl	Cu ₂ O	Total
Qz	0	101.01	0	0.11	101.16
Qz	-0.04	104.28	0	-0.39	104.29
Cu ₂ O	4.77	24.04	0.17	65.28	94.67
Cu ₂ O	0.72	12.75	0.01	88.76	102.6
SMI-1	1.98	78.48	0.32	8.94	90.51
SMI-2	4.54	61.74	0.31	2.79	71.1
SMI-2*	1.95	68.86	0.32	0.06	74.04
SMI-2*	5.09	75.4	0.92	0.25	84.15
SMI-2*	2.04	70.59	0.23	0.95	76.67
SMI-3	3.9	81.11	0.04	-0.45	88.4
SMI-3*	-0.02	81.79	0.01	0.13	82.09
SMI-4	2.07	65.4	0.35	-0.16	71.47
SMI-5	4.12	63.95	0.05	-0.03	75.5
SMI-5*	1.88	60.35	0.04	0	71.81
SMI-5*	4.19	70.16	0.02	0.34	79.08

Notes: Qz denotes quartz. Cu₂O is the crystal trapped in silicate melt inclusions (Fig.4). 2*, 3*, 5* mean the analyses were conducted in the same inclusion but different locations. DQ21: Cu +1.49 m NaCl_{aq} + SiO_{2 (gel)} + Qz, 800°C, 200 MPa, 5 days. Focused beam and 15 nA were used for cuprite determination; defocused beam with a size of 2 μm and 5 nA were used for Na-bearing silicate glass determination.

Chapter I

References

- Albrecht, M., Derrey, I.T., Horn, I., Schuth, S. and Weyer, S. (2014). Quantification of trace element contents in frozen fluid inclusions by UV-fs-LA-ICP-MS analysis. *Journal of Analytical Atomic Spectrometry*, 29(6): 1034-1041. DOI: 10.1039/c4ja00015c.
- Anderson, G. and Burnham, C. (1965). The solubility of quartz in super-critical water. *American Journal of Science*, 263(6): 494-511. DOI: 10.2475/ajs.263.6.494.
- Anderson, G. and Burnham, C. (1967). Reactions of quartz and corundum with aqueous chloride and hydroxide solutions at high temperatures and pressures. *Am. J. Sci. (United States)*, 265(1): 12-26. DOI: 10.2475/ajs.265.1.12.
- Archibald, S., Migdisov, A.A. and Williams-Jones, A. (2001). The stability of Au-chloride complexes in water vapor at elevated temperatures and pressures. *Geochimica et Cosmochimica Acta*, 65(23): 4413-4423. DOI: 10.1016/S0016-7037(01)00730-X.
- Archibald, S., Migdisov, A.A. and Williams-Jones, A. (2002). An experimental study of the stability of copper chloride complexes in water vapor at elevated temperatures and pressures. *Geochimica et Cosmochimica Acta*, 66(9): 1611-1619. DOI: 10.1016/S0016-7037(01)00867-5.
- Audetat, A. and Gunther, D. (1999). Mobility and H₂O loss from fluid inclusions in natural quartz crystals. *Contributions to Mineralogy and Petrology*, 137(1-2): 1-14. DOI: 10.1007/s004100050578.
- Audetat, A., Pettko, T., Heinrich, C.A. and Bodnar, R.J. (2008). The Composition of Magmatic-Hydrothermal Fluids in Barren and Mineralized Intrusions. *Economic Geology*, 103(5): 877-908. DOI: 10.2113/gsecongeo.103.5.877.
- Audetat, A., Zhang, L. and Ni, H. (2018). Copper and Li diffusion in plagioclase, pyroxenes, olivine and apatite, and consequences for the composition of melt inclusions. *Geochimica et Cosmochimica Acta* DOI: 10.1016/j.gca.2018.09.016.
- Bai, T.B. and Koster van Groos, A.F. (1999). The distribution of Na, K, Rb, Sr, Al, Ge, Cu, W, Mo, La, and Ce between granitic melts and coexisting aqueous fluids. *Geochimica et Cosmochimica Acta*, 63(7): 1117-1131. DOI: [https://doi.org/10.1016/S0016-7037\(98\)00284-1](https://doi.org/10.1016/S0016-7037(98)00284-1).
- Bakker, R.J. (2003). Package FLUIDS 1. Computer programs for analysis of fluid inclusion data and for modelling bulk fluid properties. *Chemical Geology*, 194(1): 3-23. DOI: 10.1016/S0009-2541(02)00268-1.
- Berndt, J., Holtz, F. and Koepke, J. (2001). Experimental constraints on storage conditions in the chemically zoned phonolitic magma chamber of the Laacher See volcano. *Contributions to Mineralogy and Petrology*, 140(4): 469-486. DOI: 10.1007/Pl00007674.
- Berry, A.J., Hack, A.C., Mavrogenes, J.A., Newville, M. and Sutton, S.R. (2006). AXANES study of Cu speciation in high-temperature brines using synthetic fluid inclusions. *American Mineralogist*, 91(11-12): 1773-1782. DOI: 10.2138/am.2006.1940.
- Berry, A.J., Harris, A.C., Kamenetsky, V.S., Newville, M. and Sutton, S.R. (2009). The speciation of copper in natural fluid inclusions at temperatures up to 700 C. *Chemical Geology*, 259(1): 2-7. DOI: 10.1016/j.chemgeo.2008.10.018.
- Blundy, J., Mavrogenes, J., Tattitch, B., Sparks, S. and Gilmer, A. (2015). Generation of porphyry copper deposits by gas-brine reaction in volcanic arcs. *Nature Geoscience*, 8(3): ngeo2351.
- Bodnar, R., Lecumberi-Sanches, P., Moncada, D. and Steele-MacInnis, M. (2014). Fluid inclusions in hydrothermal ore deposits, *Treatise on Geochemistry* 2nd Edition, pp. 119-142.
- Bodnar, R. and Sterner, S. (1987). *Synthetic Fluid Inclusions*, in "Hydrothermal Experimental Techniques", Barnes, H.L., Ulmer, G.C., eds. Wiley and Sons, New York.
- Bornhorst, T.J. (1997). Tectonic context of native copper deposits of the North American Midcontinent Rift System. *Geological Society of America special papers*, 312: 127-136.
- Bornhorst, T.J. and Mathur, R. (2017). Copper Isotope Constraints on the Genesis of the Keweenaw Peninsula Native Copper District, Michigan, USA. *Minerals*, 7(10): 185. DOI: 10.3390/min7100185.
- Brantley, S.L. (1992). The effect of fluid chemistry on quartz microcrack lifetimes. *Earth and Planetary Science Letters*, 113(1-2): 145-156. DOI: 10.1016/0012-821x(92)90216-I.
- Brantley, S.L., Evans, B., Hickman, S.H. and Crerar, D.A. (1990). Healing of microcracks in quartz: Implications for fluid flow. *Geology*, 18(2): 136-139. DOI: 10.1130/0091-7613(1990)018<0136:Homiqi>2.3.Co;2.
- Brugger, J., Etschmann, B., Liu, W., Testemale, D., Hazemann, J.L., Emerich, H., van Beek, W. and Proux, O. (2007). An XAS study of the structure and thermodynamics of Cu (I) chloride complexes in brines up to high temperature (400 C, 600bar). *Geochimica et Cosmochimica Acta*, 71(20): 4920-4941. DOI: 10.1016/j.gca.2007.08.003.
- Brugger, J., McPhail, D., Black, J. and Spiccia, L. (2001). Complexation of metal ions in brines: application of electronic spectroscopy in the study of the Cu (II)-LiCl-H₂O system between 25 and 90 C. *Geochimica et Cosmochimica Acta*, 65(16): 2691-2708. DOI: 10.1016/S0016-7037(01)00614-7.
- Butler, B.S. and Burbank, W.S. (1929). *The copper deposits of Michigan*. US Government Printing Office.
- Colomban, P. and Schreiber, D.H. (2005). Raman signature modification induced by copper nanoparticles in silicate glass. *Journal of Raman Spectroscopy*, 36: 884-890. DOI: 10.1002/jrs.1379
- Crerar, D.A. and Barnes, H. (1976). Ore solution chemistry; V, Solubilities of chalcopyrite and chalcocite assemblages in hydrothermal solution at 200 degrees to 350 degrees C. *Economic Geology*, 71(4): 772-794. DOI: 10.2113/gsecongeo.71.4.772.

Chapter I

- Derrey, I.T. Albrecht, M., Duplii, E., Botcharnikov, R. E., Horn, I., Junge, M., Weyer, S. and Holtz, F. (2017). Experimental tests on achieving equilibrium in synthetic fluid inclusions: Results for scheelite, molybdenite, and gold solubility at 800 C and 200 MPa. *American Mineralogist*, 102(2): 275-283. DOI: 10.2138/am-2017-5869.
- Dolejš, D. and Manning, C. (2010). Thermodynamic model for mineral solubility in aqueous fluids: theory, calibration and application to model fluid-flow systems. *Geofluids*, 10(1-2): 20-40. DOI: 10.1111/j.1468-8123.2010.00282.x.
- Doppler, G., Bakker, R.J. and Baumgartner, M. (2013). Fluid inclusion modification by H₂O and D₂O diffusion: the influence of inclusion depth, size, and shape in re-equilibration experiments. *Contributions to Mineralogy and Petrology*, 165(6): 1259-1274. DOI: 10.1007/s00410-013-0857-6.
- Duc-Tin, Q., Audetat, A. and Keppler, H. (2007). Solubility of tin in (Cl, F)-bearing aqueous fluids at 700 degrees C, 140 MPa: A LA-ICP-MS study on synthetic fluid inclusions. *Geochimica Et Cosmochimica Acta*, 71(13): 3323-3335. DOI: 10.1016/j.gca.2007.04.022.
- Fulton, J.L., Hoffmann, M.M. and Darab, J.G. (2000). An X-ray absorption fine structure study of copper (I) chloride coordination structure in water up to 325 C. *Chemical Physics Letters*, 330(3): 300-308. DOI: 10.1016/S0009-2614(00)01110-6.
- Garven, G. (1985). The role of regional fluid flow in the genesis of the Pine Point deposit, western Canada sedimentary basin. *Economic Geology*, 80(2): 307-324.
- Girardet, C., Plata, J., Breton, J. and Hardisson, A. (1988). Electrodiffusion of alkali-metal ions and protons in quartz: A diffusion-compensation model. *Physical Review B*, 38(8): 5648. DOI: 10.1103/PhysRevB.38.5648.
- Götze, J. (2009). Chemistry, textures and physical properties of quartz—geological interpretation and technical application. *Mineralogical Magazine*, 73(4): 645-671. DOI: 10.1180/minmag.2009.073.4.645.
- Guillong, M. and Heinrich, C.A. (2007). Sensitivity enhancement in laser ablation ICP-MS using small amounts of hydrogen in the carrier gas. *Journal of Analytical Atomic Spectrometry*, 22(12): 1488-1494. DOI: 10.1039/b709489b.
- Guillong, M., Meier, D.L., Allan, M.M., Heinrich, C.A. and Yardley, B.W. (2008). Appendix A6: SILLS: A MATLAB-based program for the reduction of laser ablation ICP-MS data of homogeneous materials and inclusions. *Mineralogical Association of Canada Short Course Series*, 40: 328-333.
- Günther, D., Audétat, A., Frischknecht, R. and Heinrich, C.A. (1998). Quantitative analysis of major, minor and trace elements in fluid inclusions using laser ablation-inductively coupled plasmamass spectrometry. *Journal of Analytical Atomic Spectrometry*, 13(4): 263-270. DOI: 10.1039/A707372K.
- Hack, A.C. and Mavrogenes, J.A. (2006). A synthetic fluid inclusion study of copper solubility in hydrothermal brines from 525 to 725 C and 0.3 to 1.7 GPa. *Geochimica et cosmochimica acta*, 70(15): 3970-3985. DOI: 10.1016/j.gca.2006.04.035.
- Halasz, I., Agarwal, M., Li, R. and Miller, N. (2007). Vibrational spectra and dissociation of aqueous Na₂SiO₃ solutions. *Catalysis Letters*, 117(1-2): 34-42. DOI: 10.1007/s10562-007-9141-6.
- Handke, M. and Mozgawa, W. (1993). Vibrational spectroscopy of the amorphous silicates. *Vibrational Spectroscopy*, 5(1): 75-84. DOI: 10.1016/0924-2031(93)87057-Z.
- Hedenquist, J. and Richards, J. (1998). The influence of geochemical techniques on the development of genetic models for porphyry copper deposits. *Reviews in Economic Geology*, 10(10): 235-256. DOI: 10.5382/Rev.10.10.
- Hofmeister, A.M. and Rossman, G.R. (1985). Exsolution of metallic copper from Lake County labradorite. *Geology*, 13(9): 644-647. DOI: 10.1130/0091-7613(1985)13<644:Eomcfl>2.0.Co;2.
- Holzheid, A. and Lodders, K. (2001). Solubility of copper in silicate melts as function of oxygen and sulfur fugacities, temperature, and silicate composition. *Geochimica et cosmochimica acta*, 65(12): 1933-1951. DOI: 10.1016/S0016-7037(01)00545-2.
- Ikehata, K., Chida, K., Tsunogae, T. and Bornhorst, T.J. (2016). Hydrothermal Native copper in ocean island alkali basalt from the Mineoka Belt, Boso Peninsula, Central Japan. *Economic Geology*, 111(3): 783-794. DOI: 10.2113/econgeo.111.3.783.
- Ikehata, K. and Hirata, T. (2012). Copper isotope characteristics of copper-rich minerals from the Horoman peridotite complex, Hokkaido, northern Japan. *Economic Geology*, 107(7): 1489-1497. DOI: 10.2113/econgeo.107.7.1489.
- Jochum, K.P., Nohl, L., Herwig, K., Lammel, E., Toll, B. and Hofmann, A. W. (2005). GeoReM: a new geochemical database for reference materials and isotopic standards. *Geostandards and Geoanalytical Research*, 29(3): 333-338. DOI: 10.1111/j.1751-908X.2005.tb00904.x.
- Jolly, W.T. (1974). Behavior of Cu, Zn, and Ni during prehnite-pumpellyite rank metamorphism of the Keweenaw basalts, northern Michigan. *Economic geology*, 69(7): 1118-1125. DOI: 10.2113/gsecongeo.69.7.1118.
- Kats, A. (1961). Hydrogen in alpha-quartz, TU Delft, Delft University of Technology.
- Kronenberg, A.K. and Kirby, S.H. (1987). Ionic conductivity of quartz: DC time dependence and transition in charge carriers. *American Mineralogist*, 72(7-8): 739-747.
- Larson, P.B., Maher, K., Ramos, F. C., Chang, Z., Gaspar, M. and Meinert, L. D. (2003). Copper isotope ratios in magmatic and hydrothermal ore-forming environments. *Chemical Geology*, 201(3): 337-350. DOI: 10.1016/j.chemgeo.2003.08.006.
- Lee, C-T. A., Luffi, P., Chin E.J., Bouchet, R., Dasgupta, R., Morton, D.M., Roux, V.L., Yin, Q-Z. and Jin, D. (2012). Copper systematics in arc magmas and implications for crust-mantle differentiation. *Science*, 336(6077): 64-68.
- Lerchbaumer, L. and Audetat, A. (2012). High Cu concentrations in vapor-type fluid inclusions: An artifact? *Geochimica Et Cosmochimica Acta*, 88: 255-274. DOI: 10.1016/j.gca.2012.04.033.
- Li, Y. and Audétat, A. (2009). A method to synthesize large fluid inclusions in quartz at controlled times and under unfavorable growth conditions. *American Mineralogist*, 94(2-3): 367-371. DOI: 10.2138/am.2009.3054.

Chapter I

- Li, Y., Audétat, A., Lerchbaumer, L. and Xiong, X. (2009). Rapid Na, Cu exchange between synthetic fluid inclusions and external aqueous solutions: evidence from LA-ICP-MS analysis. *Geofluids*, 9(4): 321-329. DOI: 10.1111/j.1468-8123.2009.00255.x.
- Liu, W., Brugger, J., Etschmann, B., Testemale, D. and Hazemann, J.-L. (2008). The solubility of nantokite (CuCl (s)) and Cu speciation in low-density fluids near the critical isochore: An in-situ XAS study. *Geochimica et Cosmochimica Acta*, 72(16): 4094-4106. DOI: 10.1016/j.gca.2008.05.056.
- Liu, W., Brugger, J., McPhail, D. and Spiccia, L. (2002). A spectrophotometric study of aqueous copper (I)-chloride complexes in LiCl solutions between 100 C and 250 C. *Geochimica et Cosmochimica Acta*, 66(20): 3615-3633. DOI: 10.1016/S0016-7037(02)00942-0.
- Liu, W. and McPhail, D. (2005). Thermodynamic properties of copper chloride complexes and copper transport in magmatic-hydrothermal solutions. *Chemical Geology*, 221(1): 21-39. DOI: 10.1016/j.chemgeo.2005.04.00.
- Liu, W., McPhail, D. and Brugger, J. (2001). An experimental study of copper (I)-chloride and copper (I)-acetate complexing in hydrothermal solutions between 50 C and 250 C and vapor-saturated pressure. *Geochimica et Cosmochimica Acta*, 65(17): 2937-2948. DOI: 10.1016/S0016-7037(01)00631-7.
- Lowenstern, J.B. (1994). Chlorine, fluid immiscibility, and degassing in peralkaline magmas from Pantelleria, Italy. *American Mineralogist*, 79: 353-369.
- Matthews, W., Linnen, R.L. and Guo, Q. (2003). A filler-rod technique for controlling redox conditions in cold-seal pressure vessels. *American Mineralogist*, 88(4): 701-707. DOI: 10.2138/am-2003-0424.
- Mavrogenes, J. and Bodnar, R. (1994). Hydrogen movement into and out of fluid inclusions in quartz: experimental evidence and geologic implications. *Geochimica et Cosmochimica Acta*, 58(1): 141-148. DOI: 10.1016/0016-7037(94)90452-9.
- Mei, Y., Liu, W., Sherman, D.M. and Brugger, J. (2014). Metal complexation and ion hydration in low density hydrothermal fluids: ab initio molecular dynamics simulation of Cu (I) and Au (I) in chloride solutions (25–1000 C, 1–5000 bar). *Geochimica et Cosmochimica Acta*, 131: 196-212. DOI: 10.1016/j.gca.2014.01.033.
- Mernagh, T.P. and Mavrogenes, J. (2018). Significance of high temperature fluids and melts in the Grasberg porphyry copper-gold deposit. *Chemical Geology* DOI: <https://doi.org/10.1016/j.chemgeo.2018.09.040>.
- Moore, J.G. (2001). Density of basalt core from Hilo drill hole, Hawaii. *Journal of Volcanology and Geothermal Research*, 112(1-4): 221-230. DOI: 10.1016/S0377-0273(01)00242-6.
- Mountain, B. and Seward, T. (1999). The hydrosulphide/sulphide complexes of copper (I): Experimental determination of stoichiometry and stability at 22 C and reassessment of high temperature data. *Geochimica et Cosmochimica Acta*, 63(1): 11-29. DOI: 10.1016/S0016-7037(98)00288-9.
- Mountain, B. and Seward, T. (2003). Hydrosulfide/sulfide complexes of copper (I): experimental confirmation of the stoichiometry and stability of Cu (HS) 2- to elevated temperatures. *Geochimica et cosmochimica acta*, 67(16): 3005-3014. DOI: 10.1016/S0016-7037(03)00303-X.
- Nagle, F., Fink, L., Boström, K. and Stipp, J. (1973). Copper in pillow basalts from La Désirade, Lesser Antilles island arc. *Earth and Planetary Science Letters*, 19(2): 193-197. DOI: 10.1016/0012-821X(73)90114-3.
- Nash, J.T. (1976). Fluid-inclusion petrology--data from porphyry copper deposits and applications to exploration: a summary of new and published descriptions of fluid inclusions from 36 porphyry copper deposits and discussion of possible applications to exploration for copper deposits. US Govt. Print. Off.
- Neumann, J., Zhong, T. and Chang, Y. (1984). The Cu-O (Copper-Oxygen) system. *Journal of Phase Equilibria*, 5(2): 136-140. DOI: 10.1007/BF02868948.
- Pinto, V.M., Hartmann, L.A. and Wildner, W. (2011). Epigenetic hydrothermal origin of native copper and supergene enrichment in the Vista Alegre district, Paraná basaltic province, southernmost Brazil. *International Geology Review*, 53(10): 1163-1179. DOI: 10.1080/00206810903464547.
- Pitzer, K.S. and Sterner, S.M. (1994). Equations of state valid continuously from zero to extreme pressures for H₂O and CO₂. *The Journal of chemical physics*, 101(4): 3111-3116. DOI: 10.1063/1.467624.
- Pouchou, J.-L. and Pichoir, F. (1991). Quantitative analysis of homogeneous or stratified microvolumes applying the model "PAP", *Electron probe quantitation*. Springer, pp. 31-75.
- Reiter, F., Forcey, K. and Gervasini, G. (1993). A compilation of tritium-material interaction parameters in fusion reactor materials. Commission of the European Communities.
- Rempel, K.U., Liebscher, A., Meixner, A., Romer, R.L. and Heinrich, W. (2012). An experimental study of the elemental and isotopic fractionation of copper between aqueous vapour and liquid to 450° C and 400bar in the CuCl-NaCl-H₂O and CuCl-NaHS-NaCl-H₂O systems. *Geochimica et Cosmochimica Acta*, 94: 199-216. DOI: 10.1016/j.gca.2012.06.028.
- Ripley, E.M. and Brophy, J.G. (1995). Solubility of copper in a sulfur-free mafic melt. *Geochimica et cosmochimica acta*, 59(23): 5027-5030. DOI: 10.1016/0016-7037(95)00387-8.
- Roedder, E. (1984). *Fluid Inclusions*. Fluid Inclusions.
- Rottier, B., Rezeau, H., Casanova, V., Kouzmanov, K., Moritz, R., Schlöglöva, K., Wälle, M. and Fontboté, L. (2017). Trace element diffusion and incorporation in quartz during heating experiments. *Contributions to Mineralogy and Petrology*, 172(4): 23. DOI: 10.1007/s00410-017-1350-4.
- Schmidt, C., Watenphul, A., Jahn, S., Schäpan, I., Scholten, L., Newville, M., G. and Lanzirotti, A. (2018). Copper complexation and solubility in high-temperature hydrothermal fluids: A combined study by Raman, X-ray fluorescence, and X-ray absorption spectroscopies and ab initio molecular dynamics simulations. *Chemical Geology*, 494: 69-79. DOI: 10.1016/j.chemgeo.2018.07.018.

Chapter I

- Scofield, N. (1980). Mineral chemistry applied to interrelated albitization, pumpellyitization, and native copper redistribution in some Portage Lake Basalts, Michigan.
- Seward, T. and Barnes, H. (1997). Metal transport by hydrothermal ore fluids. *Geochemistry of hydrothermal ore deposits*: 435-486.
- Sherman, D.M. (2007). Complexation of Cu⁺ in hydrothermal NaCl brines: ab initio molecular dynamics and energetics. *Geochimica et Cosmochimica Acta*, 71(3): 714-722. DOI: 10.1016/j.gca.2006.09.015.
- Shmulovich, K., Graham, C. and Yardley, B. (2001). Quartz, albite and diopside solubilities in H₂O–NaCl and H₂O–CO₂ fluids at 0.5–0.9 GPa. *Contributions to Mineralogy and Petrology*, 141(1): 95-108. DOI: 10.1007/s00410000224.
- Shmulovich, K., Yardley, B. and Graham, C. (2006). Solubility of quartz in crustal fluids: experiments and general equations for salt solutions and H₂O–CO₂ mixtures at 400-800°C and 0.1-0.9 GPa. *Geofluids*, 6(2): 154-167. DOI: 10.1111/j.1468-8123.2006.00140.x.
- Simon, A.C., Frank, M.P., Pettke, T., Candela, P.A., Piccoli, P.M., Heinrich, C.A. and Glascock, M. (2007). An evaluation of synthetic fluid inclusions for the purpose of trapping equilibrated, coexisting, immiscible fluid phases at magmatic conditions. *American Mineralogist*, 92(1): 124-138. DOI: 10.2138/am.2007.2066.
- Sorby, H.C. (1858). On the Microscopical, Structure of Crystals, indicating the Origin of Minerals and Rocks. *Quarterly Journal of the Geological Society*, 14(1-2): 453-500. DOI: 10.1144/gsl.jgs.1858.014.01-02.44.
- Steele-MacInnis, M., Ridley, J., Lecumberri-Sanchez, P., Schlegel, T.U. and Heinrich, C.A. (2016). Application of low-temperature microthermometric data for interpreting multicomponent fluid inclusion compositions. *Earth-science reviews*, 159: 14-35. DOI: 10.1016/j.earscirev.2016.04.011.
- Stoiber, R.E. and Davidson, E.S. (1959). Amygdule mineral zoning in the Portage Lake lava series, Michigan copper district; Part II. *Economic Geology*, 54(8): 1444-1460. DOI: 10.2113/gsecongeo.54.7.1250.
- Student, J. and Bodnar, R. (1999). Synthetic fluid inclusions XIV: coexisting silicate melt and aqueous fluid inclusions in the haplogranite–H₂O–NaCl–KCl system. *Journal of Petrology*, 40(10): 1509-1525.
- Swamy, V., Saxena, S.K., Sundman, B. and Zhang, J. (1994). A thermodynamic assessment of silica phase diagram. *JOURNAL OF GEOPHYSICAL RESEARCH-ALL SERIES-*, 99: 11,787-11,787. DOI: 10.1029/93JB02968.
- Thomas, R. (1994). Fluid evolution in relation to the emplacement of the Variscan granites in the Erzgebirge region: a review of the melt and fluid inclusion evidence. *Metallogeny of collisional orogens*. Czech Geological Survey, Prague: 70-81.
- Thompson, R.A. and Helz, G.R. (1994). Copper speciation in sulfidic solutions at low sulfur activity: Further evidence for cluster complexes? *Geochimica et Cosmochimica Acta*, 58(14): 2971-2983. DOI: 10.1016/0016-7037(94)90172-4.
- Uematsu, M. and Frank, E. (1980). Static dielectric constant of water and steam. *Journal of Physical and Chemical Reference Data*, 9(4): 1291-1306. DOI: 10.1063/1.555632.
- Var'yash, L. (1992). Cu (I) complexing in NaCl solutions at 300 and 350 C. *Geochem. Int.*, 29(3): 84-92.
- Verhoogen, J. (1952). Ionic diffusion and electrical conductivity in quartz. *American Mineralogist*, 37(7-8): 637-655.
- Walther, J. and Orville, P. (1983). The extraction-quench technique for determination of the thermodynamic properties of solute complexes: application to quartz solubility in fluid mixtures. *American Mineralogist*, 68(7-8): 731-741.
- Wang, C.Y., Zhou, M.F., Qi, L., Hou, S., Gao, H., Zhang Z., Malpas J., 2006. The Zhaotong native copper deposit associated with the Permian Emeishan flood basalts, Yunnan, Southwest China. *International Geology Review*, 48(8): 742-753. DOI: 10.2747/0020-6814.48.8.742.
- Weege, R. and Pollack, J. (1971). Recent developments in the native-copper district of Michigan, *Society of Economic Geologists Guidebook for Field Conference, Michigan Copper District*, pp. 18-43.
- White, S. (1970). Ionic diffusion in quartz. *Nature*, 225(5230): 375-376. DOI: 10.1038/225375a0.
- Williams-Jones, A.E., Migdisov, A.A., Archibald, S.M. and Xiao, Z. (2002). Vapor-transport of ore metals. *Water–Rock Interaction, Ore Deposits, and Environmental Geochemistry: A Tribute to David A. Crerar*: 279-306.
- Withers, A. and Behrens, H. (1999). Temperature-induced changes in the NIR spectra of hydrous albitic and rhyolitic glasses between 300 and 100 K. *Physics and Chemistry of Minerals*, 27(2): 119-132. DOI: 10.1007/s002690050248.
- Woodruff, L., Daines, M., Cannon, W. and Nicholson, S. (1995). The thermal history of the Midcontinent rift in the Lake Superior region: implications for mineralization and partial melting. *Proceedings of the International Geological Correlation Program Field Conference and Symposium on the Petrology and Metallogeny of Volcanic and Intrusive Rocks of the Midcontinent Rift System, Duluth, MN, USA*, pp. 213-214.
- Xiao, Z., Gammons, C. and Williams-Jones, A. (1998). Experimental study of copper (I) chloride complexing in hydrothermal solutions at 40 to 300 C and saturated water vapor pressure. *Geochimica et cosmochimica acta*, 62(17): 2949-2964. DOI: 10.1016/S0016-7037(98)00228-2.
- Xie, Z. and Walther, J.V. (1993). Quartz solubilities in NaCl solutions with and without wollastonite at elevated temperatures and pressures. *Geochimica et Cosmochimica Acta*, 57(9): 1947-1955. DOI: 10.1016/0016-7037(93)90086-C.
- Xu, Z. and Zhang, Y. (2002). Quench rates in air, water, and liquid nitrogen, and inference of temperature in volcanic eruption columns. *Earth and Planetary Science Letters*, 200(3): 315-330. DOI: 10.1016/S0012-821x(02)00656-8.
- Zajacz, Z., Seo, J.H., Candela, P.A., Piccoli, P.M. and Tossell, J.A. (2011). The solubility of copper in high-temperature magmatic vapors: a quest for the significance of various chloride and sulfide complexes. *Geochimica et cosmochimica acta*, 75(10): 2811-2827. DOI: 10.1016/j.gca.2011.02.029.
- Zhang, D., Zhou, T., Yuan, F., Fiorentini, M.L., Said, N., Lu, Y. and Pirajno, F. (2013). Geochemical and isotopic constraints on the genesis of the Jueluotage native copper mineralized basalt, Eastern Tianshan, Northwest China. *Journal of Asian Earth Sciences*, 73: 317-333. DOI: 10.1016/j.jseas.2013.04.043.

Chapter I

- Zhang, L., Audétat, A. and Dolejš, D. (2012). Solubility of molybdenite (MoS₂) in aqueous fluids at 600–800° C, 200MPa: A synthetic fluid inclusion study. *Geochimica et cosmochimica acta*, 77: 175-185. DOI: 10.1016/j.gca.2011.11.015.
- Zhang, Y., Jenkins, J. and Xu, Z. (1997). Kinetics of the reaction $H_2O + O \leftrightarrow 2 OH$ in rhyolitic glasses upon cooling: Geospeedometry and comparison with glass transition. *Geochimica et Cosmochimica Acta*, 61(11): 2167-2173. DOI: 10.1016/S0016-7037(97)00054-9.
- Zhang, Y., Xu, Z. and Behrens, H. (2000). Hydrous species geospeedometer in rhyolite: improved calibration and application. *Geochimica et Cosmochimica Acta*, 64(19): 3347-3355. DOI: 10.1016/S0016-7037(00)00424-5.
- Zhang, Z., Mao, J., Wang, F. and Pirajno, F. (2006). Native gold and native copper grains enclosed by olivine phenocrysts in a picrite lava of the Emeishan large igneous province, SW China. *American Mineralogist*, 91(7): 1178-1183. DOI: 10.2138/am.2006.1888.
- Zhu, B., Hu, Y., Zhang, Z., Chang, X. (2003). Discovery of the copper deposits with features of the Keweenawan type in the border area of Yunnan and Guizhou provinces. *Science in China Series D: Earth Sciences*, 46(1): 60-72.

Chapter IIA

An experimental study of the elemental and Cu isotopic fractionation between cuprite and water/acetate hydrothermal fluids to 250°C and 30 MPa

Dongmei Qi^{a*}, Harald Behrens^a, Marina Lazarov^a, Roman Botcharnikov^b,

Chao Zhang^a, Christian Ostertag-Henning^c, Stefan Weyer^a

^aInstitute of Mineralogy, Leibniz Universität Hannover, Callinstrasse 3, Hannover, D-30167, Germany

^bInstitute of Geosciences, Johannes Gutenberg University Mainz, J.-J.-Becher-Weg 21, Mainz, D-55128, Germany

^cFederal Institute for Geosciences and Natural Resources (BGR), Hannover, Germany

(*d.qi@mineralogie.uni-hannover.de)

Abstract

Copper content and isotope fractionation has been determined experimentally between cuprite and H₂O±acetate hydrothermal fluids. The experiments were conducted in a Au reaction cell at temperature range of 100°C -250°C, pressure of 5 MPa - 30 MPa up to 72 hours in pure water and 0.2 mol/kg HAc/KAc solutions (equimolar), with all starting solutions acidity of 4.5. The hydrothermal equipment used in this study enables time series in situ fluid sampling. At 250°C, native copper has not been observed within 6 hours, but it has deposited at the surface of the Au substrates as well as the cuprite in acetate bearing system after 24 hours. For long run periods of 72 hours, tenorite (CuO) has been exclusively observed in acetate-bearing systems at 150°C and 250°C. While native Cu was produced in pure water after 72 hours. Four competing reactions control the variations of Cu concentration and isotopic composition, i.e., cuprite dissolution, Cu(I) disproportionation into Cu(II) and native Cu, oxidation of Cu(I)/Cu(0) to Cu(II) and decomposition of acetate into methane and carbon dioxide.

In the early stage of cuprite dissolution, Cu content of the liquid obviously increase with time, but solubility decreases with temperature. At 250°C, pressure has significant effect on cuprite solubility when it changes from 5 MPa to 10 MPa. At constant conditions (250°C, 20 MPa, 72 hours) the dissolved Cu in water is ca. 3 µg/g which is by an order of magnitude lower than in the acetate-bearing solution. Subsequently Cu(I) disproportionation and the acetate decarboxylation processes have led to a significant Cu content drop. Accordingly, Cu(I) disproportionation reaction has a weak influence on isotope fractionation, i.e., $\Delta^{65}\text{Cu}_{[\text{native Cu-Cu(I)}]}$ are $0.09 \pm 0.09\%$. However, even in a single run the isotope composition of native Cu which has deposited at different locations (i.e., on Au substrates and in cavities of cuprite pellet) can be different. This difference is caused by the reaction mechanism and its precursor mineral or source fluids. Further oxidation of Cu(I)/Cu(0) to CuO induces the most significant fractionation, i.e. $\Delta^{65}\text{Cu}_{[\text{CuO-Cu(I)}]}$ values of $0.35 \pm 0.05\%$. The precipitation of CuO from Cu²⁺ and Cu⁺-bearing fluids may lead to a fractionation up to 0.7%.

In comparison to other studies, our data imply that hundreds ppm Cu transported by acetate-bearing fluids and subsequent metal precipitation due to instability of the complexing ligand. This may explain the enrichment of copper in sediment-hosted Cu ore deposit.

1. Introduction

Aliphatic acids that originate from biodegradation and catalytic aquathermolysis reactions of kerogen are widespread in oil field waters (potential precursors for petroleum; Cordell, 1972) as well as in sedimentary basins (e.g., Fisher, 1987). More emphasis from field and laboratory studies has been put on the acetic acid/acetate than the other short-chain aliphatic acids, primarily because of its higher abundance (0.5 wt% in oil field waters; Willey et al., 1975; Carothers and Kharaka, 1978), relative chemical simplicity and stability at basinal waters (i.e., projected half-lives of over 5 billion years at 100°C; Palmer and Drummond, 1986; Bell et al., 1994). The fact that high concentrations of acetate exist in basin brines has led to speculation as to their roles in geologic processes, including (i) the mass transport of metals such as Cu (Liu et al., 2001), Fe (Kharaka et al., 1983; Drummond and Palmer, 1985; Bell et al., 1994), Zn (Hennet et al., 1988; Giordano and Drummond, 1991; Borg and Liu, 2010), Mg (Semmler et al., 1990; Fein, 1991), Pb (Hennet et al., 1988; Giordano, 1989; Yang et al., 1989), Al (Fein, 1991; Benezeth et al., 1994) and Cd (Bénézech and Palmer, 2000); (ii) the dissolution and/or precipitation of both carbonates and aluminosilicates (e.g., Surdam and Crossey, 1985; Kharaka et al., 1986; Lundegard and Land, 1986); and (iii) the migration of methane (Carothers and Kharaka, 1978; Kharaka et al., 1983; Drummond and Palmer, 1986). The importance of acetic acid in the above-mentioned processes depends in part on its reactivity under the pressure-temperature conditions prevalent in the basin environment.

Therefore, the stability of acetate ions in hydrothermal fluids is of great importance. Although decomposition of acetate was generally found to be the dominant reaction at temperature below 400°C (Kharaka et al., 1983; Palmer and Drummond, 1986), there are exceptions that other reactions could be favored over decarboxylation in appropriate geologic settings, e.g., acetic acid was converted to ketene at temperature as low as 268 to 330°C (Child and Hay, 1964). Moreover, Sverjensky et al. (2014) demonstrated that the fluids in subduction zones contain abundant ionic organic carbon species that are mainly acetate ions which can be rather stable at high temperature and high pressure (e.g., 600°C, ≥ 2900 MPa). Sverjensky et al. (2014) also proposed that diamond is likely to precipitate from fluids containing acetate. It is likely that acetic acid exists metastably with respect to its decomposition products. The question whether the decarboxylation reaction occurs can be readily answered by considering the temperature of the system in addition to the presence of mineral catalyzer.

Hydrothermal studies in stainless steel vessels (Kharaka et al., 1983), Ti vessels, Au cups or bags, silica tubes, and Pyrex tubes (Palmer and Drummond, 1986) have shown that aqueous solutions of acetic acid are relatively stable under thermal stress (half-lives of ca. 300- 1.2×10^5 hours at 350°C), however, if suitable catalytic surface is present decarboxylation can be completed within a considerably short period (e.g., less than 100 hours at 350°C with the presence of magnetite or hematite). Thus, the presence of the mineral surface acting as a true catalyst, remaining unchanged, or playing a role as reactant has yet to be fully understood.

It has been suggested that metal-acetate complexes may also contribute to the formation of sediment-hosted base metal deposits, such as Mississippi Valley-type Pb-Zn deposits (e.g., Barnes, 1979; Giordano and Barnes, 1981; Giordano, 1985). Furthermore, organic matters may act as reductant and facilitate the precipitation of copper

sulfides in sediment-hosted copper ores (Sun and Püttmann, 2000; Hitzman et al., 2010). Thus, Cu-acetate complexes may provide better knowledge to understand the transport process of Cu in low-temperature geological environments. A detailed study of cuprite in acetate-bearing solutions has been conducted by Liu et al. (2001), they concluded that Cu(I)Ac and CuAc_2^- are the stable Cu species in fluids and decarboxylation of acetate does not occur in most of their runs even at 250°C due to the unchanged fluid acidity. However, this evidence is not sufficient for understanding the decarboxylation rate at run condition if cuprite acts as a catalyzer. In the case of decarboxylation in Fe-bearing system, Kharaka et al. (1983) found that the decomposition of acetic acid does not change the fluid acidity. Indeed, the pH values of fluids remains constant (~ 3.1) throughout the total consumption of acetic acid over a period of ~ 4000 hours (Kharaka et al., 1983).

In this study, we conducted a series of experiment to investigate the cuprite dissolution in water and acetate/acetic acid-bearing fluids at temperatures 100°C - 250°C and pressures 5 MPa - 30 MPa. Based on the Cu concentration variation and isotopic signature we could understand reaction mechanism between cuprite and fluids. In addition, the experimental products and results can help to understand whether cuprite has catalytic effect on acetate decomposition.

2. Experimental and analytical procedures

2.1 Reagents and material

Solid starting material, sintered pellets of Cu_2O , was used. This has the advantage that relic starting material can be easily separated from quenched material and that the weight change of the pellet gives an estimate of copper solubility in the fluid. Copper (I) oxide (cuprite) powder (97% purity, purchased from Sigma-Aldrich) was used for pellet material. The round disks, ~ 1 g, 13 mm diameter and 2 mm thickness, were sintered at 930°C, $\log f\text{O}_2 = -2$ for 24 hours (cuprite pellets sintered at other conditions were compared and listed in Appendix A1). The X-ray-powder diffraction (XRD) and electron microprobe analyses show that the composition of the pellets (surface and cross-section) was pure Cu_2O . More details about chemical quantifications are given in Appendix.

Crystalline anhydrous potassium acetate was purchased from *Alfa Aesar*, with a purity of 99%. Analytical-grade acetic acid (glacial, 100%) was acquired from *Merck*. Stock solutions were prepared using fresh 18 m Ω , double-deionized water. The pH buffers (0.2 m HAc/KAc, hereafter Ac and *m* refer to acetate and mol/kg) were prepared with a concentration ratio of 1:1 to optimize the buffer capacity. In general, two types of experimental solutions, namely pH buffered solutions (pH=4.6) and non-pH buffered solutions, have been used throughout this study (details are listed in Table 1).

Acetic-acid-acetate buffers are widely used for pH control in laboratory experiments (e.g. Liu et al., 2001; Palmer, 2011). The application of this buffer is due to a well-defined ionization constants of acetic acid at elevated temperatures (Mesmer et al., 1989) and the relatively higher threshold temperature for decarboxylation of acetate ($\geq 300^\circ\text{C}$; Kharaka et al., 1983; Drummond and Palmer, 1986; Palmer and Drummond, 1986). Given the fact that decarboxylation rates of acetate (in the absence of catalytic active minerals) at 200°C and 300°C are $1.81 \times 10^{-8} \text{ s}^{-1}$

and $8.17 \times 10^{-8} \text{ s}^{-1}$, respectively (Kharaka et al., 1983), the final concentration of acetate in this study changes less than 2% (a duration of 72 hours).

2.2 Fluid sampling procedure

Investigation of cuprite and hydrothermal fluids interaction at temperature and pressure up to 250°C and 30 MPa was carried out in hydrothermal equipment allowing for in situ sampling fluid with time (Seyfried et al., 1979).

The stainless steel autoclave (250 ml, I.D.: 55 mm, O.D.: 95 mm, height of 100 mm) was purchased from Parr Instrument Company, installed with three thermocouples and pressure manometer. Fig.1 shows the setup of this hydrothermal vessel. The vessel worked in such a way that aqueous solutions could be ‘squeezed’ from the reaction cell by a force exerted on water surrounding the cell by a high pressure hydraulic pump. For this procedure, the reaction cell must be deformable without rupturing and therefore was constructed of gold. The Au reaction cell consisted of a lower cylindrical-shaped gold body and star-like-conic end (Fig.1), with a volume of ~60 ml (I.D. 37.5 mm, O.D. 38.3 mm and a height of 60 mm). The Au reaction cell was prepared in-house by a piece of Au foil, it was later reshaped and welded shut under Argon flow. The brink of the gold reaction cell was previously wrapped with Teflon bands (<270°C) prior to loading for better sealing. The titanium head fitted snugly into this Au reaction cell and served as a cap; the gold extended approximately to the flared portion of the head. A seal between the titanium head and the titanium collar was established by six thrust bolts threaded into a retainer plate. These bolts forced the titanium head against the collar, thereby making a pressure seal against the collar, which led to making a pressure seal against the gold. These bolts were tightened with torch wrench with a force 2 N·m. Titanium was used in the construction of the reaction cell top because it is highly inert to such natural fluids as sea water, brines, and many dilute acids, even at the elevated temperatures. Moreover, the titanium parts were passivated at 450°C for an hour in atmospheric furnace prior to usage. The whole assembly was held in a stainless pressure vessel and secured within a furnace. The steel autoclave was filled with water served as the pressure medium. A separated pressure line leading to the steel bomb allowed water to be pumped. Three Type-J (iron-constantan) thermocouples with different lengths in direct contact with water in the autoclave adjacent the reaction cell provided a primary input for temperature control. The whole assemblage was sealed in such way as to prevent interchange of the material between the sample cell and the steel autoclave. The steel pressure vessel was covered by a ceramic furnace and isolation coat outside.

After loading cuprite pellets, a small piece of Au foil and ~30 ml aqueous solution in Au reaction cell, the preparation of the experimental vessel follows the above-mentioned procedure. The pressure was regulated by an additional pressure pump which enabled to build up or release pressure automatically. Temperature was set by an electronic controller connected to three thermocouples inside the Parr autoclave. Pressure was increased before increasing temperature with the purpose to check the possible leakage. Upon reaching experimental pressure and temperature, fluids were transported through a titanium capillary tubing (I.D.: 1.60 mm, O.D.:6.35mm, length: 25mm) to the titanium sampling container by opening a three-way titanium valve.

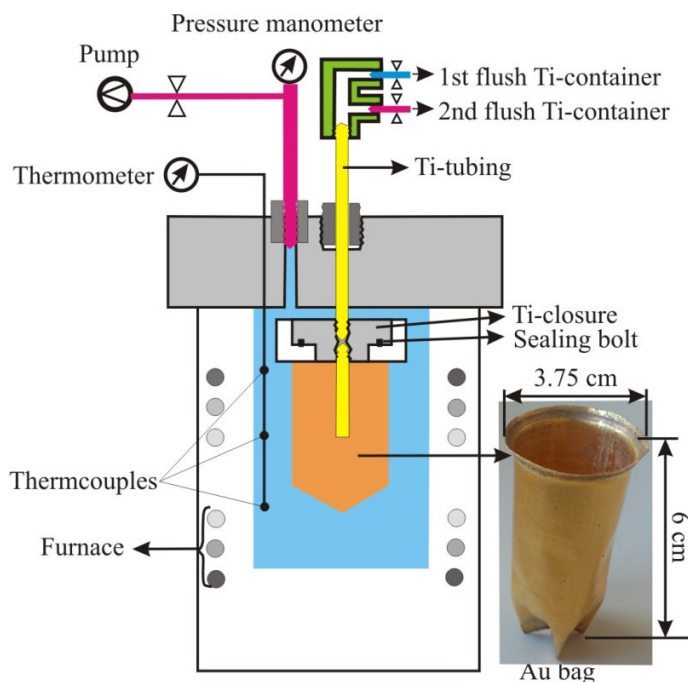


Figure 1 Schematic drawing of the fluid reactor

In-situ sampling was carried out by two steps: (i) opening of the 1st sampling valve (Fig.1) to flush the pathways and collected the flush liquid in a 1st titanium container, and quickly closing this valve; (ii) opening of the 2nd valve (Fig.1) to collect the experimental fluids in a 2nd container and closing the valve. Sometimes, another independent sampling was necessary for fluid acidity determination (Tables 2, 3). The small mass change in the total fluid mass (i.e., 1 g per sample and ~30 g of total solution loaded in the Au reaction cell) by sampling results in an instant pressure decrease of ~3 MPa in the autoclave. Then the pressure pump starts to adjust the pressure automatically within few seconds. Afterwards, the sampling containers were cooled with compressed air gun for 10-20 min. The obtained fluids (excluding the fluids for pH measurements) were transferred into Teflon vials and processed immediately with 1 mol/l HCl and deionized water to avoid possible precipitation. The solids, such as cuprite pellets and Au foil, were dried at room temperature and weighed again. The Au bag was digested with 6 mol/l HCl at 60°C for 24 h. Afterwards, the Au bag was taken out and rinsed with water. All fluids were evaporated to dryness on a 90°C hotplate. The dryness was dissolved in 3% HNO₃ and two batches from this solution were further diluted with 3% HNO₃ for further analyses (ICP-OES and MC-ICP-MS measurements).

After each run, the deformed Au reaction cell was annealed at 850°C for 15 min and reshaped by hand, this procedure was usually repeated several times until the shrunk Au bag was recovered back to its cylindrical shape. The inner surface of titanium containers were carefully checked for any corrosion under a microscope. When it was necessary, the containers were immersed in 10% HNO₃ for 4h at 180°C, and the above passivation procedure was repeated.

Table 1 listed the details of each experiment. Five series of experiments were performed to study the interaction of cuprite in hydrothermal fluids, i.e., run duration, temperature, pressure, water with/without pH buffer and temperature cycling. Run duration was set to 24 and 72 hours, temperatures were 100-250°C, pressures were 5-30 MPa and pH buffer (0.2 m HAc/KAc) was added in most runs, excluding run Cp41 in which only water was added. The cycling experiments were conducted at temperature between 150°C and 250°C with time interval of 24 hours at 20 MPa.

3. Analytical procedures

3.1 Solid sample analyses

Scanning electron microscopy (JOEL JSM-6390A SEM) coupled to an energy-dispersive X-ray analysis system (Bruker Quantax 200 EDXS) was employed to characterize the composition of the solid samples qualitatively. An acceleration voltage was set to 30.0 kV.

X-ray powder diffraction (XRD) was performed to identify the composition of cuprite pellets by using CuK α radiation between 5° and 85° in the step of 0.02° (Bruker D8). The WinXPow software (STOE) and the powder diffraction file were used for data evaluation.

The major element composition of the products was determined using a Cameca SX 100 electron probe microanalyzer (EPMA). Standards include native metals (Cu and Au), jadeite (Na), orthoclase (K), and synthetic NaCl (Cl) and Fe₂O₃ (Fe). A sample current of 15 nA and an acceleration voltage of 15 kV were used for all analyses. Raw data were corrected using the standard “PAP” procedure (Pouchou and Pichoir, 1991). Beam size of 1-2 μ m and sample current of 10-15 nA were applied to different minerals.

3.2 Copper isotope microanalysis

A femtosecond laser ablation system (Solstice, Spectra-Physics, USA) coupled to a Neptune Plus (Thermo Scientific, Germany) multi-collector-ICP-MS was used to measure the Cu isotope composition of samples and reference materials. In addition to the two isotopes, four Ni isotopes (⁶⁰Ni, ⁶¹Ni, ⁶²Ni and ⁶³Ni) were simultaneously measured. For the Ni source, we used 1 μ g/g Ni NIST SRM 986 standard solution, which was added via a quartz glass spray chamber (double pass Scott design) and a PFA micro-flow nebulizer (uptake rate ~100 μ L/min). The measured ⁶²Ni/⁶⁰Ni was used for the internal instrumental mass bias correction. For a detailed description, see Lazarov and Horn (2015). Samples have been measured against the NIST SRM 976 Cu-metal standard.

In addition, the cpy1 and cpy2 chalcopyrite from Lazarov and Horn (2015) were measured as the unknown standards to verify if the laser energy was set to the appropriate level and if the obtained $\delta^{65}\text{Cu}$ values agreed with the values for the solution reported by Lazarov and Horn (2015). Reference materials and samples (excluding Au foils) were ablated along lines. Au foils covered by thin Cu layers were analyzed by raster pattern. A spot diameter of 40 μ m and laser repetition rates of 5 Hz and 10 Hz for NIST SRM 976 and cpy2, respectively, resulted in signal

Chapter IIA

intensities of $\sim 15V$ on mass 65 (^{65}Cu). To maintain similar intensities as the standard, cuprite pellets, tenorite crystals and native Cu crystals on Au foil were generally analyzed with a repetition rate of 5-7 Hz, 2 Hz, 6-10 Hz and 2-12 Hz, respectively. For native copper precipitates, a raster ablation pattern was used due to relatively low Cu concentrations in samples as well as low Cu signal intensities, in addition, the repetition rates of standards (NIST SRM 976, cpy1 and cpy2) were adjusted accordingly. The overall double relative standard error (2RSE, 2σ) for samples is less than 0.1‰, which is calculated by the propagation of the within-run RSEs of a sample and its two bracketing standards.

3.3 Fluids treatment and analysis

The pH values of the solutions were measured with an *InLab[®] Flex-Micro* pH combination electrode (*Mettler Toledo GmbH, Germany*).

Inductively coupled plasma-optical emission spectrometer (ICP-OES) (*Varian 715-ES, Varian GmbH, Germany*) equipped with a patented VistaChip CCD simultaneous detector was used in the determination of elemental concentrations of sampled solutions. The samples were introduced with a concentric nebulizer and a cyclonic spray chamber. A total of 8 representative samples were analyzed for their elemental composition (Na, K, Ti, Fe, Ni, Cu, Rb and Cs). Sampled in situ fluids and quench fluids were mainly prepared with 3% HNO_3 .

In situ and quenched fluids were diluted to $\sim 0.5 \mu\text{g/g}$ Cu in 3% HNO_3 and doped with $1 \mu\text{g/g}$ Ni NIST SRM 986 standard solution. The simultaneously measured $^{62}\text{Ni}/^{60}\text{Ni}$ ratio of the Ni NIST SRM 986 standard solution was used for calculation of the instrumental mass bias correction. The Cu NIST SRM 976 standard solution was used for the standard-sample-standard bracketing, usually with 2-3 samples run between two standards. Measurements were run with the same cup configuration and method file as for the the LA-MC-ICP-MS measurements, using an increased measurement time of 250 s. The internal uncertainty for each single measurement was better than 0.01 ‰ (2RSE), while the daily reproducibility of the standard and samples was better than 0.06‰ (2SD). Repeatedly-processed an in-house Cu standard solution (cuprite, $\delta^{65}\text{Cu}=0.42$) was 0.02‰ heavier than the initial solution, and thus showed no significant isotopic fractionation during the chemical process.

Table 1 Experimental detail of Cu_2O - H_2O -acetate systems and the formation of new phases

SNO	system	Time hours	Temperature °C	Pressure MPa	New phases	Native Cu on Au on substrate cuprite
Cp27	$\text{Cu}_2\text{O} + \text{H}_2\text{O} + \text{pH buffer}$	24	100	20	N	N
Cp22	$\text{Cu}_2\text{O} + \text{H}_2\text{O} + \text{pH buffer}$	72	150	20	Tenorite, $\text{Au}_{92}\text{Cu}_8$	N
Cp26	$\text{Cu}_2\text{O} + \text{H}_2\text{O} + \text{pH buffer}$	24	200	20	N	N
Cp43	$\text{Cu}_2\text{O} + \text{H}_2\text{O} + \text{pH buffer}$	6	250	20	N	N
Cp29	$\text{Cu}_2\text{O} + \text{H}_2\text{O} + \text{pH buffer}$	24	250	5	Native Cu	Y
Cp30	$\text{Cu}_2\text{O} + \text{H}_2\text{O} + \text{pH buffer}$	24	250	10	Native Cu	Y
Cp31	$\text{Cu}_2\text{O} + \text{H}_2\text{O} + \text{pH buffer}$	24	250	30	Native Cu	Y
Cp24	$\text{Cu}_2\text{O} + \text{H}_2\text{O} + \text{pH buffer}$	72	250	20	Tenorite, $\text{Au}_{92}\text{Cu}_8$	N
Cp41	$\text{Cu}_2\text{O} + \text{H}_2\text{O}$	72	250	20	Native Cu	Y Tiny
Cp40	$\text{Cu}_2\text{O} + \text{H}_2\text{O} + \text{pH buffer}$	72	150-250-150	200	Native Cu	Y

Notes:

N and Y mean the presence of certain mineral phases.

4. Results

4.1 Formation of new minerals

The presence of newly formed minerals tenorite (CuO), $\text{Au}_{92}\text{Cu}_8$ and native Cu is listed in Table 1. The formation of native copper is exclusively found at 250°C runs with acetate (run periods of 24 hours) and without the presence of acetate (run periods of 24 hours). The formation of tenorite and $\text{Au}_{92}\text{Cu}_8$ are only found in acetate bearing system for long periods (72 hours) at 150°C and 250°C . The presence of Cu minerals with respect to time is shown in Fig. 2.

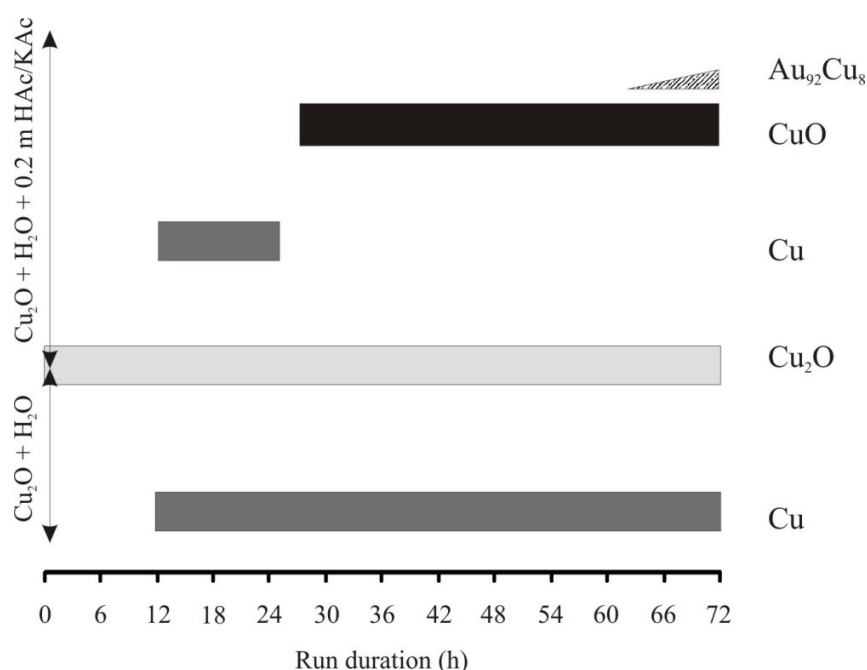
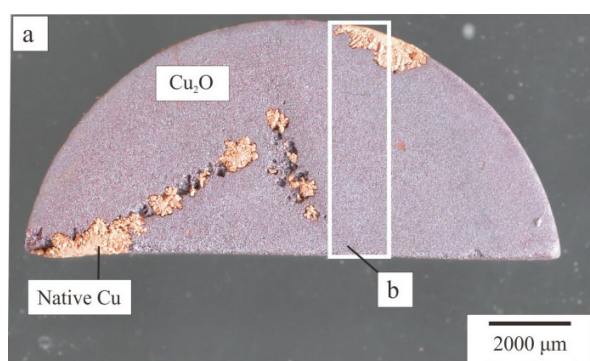


Figure 2 The presence of different Cu bearing minerals as a function of time at 250°C . Note that tenorite was also formed at 150°C . Cu -native copper; Cu_2O -cuprite; CuO -tenorite.

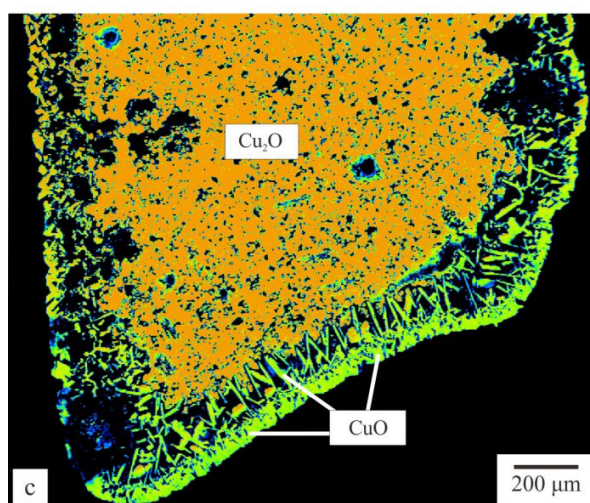
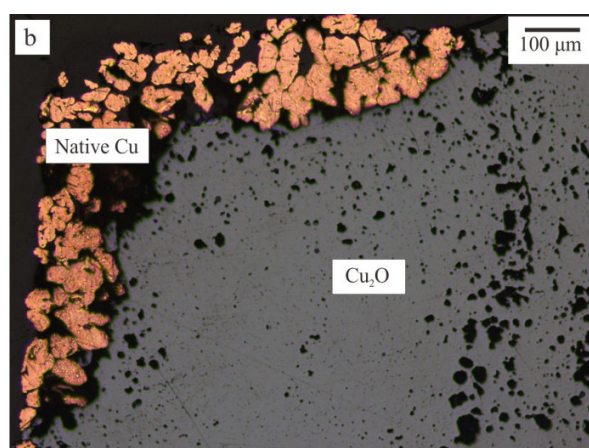
We conducted a series of time dependent experiments (e.g., run durations of 6-72 hours) at 250°C and 20 MPa with/without the addition of acetate to understand the appearance of mineral phases at different stages. With the time elapses, we found out in acetate-bearing systems: (i) there was almost no native Cu precipitation on Au substrate within 6 hours, which is verified by the ICP-OES analysis of dissolved Cu from Au reaction cell as well as by in situ LA-MC-ICP-MS analysis of Au foil of this run. (ii) Ample amount of native Cu deposits have been observed after 24 hours runs, which also enables the quantitative in situ LA-ICP-MS analysis. The precipitation of native Cu occurs in two localities: i.e. fully covering Au foil and Au reaction cell, and filling the cracks and cavities of cuprite pellets (Fig.3a, b). It is worth noting that the Au reaction cell covered by Cu precipitates starts from the maximum filling of solution rather than a local area where cuprite may locate. The mass gain of small Au foils indicates that the

Chapter IIA

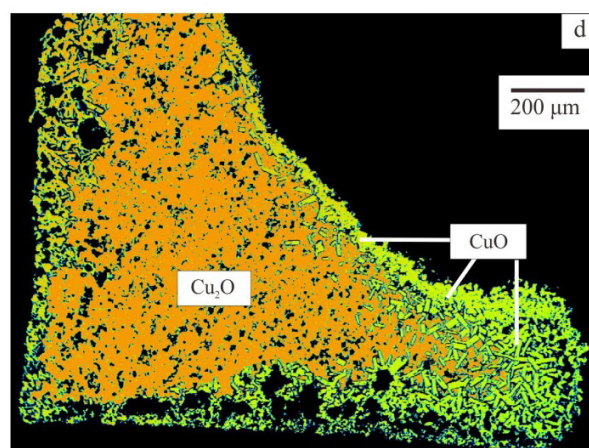
maximum thickness of the thin Cu layer is less than 2 μm . (iii) After 72 hours, a growth zone of tenorite crystals has been observed at the rims of initial cuprite (Fig. 3c, d, e). It is noteworthy that little micron-sized $\text{Au}_{92}\text{Cu}_8$ nuggets have been enclaved at the rim of tenorite (Fig. 3e, f; the composition of the nuggets were determined by EMP analysis). In addition, Au foils are covered by a black tenorite layer (determined by Raman spectra). A comb-like growth pattern of tenorite is shown in Fig. 3c, d and f. Outer rims of cuprite are covered by massive precipitation of aggregated tenorite, which kept the original shape of the cuprite (Fig. 3c, d). Between the outer rims and the interior cuprite, there are columnar minerals growing from the non-crystalline outer rim to interior cuprite. The appearance of columnar mineral is probably because acetic solution is corrosive and dissolves cuprite strongly, which supports more tenorite crystals to growth within the free vacancy. There are pores left in the growing zone of tenorite due to the density difference between these two minerals. Another comparable experiment was performed with pure water at similar conditions (250°C, 20 MPa, 72 hours). Interestingly, only little amount of native copper has been formed in pure H_2O system. Native Cu is only deposited on one side of the Au foil, in addition, tiny native Cu deposits are found at the rim of cuprite. Thus, the presence of tenorite is directly linked to the addition of acetate to the system.



Cp30 $\text{Cu}_2\text{O} + \text{H}_2\text{O} + 0.2 \text{ m HAc/KAc}$, 250°C, 10 MPa, 24 h



Cp24 $\text{Cu}_2\text{O} + \text{H}_2\text{O} + 0.2 \text{ m HAc/KAc}$, 250°C, 20 MPa, 72 h



Cp22 $\text{Cu}_2\text{O} + \text{H}_2\text{O} + 0.2 \text{ m HAc/KAc}$, 150°C, 20 MPa, 72 h

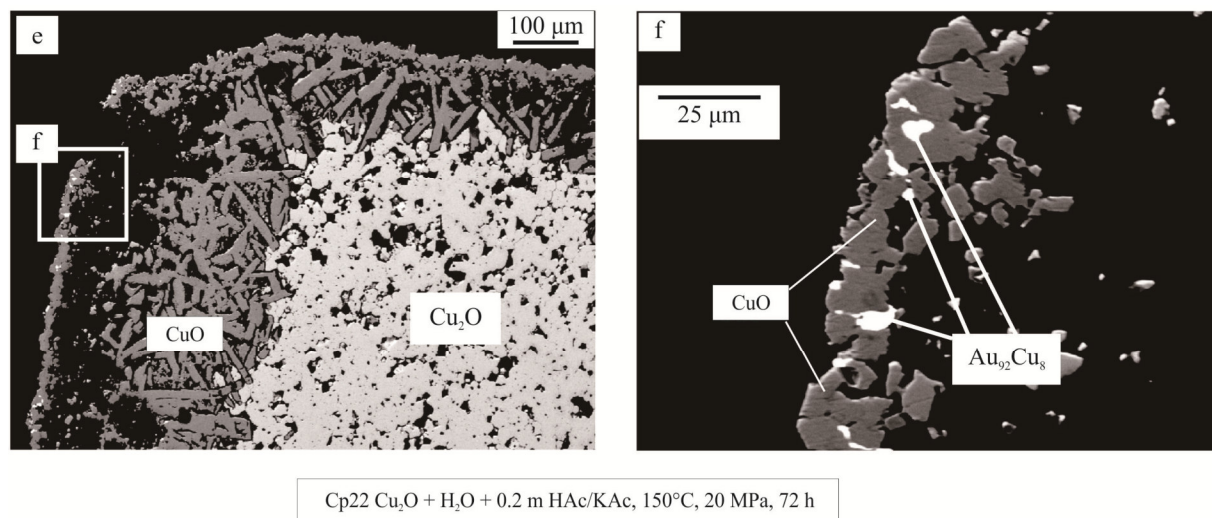


Figure 3 Images of cuprite pellets after reaction with 0.2 m HAc/KAc at 20 MPa. (a) A microscopic image of the surface of the retrieved cuprite pellet in 250°C run after 24 h. Native copper has been observed in vugs of cuprite pellet. (b) Back scattered image of the cross-section of the same cuprite pellet in white square of (a). Native copper has a well crystalline structure. Grain size of native Cu ranges from 20 μm to 100 μm . (c) Cuprite is retrieved in 250°C run after 72 h. Surfaces of the cuprite are fully covered by tenorite which appears as comb-like structure (for more details see text). The thickness of the outer rim is ~ 200 μm . The length of the columnar tenorite is ~ 100 μm . (d) A detached piece from the retrieved cuprite of Fig.3e is collected in a 150°C run after 72 h. (e) An overall cuprite is collected close to the Au reaction cell. Outer rims of the cuprite are covered by tenorite. The length of the columnar tenorite is smaller than that of Cp24 (Fig. 3c), i.e., < 100 μm . f - The coexistence of tenorite and $\text{Au}_{92}\text{Cu}_8$ nuggets. The nuggets generally $< 15\mu\text{m}$ appear at the outer rim of tenorite in both 150°C and 250°C runs.

4.2 Raman spectra of tenorite

Fig. 4 shows the Raman spectra of tenorite standards as well as the newly formed tenorite in 150°C and 250°C runs. CuO-std-1 is a compressed pellet which is made up of CuO powder and CuO-std-2 is a sintered tenorite powder pellet at 760°C, 1 atm. and for 24 hours. The spectra of tenorite standards present typical peaks at 291, 338, 623 and a broad band at 1050 - 1200 cm^{-1} . These peaks can also be found in the wavelength of newly formed tenorite at 150°C and 250 runs (Fig.2). Another peak at 2627 cm^{-1} is likely to be assigned to carbon, implying a possible relic of graphite. However, discernible graphite has not been found after these experiments.

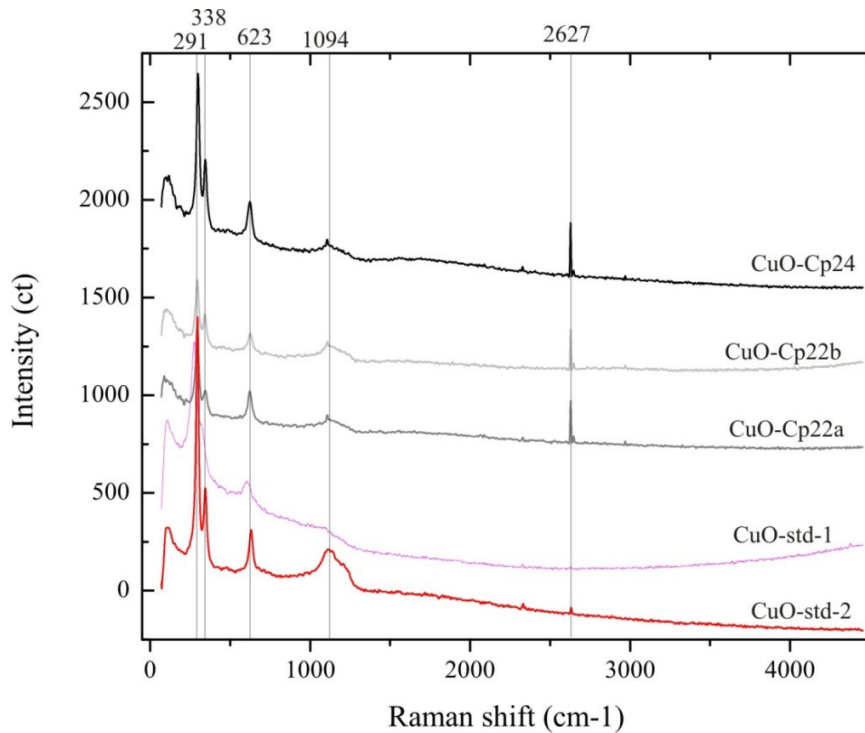


Figure 4 Raman spectra of cuprite and tenorite. CuO-std-1 and CuO-std-2 are tenorite standards: std-1 is pressed CuO powder pellet without further treatment, std-2 is sintered tenorite powder pellet at 760°C, 1 atm. for 24 hours. Typical tenorite bands are at 291, 338, 623 and 1094 cm⁻¹. A Raman shift at 2627 cm⁻¹ may be related to graphite.

4.3 Calculation of Cu isotope composition of initial cuprite pellets

The sintered cuprite pellets are found to be chemically homogeneous (details are given in Appendix A1), however, they are isotopically heterogeneous. The surface of cuprite pellet in contact with air is depleted in light Cu isotope due to preferentially evaporation of the light isotope during sintering at ~1000°C. To better constrain the isotope composition of the initial pellets, we separated these pellets into two groups: (1) freshly prepared cuprite pellets without further treatment were used in the runs of Cp21-Cp34. (2) Cuprite pellets were polished from both maximum exposed surface, i.e., a thickness of 200 μm has been removed from both sides. These treated pellets were firstly cut into two pieces, one was kept as reference starting pellet for later analysis and the other was added to the solution for reaction. The treated pellets were used for the experiments Cp35 - Cp44.

The average isotopic composition of the cuprite pellets were calculated based on the initial and residual pellet by the following steps:

(i) An example is selected from Group 2 cuprite pellet which defines clearly the isotope composition of the initial and relic cuprite (Fig. 5). It is evident that δ⁶⁵Cu values decrease with distance from rim to core (Fig.5, 6), and the correlation can be simplified as linear relation via

$$y = a + b \cdot \Delta x \quad (1)$$

Chapter IIA

where y and Δx mean the measured $\delta^{65}\text{Cu}$ values and distance from rim to core, respectively. a and b can be derived from the linear regression of the known $\delta^{65}\text{Cu}$ value and distance (examples are given in Fig.6).

(ii) The cuprite pellet has a dimension of 13 mm diameter and 2 mm thickness, hence the area of the top and bottom bases is ca. 3 times larger than the lateral area. Therefore, more materials will be dissolved from the surface than the lateral area. Here we consider the removed material from both top and bottom bases. In the case of Cp43, we can estimate the integrated area of the reacted cuprite using Eq. (1) and data in Fig.6 as follows:

$$\begin{aligned}
 f_1 &= \int_0^{26} (0.65 - 0.002x_1) dx & (2) \\
 &= [0.65x_1 - 0.001x_1^2]_0^{26} \\
 &= 0.65 \times (26 - 0) - 0.001 \times (26 - 0)^2 \\
 &= 18 \text{ } \text{‰} \cdot \mu\text{m}
 \end{aligned}$$

$$\begin{aligned}
 f_2 &= \int_0^{11} (0.32 - 0.002x_2) dx & (3) \\
 &= (0.32x_2 - 0.001x_2^2)_0^{11} \\
 &= 0.32 \times (11 - 0) - 0.001 \times (11 - 0)^2 \\
 &= 9 \text{ } \text{‰} \cdot \mu\text{m}
 \end{aligned}$$

where f_1 and f_2 describe the integrated area as a function of y (Eq.(1)) and distances, the unit of which is $\text{‰} \cdot \mu\text{m}$.

(iii) The initial (e.g., Cp43-1, Fig. 5) and residual (e.g., Cp43-2, Fig. 4) cuprite pellets and the Eqs. (2, 3) can help to define the average Cu isotope composition of the reacted cuprite which is responsible for the reaction and has been dissolved in fluids. Thus, the average integrated area or the isotope composition of the reacted cuprite is calculated by

$$\begin{aligned}
 \delta^{65}\text{Cu}(\text{‰}) &= \frac{f_1 + f_2}{\Delta x_1 + \Delta x_2} & (4) \\
 &= \frac{(18+9) \text{ } \text{‰} \cdot \mu\text{m}}{(26+11) \mu\text{m}} \\
 &= 0.57\text{‰}
 \end{aligned}$$

where Δx_1 and Δx_2 are 26 μm and 11 μm (in the case of Cp43, Figs.5, 6)

In the case of Group I cuprite pellets, we measured a cuprite pellet (without reaction) to derive linear correlation as Eqs. (1-3). The relic cuprite pellets after run Cp21-Cp34 are compared with this pellet which may not be identical to the initial cuprite of each run but can be representative to derive the value of the reacted cuprite (Eq.(5)). The estimated uncertainty of the Cu isotope composition from Eq.(4) is 0.2‰ (2 σ).

Chapter IIA

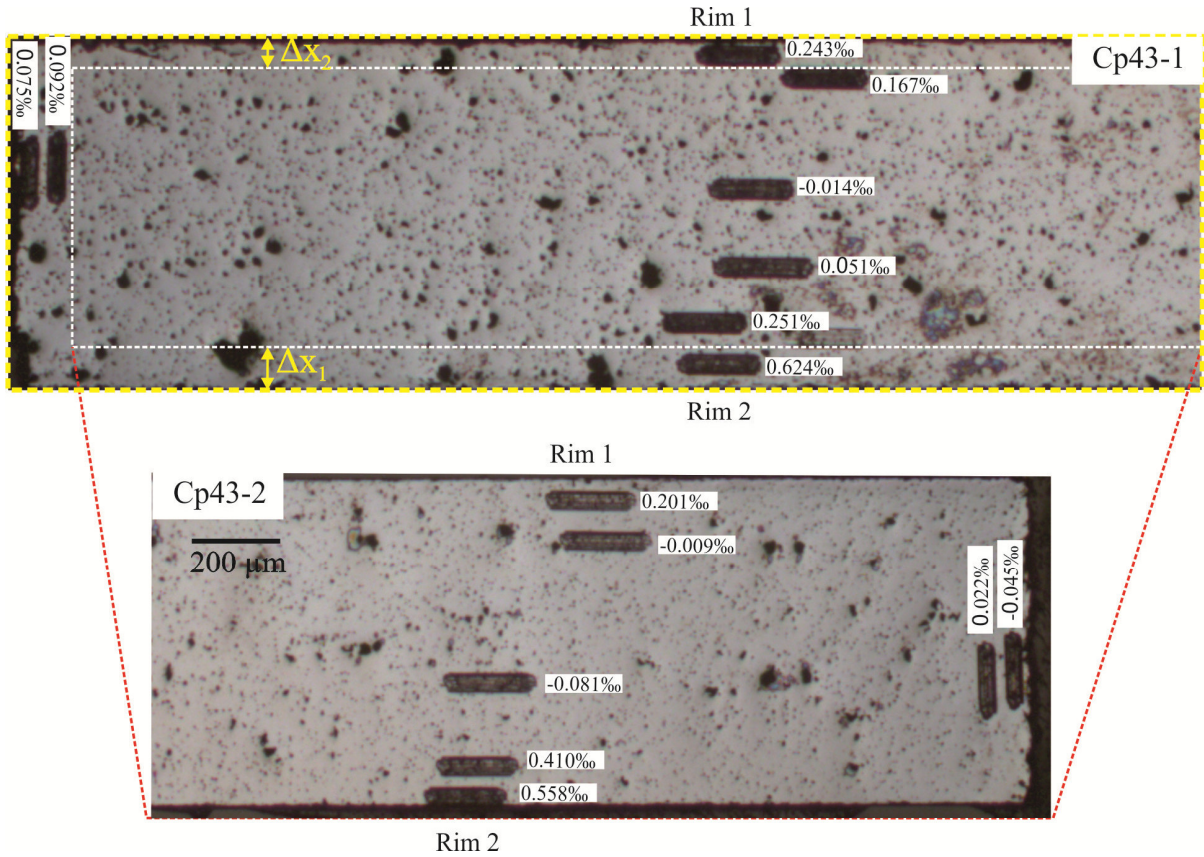


Figure 5 Cuprite pellet before (Cp43-1) and after (Cp43-2) reaction with acetic solution. The black thick lines are laser ablated lines and Cu isotope compositions are given next to the lines. The highlighted white box in Cp43-1 represents the remaining area after the reaction, which is also shown in the red area. The reacted area is calculated by Eq.(1-4), which yields a $\delta^{65}\text{Cu}$ value of $0.57 \pm 0.20\text{‰}$.

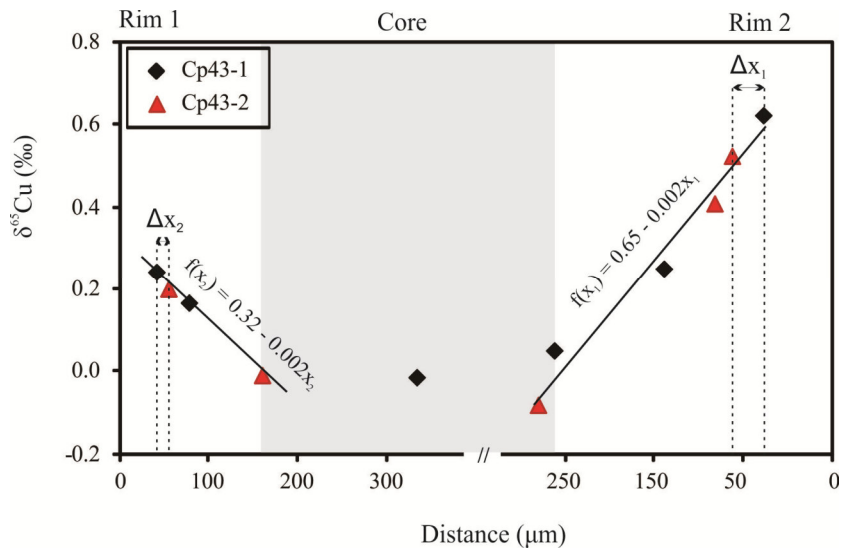


Figure 6 $\delta^{65}\text{Cu}$ values of cuprite as a function of distance. The cuprite pellets are prior to and after run Cp43 (Fig.5). The distance is expressed as the distance from one rim to another.

Chapter IIA

Table 2 Results of experiments in Cu₂O-H₂O-HAc/KAc systems at 20 MPa

SNO	t	pH ini.	pH 1 st fl	Elements concentration						Cu isotope composition($\delta^{65}\text{Cu}$)							
				Cu		Rb		solution MC-ICP-MS		in situ LA-ICP-MS		res.		Cu ₂ O*		Cu†	
				1 st fl μg/g	2 nd fl μg/g	res. μg/g	1 st fl μg/g	2 nd fl μg/g	ini. μg/g	1 st fl %	2 nd fl %	CuO %	Cu† %	CuO %	Cu† %	Cu ₂ O* %	Cu† %
Cu₂O+H₂O+pH buffer																	
Cp27	0	4.66±0.08	4.58±0.03	13	364	339	436										
	0.5			24		459											
	1			55		467											
	3			136		429											
	6			164		425											
	24			438		436											
Cp22	0	4.60±0.12	4.61±0.11	104	52	2860	314	503	464								
	0.5			88	114		490	466									
	1			157	203		459	450									
	3			299	238		543	340									
	7			356	340		455	433									
	24			359	339		464	464									
	48			320	300		464	464									
	72			263	221		464	464									
Cp26	0	4.66±0.08	4.50±0.08	1103	/		406	436									
	0.5			74			439										
	1			109			432										
	3			137			417										
	7			126			365										
	24			126													

Chapter IIA

Table 2 continued

SNO	t	Elements concentration						Cu isotope composition($\delta^{65}\text{Cu}$)										
		pH		Cu		Rb		in situ LA-ICP-MS		MC-ICP-MS		res.		CuO				
		imi	1 st fl	1 st fl	2 nd fl	res.	1 st fl	2 nd fl	1 st fl	2 nd fl	1 st fl	2 nd fl	res.	Cu ₂ O*	CuO	Cu [†]	Cu [‡]	
h	µg/g	µg/g	µg/g	µg/g	µg/g	µg/g	µg/g	%	%	%	%	%	%	%	%	%	%	
Cu ₂ O+H ₂ O+pH buffer																		
Cp24	0	4.60 ±0.12	4.67 ±0.10	277	103	1244	206	121	464	0.86±0.01	0.83±0.01	1.25 ±0.01	1.57 ±0.20	1.17 ±0.05	/	/	/	/
	0.5			98	163		124	456		0.76±0.01	0.76±0.01							
	1			93	97		449	446		0.81±0.01	0.84±0.01							
	3			77	73		418	414		1.09±0.01	1.04±0.01							
	7			66	72		404	403		1.12±0.01	1.21±0.01							
	24			60	69		464	464		1.07±0.01	1.21±0.01							
	48			65	64		464	464		0.83±0.01	1.17±0.01							
	72			43	69		464	464		0.88±0.01	1.02±0.01							
Cp43	1	4.66 ±0.08	4.50 ±0.08	56	81		497	436		-0.19±0.01	0.56 ±0.01	0.41 ±0.20	/	/	/	/	/	/
	6			82			416			0.15±0.01								
Cu ₂ O+H ₂ O																		
Cp41	1	4.53	6.28±0.12	3	3		556	516		-0.230±0.01	0.056	0.542	/	0.581	0.430			
	12	±0.04	6.57±0.04	3			569			0.415±0.01	±0.01	±0.20		±0.109	±0.03			
	72		7.49±0.13	1			459			0.249±0.01								

Notes

Abbreviations: 1st fl and 2nd fluid for the first and second sampled fluids (at once), *imi*, and *res.* for initial stock solution and residual fluid in Au reaction cell, respectively.

pH values of fluids are measured at room temperature for both stock solutions and sampled fluids during the run. As mentioned in text that 1st sampled fluids were usually used for pH determination. pH uncertainties are 95% confidences limits about the mean.

Elemental (Cu and Rb) concentrations are calibrated against dilution factor of Rb. The uncertainties are better than 10% (2SD), which is determined by ICP-OES. Cu₂O*, Cu[†] and Cu[‡] represent starting cuprite, native copper precipitated on Au foil and Au bag after a single run, respectively.

The isotope composition of Cu₂O* is based on Eqs.(1-4). Note that cuprite pellets of Cp22-Cp27 belong to Group I (no original cuprite pellets have been kept), Cp41 and Cp43 belong to Group II (cuprite pellets prior to and after experiments have been preserved).

in situ LA-MC-ICP-MS has been used to determine the isotope composition of Cu₂O* and Cu[†], *solution nebulized MC-ICP-MS* has been used to determine the isotope composition of fluids and Cu[‡].

The uncertainties of Cu isotope data acquired by solution MC-ICP-MS and *in situ* LA-ICP-MS are given by the two-sigma errors of the triplicated analyses.

4.4 Pressure medium dilution effect on elements concentration

~500 $\mu\text{g/g}$ Rb has been doped into the stock solutions (precise amount of Rb in solutions has been determined by ICP-OES; Table 2). However, Rb content decreases after certain time in some runs (Fig. 7a, b). It is clearly indicated from Fig.7a, b that Rb content decreases by ~30% (~100 $\mu\text{g/g}$) at 72 hours relative to initial Rb content. Concomitantly, Cu content shows a similar decreasing trend in Fig. 7a, i.e., reducing by 43% relative to its maximum value. As the run conditions have been controlled under liquid-saturated condition, therefore, there is no Rb partitioning between different phases (e.g., liquid and vapor). The possible explanation for these conjoint decreasing trends is an introduction of H_2O by pressure medium during extraction, which can be supported by the constant isotope data (Fig.7d). Thus, a correction for all data has been made based on the dilution factor of initial Rb and sampled Rb values, results are tabulated in Table 2. The original data which have been analyzed by ICP-OES are shown in Appendix A4-1.

The data of two fluids (both 1st flush pathway fluid and 2nd extracted fluid were sampled at the same time) show that the differences in elemental concentrations and isotopic compositions are within the range of uncertainty (Figs.7a-d). This also indicates that the formation of quench products has insignificant effect on elemental and isotopic variation during fluid extraction. Later on we extracted two samples per time but only quantitatively analyze the 2nd extracted fluid and used the 1st fluid sample for pH determination.

Chapter IIA

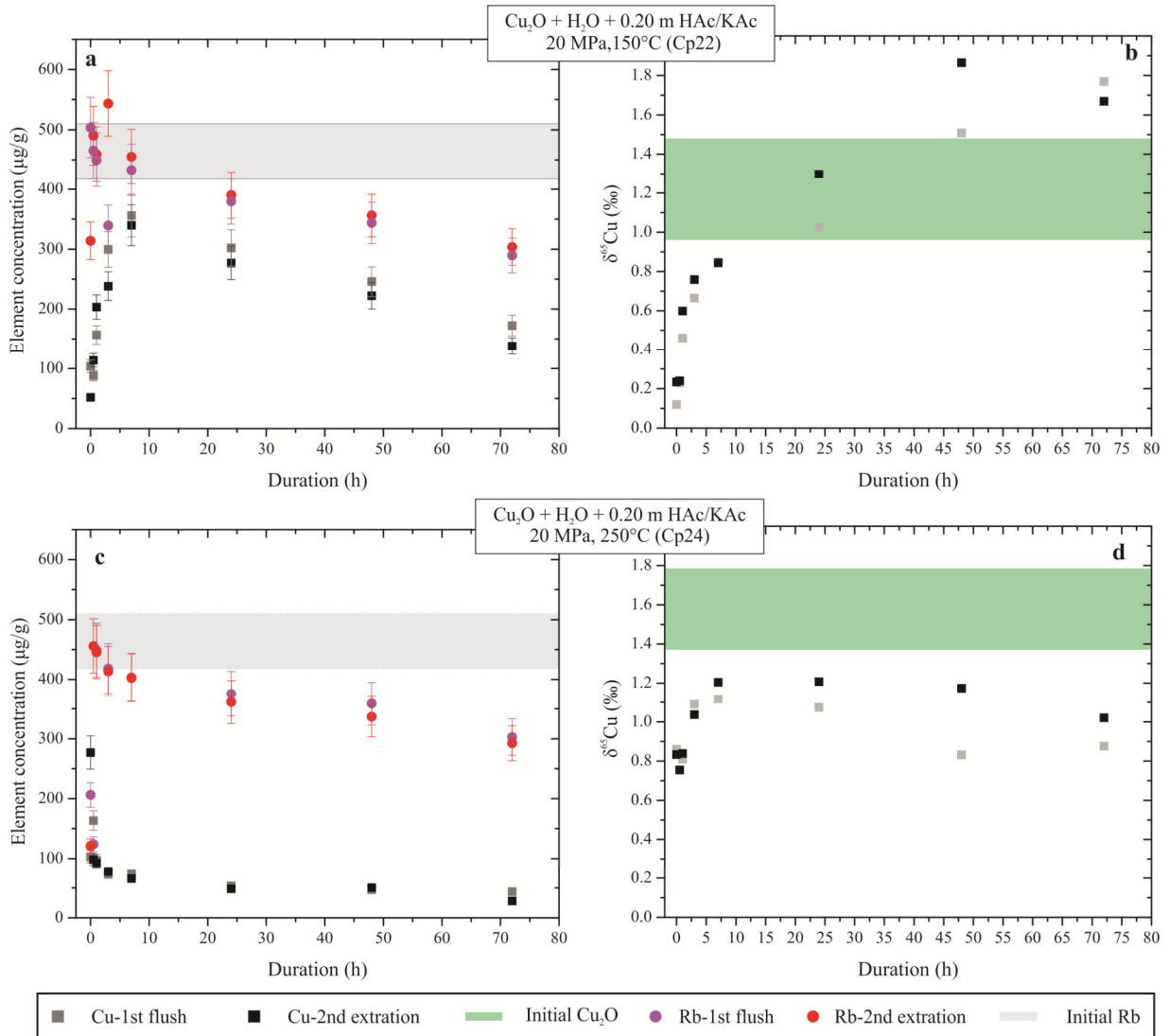


Figure 7 Elements concentration (a, c) and Cu isotope fractionation (b, d) as a function of run duration at 250°C and 20 MPa. (a, c) Rb and Cu contents without dilution factor correction (Original data are listed in Appendix Table A4-1).

4.5 Cu concentration and isotope signature of fluids in Cu_2O -HAc/KAc system at 20 MPa

Elements content and Cu isotopic composition of different phases are tabulated in Table 2. Fig.8 shows the Cu concentration and isotope fractionation as a function of run duration. Fig.8a shows the Cu concentration increases sharply with time, ranging from ~ 0 µg/g at 100°C onset of the reaction between cuprite and acetic solution to ~ 400 µg/g after 24 hours. $\delta^{65}\text{Cu}$ values of fluids continuously increase from -0.1% to $+1.2\%$ with time (Fig.7b), and no plateau has been observed. At 150°C, Cu concentration increases steeply by factors of 7, reaching 350 µg/g Cu after 6 hours (Fig.7a). $\delta^{65}\text{Cu}$ values of fluids continuously increase from $+0.1\%$ to $+1.8\%$ with time (Fig.7b), and no plateau has been observed. At 200°C, Cu concentration is almost doubled from 74 µg/g at 0.5 hour to 126 µg/g at 24 hour (Fig.8c). $\delta^{65}\text{Cu}$ values of fluids decrease from $+1.0\%$ to $\sim 0\%$ within 1 hours and increase to $+0.6\%$ after 6

Chapter IIA

hours, and a plateau has been observed in Fig.7b. The abnormal high Cu concentration (174 $\mu\text{g/g}$) and Cu isotope signature of the sampled fluid at 1 hour in Fig. 8c may be related to some remnants of Cu bearing phases from previous run which has deposited in the pathway. Strikingly, a rapid decreasing trend of Cu content is observed within 6 hours at 250°C (Fig. 8c), reducing from ~ 300 $\mu\text{g/g}$ to ~ 50 $\mu\text{g/g}$. The decreasing trend of Cu may be due to decarboxylation of acetate (explained in *Discussion*). $\delta^{65}\text{Cu}$ values of fluids sampled in 250°C runs increase from 0.8‰ to 1.2 ‰ within 6 hours and keep constant at +1.2 ‰ after 6 hours (Fig.7b).

Constant Cu contents can be reached within 24 hours (excluding 100°C run), which may indicate that the cuprite solubility has been reached at these run conditions. The Cu isotopic equilibrium between cuprite and dissolved Cu cannot be defined easily at temperatures of 150°C and 250°C (Fig. 7b, 7d), which is a result of oxidation, i.e., the formation of tenorite. Whereas Cu isotopic equilibrium can be reached within 24 hours for 100°C and 200°C runs in which there are no new phases formed.

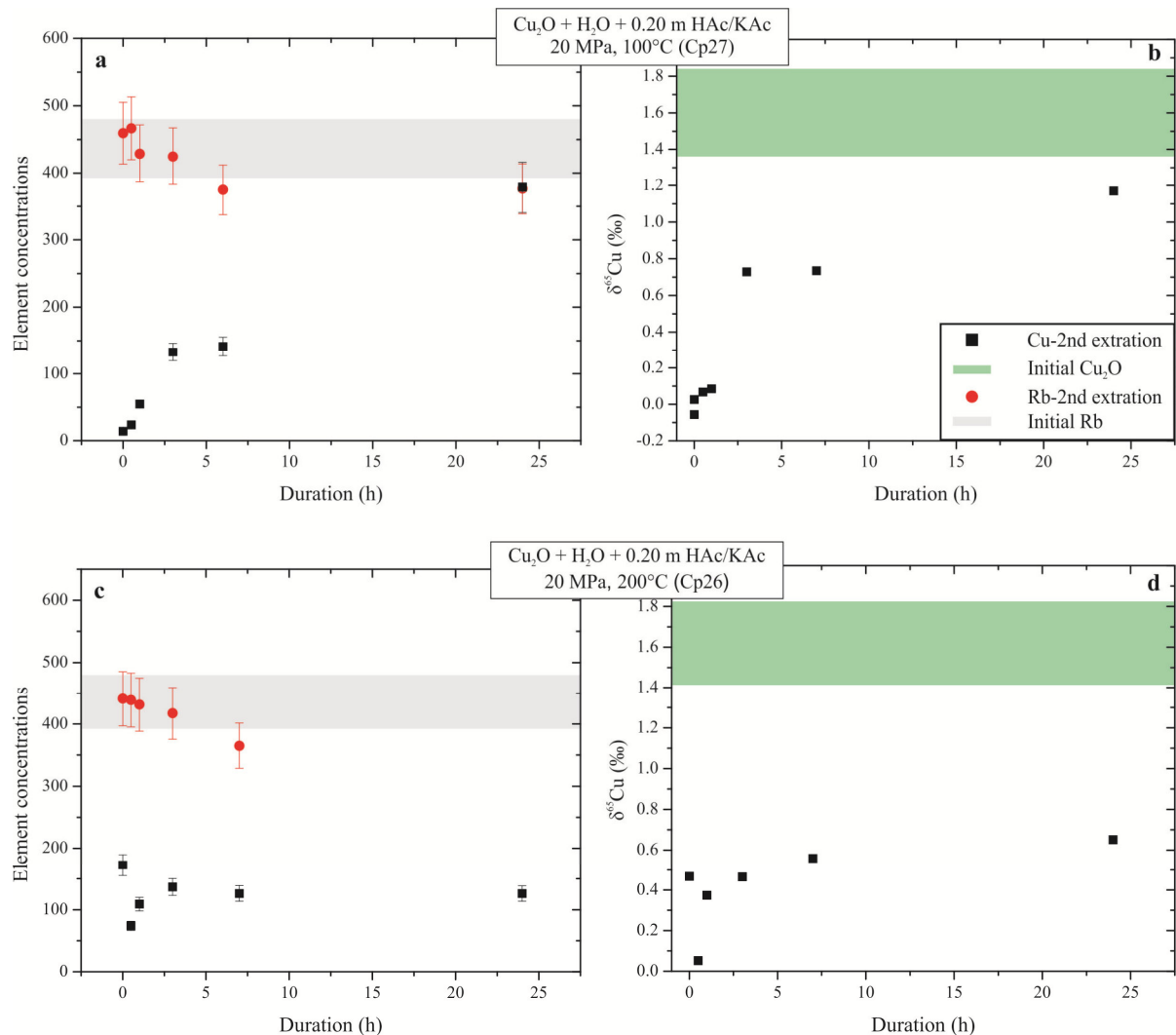


Figure 8 Elements concentration and Cu isotope fractionation as a function of run durations. All experiments were conducted in water under pH buffered condition at 20 MPa. (a, b) 100°C, 24 hours; (c, d) 200°C, 24 hours.

4.6 T, P, pH effects on cuprite dissolution

Fig.9 depicts the influences of temperature, pressure and fluid acidity on Cu contents in fluid. It is apparent that temperature has a negative effect on Cu_2O solubility (Fig.9a), decreasing from 380 $\mu\text{g/g}$ Cu at 100°C to 80 $\mu\text{g/g}$ Cu at 250°C. Our data are by up to 2 orders of magnitudes higher than the data of Liu et al. (2001) in which Cu contents are $\leq 45 \mu\text{g/g}$ in all temperature ranges (Fig.9a).

Fluids in both runs (with/without pH buffer) were sampled periodically. Cu content in pure water ranges from 1 to 3 $\mu\text{g/g}$ over 72 hours (Cp41; Table 3). On the contrary, dissolved Cu decreases from 350 to 50 $\mu\text{g/g}$ in acetate solution over 72 hours (Cp24; Table 2), which may be due to acetate decomposition. Although there is only one experiment which has been conducted without pH buffer, Cu concentration is strongly enhanced by at least 17 times, i.e., $\geq 50 \mu\text{g/g}$ in H_2O -pH buffer solution and $\leq 3 \mu\text{g/g}$ in pure water (Fig. 9b).

Pressure has an effect on cuprite solubility by increasing from 52 $\mu\text{g/g}$ at 5 MPa to 100 $\mu\text{g/g}$ at 10 MPa (Fig. 9c). Cu content remains $\sim 80 \mu\text{g/g}$ in the pressure range from 20 MPa to 30 MPa.

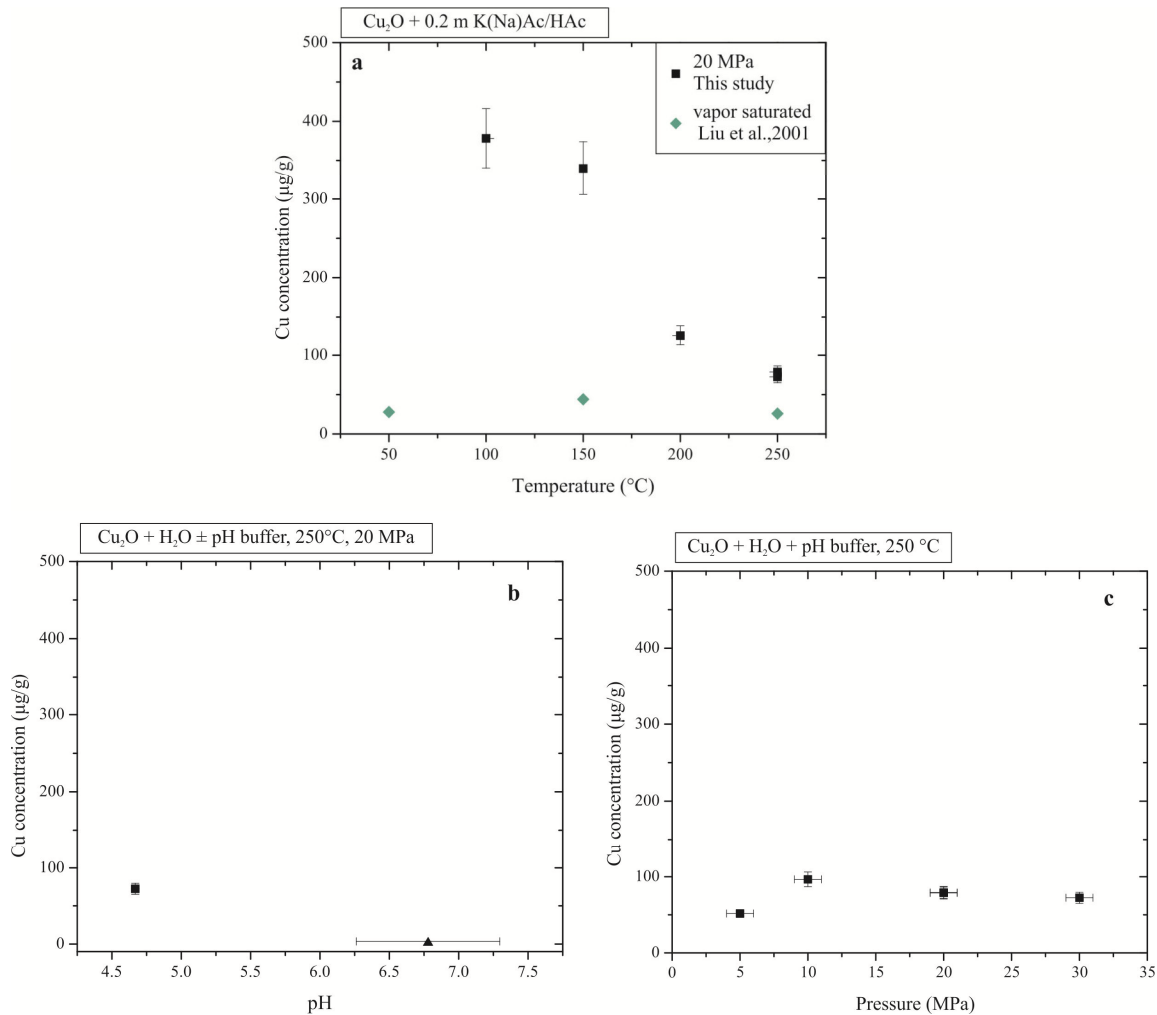


Figure 9 Cu content as functions of temperature (a), fluid acidity (b) and pressure (c) in $\text{H}_2\text{O} \pm$ acetate systems. pH buffer denotes 0.2 m HAc/KAc. Note that the pH values of sampled fluids in pure water system changes from 6.28 to 7.49 after 1 and 72 hours, respectively. The average pH value is shown in (b).

Chapter IIA

Table 3 Results of experiments in $\text{Cu}_2\text{O-H}_2\text{O-HAc/KAc}$ systems at 250°C

SNO	t	T	Elements concentration				Cu isotope composition						
			pH ini.	pH 1 st fl.	Cu	Rb	solution MC-ICP-MS		in situ LA-ICP-MS				
h	°C	ini.	res. µg/g	2 nd fl µg/g	2 nd fl µg/g	ini. µg/g	2 nd fl %	res. %	Cu ₂ O* %	Cu %	Cu [†] %	Cu [‡] %	
Cp29	1	250	4.66±0.08	4.30±0.05	118	32	447	436	0.73±0.02	1.57±0.02	1.51±0.20	1.04±0.14	0.97±0.03
	6				52		414		1.37±0.01		<i>0.49±0.03</i>		
	24				19		436		1.51±0.03		<i>0.75±0.02</i>		
Cp30	1	250	4.66±0.08	4.37±0.05	86	64	436	436	0.30±0.02	1.23±0.01	1.34±0.20	1.04±0.10	0.92±0.02
	6				97		426		0.80±0.01		<i>0.60±0.02</i>		
	24				53		436		0.92±0.02		<i>0.51±0.02</i>		
Cp31	1	250	4.66±0.08	4.29±0.10	80	29	426	436	0.52±0.01	1.56±0.03	1.33±0.20	1.00±0.13	0.95±0.03
	6				79		440		1.00±0.02		n.m.		
	24				53		402		1.24±0.02				
Cp40	1	150	4.66±0.08	4.78±0.06	51	67	456	436	0.07±0.01	0.18±0.02	0.36±0.20	0.14±0.08	0.52±0.03
	6	150			92		480		0.17±0.01		<i>0.14±0.02</i>		
	24	150			59		499		0.26±0.02				
	25	250			87		498		0.39±0.01				
	31	250			58		492		0.47±0.02				
	49	250			61		436		0.92±0.01				
	50	150			49		436		0.94±0.03				
	56	150			41		436		0.25±0.03				
	74	150			13		436		-0.07±0.01				

Notes

Cu^{\parallel} , Cu^{\dagger} and Cu^{\ddagger} represent native copper precipitated on cuprite, Au foil and Au bag after a single run, respectively. Cuprite pellets of Cp29-Cp31 belong to Group I (no original cuprite pellets have been kept), cuprite of Cp40 belongs to Group II (cuprite pellets prior to and after experiments have been preserved). The italic $\delta^{65}\text{Cu}$ values denote that the ablated lines in cuprite of the runs Cp29, Cp30 and Cp40 are adjacent to that of newly crystallized native Cu. Elemental (Cu and Rb) concentrations are calibrated against dilution factor of Rb. The uncertainties are better than 10% (2SD), which is determined by ICP-OES. The uncertainties of Cu isotope data acquired by solution MC-ICP-MS and in situ LA-ICP-MS are given by the two-sigma errors of the triplicated analyses.

4.7 Cu(I) disproportionation effect on Cu isotope fractionation

As it is stated previously, no native Cu has been formed within 6 hours, and the precipitates are exclusively observed during the period of 7-24 hours at 250°C (Fig.2). This phenomenon may be explained by Cu(I) disproportionation reaction (1):

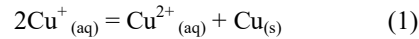


Fig.10a shows a slight decrease of Cu content in fluids with time. This can be explained by native Cu precipitates on cuprite, which hampers the further cuprite dissolution by forming a protection layer of Cu at the cuprite surface. The mass of native Cu precipitation can be estimated from the mass gain of Au foil and Au reaction cell, the later one is achieved by solution measurement, i.e., dissolving Au reaction cell in HCl solutions and analyzing Cu content by ICP-OES measurement. The estimation shows up to 120 µg Cu precipitates on Au substrates, which results in $\leq 8\%$ Cu(II)_{aq} and $\geq 92\%$ Cu(I)_{aq} in the aqueous fluids based on reaction (1). The isotopic compositions of fluids containing both Cu²⁺ and Cu⁺ species are generally similar to or slightly higher than those contain solely Cu⁺ species (Fig.10b).

Native copper precipitates yield similar isotope signature as their source. On the one hand, the δ⁶⁵Cu values of native Cu deposits on Au foil are similar to that of Cu⁺-bearing fluids, i.e., δ⁶⁵Cu values of 1.71‰ and 1.72‰ at 5 MPa and 1.04‰ and 1.16‰ at 10 MPa (Fig.10b; Cp29 and Cp30 in Table 3). On the other hand, the Cu isotope compositions of native Cu deposits on cuprite yield similar values to the adjacent relic cuprite, i.e., δ⁶⁵Cu values of 0.63‰ and 0.69‰ at 5 MPa and 0.60‰ and 0.54‰ at 10 MPa (Fig.10b; Cp29 and Cp30 in Table 3). Quite different δ⁶⁵Cu values of native Cu are observed at different localities, implying different formation mechanisms, i.e., reduction of aqueous Cu(I) species to native Cu in the fluid and reduction of cuprite to native Cu which is aided by H₂ production at the early stage of decarboxylation and local material transport.

Without the presence of pH buffer (at 20 MPa), isotope compositions among cuprite, equilibrated fluid, native Cu and associated fluid show very little variations, implying neutral fluid environment does not favor isotope fractionation.

To sum up, Cu(I) disproportionation induces less significant isotope fractionation, Δ⁶⁵Cu_{native Cu-Cu(I)} of 0.09±0.09‰.

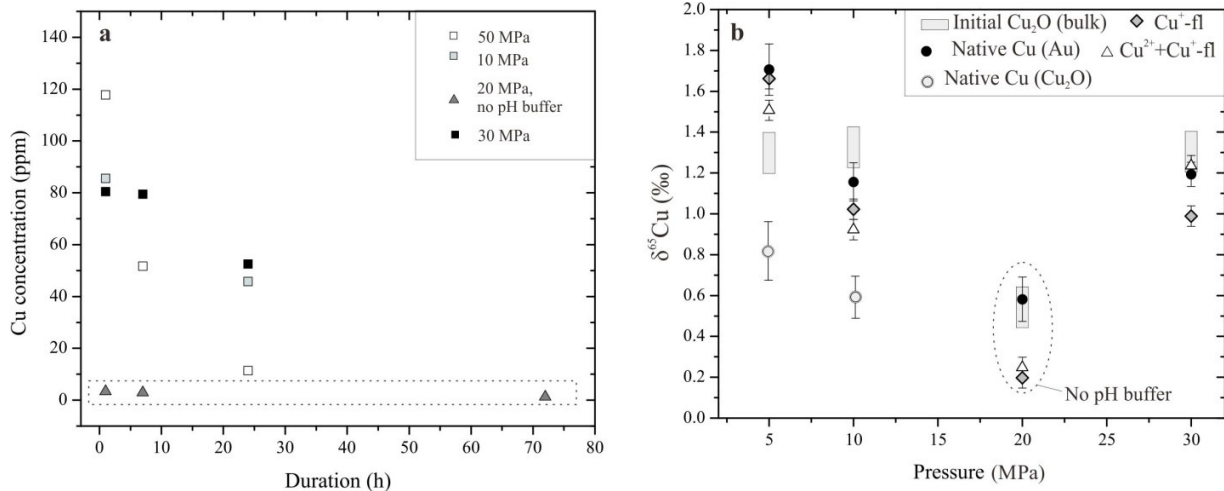


Figure 10 The variation of Cu concentration and isotope composition associated with native Cu precipitation. All experiments were conducted at 250°C with and without pH buffer (marked with dashed area). (a) Cu content variation as functions of run duration and pressure. (b) Cu isotope composition as function of pressure. Native Cu(Au) denotes native Cu precipitates on Au foil; Native Cu(Cu_2O) denotes native Cu precipitates on cuprite. Cu^+ -fl. means the fluid contains Cu^+ cations. $\text{Cu}^{2+} + \text{Cu}^+$ -fl represents the fluid contains both Cu^{2+} and Cu^+ , which were sampled at the final stage (either 24 hours or 72 hours).

Cu(I) disproportionation effect on Cu isotope fractionation has further been investigated by temperature oscillating experiment, i.e., T alternating between 150°C to 250°C. The result shows that Cu concentration increases from 50 $\mu\text{g/g}$ at 150°C to 90 $\mu\text{g/g}$ at 250°C, and decreases continuously to ~ 0 $\mu\text{g/g}$ when temperature sets back to 150°C (Fig. 11a). The isotopic compositions of dissolved Cu(I) in fluids at 150°C and 250°C remain constant at ~ 0 ‰. Cu(I) disproportionates into Cu(II) and native Cu is likely faster at 250°C, which may trigger the precipitation of native Cu on the surface of Au foil and cuprite. The isotope fractionation between Cu(I) species and native Cu can be induced by disproportionation reaction, i.e., $\Delta^{65}\text{Cu}_{\text{native Cu-Cu(I)}}$ and $\Delta^{65}\text{Cu}_{\text{native Cu-Cu}_2\text{O}}$ values are 0.04 ± 0.05 ‰ and 0.08 ± 0.05 ‰ (Fig.11b; Table 3). Due to the native Cu precipitation, Cu content and Cu isotope composition of fluids continuously decrease even at 150°C (Fig. 11a, b).

Chapter IIA

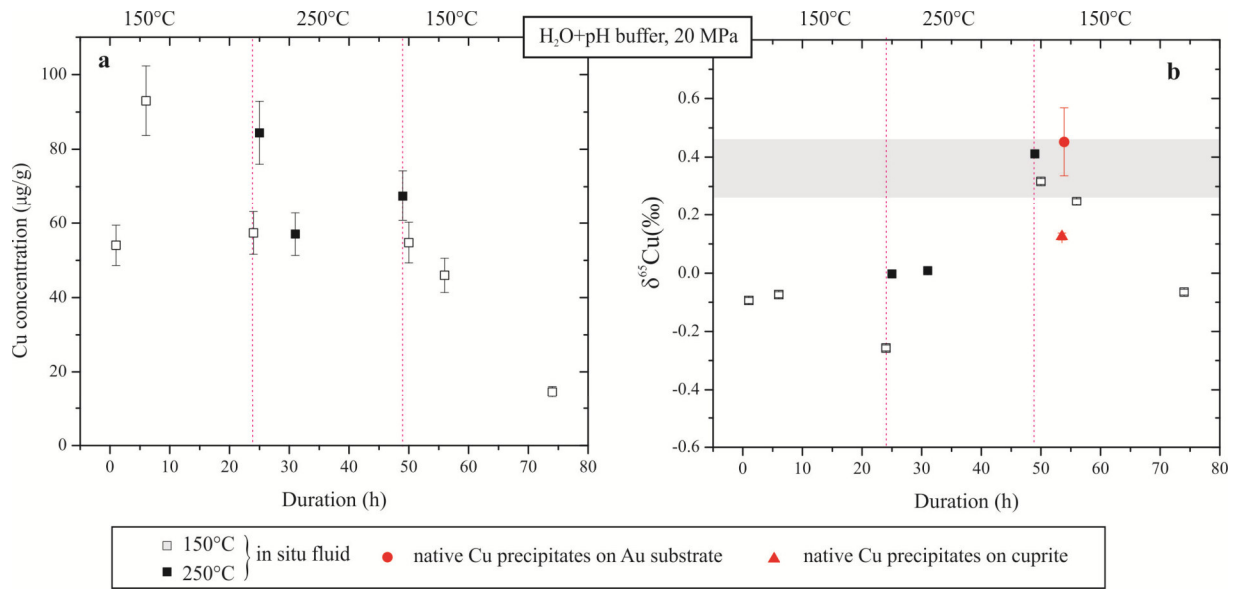


Figure 11 The variation of Cu concentration (a) and isotope composition (b) as functions of run duration and temperature. Dashed lines with arrow suggest the likelihood of isotope fractionation associated with Cu(I) disproportionation process.

4.8 Oxidation of Cu(I) to Cu(II)

Tenonite produced in acetate-bearing solution at 150°C and 250°C for 72 hours yields a constant $\delta^{65}\text{Cu}$ value of 1.2‰ (Fig.12). The most significant isotope fractionation is induced by oxidation of Cu(I) to Cu(II), i.e., ~1‰ at 150°C and ~0.4‰ at 250°C (Fig.12). Note that fluids at oxidized condition may contain Cu^{2+} as well as Cu^+ , however, the amount of Cu^+ in fluids cannot be easily estimated. This implies that fluids associated the oxidation process are enriched in heavy isotope (^{65}Cu). The precipitation of tenonite can also induce isotope fractionation, i.e., ~0.7‰ at 150°C and ~0.1‰ at 250°C (Fig.12). Tenonite as a stable phase precipitated at different temperatures (150°C and 250°C) yield the same isotope signature of 1.2‰.

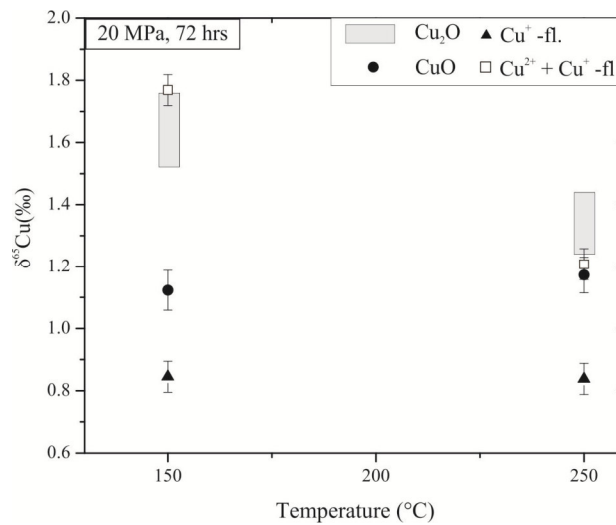


Figure 12 $\delta^{65}\text{Cu}$ values of fluids, initial cuprite (Cu_2O) and tenonite (CuO). Runs are Cp22 (150°C, 20 MPa, 72 hrs) and Cp24 (150°C, 20 MPa, 72 hrs)

5. Discussion

5.1 Cu speciation in hydrothermal fluids

The potential-pH diagram (Pourbaix diagram; Fig. 13) for copper in water has been studied by Beverskog and Puigdomenech (1997). The hydrolysis of copper (I) and (II) is included with two and four hydroxide complexes, respectively. The pourbaix diagrams of Beverskog and Puigdomenech (1997) show that the stable solid phases of copper at 25°C to 200°C at ~0.1 µg/g of dissolved species are native Cu, Cu₂O and CuO, and at 300°C only native Cu and CuO are stable.

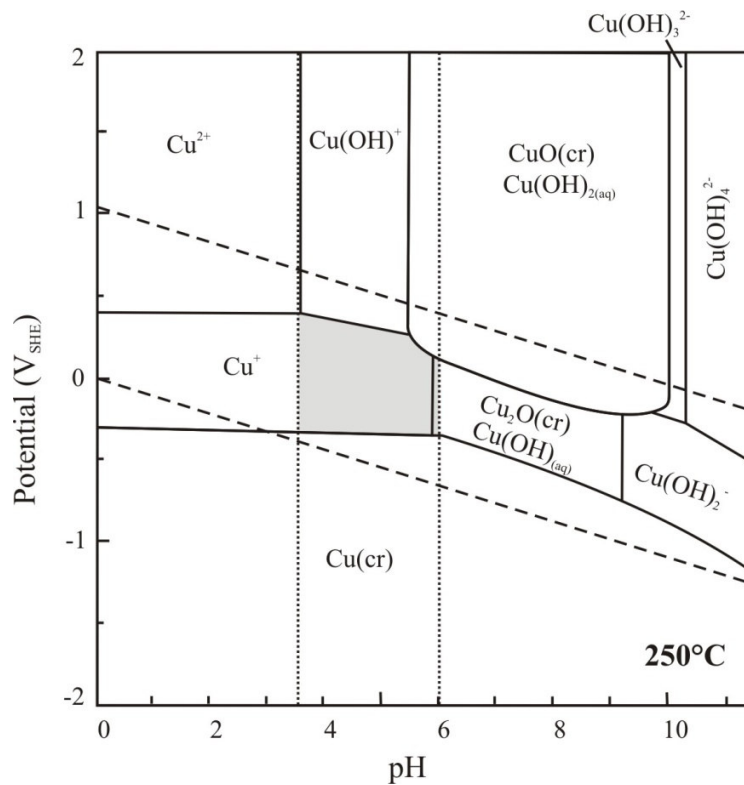


Figure 13 Pourbaix (potential-pH) diagram for copper at 250°C at $[Cu(aq)]_{tot} = 0.06 \mu\text{g/g}$ (modified from Beverskog and Puigdomenech (1997)). The parallel sloping dashed lines in the Pourbaix diagrams represent the stability of water at a partial pressure of gaseous species equal to 1 atm. The upper dashed line represents the oxygen equilibrium line ($O_2(g)/H_2O(l)$), and potential above this line will oxidize water resulting in oxygen evolution. The lower dashed line represents the hydrogen line ($H^+/H_2(g)$), and potential below this will result in hydrogen evolution. Two dotted lines represent the fluid acidity change at run condition (calculated against the ionization of water at 250°C). *cr* is an abbreviation of crystal. The shaded area represents the possible potentials and pH values of the run in pure H₂O (Cp41).

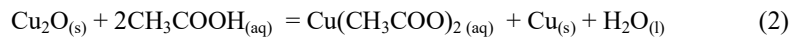
In the system of cuprite and water, the pH values range from 4.53 (stock solution) to 7.58 for a duration of 72 hours (note that the pH values are determined at 25°C; Tables 2, 3). Considering the self-ionization of water at 250°C, the corresponding pH values are adjusted and shown in Fig.13 (two parallel dotted lines). The area within

Chapter IIA

two dashed lines defines the stability of water at given condition (250°C and 0.1 MPa). Oxygen will be generated when the potential is higher than the upper dashed line, hydrogen is produced when potential is below the lower dashed line. At run conditions, there are no detectable gases (including H₂) produced during the experiment (results are given in Table 4). Thus, it is likely that the reaction occurs within the stability field of water without producing any gases. It is also clear that Cu⁺ is the dominant species in fluid (Gray region in Fig.13). However, this heterogeneous reaction may lead to certain changes in oxygen fugacity especially in the vicinity of cuprite and Au substrate. Furthermore, the presence of native Cu, the changes of fluid acidity and the absence of H₂ support a similar Cu(I) disproportionation reaction (1) as mentioned in previous chapter.

The transport of copper (cuprite) in acetate solutions has been well studied by Liu et al. (2001) using silica tube technique at a temperature range of 50°C-150°C over NaAc concentration from 0.1 m to 2 m (note that HAc and NaAc are always equimolar in the solution). In addition, their 250°C runs were unsuccessful due to the explosion of silica tubes, which may be caused by the overpressure generated by the decarboxylation of acetate. Liu et al. (2001) calculate that the hydrolysis reaction rate of Cu⁺ is by almost 9 orders of magnitude slower than the reaction with acetate, also the affinity of Cu⁺ to acetate is much higher than that to H₂O (Lai et al., 2018). Also, this is supported by the data in this study that Cu concentration in pure water is 20 times lower than that in acetate-bearing system. Solubility investigation (Liu et al., 2001) and molecular dynamic simulation (Lai et al., 2018) suggest that Cu(I) exists exclusively as Cu(I)Ac in acetate solutions at temperature up to 150°C, the possible complexes are [Cu(CH₃COO)(H₂O)] and [(CH₃COO)₂Cu]⁻ (Lai et al., 2018).

However, native Cu and tenorite are the main solid products formed the system of cuprite and water ± acetate (0.2 m HAc/KAc) at 250°C (for more details see *Results*). Formation of native Cu in acetate solutions is exclusively observed in 24 hours runs, the reaction may be similar to what proposed by Ball and Portwood (1994):



Intriguingly, tenorite, more oxidized mineral, is observed in acetate solutions at 150°C and 250°C for 72 hours runs. Very little Au₉₂Cu₈ nuggets (<15 μm) found at the rim of tenorite (Fig.3e, f), which may be the relic of native Cu on Au reaction cell. The formation of tenorite on both cuprite and Au foils are possibly explained by following reactions.



Comparable run (more details are given in Appendix A2) have confirmed that acetic acid has been completely decomposed with the production of CO₂ and CH₄ (Table). Subsequently, CO₂ may act as an oxidant via reaction (3), the production of C (graphite) may be supported by Raman spectra (Fig.4). The produced oxygen will be further consumed by the oxidation reactions (4-6) to form tenorite.

However, the precipitation of tenorite can also be attributed to $\text{Cu}(\text{CH}_3\text{COO})_2$. The breakdown of metal acetate complexes into metal oxide is possible. Palmer and Drummond (1986) conducted a series of experiments to investigate the titanium oxide solubility in acetate and/or acetic acid at a temperature range of 360°C-440°C. Experiments conducted either in acetic acid solutions or in exclusively sodium acetate showed no changes of the titanium surface. However, a significant amount of recrystallization of TiO_2 surface layer was found in the run with equimolar acetic acid/sodium acetate solution. The overall concentration of acetate ions strongly affects the solubility of titanium oxide. They also suggested that the high concentration of titanium acetate ($\text{Ti}(\text{AC})_{2+n}^{-n}$) in solution can lead to the gradual deposition of TiO_2 during the experiment as the concentration of acetic acid declines.

5.2 Acetate effect on metal transport and deposition

Acetic acid was found to decompose faster than acetate (Kharaka et al., 1983; Palmer and Drummond, 1986; Bell et al., 1994). The C-C bond in the adsorbed acetate ion may be more destabilized compared to the adsorbed acetic acid molecule, but react more slowly because of the lack of a neighboring adsorbed H atom.

Kharaka et al. (1983) used a same vessel as this study to investigate of thermal decarboxylation of acetic acid as well as the Fe concentration in fluids at 200°C, 300°C and 1.5, 8.5 bar, respectively. Runs were carried out in HAc and NaAc solutions for periods of up to 4400 hours. At 200°C, Fe concentration in pure acetic acid initially increases from 5580 $\mu\text{g/g}$ to 7090 $\mu\text{g/g}$, and decreases to almost half after 650 hours, e.g., 4100 $\mu\text{g/g}$ at 1146 hour (Fig.14a). Note that the pH of the solution remains constant even all acetic acid is consumed, i.e., pH values of 3.11 ± 0.08 . The trend of Fe concentration with time is comparable to the evolution of Cu concentration at 150°C run in this study, rising from 50 to 350 $\mu\text{g/g}$ within 6 hours, and reduces to 150 $\mu\text{g/g}$ at 24 hour. At higher temperatures (250°C and 300°C) and in pure acetic acid system, an initial decreasing trend is observed commensurate with the Fe and Cu_2O dissolution. Kharaka et al. (1983) also found that iron concentration in the sodium acetate solutions were $<1 \mu\text{g/g}$ and decarboxylation was found to be orders of magnitude slower. An explanation of this phenomenon is that the dissolution, or oxidation, of iron is mainly promoted by the acetic acid content of the solution due to the formation of $[\text{FeAc}_2]_{\text{aq}}$ which is predicted to be the dominant iron acetate complex at these conditions (Drummond and Palmer, 1985) and is independent of the acetate anion concentration. Since the half lives of acetic acid in stainless steel are ca. 2400 hours and ca. 10000 hours at 300°C and 200°C, respectively (Kharaka et al., 1983), the acetic acid is almost consumed over a period of 4400 hours at 300°C so that Fe content decreases over time. The increment of Fe and Cu concentrations is inversely proportion to temperature (Fig.14a, b). Furthermore, the concentration of the acetic acid promotes the metal enrichment, and it is likely that the decarboxylation of acetic acid which attenuates the metal concentration.

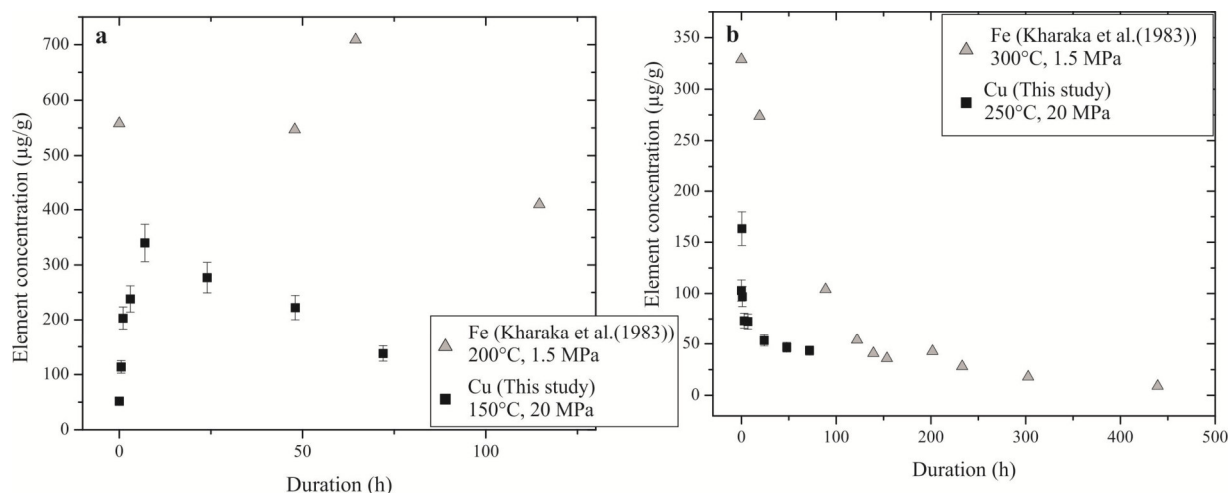
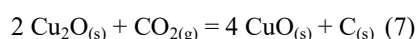


Figure 14 Cu and Fe concentrations as functions of time and temperature. (a) Cu and Fe contents at temperature $\leq 200^{\circ}\text{C}$, liquid- and vapor-saturated conditions, respectively; (b) Cu and Fe contents at temperature $> 200^{\circ}\text{C}$, liquid- and vapor-saturated conditions, respectively. Fe concentration data are taken from Kharaka et al. (1983). Their runs were conducted in the same equipment as used in this study but at vapor-saturated condition, and reactions took place between Fe (stainless steel) and 0.5 m HAC/NaAc solutions. In order to better compare the data in a similar range, some changes of the data from Kharaka et al. (1983) have been made, i.e., reaction time and Fe concentration data of the 200°C run are reduced by an order of magnitude.

Experiments similar to Cp24 and Cp40 ($\text{Cu}_2\text{O} + \text{H}_2\text{O} \pm \text{KAc}/\text{HAc}$) have been done to investigate the compositions of gas phase generated in the system (Experimental details are given in Appendix A2). Additionally, one run has been conducted in pH buffered solution, and all results are tabulated in Table 4. It is clear that methane (CH_4) and carbon dioxide (CO_2) are the dominant reaction products of both pH buffered runs. Interestingly, 0.2 mol/kg acetic acid has been fully consumed in KCl system (with KAc/HAc), whereas some acetic acids can still be detected after the run with H_2O and KAc/HAc. This may support the finding of Bell et al. (1994) that the presence of chloride can also speed up decarboxylation reaction. Furthermore, the generated CO_2 may be act as an oxidant, which will help to oxidize Cu(I) to Cu(II) via the following reaction.



The production of carbon is possible during this oxidation process. A direct evidence is the coexistence of carbon and tenorite, which has been measured by Raman spectra in Fig.4.

Table 4 Compositions of gas phase products in 250°C and 20 MPa runs

SNO	System	Time hrs	CH_4 mol%	CO_2 mol%	H_2 mol%	Acetone mol%	Presence of acetic acid
Cp45	$\text{Cu}_2\text{O} + \text{H}_2\text{O}$	72	/	/	/	/	N
Cp46	$\text{Cu}_2\text{O} + \text{H}_2\text{O} + 0.2 \text{ m HAC}/\text{KAc}$	72	49	51	/	52	Y
Cp47	$\text{Cu}_2\text{O} + \text{KCl} + 0.2 \text{ m HAC}/\text{KAc}$	72	56	44	/	6	N

Notes:

Starting and gas compositions of each experiment are given in Appendix table A2.

N and Y denote the absence and the presence of certain phase.

5.3 Fractionation mechanism

Although the nature of the reaction has not yet been identified unequivocally, it is possible that four reactions competing during the fluid-cuprite interaction, namely cuprite dissolution (step 1), Cu(I) disproportionation in the fluid (step 2) and oxidation of Cu(I)/Cu(0) to Cu(II) (only takes place in acetate bearing system; step 3) and acetate decarboxylation (step 4). Step (2) and step 3 are responsible for isotope fractionation.

Comparing temperature cycling and constant temperature experiments, it is certain that Cu(I) disproportionation reaction rate is faster at high temperature (250°C) than low temperature, i.e., native copper occurs in all 250°C runs (e.g., 24 hours in H₂O-KAc/HAc system and 72 hours in pure water). The isotope data indicate that Cu⁺ dominant fluid sampled at early stage yields generally similar $\delta^{65}\text{Cu}$ values to that consists of a mixture of Cu⁺ and Cu²⁺ (Fig. 10b). Concomitantly, the reduction of Cu(I) to native Cu yields fractionation of ~0‰. This conclusion is in a good agreement of chapter III which investigated the isotope fractionation between Cu(II) and Cu(0) using Cu electroplating method. A major conclusion is that the observed isotope fractionation is controlled by the reduction of Cu(II) to Cu(I) and is less significantly affected by the reduction of Cu(I) to native Cu. However, even in a single run the isotope signature of native Cu deposited at different locations can be different (up to 1‰; Fig.10b). Thus, $\delta^{65}\text{Cu}$ value of native Cu is strongly dependent on its precursor mineral or source fluids.

Step 3 may be initiated by decarboxylation of acetate because methane and carbon dioxide are found in a comparable run. Although the mechanism of oxidation of Cu(I) and / or Cu(0) into tenorite remains enigma, this process will certainly induce isotope fractionation. The initial Cu⁺ dominant fluids has a $\delta^{65}\text{Cu}$ value of 0.8‰ (at 150°C and 250°C), much lower than the initial cuprite (Fig. 12). After 24 hours, the decomposition of acetate releases gases (CH₄ and CO₂) which may lead to the destabilization of copper acetate (likely CuAc) and/or cuprite and native Cu oxidation. The fluid dominated by Cu²⁺ will have a higher $\delta^{65}\text{Cu}$ value than that of Cu⁺ fluid, i.e., $\delta^{65}\text{Cu}$ values are 1.8‰ and 1.2‰ for Cu²⁺ fluids at 150°C and 250°C, respectively. When the concentration of copper exceeds certain mineral solubility, which will result in the gradual precipitation of oxides, e.g., tenorite (analogous to the findings of Palmer and Drummond (1986)). The isotope fractionation between tenorite and Cu(I)-bearing fluids is $0.35 \pm 0.05\%$ at both 150°C and 250°C. The precipitation of Cu mineral from the solution can also yield isotope fractionation, e.g., up to 0.4‰ lighter than the solution (Maréchal and Sheppard, 2002; Ehrlich et al., 2004). However, in our case the precipitation of tenorite may induces isotope fractionation of up to 0.7‰ due to the possible mixing of Cu²⁺ and Cu⁺ in fluids.

5.4 Implications

Researchers have placed less emphasis on the complexation between acetate and Cu(I) ion due to (i) the lower stability of Cu-Ac complexes and (ii) the low concentration of acetate relative to Cl⁻. However, experimental investigation (Drummond and Palmer, 1986) and theoretical simulation (Lai et al., 2018) prove that the first factor has been overstated, and their results suggest that metal-acetate (e.g., CuAc_(aq)) complexes are stronger than the analogous chloro-complexes and the high stability of the acetate complexes in aqueous may account for a large proportion of metal transport in deep sedimentary basins.

Chapter IIA

The lack of evidence of acetate/acetic acid in natural systems is undoubtedly attributed to several factors. Many of the hydrothermal and ore-forming fluids of interest are contained only in fluid inclusions. It is rather difficult to preserve acetic anions in miniscule volume of fluid over a reasonable geological time because decarboxylation at elevated temperature is rapid, especially when the system contains catalytic active mineral (e.g., hematite (Bell et al., 1994), cuprite (this study)). However, there are evidences that up to 1 m acetate may exist in the original ore fluids of a polymetallic mineral deposit in Northern Caucasus (Germanov and Mel'Kanovitskaya, 1975; Drummond and Palmer, 1986). Furthermore, up to 0.08 m (i.e., 4900 $\mu\text{g/g}$) aliphatic acid (possibly acetic acid) has been detected in sedimentary basin brines at San Emidio Nose oil field, California (Carothers and Kharaka, 1978).

It is evident from this study that acetate is capable of the transportation of metals in hydrothermal solutions by acetate complexing at low temperature. There are several hydrothermal metal transport processes related to copper in which carboxylation may play a vital role, including (1) the formation of sediment-hosted stratiform Cu ore (e.g., Azaraien et al., 2017), (2) reaction with sulfate to produce H_2S which helps Cu precipitation (Sun and Püttmann, 2000). For these processes to be effective, the metal-carboxylate complexes must be sufficiently stable with respect to other competing metal ions and ligands and, in case 1, a mechanism must exist to cause metal deposition at ore concentrations. Among the many mechanisms known to cause the precipitation of metals from solution, instability of the complexing ligand (acetate) due to decomposition as the brine encounters catalytic and / or reactive oxidant minerals provides an additional mechanism (Ti_2O precipitation (Palmer and Drummond, 1986) and CuO precipitation (this study)).

Sediment-hosted stratiform Cu ores account for significant proportion of the world's Cu, e.g., ca.3.3 Mt at White Pine native Cu mine (Brown, 2009), and ca. 0.6 Mt at Rammelsberg deposit (Large and Walcher, 1999). The source of copper in sediment-hosted stratiform copper deposits is commonly attributed to the leaching of copper from large volumes of footwall red beds (Rose, 1976; Hitzman et al., 2005). Previous studies have stated that ppm level of Cu (typically 5-50 $\mu\text{g/g}$) is enough to form these tonnage Cu ores (commonly the footwall red beds are hundreds of km^3 : White, 1971; Hitzman et al., 2005). A recent estimation from Brown (2009) shows that 20 $\mu\text{g/g}$ Cu leached out from the red bed can lead to a 1 Mt Cu deposit over a million year. More to this point, Giordano (1985) concluded that at least 10 $\mu\text{g/g}$ metal (Pb, Zn) acetate complexes are required to form a sediment-hosted Pb-Zn deposit (e.g., Mississippi Valley-Type deposit). In this way, our data imply that hundreds ppm Cu transported by acetate-bearing fluids and subsequent metal precipitation due to instability of the complexing ligand may explain the enrichment of copper in sediment-hosted Cu ore deposit.

6. Conclusion

The partitioning of Cu between cuprite and $\text{H}_2\text{O} \pm 0.2$ m HAc/KAc solutions is investigated elementally and isotopically at 100-250°C and 5-30 MPa. The experiments were carried out for periods of up to 72 hours in a Parr autoclave allowing for in-situ sampling of fluid phase. Native copper and tenorite are the dominant experimental products. Native Cu forms in pure H_2O solution (run duration of 72 hours) and in acetate-bearing runs (≤ 24 hours) at 250°C. Tenorite is observed in 150°C and 250°C long-termed (72 hours) acetate-bearing runs.

Chapter IIA

The decomposition of cuprite in hydrothermal fluids was found to occur by several types of reactions: (1) simple cuprite dissolution and production of Cu(I) in hydrothermal fluids at the early stage (≤ 6 hours); (2) Cu(I) disproportionation into Cu(II) and native Cu (6-24 hours); (3) decarboxylation reaction and production of equimolar methane and carbon dioxide; (4) oxidation of Cu(I)/Cu(0) to Cu(II).

During cuprite dissolution process, Cu content in acetate solution (pH= ~4.5) is ~20 times higher than that in pure water (pH= 4.5-7.5), i.e., 70 $\mu\text{g/g}$ and 3 $\mu\text{g/g}$, respectively. In pH buffered solutions: (i) temperature correlates inversely with Cu content, i.e., decreasing from ~400 $\mu\text{g/g}$ at 100°C to ~70 $\mu\text{g/g}$ at 250°C; (ii) Cu content increases from 50 $\mu\text{g/g}$ at 5 MPa to 100 $\mu\text{g/g}$ at 10 MPa, a constant value of ~100 $\mu\text{g/g}$ is observed over a pressure range of 10-30 MPa.

The Cu(I) disproportionation reaction induces insignificant isotope fractionation, i.e., $\Delta^{65}\text{Cu}_{[\text{native Cu-Cu(I)}]}$ values of $0.09\pm 0.09\%$. It is likely that the oxidation of Cu(I) and Cu(0) to CuO is due to decarboxylation of acetate and/or acetic acid. This oxidation reaction induces substantial fractionations, i.e. $\Delta^{65}\text{Cu}_{[\text{CuO-Cu(I)}]}$ values are $0.35\pm 0.05\%$ at 150°C and 250°C. The accompanying precipitation of CuO from Cu(II) may lead to a fractionation of 0.10 ± 0.02 to $0.70\pm 0.01\%$ at 150°C and 250°C, respectively.

This study indicates that acetate plays a dual role in copper transport and deposition. On the one hand, the presence of acetate strongly enhances Cu content up to 400 $\mu\text{g/g}$, implying that acetate complexation can be responsible for metal transport in hydrothermal fluids. On the other hand, decarboxylation of acetate substantially decreases the dissolved Cu and aid the precipitation of Cu-bearing minerals (e.g., native Cu and tenorite). These findings may help to explain the enrichment of copper in sediment-hosted Cu ore deposit.

Acknowledgments

This research was supported by the German Academic Exchange Service (DAAD-57076462) and Graduate School GeoFluxes. We thank U. Kroll, A. Reimer and J. Feige for their technical support.

Chapter IIB

**Partitioning behavior of Cu and its isotopes between cuprite and
K(Na)Cl-bearing hydrothermal fluids to 250°C and 30 MPa:
constraints from in situ hydrothermal fluid**

Dongmei Qi^{a*}, Harald Behrens^a, Marina Lazarov^a, Roman Botcharnikov^b, Chao Zhang^a, Stefan Weyer^a

^aInstitute of Mineralogy, Leibniz Universität Hannover, Callinstrasse 3, Hannover, D-30167, Germany

^bInstitute of Geosciences, Johannes Gutenberg University Mainz, J.-J.-Becher-Weg 21, Mainz, D-55128, Germany

(*d.qi@mineralogie.uni-hannover.de)

Abstract

Copper solubility and isotope fractionation has been determined experimentally between cuprite and KCl-bearing hydrothermal fluids at temperatures of 100°C -250°C, pressures of 5 MPa - 30 MPa for up to 72 hours. Aqueous solutions contained 0.14 - 0.72 mol/kg chloride solutions (with/without the presence of pH buffer, 0.2 m HAc/KAc), with all starting solutions acidity of 4.5. This study utilized deformable gold-cell technology, which allowed time-series sampling of solution during cuprite dissolution and isotope exchange. At 250°C, native copper as an additional stable mineral is produced and mainly deposits on Au substrate. Three competing reactions control the variations of Cu concentration and isotopic composition at 250°C, i.e., cuprite dissolution, Cu(I) disproportionation into Cu(II) and native Cu, and decomposition of acetate into methane and carbon dioxide.

At the early stage (<24 hours) of the cuprite dissolution process, constant Cu content can be achieved within 6 hours at 100°C - 250°C. Cu content is strongly dependent on temperature, salinity (KCl_{aq} concentration) and fluid acidity and almost independent of pressure. The dissolved Cu in pH buffered KCl-bearing solution (pH=4.5) is ca. 2 log units higher than that in pure solution where fluid acidities vary from 4.5 to 9.3. In pH buffered solutions: (i) increasing temperature from 100 to 250°C promotes Cu dissolution from 1000 $\mu\text{g/g}$ to ~3000 $\mu\text{g/g}$ at 0.41 m KCl_{aq} . (ii) Increasing salinity significantly increases Cu content by a factor of 3, i.e., 1200 $\mu\text{g/g}$ and 3600 $\mu\text{g/g}$ at 0.14 m and 0.71 m KCl_{aq} , respectively.

Subsequent Cu(I) disproportionation induces isotope fractionation, i.e., $\Delta^{65}\text{Cu}_{[\text{native Cu-Cu(I)}]}$ value are $0.15\pm 0.07\%$. The data indicate that reduction of Cu(I) to native Cu has less significant effect on isotope fractionation.

The gas spectrometry measurement shows that equimolar methane and carbon dioxide has been generated due to acetate decarboxylation. Moreover, the discernible dissolved Cu reduction after 6 hours at 250°C runs may be related to decomposition of acetic acid.

The results of this study show that chloride in addition to acetate can be strong complexation ligands, which significantly increase Cu content in hydrothermal fluids to ~4000 $\mu\text{g/g}$. Our findings can help to understand the enrichment of Cu in sedimentary settings.

1. Introduction

Fluids play an important role in a variety of processes in the Earth's crust and upper mantle. The majority of economic copper deposits are hydrothermal in origin, and the presence of an aqueous fluid phase helps to transport metals over long distances, and eventually deposit them as ore minerals. In hydrothermal fluids, the stability of aqueous metal complexes which results in metal ions transport is controlled by the physicochemical environment (e.g., Heinrich et al., 1999; Harris et al., 2003; Redmond et al., 2004; Harris et al., 2005; Landtwing et al., 2005). Ore-forming fluids cover wide ranges in temperature (25 to >600°C), pressure (0.1 to >500 MPa) and compositions ranging from nearly pure water to highly saline fluids (>50 mol% NaCl, KCl, CaCl₂ and FeCl₂) (Brugger et al., 2016).

At room temperature and atmospheric condition, the stable oxidation states of copper are cupric and metallic copper. The Cu⁺ ion is unstable and tends to disproportionate to Cu(s) and Cu²⁺ in aqueous solution (Brugger et al., 2007; Moynier et al., 2017). Cu(I) becomes more stable than Cu(II) in aqueous fluid and vapor at elevated temperature (>100°C). In hydrothermal fluids, Cu would readily form either chloride or hydrosulphide species, depending on P-T-X conditions and ligand availability (Mountain and Seward, 1999, 2003; Etschmann et al., 2010). Numerous studies of fluid inclusions from copper deposits and fluid composition of modern hydrothermal systems indicate that chloride is one of the most important complex ligand in ore-forming fluids (e.g., Barnes, 1979; Heinrich et al., 1989). For sedimentary-hosted copper deposits, usually formed at low temperature (<200°C), copper chloride complexes are suggested to be important for copper transport. Spectroscopic (e.g. Fulton et al., 2000a; Liu et al., 2002; Berry et al., 2006; Brugger et al., 2007), experimental (Xiao et al., 1998; Liu et al., 2001; Hack and Mavrogenes, 2006) and thermodynamic (Liu and McPhail, 2005; Sherman, 2007) investigations suggest that the dominant Cu(I) chloride complexes are linear complexes, i.e. [H₂O-Cu-Cl]⁰ and [Cl-Cu-Cl]⁻ at temperature above 100°C. The linear dichloro Cu⁺ species as [CuCl₂]⁻ is the only Cu⁺ chloride complex stable over the range of salinities (up to 17 mol kg⁻¹) typical of natural fluids at the temperatures of ore-deposition (up to 450°C) (Berry et al., 2006; Brugger et al., 2007; Cauzid et al., 2007).

Deciphering metal transport and enrichment during hydrothermal and other geological processes is complicated due to a variety of pressure-temperature conditions and variable compositions of fluids interacting with the lithosphere. The precise transition metal isotope ratios (e.g., Fe, Cu and Zn) can help to answer the longstanding questions on the source of the metals and mineralization processes in ore-forming systems. Among the transition metals, copper has received the greatest attention among researchers interested in applying metal stable isotope to mineral deposits. Copper has two stable isotopes (⁶³Cu and ⁶⁵Cu with the abundances of 69.17% and 30.83%, respectively, Shields et al., 1964) and its isotopic ratio is commonly expressed in δ notation ($\delta^{65}\text{Cu} (\text{‰}) = [((^{65}\text{Cu}/^{63}\text{Cu})_{\text{sample}} / (^{65}\text{Cu}/^{63}\text{Cu})_{\text{NIST-SRM 976}}) - 1] \times 1000$, NIST SRM 976 denotes the standard reference material of Cu). Due to the recent advances in multi-collector ICP-MS (MC-ICP-MS) and high precision measurements, Cu isotopes have been used to fingerprint the sources and/or processes involved in solar system, subduction zones,

Chapter IIB

mantle plumes and the crust (e.g., Luck et al., 2005; Savage et al., 2015; Busigny et al., 2018). To date, the overall $\delta^{65}\text{Cu}$ values range from -16.5‰ to 10‰ in nature (Moynier et al., 2017).

High temperature magmatic processes yield almost no noticeable isotope fractionation, with $\delta^{65}\text{Cu}$ values averaging to $\sim 0.07 \pm 0.10\%$ which is believed to represent the bulk Earth composition (e.g. Li et al., 2009a; Liu et al., 2015; Savage et al., 2015; Huang et al., 2016; Moynier et al., 2017). In contrast, a very large Cu isotope fractionation was observed during redox processes at low temperature. For instance, in low temperature (40°C) sediment-hosted copper deposits the isotope compositions of Cu(II) minerals are up to 3.86‰ higher than that of covellite (Asael et al., 2012b). Rouxel et al. (2004) found that low temperature alteration of sulfides from hydrothermal sea-floor vents produces secondary copper minerals enriched in ^{65}Cu , whereas the actual high-temperature precipitation process (massive sulfides deposition) did not lead to variation in $\delta^{65}\text{Cu}$. Markl et al. (2006) studied the primary and secondary copper minerals from hydrothermal veins in the Schwarzwald mining district, south Germany. They found that secondary Cu(II) minerals were formed at the expense of the primary Cu(I) minerals during interaction with low temperature (<50°C) oxidizing solutions. Moreover, they found that the isotope composition of Cu(II) minerals are up to 3.69‰ higher than those of Cu(I) minerals on the same specimen, whereas alteration of the primary Cu(I) mineral to cuprite does not affect the $\delta^{65}\text{Cu}$ value significantly. Experimental determinations of Cu redox state change suggest that Cu isotopes fractionate up to 4.12‰ at temperature lower than 100°C, e.g., the precipitation of Cu(I) minerals from aqueous Cu(II) solutions (Zhu et al., 2002; Ehrlich et al., 2004), the electrochemical reduction of aqueous Cu(II) species to Cu(0) (Qi et al., submitted), oxidative leaching of Cu(I) mineral to aqueous Cu(II) solutions (Mathur et al., 2005; Fernandez and Borrok, 2009b; Pękala et al., 2011).

Based on theoretical calculations of equilibrium isotopic fractionation (Urey, 1947) at elevated temperature will become less pronounced, especially where mass differences between isotopes are small (e.g. for Cu, Fe and Zn). However, studies by Larson et al. (2003) and Graham et al. (2004) suggest that significant Cu isotope fractionation occurs at temperatures above 200°C in ore forming system. Yet, very limited attempt has been made to quantitatively measure the copper isotope fractionation in hypogene ore-forming systems. An experimental study by Rempel et al. (2012) demonstrates that isotopic partitioning between vapor and liquid-phase has been observed up to 0.69‰ at temperature up to 450°C and pressure up to 40 MPa. These findings are consistent with the theoretical prediction that isotopic partitioning up to 2.5‰ may occur during boiling process (Seo et al., 2007). Additionally, the isotopic signature of the dissolved Cu in fluids is up to 1‰ lighter than the precursor chalcopyrite during mineral dissolution processes at temperature of 250°C and 300°C and vapor saturated pressure (Maher et al., 2011). Their results also reveal that the isotope fractionation is controlled by several parameters such as pH, salinity, and partition between liquid and vapor phases.

However, a major impediment to the interpretation of Cu isotope data as well as fractionation during fluid-mineral interaction is that the hydrothermal fluids and aqueous species are well preserved and are not overprinted by retrograde exchange processes (e.g., quenched phases are produced by fluid cooling). We have conducted a series of fluid ($\text{KCl}_{\text{aq}}/\text{NaCl}_{\text{aq}}$) - mineral (cuprite) interaction experiments in Au reaction cell at 100°C-250°C, 5 MPa-30 MPa over a range of salinities and with/without the presence of pH buffer. In addition, the experimental vessel used in

this study allows for on-line sampling liquid phased. Our objectives are: (i) to determine the partitioning behavior of Cu between crystalline material and the fluid phase as a function of P, T, and fluid chemistry; (iii) to understand the mechanism controlling the Cu isotope fractionation; (ii) to unravel the process during cuprite dissolution process by using concentration and the isotopic data; (iv) to gain insight into the natural weathering history of ore deposit during aqueous water-rock interactions at low-temperature.

2. Experimental and analytical procedures

Experimental and analytical procedures are similar to Chapter IIA.

2.1 Experiments setup

Due to the matrix effect of $^{23}\text{Na}^{40}\text{Ar}$ and $^{23}\text{Na}_2^{16}\text{O}^{1}\text{H}$ complexes on the mass of ^{63}Cu , NaCl-bearing solution was only use in one run (Cp6), and KCl-bearing solutions were used in most runs. Table 1 listed the details of each experiment. Six types of experiments were performed to study the interaction of cuprite in hydrothermal fluids, i.e., run duration, temperature, pressure, salinity (KCl_{aq} concentration), with/without pH buffer and temperature cycling. Run duration was set to 24 and 72 hours, temperatures were 100°C, 150°C, 200°C and 250°C, pressures were 5 MPa, 10 MPa, 20 MPa and 30 MPa and KCl concentration was varied between 0.14 m and 0.7 m, pH buffer (0.2 m HAc/KAc) was added in most runs excluding run Cp42 in which only 0.41 m KCl_{aq} solution was added. The cycling experiments were conducted at temperature between 100°C and 250°C at 20 MPa.

2.2 Chromatographic purification

For isotopic analyses of the Na-bearing samples, Cu was separated from the matrix to avoid potential isobaric interferences from the $^{23}\text{Na}^{40}\text{Ar}$ and $^{23}\text{Na}_2^{16}\text{O}^{1}\text{H}$ complexes on the mass of ^{63}Cu (Zhu et al., 2000). The purification was done by ion-exchange chromatography following a modified method described by Maréchal et al. (1999) and Borrok et al. (2007). The digested samples were taken up in 1 ml of 9 mol/l HCl (hereafter M denotes mol/l), and purified Cu fractions were obtained by passing the solution through Bio-Rad® AG MP-1 (100-200 mesh, chloride form) anion resin in 2 ml Bio - Rad® columns. Prior to loading the sample, the resin was cleaned once with 12 ml 9 mol/l HCl and twice with 10 ml 3 mol/l HNO_3 , alternating with M.Q. H_2O . It was subsequently conditioned by 12ml 9 mol/l HCl. The samples were loaded on the resin, the matrix was removed with 8 ml 9 mol/l HCl, then Cu was eluted from the columns with 18 ml 5mol/l HCl + 0.001% H_2O_2 . After separation, all sample aliquots were dried and dissolved in 3% HNO_3 , and diluted to a final concentration of approximately 500 ppb Cu for MC-ICP-MS analyses.

Chapter IIB

Table 1 Run conditions and formation of new minerals during cuprite-KCl_{liq} interaction

SNO	System	Temperature		Pressure MPa	Time hrs	Native		Native	
		°C				Cu	Au	Cu	on cuprite
Cp28	Cu ₂ O + 0.41 m KCl + pH buffer	100		20	24	N	N	N	N
Cp38	Cu ₂ O + 0.41 m KCl + pH buffer	150		20	24	N	N	N	N
Cp25	Cu ₂ O + 0.41 m KCl + pH buffer	200		20	24	N	N	N	N
Cp23	Cu ₂ O + 0.41 m KCl + pH buffer	250		20	72	Y	Y	Y	tiny
Cp42	Cu ₂ O + 0.41 m KCl	250		20	72	Y	Y	Y	tiny
Cp32	Cu ₂ O + 0.41 m KCl + pH buffer	250		5	24	Y	Y	Y	tiny
Cp33	Cu ₂ O + 0.41 m KCl + pH buffer	250		10	24	Y	Y	Y	tiny
Cp34	Cu ₂ O + 0.41 m KCl + pH buffer	250		30	24	Y	Y	Y	tiny
Cp44	Cu ₂ O + 0.14 m KCl + pH buffer	250		20	24	Y	Y	Y	tiny
Cp35	Cu ₂ O + 0.14 m KCl + pH buffer	250		20	24	Y	Y	Y	tiny
Cp36	Cu ₂ O + 0.27 m KCl + pH buffer	250		20	24	Y	Y	Y	tiny
Cp37	Cu ₂ O + 0.71 m KCl + pH buffer	250		20	24	Y	Y	Y	tiny
Cp39	Cu ₂ O + 0.41 m KCl + pH buffer	150-250-150		20	72	Y	Y	Y	tiny
Cp6	Cu ₂ O + 0.90 m NaCl + pH buffer	100-250-150		20	72	Y	Y	Y	tiny

Note:

N and *Y* denote the absence or the presence of native copper after each run.

3. Results

3.1 Formation of new minerals

The solid phases, starting cuprite, newly formed native copper and quench product cuprous chloride are shown in Fig.1. The starting pellet shows a porous structure, with higher porosity near the outer rims compared to the interior (Fig.1a). This is probably due to the combustion of polyvinyl alcohol which was added during preparation to improve the pellet quality. Assuming an ideal cylindrical shape of the sintered pellet, the mass determination of cuprite pellet indicates that the density of the cuprite pellet is 4.5 - 5.0 g/cm³ lower than the theoretical value (6.11 g/cm³), resulting the porosity of 18-26% relative to the theoretical density. The XRD and EMP analyses (shown in Appendix A1) confirm that the pellet is made up of Cu₂O under the sintering conditions 930°C, 24 hours and log $fO_2 = -3$ (other sintering condition is also compared and listed in Appendix A1).

Copper-chloride-bearing precipitates have been found at the surfaces and rims of cuprite (Fig.1b,d). SEM, Raman spectroscopy and qualitative EMP analyses indicate that the phase is composed of Cu, Cl and H₂O, with a Cu/Cl atomic ratio of 1:1 (the total oxides ratio is ~50 wt%), and possible formula of this phase is CuCl(H₂O)_n. This phase might be a quench product due to its absence in the interior of cuprite.

Intriguingly, the golden colored Au foils turn into reddish color after all 250°C runs (Fig.1c). The SEM analyses identify this deposit as native Cu. Native copper occurs at two localities, which is predominated by deposition on Au substrate and to a lesser extent Cu is attached to the rim of cuprite (Fig.1c). In the presence of the pH buffer, both sides of Au foils are covered by the native Cu deposits. Additionally, the growth of native copper crystal on Au foil surrounding the cuprite rim can be observed (e.g., Fig.1c). From the mass gain of the Au foil as well as the quantitative Cu content determination (ICP-OES analyses of Cu deposits on Au reaction cell), the estimated Cu layer thickness is less than 4 μm (Cp37, Fig.1c). In the absence of pH buffer (only one run Cp42 is conducted with Cu₂O and KCl solution), the native copper precipitates occur only at one side of the Au foil as well as the cuprite where a discernible zone was found (Fig. 1e). Under 100× objective, native copper was found to be surrounded by gray precipitates (Fig.1f) which cannot be identified by Raman and SEM. In addition, these gray precipitates cannot be found in the interior of a cross-section of cuprite, implying this phase must be a quench product.

Precipitates in residual solutions collected from the Au reaction cell are found to be fine cuprite precipitates and blue copper chloride deposits which were collected from the 150°C run (Cp21). The composition of these precipitates was identified by SEM analysis.

Chapter IIB

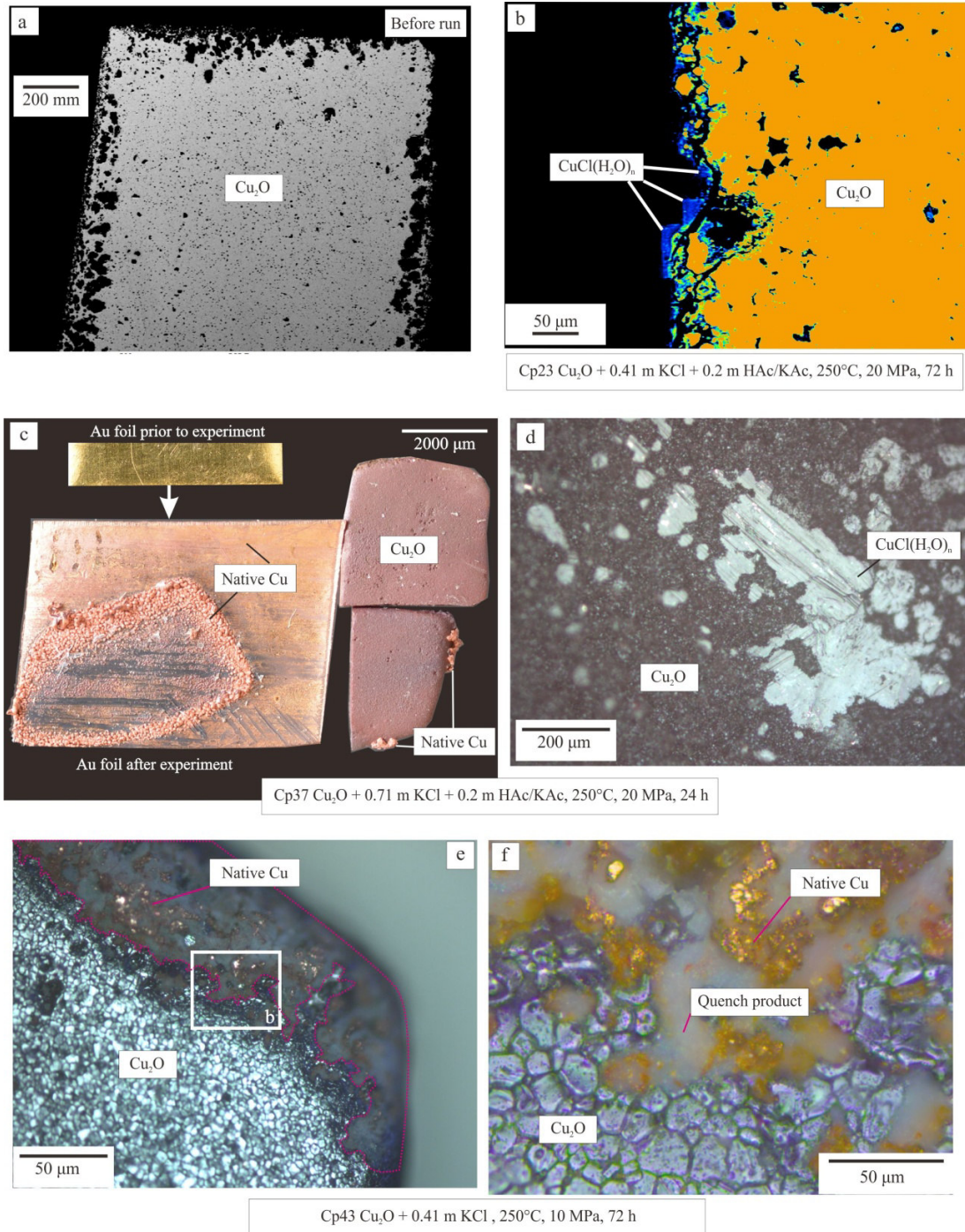


Figure 1 Images of cuprite pellets before and after reaction with pH buffered KCl-bearing solutions. (a) Back scattered image (BSE) of a cross-cut cuprite pellet prior to experiment. Rims tend to be more porous than the interior. (b) BSE image of a cuprite (in orange color) after run at 250°C, 200°C, for 72 hours. The tabular copper chloride phase (in blue color) is observed at the rim of the cuprite. (c) Au foils prior to and after run Cp37. Native Cu crystals up to 150 μm are observed at the surface of Au foil and rims of cuprite pellet. (d) Microscopic image (under reflected light) of copper chloride (quenched phase) at the surface of cuprite after run with 0.71 m KCl_{aq} at 250°C and 20 MPa. (e) Microscopic image (under reflected light) of the reacted cuprite. Rims are covered by native Cu and quench product. More details of the white box in (e) is shown in (f). (f) Spatial relationship among native Cu, cuprite and quench product.

Chapter IIB

Table 2 Results of experiments in the Cu₂O-KCl-HAC/KAC system at 20 MPa

SNO	t	pH ini.	pH 1 st fl.	Elements concentration										Cu isotope composition(δ ⁶⁵ Cu)							
				Cu		Rb		res.		1 st fl		2 nd fl		solution MC-ICP-MS		res.		in situ LA-ICP-MS			
	h	μg/g	μg/g	μg/g	μg/g	μg/g	μg/g	μg/g	μg/g	μg/g	μg/g	μg/g	%	%	%	%	%	%	%		
Cp28	0	4.64	4.63	207	3814	398	458						0.91±0.01	1.04±0.02	1.69±0.20						
	0.5	±0.04	±0.08	371		396							0.88±0.02								
	1			532		409							0.85±0.01								
	3			805		458							0.79±0.01								
Cp38	6			1349		458							0.85±0.01								
	24			1618		458							0.86±0.01								
	1	4.64	4.78	650	4295	458	458						0.29±0.02	0.21±0.01	0.61±0.20						
	6	±0.04	±0.16	1552		458							0.24±0.01								
Cp25	24			2970		458							0.21±0.03								
	0	4.64	4.74	1083	2695	420	458						0.98±0.01	1.08±0.03	1.49±0.20						
	0.5	±0.04	±0.08	1192		402							0.92±0.01								
	1			1356		393							0.92±0.01								
Cp23	3			2203		458							0.95±0.01								
	7			2727		458							0.95±0.01								
	24			3262		458							0.92±0.02								
	0	4.46	4.85	712	3324	363	450						0.81±0.02	0.81±0.01	1.29±0.20	0.42±0.06	0.98±0.03				
	0.5	±0.28	±0.12	1474	1606	435	430						0.85±0.01	0.86±0.01							
	1			1848	1950	446	417						0.85±0.03	0.86±0.01							
	3			2239	2593	411	415						0.84±0.01	0.84±0.03							
	7			2817	3301	389	395						0.85±0.02	0.87±0.01							
Cp42	24			3066	3320	397	427						0.84±0.01	0.84±0.03							
	48			2788	3327	450	450						0.90±0.03	0.87±0.01							
	72			2650	3050	450	450						0.89±0.01	0.85±0.01	0.50±0.20	0.48±0.06	0.48±0.02				
	1	4.46	5.54±0.01	98	88	502	485						0.10±0.02	0.10±0.02							
72	±0.08	6.81±0.25	152		461								0.23±0.02								
		9.28±0.01	41		485								0.04±0.01								

Notes:

Abbreviations: 1st fl and 2nd fl for the first and second sampled fluids (per time), *ini.* and *res.* for initial stock solution and residual fluid in Au reaction cell, respectively.

pH values of fluids are measured at room temperature for both stock solutions and sampled fluids during the run. As mentioned in text that 1st sampled fluids were usually used for pH determination. pH uncertainties are 95% confidences limits about the mean.

Elements (*Cu* and *Rb*) concentration uncertainties are better than 10% (2SD), which is determined by ICP-OES.

Cu_2O^* , Cu^{\dagger} and Cu_4^{\ddagger} represent starting cuprite, native copper precipitated on Au foil and Au bag after a single run, respectively.

The isotope composition of Cu_2O^* is based on the Eqs.(1-4) which has been described in Chapter IIA. Cuprite pellets of Cp23-Cp28 belong to Group I (no original cuprite pellets have been kept), cuprite of Cp39-Cp42 belong to Group II (cuprite pellets prior to and after experiments have been preserved).

in situ LA-MC-ICP-MS has been used to determine the isotope composition of Cu_2O^* and Cu^{\dagger} , *solution nebulized MC-ICP-MS* has been used to determine the isotope composition of fluids and Cu_4^{\ddagger} .

The uncertainties of Cu isotope data acquired by solution MC-ICP-MS and *in situ* LA-ICP-MS are given by the two-sigma errors of the triplicated analyses.

3.2 Elements concentration and Cu isotope fractionation as a function of run duration

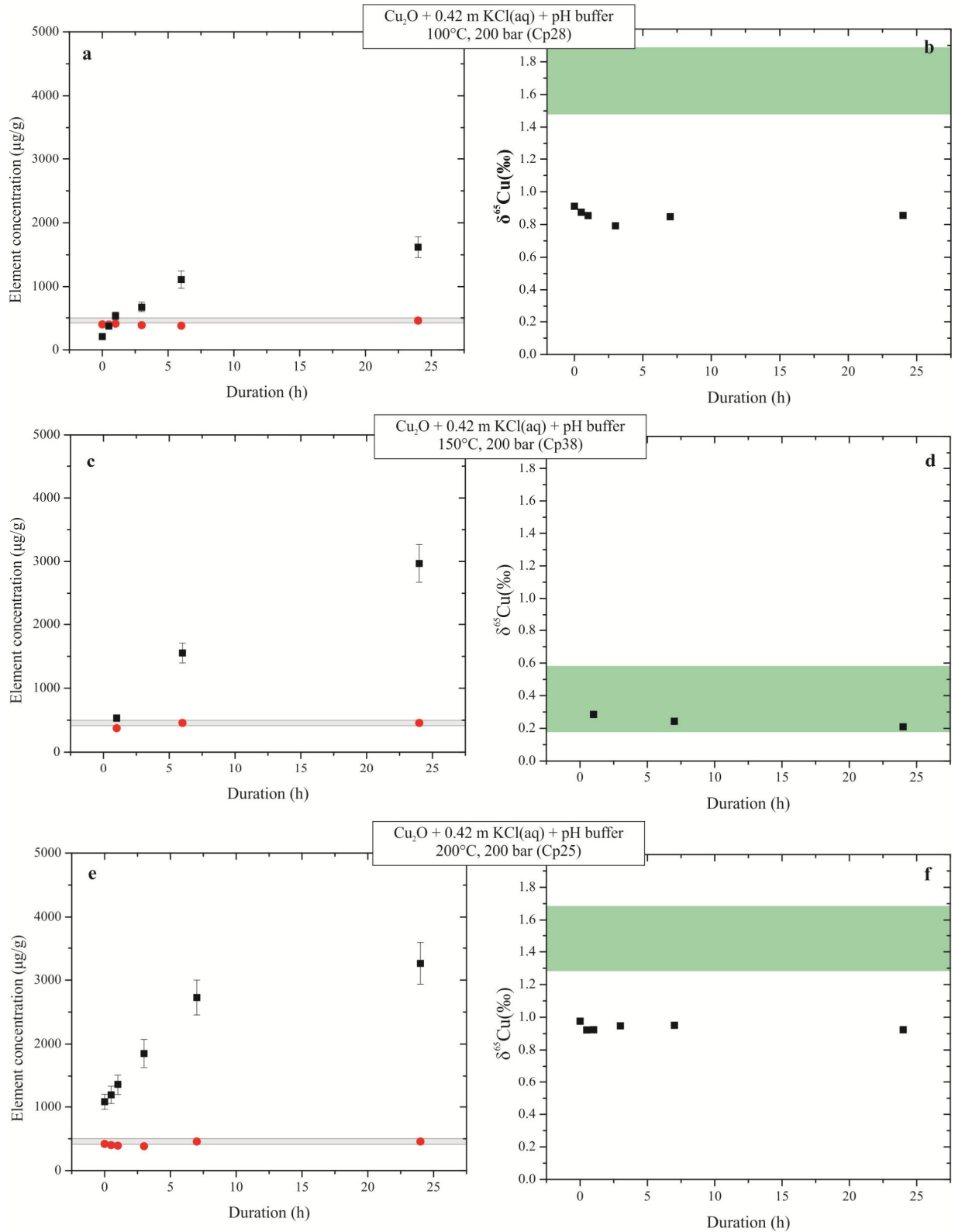
In the presence of pH buffer, pH values of the sampled fluids are in good agreements with the stock solutions, i.e., 4.77 ± 0.18 (Table 2, 3, 4). Without the presence of pH buffer (Cp42), the fluid acidity decreases with time, i.e., pH values of fluids rise from 5.54 to 6.81 and 9.28 after 1 hour, 12 hours and 72 hours, respectively (Table 1). Therefore, experiments are done in two fluids, i.e., acidic and neutral-basic fluids.

In 250°C run two fluids (i.e., 1st fluid is to flush pathway and 2nd fluid is similar to run fluids, mentioned above) have been sampled and the results indicate that there is almost no difference in elemental concentrations and isotopic compositions (Fig.2g, h). Later on we extracted two samples per time but only quantitatively analyze the 2nd extracted fluid and used the 1st fluid sample for pH determination. The results of elements concentration (all calibrated against dilution factor of Rb, see *Chapter IIA results*) and Cu isotope compositions are tabulated in Table 2.

Fig.2 shows the results from fluids collected from the runs with buffered KCl solution (at 0.42 m) at 20 MPa. Fig. 2a depicts that Cu concentration increases by factors of ~6 from 240 $\mu\text{g/g}$ to 1350 $\mu\text{g/g}$ within 6 hours at 100°C. As it is shown in Fig.2c, Cu concentration increases from 530 $\mu\text{g/g}$ to 2100 $\mu\text{g/g}$ when the temperature increases to 150°C. At 200°C, the Cu concentration gets doubled from 1100 to 2200 $\mu\text{g/g}$ within 6 hours (Fig.2e). The data agree within error for 6 and 24 hours, implying that the dissolution process is likely to be finished within 6 hours. When the temperature is elevated to 250°C, the Cu concentration rises steeply from 700 $\mu\text{g/g}$ to 3300 $\mu\text{g/g}$ within first 6 hours and is constant for the following 18 hours (Fig.2g). In all temperature ranges (100-250°C), it is likely that Cu content reaches constant within 24 hours.

At 150°C run, the initial and the final cuprite pellet are preserved and the isotope compositions can be well characterized. The isotopic data show that fluids of 150°C run yield slight lower or similar isotopic composition as their precursor cuprite (Fig. 2d). Since initial cuprite pellets of 100°C, 200°C and 250°C runs were not preserved, it is shown from Fig.2b, f and h that fluids yield much lower Cu isotope composition than expected possibly due to not well-defined isotopic values of initial cuprite in these runs. Therefore, there is almost no isotope fractionation between initial cuprite and fluids during cuprite dissolution process.

Chapter IIB



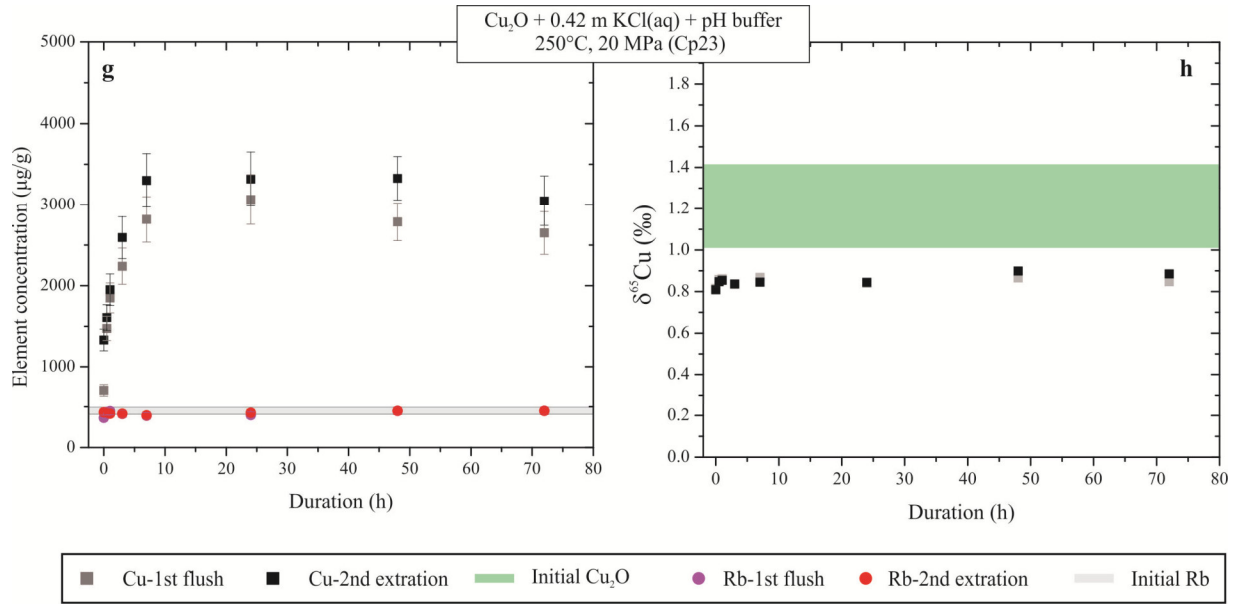


Figure 2 Elements concentration and Cu isotope composition as functions of run duration. All experiments were conducted in pH buffered KCl solutions at 20 MPa. (a, b) 100°C , 24 hours; (c, d) 150°C , 24 hours; (e, f) 200°C , 24 hours; (g, h) 250°C , 72 hours.

3.3 T, P, Cl and pH effects on cuprite dissolution process

Temperature, pressure, chloride concentration and pH effects on Cu content are shown in Fig.3. Among these factors, temperature, chloride concentration and fluid acidity strongly enhance the Cu content in fluids, whereas pressure has insignificant effect on Cu concentration. The details of the evolution of each set of experiments with time are presented in Table 2. Here, we take the concentration at 24 hours of each series.

In this study, a positive correlation between copper concentration and temperature is indicated from Fig.3a. Cu concentration increases steeply from $1600 \mu\text{g/g}$ at 100°C to $3000 \mu\text{g/g}$ at 150°C . At temperature $\geq 150^\circ\text{C}$, the enhancement of Cu concentration shows no dependence on temperature increment, i.e., $\sim 3000 \mu\text{g/g}$ Cu at temperature range of 150°C - 250°C . Liu et al. (2001) reported cuprite solubility data by using the silica tube technique (more details are given by Seward (1976)). They conducted experiments with cuprite and pH buffered NaCl solutions at vapor-saturated pressure ($<4 \text{ MPa}$; estimated from H_2O -NaCl phase diagram of Driesner and Heinrich (2007)). The pH buffered added in our study is similar to Liu et al. (2001). However, our data are much lower than the cuprite solubility data of Liu et al. (2001), especially at low temperature. This is probably due to sampling strategy, i.e., a collection of in situ hydrothermal fluids (this study) vs. bulk fluids containing possible cuprite particles (Liu et al. (2001)). In addition, the pressure is much lower in the experiments of Liu et al (2001) than ours, i.e., $<4 \text{ MPa}$ and 20 MPa (in general), respectively. Thus, the dominant transport medium either vapor or liquid may cause certain difference in metal transport process.

Chapter IIB

Fig.3b reveals the variation of Cu content with respect to fluid salinity at 250°C. The cuprite solubility data of Liu et al. (2001) demonstrate a positive correlation between Cu content and NaCl content (Fig.3b). It is worth noting that our data are in good agreement with Cu_2O solubility data of Liu et al. (2001) when chloride concentration is lower than 0.4 m (Fig.3b). In this study, a relative constant Cu concentration of $\sim 3200 \mu\text{g/g}$ is observed at Cl content of 0.4 - 0.9 m, which is almost half of the reported data of Liu et al. (2001) (Fig.3b).

Fig. 3c compares the results of the runs with and without pH buffer at the same condition of 250°C, 20 MPa and 72 hours. In comparison to a pH buffered system ($\text{pH} = 4.5 \pm 0.5$), the unbuffered fluids turn into basic ($\text{pH} = 9.3$) after 72 hours. Intriguingly, Cu concentration in pH buffered solution is by almost one order of magnitude higher than the fluids without pH buffer (Fig. 3c). This difference may be explained by the reaction kinetics which are slowed down in absence of the acetate buffer.

The increment of pressure from 5 MPa to 30 MPa has almost no effect on Cu content, producing $\sim 4000 \mu\text{g/g}$ Cu in 250°C fluids (Fig. 3d).

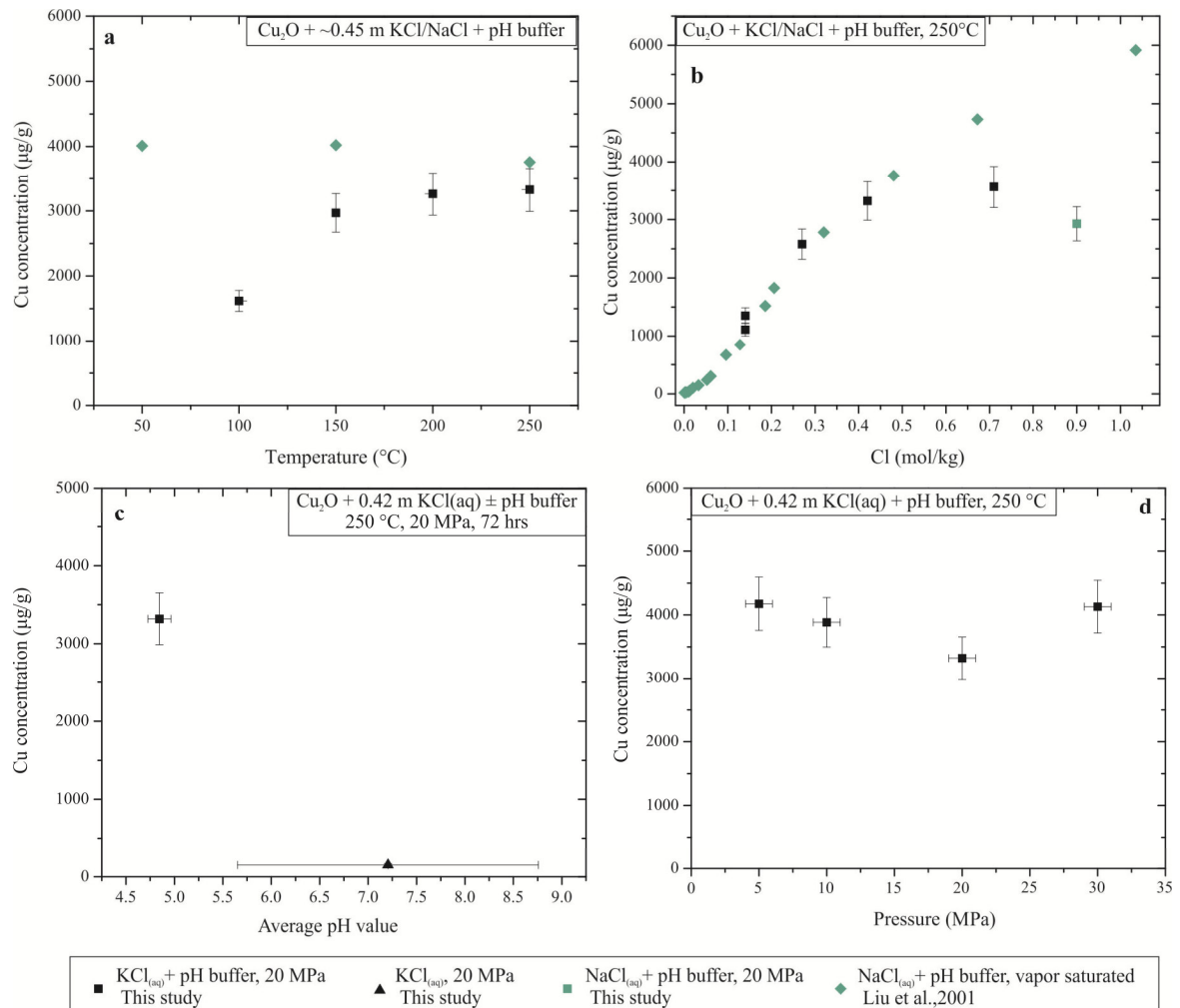


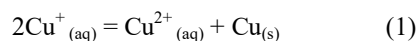
Figure 3 Cu content in fluids as functions of temperature (a), chloride concentration (b), pH (c) and pressure (d). Comparable cuprite solubility data are taken from Liu et al. (2001). Note that the pH values of unbuffered run change from 5.54 (1 hour) to 6.81 (12 hours) and 9.28 (72 hours), averaging 7.38 ± 1.54 (in (d)).

Table 3 Results of pressure and salinity series in the Cu₂O-KCl-HAc/KAc system at 250°C

SNO	t	pH ini.	pH 1 st fl.	Elements concentration				Cu isotope composition				
				Cu 2 nd fl µg/g	Cu res. µg/g	Rb ini. µg/g	Rb res. µg/g	2 nd fl % %	res. % %	Cu ₂ O* % %	in situ LA-ICP-MS Cu† % %	Cu‡ % %
Cp32	1	4.64±0.04	4.41±0.18	1717	1170	415	458	0.69±0.01	0.65±0.01	1.51±0.20	1.04±0.14	0.97±0.03
	6			4121		458		0.72±0.02				
	24			279		482		0.58±0.01				
Cp33	1	4.64±0.04	4.69±0.41	2355	1904	436	458	1.03±0.02	0.87±0.01	1.34±0.20	1.04±0.10	0.92±0.02
	6			3883		401		0.93±0.01				
	24			2678		458		0.98±0.01				
Cp34	1	4.64±0.04	4.37±0.19	2714	1938	444	458	0.97±0.04	0.85±0.01	1.33±0.20	1.00±0.13	0.95±0.03
	6			4129		432		0.86±0.01				
	24			2280		419		0.93±0.01				
Cp35	1	4.64±0.04	4.82±0.32	960	263	534	464	0.41±0.03	0.14±0.01	0.46±0.20	0.36±0.11	0.22±0.01
	6			1352		497		0.26±0.04				
	24			857		549		0.38±0.01				
Cp36	1	4.62±0.04	4.78±0.34	1958	2043	457	453	0.35±0.01	0.40±0.01	0.44±0.20	0.47±0.07	0.26±0.02
	6			2579		452		0.33±0.01				
	24			1641		436		0.40±0.02				
Cp37	1	4.55±0.04	4.92±0.34	2025	4562	457	463	0.14±0.01	0.21±0.01	0.56±0.20	0.03±0.12	0.01±0.03
	6			3564		416		0.07±0.01				
	24			3802		409		0.18±0.02				

3.4 The influence of the disproportionation of Cu(I) on Cu concentration and isotope fractionation

As mentioned before, native copper formation occurs exclusively at 250°C, which may be explained by Cu(I) disproportionation reaction (1).



Thus, this phenomenon was systematically investigated at 250°C with run time of 24 hours and varying Cl content and pressure.

In several runs, Cu concentration drops after 6 hours, i.e., loss of < 30% of dissolved Cu in solution (Fig.4a, c). This may be explained by Eq.(1) that up to 15% of dissolved Cu are deposited as native Cu, which reduces the total dissolved Cu in solution. The amount of native Cu precipitation is summarized from the mass gain of Au foil and Cu concentration of Au reaction cell (ICP-OES determination), which is in a good agreement with the estimation that <15% Cu is involved with native Cu deposition. On the other hand, there are two types of Cu species coexisting in the solution, i.e., Cu(II)_{aq} and Cu(I)_{aq} accounts for < 15% and > 85%, respectively. Cu content in the fluids keeps constant with native Cu precipitation when chloride concentration is above 0.41 m and pressure is 20 MPa (Fig. 4c).

However, there are other reasons contributing to Cu content reduction for 5 MPa and 30 MPa runs. The reason for the Cu concentration drop at 5 MPa is probably caused by a pressure decrease to 0.4 MPa after 6 hours reaction due to the malfunction of pressure pump. Even though the fluid sample was collected after 3 hours when the pressure was readjusted back to ~5 MPa, the final Cu concentration is 5 times lower than the maximum at 6 hours. In this case, Cu transport was controlled under vapor saturated condition rather than liquid saturated condition, which strongly lowers the Cu content (e.g., Rempel et al., 2012). Moreover, Cu isotopic data of the fluid sampled at 6 hours (fluid dominated by Cu⁺ species) is higher than that at 24 hours (fluid mixed with Cu⁺ and Cu²⁺; Fig. 4b), which may be expected that light isotope ⁶³Cu enters more readily in the vapor phase (dominant phase for the 6 hours). Additionally, a possible vapor + salt immiscibility field is also generated at this condition (based on the H₂O-NaCl phase diagram of Driesner and Heinrich (2007)). In the case of 30 MPa run, a reduction of Cu concentration at 24 hours is likely due to less sampled fluids than that at 6 hours, i.e., ~0.5 ml and ~1ml, respectively.

The isotopic compositions of native Cu have been analyzed by solution MC-ICP-MS (for Cu precipitates on Au bag) and in situ LA-MC-ICP-MS (for Cu precipitated on small pieces of Au foils). Data of both analyses are in good agreement, and the results are given in Table 3. To rule out any existing and/or superimposed Cu-bearing phases in reaction cell, here we use the data of in situ LA-MC-ICP-MS analyses. The isotope compositions of precipitated Cu on Au foils show a constant δ⁶⁵Cu value of ~1.0‰ in the pressure range of 5 MPa- 30 MPa. Whereas native Cu yields δ⁶⁵Cu values of 0.03‰ to 1.51‰ in runs with 0.14 m - 0.71 m KCl_{aq} solutions. The isotopic difference of native Cu may be due to different starting material, i.e., intact (Group I) and treated cuprite (Group II) pellets were used for pressure and salinity series runs, respectively.

As it is indicated from previous chapter IIA that fluids sampled within 6 hours at 250°C are dominated by Cu⁺ cations, whereas fluids sampled at late stage (e.g., > 24hours) likely incorporate Cu²⁺ cations (<15%) in addition to Cu⁺ cations (>85%). Accompanying native Cu precipitation, Cu(I) disproportionation reaction (7) induces certain isotope fractionation among different species. Fluids containing Cu²⁺ and Cu⁺ species yield similar or slightly higher

Chapter IIB

$\delta^{65}\text{Cu}$ values than the Cu^+ -bearing fluids (excluding 5 MPa run; Fig.4 b, 4d). It is evident that the average Cu isotope compositions of native Cu are $0.15\pm 0.07\%$ higher than the Cu^+ -bearing fluids (Fig.4 b, 4d).

The isotope compositions of fluids extracted from 5 MPa run show a different trend, i.e., $\delta^{65}\text{Cu}$ values of 0.72% and 0.58% for fluids sampled at 6 and 24 hours, respectively. This is probably due to a pressure drop from 5 MPa to 0.4 MPa at the early stage (mentioned above), vapor phase is not as competent as liquid phase in transporting isotopes. Thus a lowered isotope composition at vapor saturated condition (<6 hours) is expected.

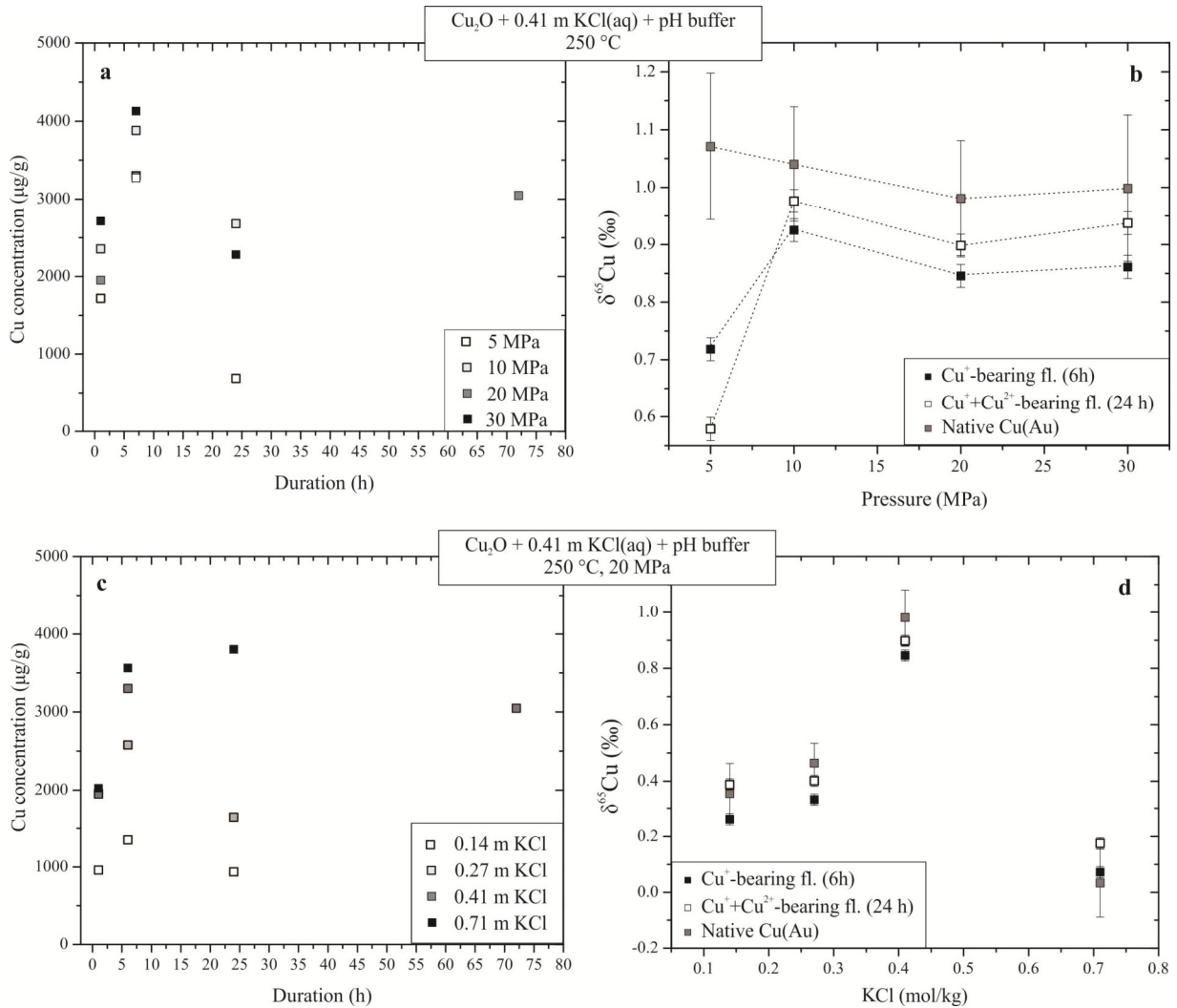


Figure 4 Variation of Cu concentration and Cu isotopic composition with respect to native Cu precipitation on Au foils. (a,b) Pressure series. (c, d) Salinity series. Cu^+ -fl. means the fluid containing Cu^+ cations. $\text{Cu}^{2+} + \text{Cu}^+$ -fl represents the fluid containing both Cu^{2+} and Cu^+ , which were sampled during native Cu precipitation.

4. Discussion

4.1 Cu speciation in fluids

Cu solubility studies (e.g., Xiao et al., 1998; Liu et al., 2001), spectroscopic investigation (e.g., Brugger et al., 2007; Schmidt et al., 2018) are in general agreement that copper is transported as Cu(I) in hydrothermal fluids, predominantly as linear $\text{CuCl}_2^-(\text{aq})$ complexes, the stability of which increases with temperature (Fig.5). The thermodynamic properties of copper (I) chloride complexes have been reviewed by Liu and McPhail (2005).

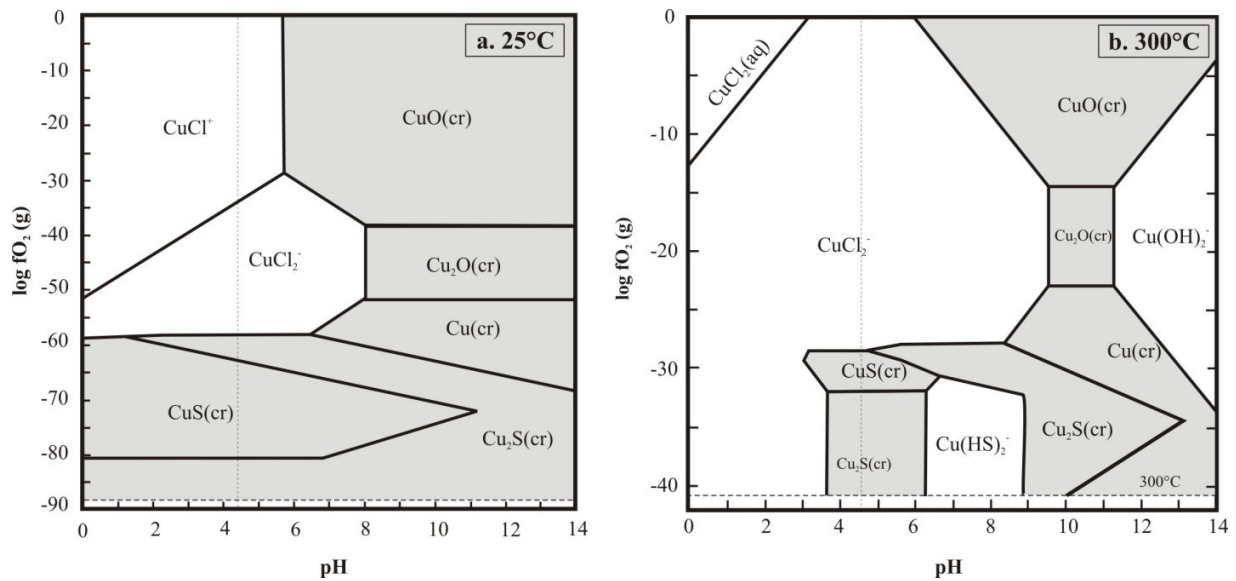
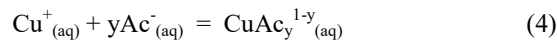
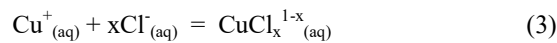
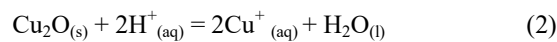
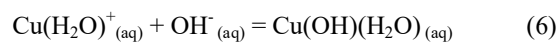
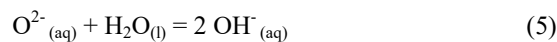


Figure 5 Mineral solubility and dominant aqueous complexes for Cu in hydrothermal solutions at 25°C (a) and 300°C (b) (Etschmann et al., 2010). The thermodynamic modeling is assumed at the condition: $\text{Cu}_{\text{tot}} = 10^{-3} \text{ m}$, $a_{\text{Cl}^-} = 2 \text{ m}$, $a_{\text{S}} = 0.2 \text{ m}$.

A thermodynamic model of Liu et al. (2001) suggest the following possible reactions between cuprite and fluids at temperature $\leq 250^\circ\text{C}$:



where subscripts x and y represent the number of chloride and acetate ligands, respectively. The presence of Cu-hydroxide complexes is unlikely in all pH buffered runs due to the pH range (approximately 4.6 ± 0.5 in this study), and the hydrolysis constants for Cu(I) is much lower than that of copper chloride and copper acetate ($\log K_{\text{CuOH}} = -6.39$ at 250°C , $\log K_{\text{CuCl}} = 3.76$ at 150°C and 3.97 at 250°C , $\log K_{\text{CuAc}} = 2.26$ at 150°C ; Liu et al. (2001)). In comparison to the pH buffered system, Cu content is strongly reduced in the unbuffered system, accompanying by a decrease in acidity (from 4.5 to 9.3). The possible reactions are:



Chapter IIB

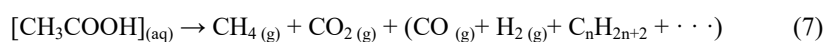
According to Liu et al. (2001), the speciation of copper at our run conditions (solutions with Cl⁻ concentration >0.1 m and temperature of 150°C - 250°C) suggests that CuCl₂⁻ and CuCl_(aq) are the major species in solution, accounting for > ~60 mol % CuCl₂⁻ and < ~35 mol % CuCl_(aq), respectively, with little contribution of CuCl₃²⁻ (< ~5 mol %).

The Cu(I) disproportionation reaction or the coexistence of Cu⁰, Cu⁺ and Cu²⁺ in fluids are not been favored by the current spectroscopic studies (e.g., Collings et al., 2000; Berry et al., 2006; Schmidt et al., 2018) and the phase diagram (e.g., Fig.5). Although spectroscopic analysis has confirmed the formation of native copper and mixture of Cu⁺ ([CuCl₂]) and Cu²⁺ in the fluid, these phenomena are attributed to beam damage (Berry et al., 2006).

However, there are other evidences supporting the possibility of the Cu(I) disproportionation reaction. The aqueous cupric chloride complexes can be stable up to 175°C in oxidized NaCl solutions determined by EXAFS (Collings et al., 2000). Solid state reaction demonstrates that cuprite disproportionates into CuO and Cu at temperature >200°C and pressure higher than 5000 MPa (Belash et al., 1977; Webb et al., 1990). In nature, Thornber (1985) proposed the likelihood of Cu(I) disproportionation reaction (Eq.(1)) in supergene environment and suggested that this reaction is favored by the existing metallic surface for native Cu nucleation in a region of pH <6. In order to verify whether the formation of native Cu and Cu(I) disproportionation reaction is dependent on the experimental vessel, we performed additional experiments with cuprite in NaCl/HCl/NaCl+acetate solutions in cold seal pressure vessel with a log₁₀fO₂ of ~NNO+2.3 (Details are given in Appendix A3). Native Cu precipitates on Au capsules have been confirmed in these runs. Without apparent reducing agent and direct spectroscopic evidence of Cu²⁺, our favored explanation for the formation of native copper is disproportionation of Cu⁺ at run condition (i.e., 250°C;).

4.2 Thermal decarboxylation of acetate

Decarboxylation is a term for the decomposition of carboxylic acids where the carboxyl group is liberated, usually involves cleavage of the C-C bond. The decarboxylation of aqueous acetic acid can be represented by the general equation:



The thermally induced decarboxylation of acetate has been well studied by (Kharaka et al., 1983; Drummond and Palmer, 1986; Palmer and Drummond, 1986; Bell et al., 1994). Indeed, acetate can survive at low hydrothermal temperature (e.g., 100°C) over billion years to promote the mobility of metals as acetate complexes (Drummond and Palmer, 1986; Bell et al., 1994). With the temperature increase, the decarboxylation rates are enhanced, e.g., 9000 h at 360 °C (in gold reaction cell; Palmer and Drummond, 1986). The principal products of acetic acid decomposition are generally CH₄ and CO₂, but varying amounts of CO, H₂, and volatile hydrocarbons are also observed (e.g., Kharaka et al., 1983; Palmer and Drummond, 1986).

Experimental determinations of decarboxylation rates in stainless vessel (Kharaka et al., 1983), Ti vessel, Au cups, silica tubes and Pyrex tubes (Palmer and Drummond, 1986) have shown that, although aqueous solutions of acetic acid are relatively stable and the decomposition reaction is sluggish, decarboxylation can be enhanced by a

Chapter IIB

suitable catalytic mineral surface. As a matter of fact, decarboxylation is used to test the catalytic properties of metals, which can be served as potentially useful industrial catalysts (Rajadurai, 1987; Kim and Barteau, 1988).

Catalytic effects of mineral surfaces on decarboxylation of acetic acid and acetate have been investigated by Palmer and Drummond (1986) and Bell et al. (1994). Passivated titanium cell (surface covered by TiO₂) and Au cell do not catalyze aqueous decarboxylation reactions, in contrast hematite and synthetic minerals such as pyrite and magnetite affect profoundly the decomposition of acetic acid and result in rapid reaction kinetics (Bell et al., 1994). For example, at 350°C the half-life for acetic acid decomposition is ca. 5000 hours in titanium cell with the presence of TiO₂ (Palmer and Drummond, 1986), however, the half life can be shorted to ca. 100 hours with the presence of hematite in the same vessel (Bell et al., 1994). In addition, Drummond and Palmer (1986) demonstrated that the presence of acetic acid / acetate accelerated the equilibration of the hematite-magnetite oxygen buffer, and extended the useful temperature range of the oxygen buffer below 300°C.

The result of gas components obtained after a duplicate run in the system of KCl- HAc-KAc (details are given in Appendix A2) has been compared with water±acetate systems and all data acquired at 250°C and 20 MPa for 72 hours are tabulated in Table 4 in Chapter IIA. The data indicate that CH₄ and CO₂ are the dominant products, accounting for 56 mol% and 44 mol% (Table 4), respectively. Furthermore, no detectable acetic acid can be found, implying a total consumption of acetic acid (0.2 mol/kg). The estimation of the production of CH₄ and CO₂ can generate 20% of Cu²⁺ in the bulk solution (predominated by Cu⁺). Thus, the presence of cuprite (especially in nanoparticle form) and chloride can substantially reduce the time needed for acetic acid decomposition from ca. 2×10⁶ hours in Au reaction (Palmer and Drummond, 1986) to 72 hours. The ability of synthetic cuprite to affect the decomposition of acetic acid may be due to its surface. Note that there are pores or cavities existed at the surface of the cuprite pellet (Fig. 1a). These sites suitable for decarboxylation may function as true catalyst, such that the overall rate of decarboxylation is governed by the rates of adsorption/desorption of acetic acid molecules onto these sites and the rate of the subsequent decomposition of the adsorbed species (Palmer and Drummond, 1986). The adsorbed acetic ions enable the mobilization of metals because metal-acetate complexes are stronger than the analogous chloro-complexes (Bell et al., 1994). Apparently, dissolved Cu in the pH buffered KCl solution can be 20 times higher than that in pure KCl solutions (Fig. 3c). Note that Cu content in pure KCl solution (Cp41) increases from 98 µg/g to 152 µg/g and 41 µg/g after 1, 12 and 72 hours, respectively.

The production of native Cu is also enhanced by the presence of acetate/acetic acid, which is strongly dependent on the amount of dissolved Cu in fluids. For example, more Cu crystals (< 200 µm) grow at the interface between cuprite pellet and Au foil with the presence of acetate/acetic acid (Fig. 1c), whereas only little Cu crystals (<50 µm) has been found in the pure KCl system (Fig. 1e, f). Kharaka et al. (1983) found that there are large amount of hydrogen gas produced at the initial stage of decarboxylation. This evidence may help to understand the formation of native Cu after certain period (i.e., > 6 hours) due to possible H₂ production and disproportionation reaction.

The catalytic effect of copper bearing minerals on decarboxylation has not been well determined. We can consider analogous catalytic effect of Cu on other acid. For example, it is known that amino acid condensations are

catalyzed by copper chloride in reaction mixtures containing high concentration of NaCl. These reactions are mainly governed by the Cu(II) catalytic effect and by the water-removing force of concentrated chloride solutions.

Although the nature of the reaction has not yet been identified unequivocally, it is apparent that the presence of acetic acid and acetate may play a significant role in increasing Cu content in 250°C fluids, e.g., 3300 µg/g (with HAc and KAc) and 160 µg/g (without HAc and KAc). In addition, cuprite and/or chloride cause an extremely rapid decomposition of acetic acid.

4.3 Fractionation mechanism

Due to the complexity of our experiments, we consider the following possible steps for Cu mobilization: (i) release of copper from cuprite by dissolution reaction; (ii) disproportionation reaction of Cu(I) to Cu(II) and native Cu, which occurs in all 250°C runs; (iii) decarboxylation reaction of acetate. Among three steps, only the second step induces isotope fractionation.

The reasonable explanation for the formation of native Cu and Cu concentration (after Rb correction) starts to decrease after 6 hours in all 250°C runs is that Cu(I) disproportionation reaction occurs and predominates at late stage (>6 hours). This reaction path has been further explored by temperature cycling experiments (Cp6 and Cp39; Table 4). Fig. 6 shows that Cu concentration of fluids increases steeply at the early stage of cuprite-fluid interaction, and starts to decrease after ~30 hours when temperature increases from 150°C to 250°C. The decreasing trend of Cu in hydrothermal fluids is potentially related to the deposition of native Cu (Fig.6a, c). Subsequently, the disproportionation reaction will cause Cu isotope fractionation between different Cu oxidation states, e.g. favoring heavy isotope (⁶⁵Cu) in residual aqueous which may contain <15% Cu²⁺ and >85% Cu⁺ and slightly lower fractionation between precipitated Cu metal and dissolved Cu(I) (Fig. 6b, d). In acidic KCl solution, $\Delta^{65}\text{Cu}_{[\text{Cu(II+I)-Cu(I)}]}$ and $\Delta^{65}\text{Cu}_{[\text{Cu(0)-Cu(I)}]}$ values are ~-0.30‰ and ~0‰, respectively (Fig. 6b). In acidic NaCl solution, the isotopic fractionation determined in Fig.6d can be a qualitative estimation because no intermediate sampling between 1 and 72 hours was done at 250°C, i.e., $\Delta^{65}\text{Cu}_{[\text{Cu(II+I)-Cu(I)}]}$ and $\Delta^{65}\text{Cu}_{[\text{Cu(0)-Cu(I)}]}$ values are ~-0.40‰ and ~-0.3‰, respectively. In combination of the previous data shown in Fig. 4 (pressure and salinity series at 250°C), the fractionation between Cu(II) and Cu(0) during the disproportionation reaction is estimated to be <~-0.4‰, which is followed by isotopic re-equilibration between Cu(I) and Cu(II) in the fluid.

Chapter IIB

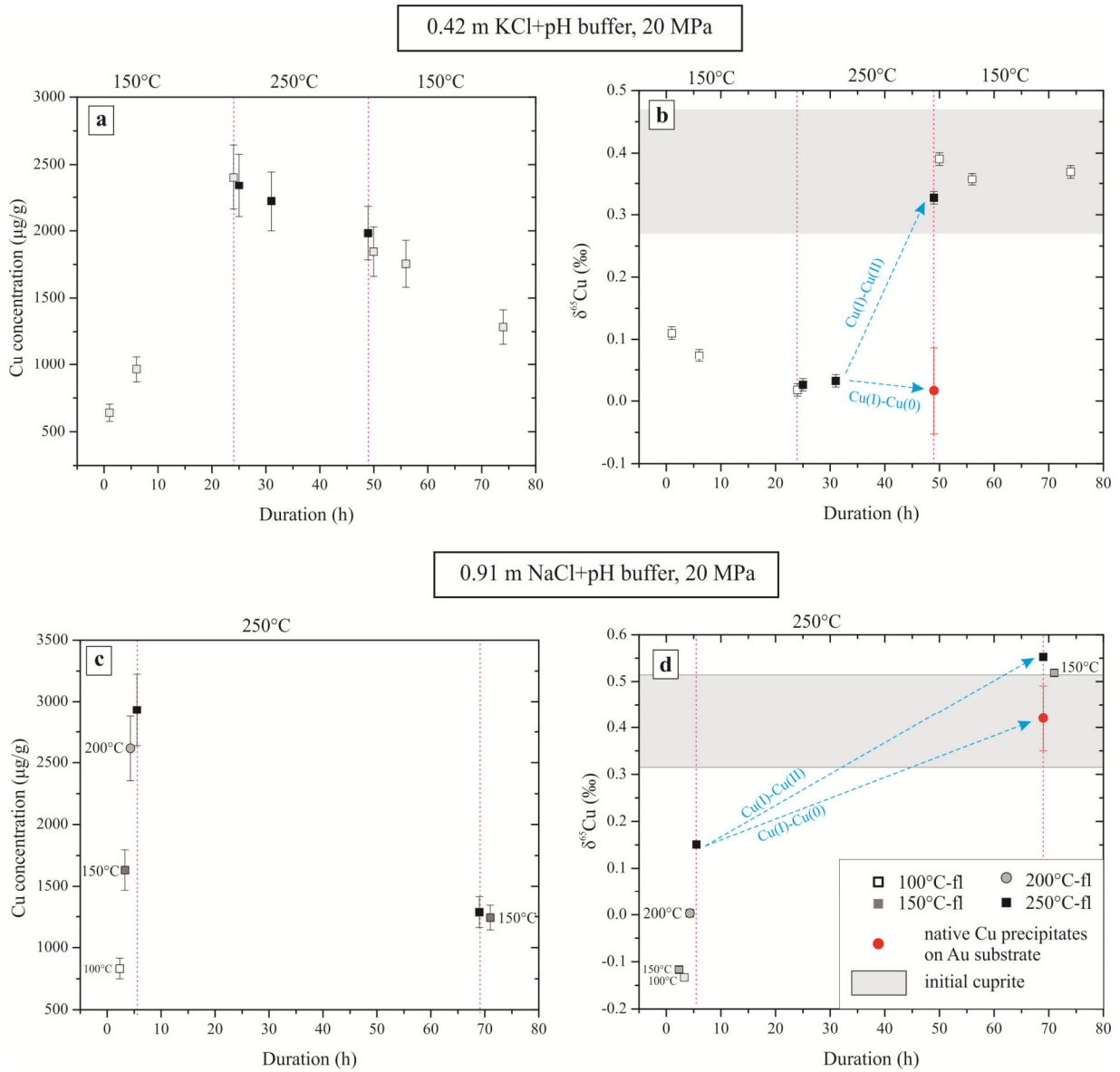


Figure 6 Cu concentration and Cu isotope fractionation in KCl and NaCl solutions. (a, c) Cu concentration variations in buffered KCl and acetic solutions. (b, d) Cu isotope fractionation between in situ fluids, native Cu and cuprite. The errors show the likelihood of isotope fractionation induced by disproportionation reaction. In order to simply the expression, Cu(II) in (b, d) represents dissolved Cu(I) and Cu(II) cations in solution. Note that the Cu(II) in the solution may account for <15%.

When does the disproportionation reaction occur at run conditions is not known precisely, we can gain insight from the predicted isotope fractionation between Cu(II) and Cu(I) in aqueous Cl-bearing solutions. The equilibrium fractionation factors is expressed as Eq.(9):

$$\begin{aligned} \Delta^{65}\text{Cu}_{\text{A-B}} (\text{‰}) &= \delta^{65}\text{Cu}_{\text{A}} - \delta^{65}\text{Cu}_{\text{B}} \\ &\approx 1000 \cdot \ln \beta_{\text{Cu(A)}} - 1000 \cdot \ln \beta_{\text{Cu(B)}} \quad (8) \end{aligned}$$

Chapter IIB

where β factors are predicted values based on species vibrational frequency. Moynier et al. (2017) summarized the β factors for Cu-bearing species (solid minerals as well as aqueous Cu complexes), which will enable us to calculate the estimated fractionation between cupric and cuprous ions. It is previously mentioned that CuCl_2^- is the dominant complexes at high temperature during the dissolution of cuprite in KCl solutions. At equilibrium, the upper and lower boundaries of isotope fractionation between Cu^{2+} and Cu^+ are derived from Eq.(9) and shown in Fig. 7, i.e., $\Delta^{65}\text{Cu}_{\text{CuCl}^+ - \text{CuCl}_2^-}$ and $\Delta^{65}\text{Cu}_{\text{CuCl}_3^- - \text{CuCl}_2^-}$, respectively. The observed $\Delta^{65}\text{Cu}$ values (0.3-0.4‰; Fig.7) at 250°C lie in the range of the predicted range (data obtained from Moynier et al. (2017)), which may explain the likelihood of Cu(I) disproportionation reaction.

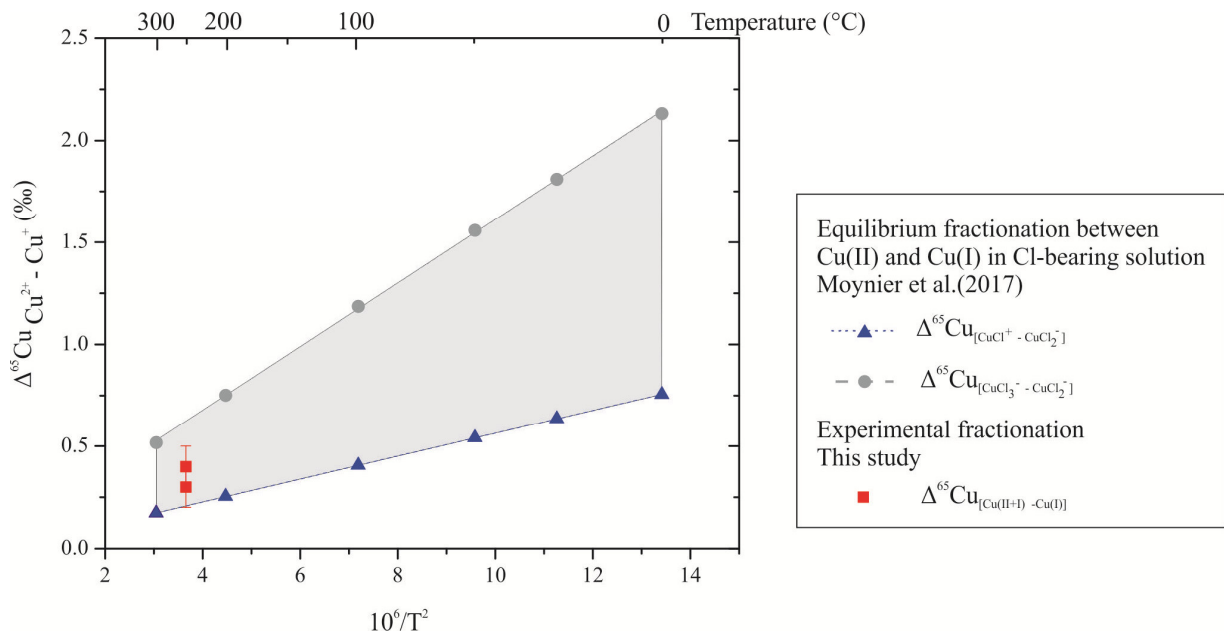


Figure 7 Isotope fractionation between aqueous cupric and cuprous chloride complexes as function of temperature. Upper (defined by gray circles) and lower (defined by blue triangular symbols) boundaries of isotope fractionation are calculated based on Eq.(9) and data in Moynier et al. (2017). The red symbols are the data calculated from Fig.6.

Chapter IIB

Table 4 Results of temperature cycling experiments in the Cu₂O-KCl/NaCl-HAc/KAc system at 20 MPa

SNO	t	T	Elements concentration					Cu isotope composition							
			pH	pH	Cl	Cu	Rb	Solution MC-ICP-MS		in situ LA-ICP-MS					
	h	°C	ini.	1 st fl	m	2 nd fl.	res.	2 nd fl.	ini.	2 nd fluid	res.	Cu ₂ O	Cu†	Cu‡	
						µg/g	µg/g	µg/g	µg/g	%	%	%	%	%	
Cu₂O+KCl+pH buffer															
Cp39	1	150	4.64±0.04	5.15±0.26	0.41	641	2543	445	458	0.11±0.01	0.44±0.02	0.37±0.20	0.02±0.07	0.05±0.02	
	6	150				965		451		0.07±0.02					
	24	150				2404		475		0.02±0.03					
	25	250				2341		401		0.03±0.01					
	31	250				2223		397		0.03±0.02					
	49	250				1982		458		0.33±0.01					
	50	150				1844		458		0.39±0.03					
	56	150				1754		458		0.36±0.01					
	74	150				1282		458		0.37±0.01					
Cu₂O+NaCl+pH buffer															
Cp6	2	100	4.54±0.04	n.m.	0.90	832	841	630	450	-0.12±0.01	0.14±0.02	0.41±0.20	0.42±0.09	0.37±0.05	
	3	150				1631		543		-0.13±0.02					
	4	200				2615		536		0.00±0.01					
	6	250				2930		470		0.15±0.02					
	70	250				1234		442		0.55±0.01					
	71	150				1214		450		0.52±0.01					

Notes:

n.m. denotes fluid acidity was not measured.

Run duration (t in hours) denotes the time after reaching the targeted temperature (e.g., 150°C of Cp39 and 100°C of Cp6).

Note that both cuprite pellets (prior to and after experiment) of Cp39 were preserved, while only the reacted pellet of Cp6 was retrieved.

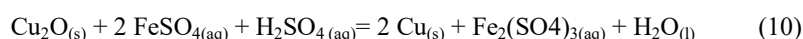
4.4 Implications

Spectroscopic investigation (Fulton et al., 2000a), experimental and thermodynamic data (Xiao et al., 1998; Liu et al., 2001) show that cuprous copper species are stable at temperature higher than 100°C. The study of Cu(I) mineral (e.g. cuprite, Cu₂O) is of practical importance for Cu transport in crustal hydrothermal fluids.

Supergene alteration occurs during weathering of primary, hypogene ore minerals, where mainly sulfides are oxidized and their metal ions are redistributed by near surface percolating ground water. The coexisting Cu⁰, Cu⁺, and Cu²⁺ minerals can be found even within a single hand specimen in this setting. Such deposits are important metal sources, which supply over 50% of the Cu production on Earth (Sillitoe, 2005). Copper not only precipitates as copper sulfide phases in the supergene system, but also precipitates as sulfates and oxides (Tittley, 1978). The low temperature weathering, where temperature-dependent fractionation might a priori be predicted to be large, and the coexistence of minerals with multivalent cationic states, make supergene alteration an ideal environment in which to study fractionation of transition metal isotopes, e.g. Cu isotopes.

In the leaching event, alteration and weathering of primary copper minerals produce a wide copper isotope range in low-temperature secondary copper minerals. The precursor Cu(I) minerals will dissolve oxidatively to release isotopically heavy copper from the solid reservoir into solution (Zhu et al., 2000; Larson et al., 2003; Rouxel et al., 2004; Mathur et al., 2005; Asael et al., 2007; Mathur et al., 2009). A sample with both native copper and cuprite from Ccatun Pucara deposit, Tintaya district, Peru, was analyzed by Larson et al. (2003). Cuprite yields a slight higher δ⁶⁵Cu value than native copper, i.e. -0.54‰ and -0.83‰, respectively. However, a detailed paragenetic relation between these minerals was not reported in this study. A possible reduction/oxidation reaction may be responsible for this small fractionation, Δ⁶⁵Cu_{[Cu(0)-Cu₂O]}} = -0.29‰. Moreover, native copper even from the same locality produces different values, e.g. 0.72‰ (Ray-2b) and -0.04‰ (Ray-1) from Ray Arizona, USA (Larson et al., 2003). This is consistent with our findings that the isotopic composition of native copper is strongly dependent on the conditions and its precursor mineral.

Interestingly, both Cu(II) and Cu(0) minerals are coexisting in one hand sample due to secondary process, which have been collected from metamorphosed Besshi-type volcanogenic massive sulfide (VMS) deposits in Japan (Ikehata et al., 2011). It is worth noting that secondary minerals show higher δ⁶⁵Cu values than inferred Cu(I) precursor mineral. Although the formation mechanism of secondary copper minerals are not fully understood yet, they proposed possible redox reactions with cuprite as the precursor mineral (Ikehata et al., 2011). Both malachite and native copper are possibly generated by reduction and/or oxidation of cuprite via



However, the production of malachite (Cu(II)) and native copper (Cu(0)) could be due to cuprite disproportionation process, similar to this study. In this sense, the experiments conducted in this study are thought to provide new evidence for what happened in nature. The oxidative dissolution of cuprite releases Cu(II) into solution whose δ⁶⁵Cu values can be higher by up to 1‰ at 150°C and 0.4‰ at 250°C, accompanying by the formation of native Cu who inherited its precursor's isotope signature but slightly lower than the Cu(II) species. Therefore, ⁶⁵Cu

has been transported from primary Cu(I) species to secondary phases, more likely to the observation of Ikehata et al. (2011).

Our experiments are of great interest to natural systems due to an appropriate pH range, 4 - 9. The results show that isotope fractionation of acidic fluids (under pH buffered conditions) is more significant than those neutral-basic (without pH buffer) fluids. The possible explanation is that Cu solubility and speciation in fluids play a vital role in isotope fractionation. Cu concentrations in acidic fluids are at least by one magnitude higher than those in neutral-basic fluids. The speciation of Cu may change from $\text{CuCl}_2^-/\text{CuAc}_2^-$ in acidic solution to Cu-bearing aqua complexes or $\text{Cu}(\text{OH})_2^-$. According to the predicted β values from Moynier et al. (2017), this change will attenuate the isotope fractionation, e.g. $\Delta^{65}\text{Cu}_{[\text{Cu}(\text{H}_2\text{O})_2^+ - \text{Cu}_2\text{O}]}$ and $\Delta^{65}\text{Cu}_{[\text{CuCl}_2^- - \text{Cu}_2\text{O}]}$ are -0.22‰ and -0.45‰, respectively.

In addition, the speciation of copper in the liquid is a function of temperature, Cl^- activity (simplified as concentration) and $f\text{O}_2$. At higher temperature, higher chloride concentration, CuCl_2^- turns into major species. Thus, isotope fractionation related to CuCl_2^- gets more pronounced than $\text{CuCl}_{(\text{aq})}$.

Pressure (fluid density) has strong influence on isotope fractionation. In pH buffered KCl solutions, low pressure (i.e. 5 MPa) favors stronger fractionation than high pressure, which is probably due to light isotope (^{63}Cu) can be easily transported by the diluted fluid. In pH buffered acetic solutions, pressure in the range of 10-20 MPa strongly fractionates Cu isotope in comparison to the high and low pressure (30 MPa and 5 MPa), $\Delta^{65}\text{Cu}$ value of -0.5‰ at 10 MPa increases to nearly -0‰ at 50 MPa and 30 MPa. Fluid densities at low and high pressure are vapor-like and dense, which are not suitable for ^{63}Cu transport in acetic fluids.

5. Conclusion

Copper content and isotope fractionation has been determined experimentally between cuprite and KCl-bearing hydrothermal fluids. The experiments were conducted in a Au reaction cell at temperature range of 100°C -250°C, pressure of 5 MPa - 30 MPa for up to 72 hours in 0.14 - 0.72 mol/kg chloride solutions (with/without the presence of pH buffer (0.2 m HAC/KAc)), with all starting solutions acidity of 4.5. Native copper is exclusively observed in all 250°C runs.

Three competing reactions control the Cu transport and precipitation processes, i.e., simple cuprite dissolution, Cu(I) disproportionation into Cu(II) and native Cu, and decomposition of acetate into methane and carbon dioxide. During the early stage (<24 hours) cuprite dissolution process, constant Cu content can be achieved within 6 hours at 100°C - 250°C. Cu dissolved in pH buffered KCl solutions is ~20 times higher than that in pure KCl_{aq} , i.e., 160 $\mu\text{g/g}$ and 3200 $\mu\text{g/g}$, respectively. In pH buffered solutions: (i) the increment of temperature and salinity strongly promotes Cu dissolution, i.e., increasing from 1000 $\mu\text{g/g}$ at 100°C to ~3000 $\mu\text{g/g}$ at 250°C and 1350 $\mu\text{g/g}$ at 0.71 m KCl to 4300 $\mu\text{g/g}$ at 0.71 m KCl; (ii) Cu content remains rather constant value of ~3500 $\mu\text{g/g}$ with pressure ranging from 5 MPa to 30 MPa. Cu isotope fractionation is induced by the Cu(I) disproportionation reaction, i.e., the average $\Delta^{65}\text{Cu}_{[\text{Cu}(0)-\text{Cu}(I)]}$ value is 0.15±0.07‰. It is likely that the reduction of dissolved Cu at 250°C after 6 hours is due to decarboxylation of acetate and/or acetic acid.

Chapter IIB

It is evident that acetate doped KCl solutions transport one magnitude more dissolved Cu than pure KCl solution, implying that acetate acts as catalyzer in dissolving more Cu in fluids. However, cuprite has an active catalytic effect on accelerating decarboxylation reaction. Our findings can help to understand the formation of sediment-hosted Cu ore deposits and weathering process in supergene environments where multivalent of Cu species are present, e.g. Cu^{2+} , Cu^+ and Cu^0 .

Acknowledgments

This research was supported by the German Academic Exchange Service (DAAD-57076462) and Graduate School GeoFluxes. We thank U. Kroll, A. Reimer and J. Feige for their technical support.

Appendix:

A1. Cuprite pellets preparation procedure

Copper (I) oxide powder (97% purity, purchased from Sigma-Aldrich) was used for pellet preparation. The pressure of the die was set 100 MPa to check the quality of the pellet. As the fragility of the pellet, an increased pressure up to 140 MPa was applied to attain better quality. After this pressure the pellet was intact but upon removal from the die module it broke into pieces. Bigger broken pieces of Cu_2O pellets were selected to do sintering later in a horizontal reduction furnace. The first batch experiment was done at 1027°C , 30 hours at atmosphere condition. The second batch was conducted CO_2 atmosphere, i.e., 927°C , $\log f\text{O}_2 = -3$, 4 hours.

All pellets were characterized by X-ray-powder diffraction on a Philips PW-1800 powder diffractometer. The WinXpow software (STOE) and the TOPAS software (Bruker) were used for data evaluation. The X-ray powder pattern of the 8 h product was further analyzed to check any impurities in the pellets (Buhl et al., 2010). The sintered samples were cut through and analyzed with XRD to check the homogeneity of the composition on the surface and cross-section. XRD analyses (Fig.A1) show that the synthesis of cuprite pellet at atmosphere condition may contain some impurities while the purity will be significantly enhanced at reduced conditions ($f\text{O}_2 = 10^{-3}$ bar).

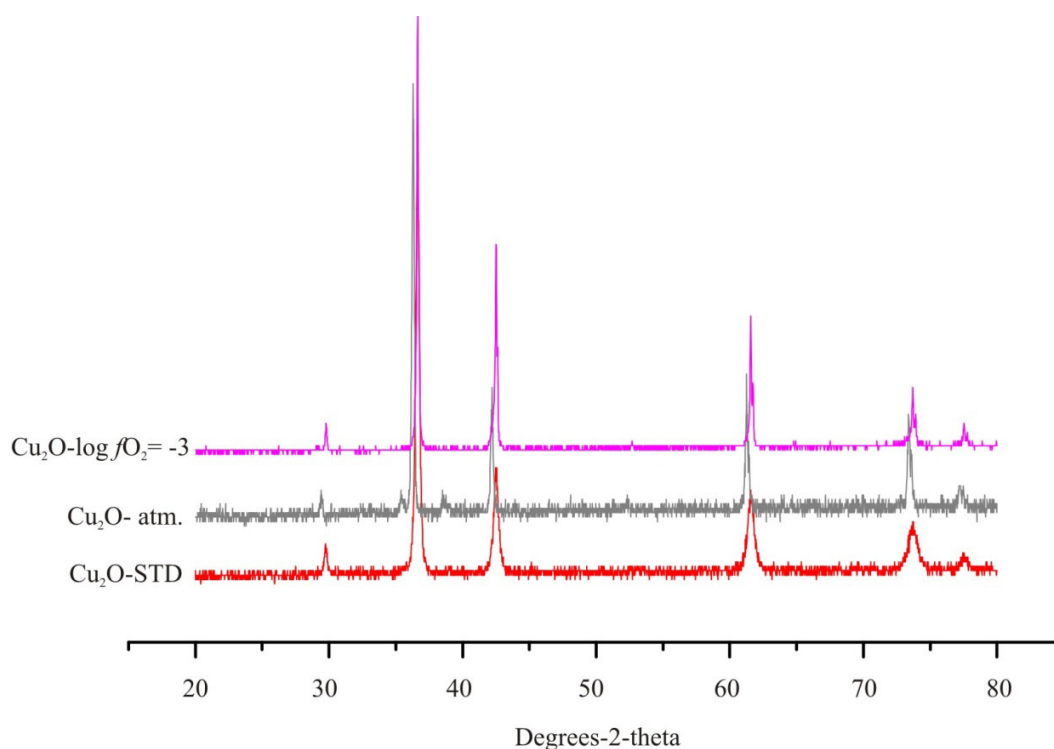


Figure A1-1 XRD analyses of synthesized cuprite pellets. Cu_2O -atm. and Cu_2O -log $f\text{O}_2$ are the cuprite pellets sintered at atmosphere condition and reduced condition, respectively (for more details see text).

Chapter IIB

Due to the fragility of cuprite pellet, an improved method by the introduction of some polyvinylalcohol was applied and used to enhance the quality. The addition of polyvinylalcohol would help to increase the mechanical stability of the pellet during preparation. The details are as follows:

- a) The mixture was prepared by adding 9 g of copper(I) oxide and 15 ml distilled water in a glass beaker;
- b) PVA, about 2 % of the copper(I) oxide weight, was weighed and loaded into the starting solution.
- c) The mixture should be stirred thoroughly for 1-2 min;
- d) The beaker was placed on a magnetic hot plate with magnetic stirrers inside to increase the system's homogeneity. The temperature was set to 80 - 100°C to cook the mixture.
- e) After 2 hours sitting on the hot plate the water was already evaporated and the powder was retrieved from the beaker.
- f) Prior to pressing into the pellet, the required amount of powder was grinded with agate mortar until the powder was fine enough.
- g) Applying 140 MPa of the steel die would be the optimum pressure to keep pellet intact, afterward the disks were ~ 1 g, 13 mm diameter and 2 mm thickness.

h) The pressed cuprite pellets were loaded in a ceramic boat which was covered by copper foils. The sintering of these pellets was done by two steps. The first step was to remove polyvinylalcohol from the pellets, which was achieved by increasing temperature at a rate of 50 K/h to 300°C and this temperature was fixed for next two hours. Secondly, these pellets were heated in the same furnace directly to 1030°C at atmospheric condition, which supposed to be in the stability field of cuprite (Neumann et al., 1984). The sintered pellets were later analyzed with EMP analyzer. The results indicate that native copper nuggets are present in cuprite pellet at this condition (Fig. A1-2a). This may be explained by Cu(I) disproportionation reaction that results in the formation of native Cu and tenorite. Native copper was found in the cuprite pellets (Fig. A1-2a) and tenorite may precipitate at the surface of native copper. Although we did not analyze the composition of the Cu foil, we observed a color change of the Cu foil from metallic color (before sintering) to black color.

i) Thus, an improved step was conducted to increase the pellet purity. Pellets after the first step (combustion of polyvinylalcohol at 300°C) were rapidly transferred to a reduction furnace which was pre-heated to 927°C, and oxygen fugacity is fixed at 10^{-3} bar, which is also in the stability field of Cu_2O . After the sintering, the Cu foils almost remained their metallic color. Moreover, the EMP analysis indicates that cuprite pellet sintered in reduced condition turns out to be pure and homogeneous (Fig. A2b). Therefore, we used the later conditions, i.e., 927°C, $\log f\text{O}_2 = -3$ and 24 hrs for all cuprite pellets preparation.

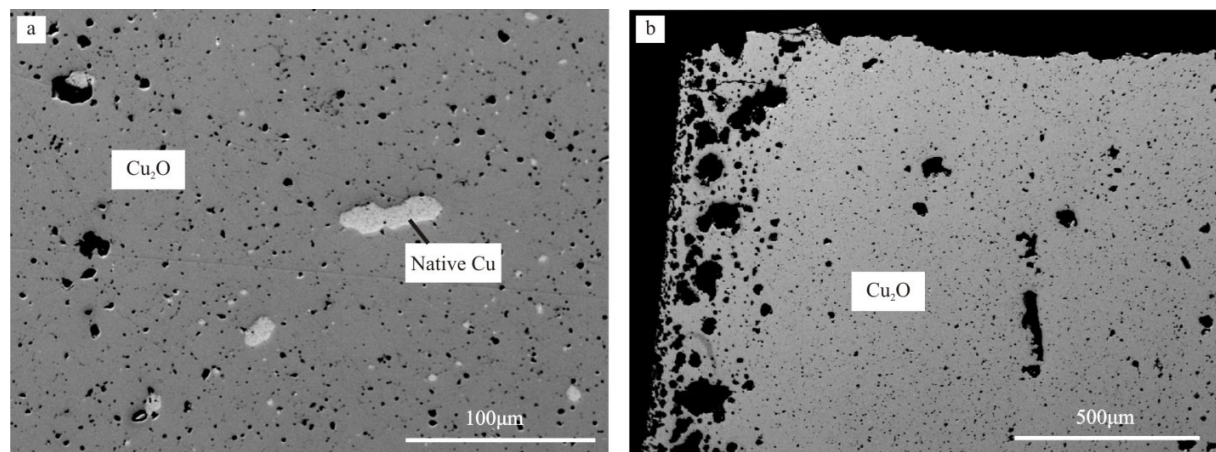


Figure A1-2 BSE images of the cross-section of cuprite pellets. a- cuprite was sintered at 1027°C and atmosphere condition for 30 hours; native Cu in addition to Cu₂O have been formed at this condition. b- cuprite was sintered at 927°C, $\log f_{\text{O}_2}$ (bar) at 10^{-3} for 24 hours. Cuprite is made up of Cu₂O.

A2. Gas phase determination

Additional runs were designed to check the possible gases produced in cuprite-fluid interaction process. Three Au capsules (4.00 mm I.D., 4.40 mm O.D. and 30 mm length) were loaded with: (i) cuprite + H₂O (similar to Cp41); (ii) cuprite + H₂O + 0.2 m HAc/KAc (similar to Cp24); (iii) cuprite + KCl_{aq} + 0.2 m HAc/KAc (similar to Cp23). The loading of each component is tabulated in Table A2. The mineral/fluid ratio is similar to the runs conducted in Au reaction cell, i.e., 0.015 (mineral/fluid by mass). All runs were conducted in the stainless autoclave at 250°C and 20 MPa with a period of 72 hours. Later the gas components in Au capsules are determined by headspace-gas chromatography in BGR (Bundesanstalt für Geowissenschaften und Rohstoffe, Hannover).

Chapter IIB

Table A2 Educts and products in 250°C and 20 MPa runs

	Starting compositions		Products
	mass [g]	n [nmol]	n [nmol]
Cp45-Cu₂O + H₂O, 72 hrs			
Cu ₂ O	0.005	31519	
H ₂ O	0.305	16924785	
H ₂			<70
CH ₄			1.3
CO ₂			114.8
Acetone			0
Cp46- Cu₂O + H₂O + 0.2 m HAc/KAc, 72 hrs			
Cu ₂ O	0.005	33475	
H ₂ O	0.299	16582463	
KAc	0.006	61692	
HAc	0.004	61647	
total solution	0.308		
H ₂			<70
CH ₄			31045
CO ₂			32351
Acetone			52
Cp46- Cu₂O +KCl + 0.2 m HAc/KAc, 72 hrs			
Cu ₂ O	0.005	70305	
H ₂ O	0.302	16776514	
KAc	0.006	62414	
HAc	0.004	62368	
KCl	0.009	125383	
total solution	0.312		
H ₂			<70
CH ₄			60688
CO ₂			48220
Acetone			6

Notes: nmol denotes 10⁻⁹ mol.

A3. Additional runs to confirm the formation of native Cu

Additional runs were designed to verify the formation of native Cu in different fluids and experimental vessels. Au capsule (3.00 mm I.D., 3.40 mm O.D. and 30 mm length) was selected as container. Three runs were conducted in cold seal pressure vessel with cuprite in 1.49 m NaCl (without pH buffer) solution at 300°C and 20 MPa, in 1.5 m HCl solution at 300°C and 20 MPa and in 0.9 m NaCl (with pH buffer) solution 250°C and 20 MPa. Inner walls of all Au capsules have been covered by native Cu precipitates (identified by SEM).

Chapter IIB

A4. Original data measured by ICP-OES (no Rb correction applied)

Table A4-1 Original Cu and Rb content in H₂O±HAc/KAc systems

SNO	Run duration hrs	Cu-1st fl. µg/g	Cu-2nd fl. µg/g	Rb-1st fl. µg/g	Rb-2nd fl. µg/g
Cp27	0		14		459
	0.5		24		467
	1		55		429
	3		133		425
	6		141		375
	24		378		376
Cp22	0	104	52	314	503
	0.5	88	114	490	466
	1	157	203	459	450
	3	299	238	543	340
	7	356	340	455	433
	24	302	277	390	380
	48	246	222	356	344
	72	172	138	304	289
Cp26	0		173		406
	0.5		74		441
	1		109		439
	3		137		432
	7		126		417
	24		126		365
Cp24	0	277	103	206	121
	0.5	98	163	124	456
	1	93	97	449	446
	3	77	73	418	414
	7	66	72	404	403
	24	49	53	376	362
	48	50	47	359	337
	72	28	44	303	292
Cp29	1		118		447
	6		52		414
	24		11		268
Cp30	1		86		436
	6		97		426
	24		46		377
Cp31	1		80		426
	6		79		440
	24		53		402
Cp43	1		64		497
	6		79		416
Cp41	1		3		556
	12		3		569
	71		1		459
Cp40	1		51		456
	6		92		480
	24		59		499
	25		87		498
	31		58		492
	49		53		383
	50		37		332
	56		33		344
74		10		323	

Chapter IIB

Table A4-2 Original Cu and Rb content in KCl±HAc/KAc systems

SNO	Run duration hrs	Cu-1st fl. µg/g	Cu-2nd fl. µg/g	Rb-1st fl. µg/g	Rb-2nd fl. µg/g
Cp28	0		207		398
	0.5		371		396
	1		532		409
	3		680		387
	6		1111		377
	24		1097		310
Cp38	1		533		376
	6		1200		354
	24		2085		322
Cp25	0		1083		420
	0.5		1192		402
	1		1356		393
	3		1853		385
	7		2200		370
	24		2490		350
Cp23	0	712	1332	363	431
	0.5	1474	1606	435	430
	1	1848	1950	446	417
	3	2239	2593	411	415
	7	2817	3301	389	395
	24	3066	3320	397	427
	48	2324	2673	375	362
	72	2042	2304	347	340
Cp6	2.3	879	832	469	630
	3.3	711	1631	315	543
	4.3	2442	2615	545	536
	5.5	2903	2930	486	470
	69	619	1234	440	442
	71	825	998	400	370
Cp42	1		98		502
	11		152		461
	72		30		353

SNO	Run duration hrs	Cu-2nd fl. µg/g	Rb-2nd fl. µg/g
Cp32	1	1717	415
	6	3275	364
	24	689	482
Cp33	1	2355	436
	6	3883	401
	24	2050	351
Cp34	1	2714	444
	6	4129	432
	24	2280	419
Cp35	1	960	534
	6	1188	530
	6	1352	497
	24	857	549
Cp44	1	714	445
	6	1112	394
	24	753	373
Cp36	1	1958	457
	6	2579	452
	24	1641	436
Cp37	1	2025	457
	6	3564	416
	24	3802	409
Cp39	1	641	445
	6	965	451
	24	2404	475
	25	2341	401
	31	2223	397
	49	1663	384
	50	1241	308
	56	1195	312
74	817	292	

Chapter IIB

References

- Asael, D., Matthews, A., Bar-Matthews, M. and Halicz, L. (2007) Copper isotope fractionation in sedimentary copper mineralization (Timna Valley, Israel). *Chemical Geology* 243, 238-254.
- Asael, D., Matthews, A., Bar-Matthews, M., Harlavan, Y. and Segal, I. (2012) Tracking redox controls and sources of sedimentary mineralization using copper and lead isotopes. *Chemical Geology* 310, 23-35.
- Azaraien, H., Shahabpour, J. and Aminzadeh, B. (2017) Metallogenesis of the sediment-hosted stratiform Cu deposits of the Ravar Copper Belt (RCB), Central Iran. *Ore Geology Reviews* 81, 369-395.
- Ball, M. and Portwood, L. (1994) The dehydration of copper (II) acetate monohydrate. *Journal of thermal analysis* 41, 347-356.
- Barnes, H. (1979) Solubilities of ore minerals. *Geochemistry of hydrothermal ore deposits*, 404-460.
- Belash, I., Peresada, G. and Ponyatovskii, E. (1977) PHYSICOCHEMICAL REACTIONS IN CU₂O AT HIGH-PRESSURES. *INORGANIC MATERIALS* 13, 544-545.
- Bell, J.L., Palmer, D.A., Barnes, H. and Drummond, S. (1994) Thermal decomposition of acetate: III. Catalysis by mineral surfaces. *Geochimica et cosmochimica acta* 58, 4155-4177.
- Bénézech, P. and Palmer, D.A. (2000) Potentiometric determination of cadmium–acetate complexation in aqueous solutions to 250° C. *Chemical Geology* 167, 11-24.
- Bénézech, P., Castet, S., Dandurand, J.-L., Gout, R. and Schott, J. (1994) Experimental study of aluminum-acetate complexing between 60 and 200 C. *Geochimica et Cosmochimica Acta* 58, 4561-4572.
- Berry, A.J., Hack, A.C., Mavrogenes, J.A., Newville, M. and Sutton, S.R. (2006) AXANES study of Cu speciation in high-temperature brines using synthetic fluid inclusions. *American Mineralogist* 91, 1773-1782.
- Beverkog, B. and Puigdomenech, I. (1997) Revised Pourbaix diagrams for copper at 25 to 300 C. *Journal of The Electrochemical Society* 144, 3476-3483.
- Bigeleisen, J. and Mayer, M.G. (1947) Calculation of equilibrium constants for isotopic exchange reactions. *The Journal of Chemical Physics* 15, 261-267.
- Borg, S.J. and Liu, W. (2010) An XAS study of zinc speciation in aqueous acetate solutions at 25–200° C. *Nuclear Instruments and Methods in Physics Research Section A: Accelerators, Spectrometers, Detectors and Associated Equipment* 619, 276-279.
- Borrok, D., Wanty, R., Ridley, W., Wolf, R., Lamothe, P. and Adams, M. (2007) Separation of copper, iron, and zinc from complex aqueous solutions for isotopic measurement. *Chemical geology* 242, 400-414.
- Brown, A.C. (2009) A process-based approach to estimating the copper derived from red beds in the sediment-hosted stratiform copper deposit model. *Economic Geology* 104, 857-868.
- Brugger, J., Etschmann, B., Liu, W., Testemale, D., Hazemann, J.-L., Emerich, H., Van Beek, W. and Proux, O. (2007) An XAS study of the structure and thermodynamics of Cu (I) chloride complexes in brines up to high temperature (400 C, 600bar). *Geochimica et cosmochimica acta* 71, 4920-4941.
- Brugger, J., Liu, W., Etschmann, B., Mei, Y., Sherman, D.M. and Testemale, D. (2016) A review of the coordination chemistry of hydrothermal systems, or do coordination changes make ore deposits? *Chemical Geology* 447, 219-253.
- Buhl, J.-C., Rüscher, C., Schomborg, L. and Stemme, F. (2010) Nanocrystalline NaBH₄-enclathrated zeolite SOD: a model for the improvement of safeness and reactivity of boron hydride based hydrogen storage systems. *Clean Technology* www.ct-si.org, ISBN 978-1-4398-3419-0 (2010) 236-239
- Busigny, V., Chen, J., Philippot, P., Borensztajn, S. and Moynier, F. (2018) Insight into hydrothermal and subduction processes from copper and nitrogen isotopes in oceanic metagabbros. *Earth and Planetary Science Letters* 498, 54-64.
- Carothers, W.W. and Kharaka, Y.K. (1978) Aliphatic acid anions in oil-field waters--implications for origin of natural gas. *AAPG Bulletin* 62, 2441-2453.
- Cauzid, J., Philippot, P., Martinez-Criado, G., Ménez, B. and Labouré, S. (2007) Contrasting Cu-complexing behaviour in vapour and liquid fluid inclusions from the Yankee Lode tin deposit, Mole Granite, Australia. *Chemical Geology* 246, 39-54.
- Child, W.C. and Hay, A.J. (1964) The thermodynamics of the thermal decomposition of acetic acid in the vapor phase. *Journal of the American Chemical Society* 86, 182-187.
- Collings, M.D., Sherman, D.M. and Ragnarsdottir, K.V. (2000) Complexation of Cu²⁺ in oxidized NaCl brines from 25°C to 175°C: results from in situ EXAFS spectroscopy. *Chemical Geology* 167, 65-73.
- Cordell, R.J. (1972) Depths of oil origin and primary migration: a review and critique. *AAPG Bulletin* 56, 2029-2067.
- Driesner, T. and Heinrich, C.A. (2007) The system H₂O–NaCl. Part I: Correlation formulae for phase relations in temperature–pressure–composition space from 0 to 1000° C, 0 to 5000bar, and 0 to 1 X NaCl. *Geochimica et Cosmochimica Acta* 71, 4880-4901.
- Drummond, S. and Palmer, D. (1985) Formation constants for aqueous ferrous acetate complexes from magnetite solubility measurements from 100° to 250° C and 250 to 1250 bars [abstr.], *Geol. Soc. Amer., Abstracts with Programs*, p. 567.
- Drummond, S. and Palmer, D.A. (1986) Thermal decarboxylation of acetate. Part II. Boundary conditions for the role of acetate in the primary migration of natural gas and the transportation of metals in hydrothermal systems. *Geochimica et Cosmochimica Acta* 50, 825-833.
- Ehrlich, S., Butler, I., Halicz, L., Rickard, D., Oldroyd, A. and Matthews, A. (2004) Experimental study of the copper isotope fractionation between aqueous Cu (II) and covellite, CuS. *Chemical Geology* 209, 259-269.

Chapter IIB

- Etschmann, B., Liu, W., Testemale, D., Mueller, H., Rae, N., Proux, O., Hazemann, J.-L. and Brugger, J. (2010) An in situ XAS study of copper (I) transport as hydrosulfide complexes in hydrothermal solutions (25–592° C, 180–600bar): Speciation and solubility in vapor and liquid phases. *Geochimica et Cosmochimica Acta* 74, 4723-4739.
- Fein, J.B. (1991) Experimental study of aluminum-, calcium-, and magnesium-acetate complexing at 80 C. *Geochimica et Cosmochimica Acta* 55, 955-964.
- Fernandez, A. and Borrok, D.M. (2009) Fractionation of Cu, Fe, and Zn isotopes during the oxidative weathering of sulfide-rich rocks. *Chemical Geology* 264, 1-12.
- Fisher, J.B. (1987) Distribution and occurrence of aliphatic acid anions in deep subsurface waters. *Geochimica et Cosmochimica Acta* 51, 2459-2468.
- Fulton, J.L., Hoffmann, M.M. and Darab, J.G. (2000) An X-ray absorption fine structure study of copper (I) chloride coordination structure in water up to 325 C. *Chemical Physics Letters* 330, 300-308.
- Germanov, A. and Mel'Kanovitskaya, S. (1975) Organic acids in hydrothermal ores of polymetallic deposits and in ground waters. *Doklady... earth sciences sections*.
- Giordano, T. (1985) A preliminary evaluation of organic ligands and metal-organic complexing in Mississippi Valley-type ore solutions. *Economic Geology* 80, 96-106.
- Giordano, T. and Barnes, H. (1981) Lead transport in Mississippi Valley-type ore solutions. *Economic Geology* 76, 2200-2211.
- Giordano, T.H. (1989) Anglesite (PbSO₄) solubility in acetate solutions: The determination of stability constants for lead acetate complexes to 85° C. *Geochimica et Cosmochimica Acta* 53, 359-366.
- Giordano, T.H. and Drummond, S. (1991) The potentiometric determination of stability constants for zinc acetate complexes in aqueous solutions to 295 C. *Geochimica et Cosmochimica Acta* 55, 2401-2415.
- Graham, S., Pearson, N., Jackson, S., Griffin, W. and O'reilly, S. (2004) Tracing Cu and Fe from source to porphyry: in situ determination of Cu and Fe isotope ratios in sulfides from the Grasberg Cu–Au deposit. *Chemical Geology* 207, 147-169.
- Hack, A.C. and Mavrogenes, J.A. (2006) A synthetic fluid inclusion study of copper solubility in hydrothermal brines from 525 to 725 C and 0.3 to 1.7 GPa. *Geochimica et cosmochimica acta* 70, 3970-3985.
- Harris, A.C., Golding, S.D. and White, N.C. (2005) Bajo de la Alumbrera copper-gold deposit: Stable isotope evidence for a porphyry-related hydrothermal system dominated by magmatic aqueous fluids. *Economic Geology* 100, 863-886.
- Harris, A.C., Kamenetsky, V.S., White, N.C., van Achterbergh, E. and Ryan, C.G. (2003) Melt inclusions in veins: linking magmas and porphyry Cu deposits. *Science* 302, 2109-2111.
- Heinrich, C., Günther, D., Audétat, A., Ulrich, T. and Frischknecht, R. (1999) Metal fractionation between magmatic brine and vapor, determined by microanalysis of fluid inclusions. *Geology* 27, 755-758.
- Heinrich, C.A., Henley, R. and Seward, T.M. (1989) Hydrothermal systems. Australian Mineral Foundation.
- Hennet, R.J., Crerar, D.A. and Schwartz, J. (1988) Organic complexes in hydrothermal systems. *Economic Geology* 83, 742-764.
- Hitzman, M., Kirkham, R., Broughton, D., Thorson, J. and Selley, D. (2005) The sediment-hosted stratiform copper ore system. *Economic geology* 100.
- Hitzman, M.W., Selley, D. and Bull, S. (2010) Formation of sedimentary rock-hosted stratiform copper deposits through Earth history. *Economic Geology* 105, 627-639.
- Huang, J., Liu, S.-A., Wörner, G., Yu, H. and Xiao, Y. (2016) Copper isotope behavior during extreme magma differentiation and degassing: a case study on Laacher See phonolite tephra (East Eifel, Germany). *Contributions to Mineralogy and Petrology* 171, 76.
- Ikehata, K., Notsu, K. and Hirata, T. (2011) Copper isotope characteristics of copper-rich minerals from besshi-type volcanogenic massive sulfide deposits, japan, determined using a femtosecond LA-MC-ICP-MS. *Economic Geology* 106, 307-316.
- Kharaka, Y.K., Carothers, W.W. and Rosenbauer, R.J. (1983) Thermal decarboxylation of acetic acid: Implications for origin of natural gas. *Geochimica et Cosmochimica Acta* 47, 397-402.
- Kharaka, Y.K., Law, L.M., Carothers, W.W. and Goerlitz, D.F. (1986) Role of organic species dissolved in formation waters from sedimentary basins in mineral diagenesis.
- Kim, K.S. and Barteau, M.A. (1988) Pathways for carboxylic acid decomposition on titania. *Langmuir* 4, 945-953.
- Lai, F., Liu, L. and Cao, W. (2018) Complexation of copper in acetate-rich low-temperature hydrothermal fluids: Evidence from ab initio molecular dynamics simulations. *Chemical Geology* 476, 100-118.
- Landtwing, M.R., Pettke, T., Halter, W.E., Heinrich, C.A., Redmond, P.B., Einaudi, M.T. and Kunze, K. (2005) Copper deposition during quartz dissolution by cooling magmatic–hydrothermal fluids: The Bingham porphyry. *Earth and Planetary Science Letters* 235, 229-243.
- Large, D. and Walcher, E. (1999) The Rammelsberg massive sulphide Cu-Zn-Pb-Ba-Deposit, Germany: an example of sediment-hosted, massive sulphide mineralisation. *Mineralium Deposita* 34, 522-538.
- Larson, P.B., Maher, K., Ramos, F.C., Chang, Z., Gaspar, M. and Meinert, L.D. (2003) Copper isotope ratios in magmatic and hydrothermal ore-forming environments. *Chemical Geology* 201, 337-350.
- Lazarov, M. and Horn, I. (2015) Matrix and energy effects during in-situ determination of Cu isotope ratios by ultraviolet-femtosecond laser ablation multicollector inductively coupled plasma mass spectrometry. *Spectrochimica Acta Part B: Atomic Spectroscopy* 111, 64-73.
- Li, W., Jackson, S.E., Pearson, N.J., Alard, O. and Chappell, B.W. (2009) The Cu isotopic signature of granites from the Lachlan Fold Belt, SE Australia. *Chemical Geology* 258, 38-49.

Chapter IIB

- Liu, S.-A., Huang, J., Liu, J., Wörner, G., Yang, W., Tang, Y.-J., Chen, Y., Tang, L., Zheng, J. and Li, S. (2015) Copper isotopic composition of the silicate Earth. *Earth and Planetary Science Letters* 427, 95-103.
- Liu, W. and McPhail, D. (2005) Thermodynamic properties of copper chloride complexes and copper transport in magmatic-hydrothermal solutions. *Chemical Geology* 221, 21-39.
- Liu, W., Brugger, J., McPhail, D. and Spiccia, L. (2002) A spectrophotometric study of aqueous copper (I)-chloride complexes in LiCl solutions between 100 C and 250 C. *Geochimica et Cosmochimica Acta* 66, 3615-3633.
- Liu, W., McPhail, D. and Brugger, J. (2001) An experimental study of copper (I)-chloride and copper (I)-acetate complexing in hydrothermal solutions between 50 C and 250 C and vapor-saturated pressure. *Geochimica et Cosmochimica Acta* 65, 2937-2948.
- Liu, W., McPhail, D. and Brugger, J. (2001) An experimental study of copper (I)-chloride and copper (I)-acetate complexing in hydrothermal solutions between 50 C and 250 C and vapor-saturated pressure. *Geochimica et Cosmochimica Acta* 65, 2937-2948.
- Luck, J.M., Ben Othman, D. and Albarede, F. (2005) Zn and Cu isotopic variations in chondrites and iron meteorites: Early solar nebula reservoirs and parent-body processes. *Geochimica Et Cosmochimica Acta* 69, 5351-5363.
- Lundegard, P.D. and Land, L.S. (1986) Carbon dioxide and organic acids: their role in porosity enhancement and cementation, Paleogene of the Texas Gulf Coast.
- Maher, K.C., Jackson, S. and Mountain, B. (2011) Experimental evaluation of the fluid-mineral fractionation of Cu isotopes at 250 C and 300 C. *Chemical Geology* 286, 229-239.
- Maréchal, C.N. and Sheppard, S.M.F. (2002) Isotopic fractionation of Cu and Zn between chloride and nitrate solutions and malachite or smithsonite at 30 degrees and 50 degrees C. *Geochim. Cosmochim. Acta* 66.
- Maréchal, C.N., Télouk, P. and Albarède, F. (1999) Precise analysis of copper and zinc isotopic compositions by plasma-source mass spectrometry. *Chemical Geology* 156, 251-273.
- Markl, G., Lahaye, Y. and Schwinn, G. (2006) Copper isotopes as monitors of redox processes in hydrothermal mineralization. *Geochimica et cosmochimica acta* 70, 4215-4228.
- Mathur, R., Ruiz, J., Titley, S., Liermann, L., Buss, H. and Brantley, S. (2005) Cu isotopic fractionation in the supergene environment with and without bacteria. *Geochimica et Cosmochimica Acta* 69, 5233-5246.
- Mathur, R., Titley, S., Barra, F., Brantley, S., Wilson, M., Phillips, A., Munizaga, F., Makshev, V., Vervoort, J. and Hart, G. (2009) Exploration potential of Cu isotope fractionation in porphyry copper deposits. *Journal of Geochemical exploration* 102, 1-6.
- Mesmer, R.E., Patterson, C., Busey, R. and Holmes, H. (1989) Ionization of acetic acid in aq. sodium chloride media: a potentiometric study to 573K and 130 bar. *The Journal of Physical Chemistry* 93, 7483-7490.
- Mountain, B. and Seward, T. (1999) The hydrosulphide/sulphide complexes of copper (I): Experimental determination of stoichiometry and stability at 22 C and reassessment of high temperature data. *Geochimica et Cosmochimica Acta* 63, 11-29.
- Mountain, B. and Seward, T. (2003) Hydrosulfide/sulfide complexes of copper (I): experimental confirmation of the stoichiometry and stability of Cu (HS)²⁻ to elevated temperatures. *Geochimica et cosmochimica acta* 67, 3005-3014.
- Moynier, F., Vance, D., Fujii, T. and Savage, P. (2017) The isotope geochemistry of zinc and copper. *Reviews in Mineralogy and Geochemistry* 82, 543-600.
- Neumann, J. P., Zhong, T., and Chang, Y.A., 1984. The Cu-O (copper-oxygen) system. *Bulletin of Alloy Phase Diagrams* 5(2): 136-140.
- Palmer, D.A. (2011) Solubility measurements of crystalline Cu₂O in aqueous solution as a function of temperature and pH. *Journal of solution chemistry* 40, 1067-1093.
- Palmer, D.A. and Drummond, S. (1986) Thermal decarboxylation of acetate. Part I. The kinetics and mechanism of reaction in aqueous solution. *Geochimica et Cosmochimica Acta* 50, 813-823.
- Pekala, M., Asael, D., Butler, L., Matthews, A. and Rickard, D. (2011) Experimental study of Cu isotope fractionation during the reaction of aqueous Cu (II) with Fe (II) sulphides at temperatures between 40 and 200 C. *Chemical Geology* 289, 31-38.
- Pouchou, J.-L. and Pichoir, F. (1991) Quantitative analysis of homogeneous or stratified microvolumes applying the model "PAP", Electron probe quantitation. Springer, pp. 31-75.
- Qi, D., Behrens, H., Lazarov, M. and Weyer, S. (----) Cu isotope fractionation during reduction processes in aqueous systems: evidences from electrochemical deposition. Submitted to *Contribution to Mineralogy and Petrology*.
- Rajadurai, S. (1987) Synthesis, structural characterization and catalytic study of ZnCrFeO₄ spinel. *Materials Chemistry and Physics* 16, 459-466.
- Redmond, P., Einaudi, M., Inan, E., Landtwing, M. and Heinrich, C. (2004) Copper deposition by fluid cooling in intrusion-centered systems: New insights from the Bingham porphyry ore deposit, Utah. *Geology* 32, 217-220.
- Rempel, K.U., Liebscher, A., Meixner, A., Romer, R.L. and Heinrich, W. (2012) An experimental study of the elemental and isotopic fractionation of copper between aqueous vapour and liquid to 450° C and 400bar in the CuCl-NaCl-H₂O and CuCl-NaHS-NaCl-H₂O systems. *Geochimica et Cosmochimica Acta* 94, 199-216.
- Rose, A. (1976) The effect of cuprous chloride complexes in the origin of red-bed copper and related deposits. *Economic Geology* 71, 1036-1048.
- Rouxel, O., Fouquet, Y. and Ludden, J.N. (2004) Copper isotope systematics of the Lucky Strike, Rainbow, and Logatchev seafloor hydrothermal fields on the Mid-Atlantic Ridge. *economic geology* 99, 585-600.
- Savage, P.S., Moynier, F., Chen, H., Shofner, G., Siebert, J., Badro, J. and Puchtel, I. (2015) Copper isotope evidence for large-scale sulphide fractionation during Earth's differentiation. *Geochemical Perspectives Letters*.

Chapter IIB

- Schmidt, C., Watenphul, A., Jahn, S., Schäpan, I., Scholten, L., Newville, M.G. and Lanzirrotti, A. (2018) Copper complexation and solubility in high-temperature hydrothermal fluids: A combined study by Raman, X-ray fluorescence, and X-ray absorption spectroscopies and ab initio molecular dynamics simulations. *Chemical Geology* 494, 69-79.
- Semmler, J., Irish, D.E. and Ozeki, T. (1990) Vibrational spectral studies of solutions at elevated temperatures and pressures. 12. Magnesium acetate. *Geochimica et Cosmochimica Acta* 54, 947-954.
- Seo, J.H., Lee, S.K. and Lee, I. (2007) Quantum chemical calculations of equilibrium copper (I) isotope fractionations in ore-forming fluids. *Chemical Geology* 243, 225-237.
- Seward, T. (1976) The stability of chloride complexes of silver in hydrothermal solutions up to 350 C. *Geochimica et Cosmochimica Acta* 40, 1329-1341.
- Seyfried, J.W., Gordon, P. and Dickson, F. (1979) New reaction cell for hydrothermal solution equipment. *Am. Mineral.*; (United States) 64.
- Sherman, D.M. (2007) Complexation of Cu⁺ in hydrothermal NaCl brines: ab initio molecular dynamics and energetics. *Geochimica et Cosmochimica Acta* 71, 714-722.
- Shields, W., Murphy, T.-J. and Garner, E. (1964) Absolute isotopic abundance ratio and the atomic weight of a reference sample of copper. *J. Res. Natl. Bur. Std.* 68.
- Sillitoe, R.H. (2005) Supergene oxidized and enriched porphyry copper and related deposits. *Econ. Geol.* 100, 723-768.
- Sun, Y.-Z., Püttmann, W. (2000) The role of organic matter during copper enrichment in Kupferschiefer from the Sangerhausen basin, Germany. *Organic Geochemistry* 31, 1143-1161.
- Surdam, R., Crossey, L.J., (1985). Organic-inorganic reactions during progressive burial: key to porosity and permeability enhancement and preservation. *Phil. Trans. R. Soc. Lond. A* 315, 135-156.
- Sverjensky, D.A., Stagno, V., Huang, F., (2014). Important role for organic carbon in subduction-zone fluids in the deep carbon cycle. *Nature Geoscience* 7, 909.
- Thornber, M., (1985). Supergene alteration of sulphides: VII. Distribution of elements during the gossan-forming process. *Chemical Geology* 53, 279-301.
- Titley, S., (1978). Geologic history, hypogene features, and processes of secondary sulfide enrichment at the Plesyumi copper prospect, New Britain, Papua New Guinea. *Economic Geology* 73, 768-784.
- Urey, H.C., (1947). The thermodynamic properties of isotopic substances. *Journal of the Chemical Society (Resumed)*, 562-581.
- Webb, A., Carpenter Jr, R., Towle, L., Skelton, E., Liu, C.-Y., 1990. Stability of the cuprite-type structure at elevated pressures and temperatures. *International Journal of High Pressure Research* 6, 107-120.
- White, W.S., (1971). A paleohydrologic model for mineralization of the White Pine copper deposit, northern Michigan. *Economic Geology* 66, 1-13.
- Willey, L.M., Kharaka, Y.K., Presser, T.S., Rapp, J.B., Barnes, I., (1975). Short chain aliphatic acid anions in oil field waters and their contribution to the measured alkalinity. *Geochimica et Cosmochimica Acta* 39, 1707-1711.
- Xiao, Z., Gammons, C., Williams-Jones, A., (1998). Experimental study of copper (I) chloride complexing in hydrothermal solutions at 40 to 300 C and saturated water vapor pressure. *Geochimica et cosmochimica acta* 62, 2949-2964.
- Yang, M.M., Crerar, D.A., Irish, D.E., (1989). A Raman spectroscopic study of lead and zinc acetate complexes in hydrothermal solutions. *Geochimica et Cosmochimica Acta* 53, 319-326.
- Zhu, X., Guo, Y., Williams, R., O'nions, R., Matthews, A., Belshaw, N., Canters, G., De Waal, E., Weser, U., Burgess, B., (2002). Mass fractionation processes of transition metal isotopes. *Earth and Planetary Science Letters* 200, 47-62.
- Zhu, X., O'nions, R., Guo, Y., Belshaw, N., Rickard, D., (2000). Determination of natural Cu-isotope variation by plasma-source mass spectrometry: implications for use as geochemical tracers. *Chemical Geology* 163, 139-149.

Chapter III

**Cu isotope fractionation during reduction processes in aqueous
systems: evidences from electrochemical deposition**

Dongmei Qi*, Harald Behrens, Marina Lazarov, Stefan Weyer

Institute of Mineralogy, Leibniz Universität Hannover, Callinstrasse 3, Hannover, D-30167, Germany

(*d.qi@mineralogie.uni-hannover.de)

(Submitted to *Contribution to Mineralogy and Petrology*)

Abstract

Redox processes are ubiquitous in Earth science, and redox transitions often lead to large fractionations of the stable isotopes of many transition metals such as copper. To get insights into the mechanisms of isotope fractionations induced by electrochemical processes, we examine the behavior of copper isotopes during the reduction reaction $\text{Cu}^{2+} + 2\text{e}^- = \text{Cu}^0$. All experiments have been conducted by applying a controlled current between the working electrode and the auxiliary electrode, i.e., the galvanostatic electrodeposition technique, in aqueous CuSO_4 solutions. Controlling parameters were tested by varying electrolyte concentration (0.01 - 1 mol kg^{-1}), stirring speed (0 - 500 rpm), current (0.1 - 0.5 A), time (35 - 600 s), and temperature (5 - 80°C). In all cases, the plated Cu metal is enriched in the light isotope (^{63}Cu) with respect to the solution. At room temperature the Cu isotopic fractionation between the electroplated Cu and electrolyte is found to increase with electrolyte concentration and stirring speed, and to decrease with current and run duration. These trends can be explained by three competing processes: copper transport in the solution, the kinetics of electrochemical reduction of copper ions and the surface diffusion at the electrode, i.e. transport becomes important at low copper concentration, low stirring speed, high currents and large amount of copper precipitation. Copper isotope fractionation has a maximum near 35°C, decreasing both towards higher and lower temperatures. In the temperature range of 35 - 80°C, the dependence of temperature on isotope fractionation can be described by

$$\Delta^{65}\text{Cu}_{\text{Cu}(0)\text{-Cu(II)}} = -(0.20 \pm 0.04) \times 10^6 \text{ T}^{-2} - (0.44 \pm 0.39)$$

where $\Delta^{65}\text{Cu}_{\text{Cu(II)-Cu(0)}}$ (‰) represents the copper isotopic composition differences between the product (electroplated copper) and the reactant (electrolyte solution, $\text{CuSO}_{4(\text{aq})}$), and T is the temperature in K. At low temperature (down to 5°C) a noticeable deviation from this trend suggests a change in the controlling mechanism, i.e., transport in the solution becomes important. Our findings in comparison to other studies imply that transformation of fivefold to sixfold coordinated aquacomplexes of Cu^{2+} to linear Cu^+ complexes is a key step during reduction of copper in aqueous solutions, inducing large negative copper isotope fractionation. These findings support that copper isotopes can be used as effective tracers of redox processes. This may have implications to various hydrothermal ore deposits, such as supergene processes, black smokers and volcanic-hosted massive sulfide.

Keywords:

Cu isotopes, Metallic Cu, Electrochemical reduction, Thermodynamic equilibrium, Kinetics

1. Introduction

Copper exists as two stable isotopes ^{65}Cu (69.17%) and ^{63}Cu (30.83%) in nature. Profound knowledge on Cu isotopes has been gained due to recent advances in multiple collector inductively coupled plasma mass spectrometry (MC-ICP-MS), and the precision of Cu isotope ratios better than 0.04‰ (1 σ) can be achieved when using Zn (Ni) doping and sample-standard bracketing techniques for instrumental mass bias correction (Maréchal et al., 1999; Zhu et al., 2000; Bigalke et al., 2010; Lazarov and Horn, 2015). Moreover, attention has focused on Cu isotopes as a geological tracer due to its significance in a variety of natural processes, such as liquid-vapor separation (Pokrovski et al., 2008; Rempel et al., 2012), multi-step equilibrium processes (Zhu et al., 2002), fluid-rock chemical interaction (Rouxel et al., 2004; Markl et al., 2006; Asael et al., 2012b; Gregory and Mathur, 2017), ore forming supergene process (Larson et al., 2003; Mathur et al., 2005; Haest et al., 2009; Mathur and Fantle, 2015), and the formation of the solar system (Luck et al., 2005; Barrat et al., 2012). Such processes generate pronounced variation in copper isotope composition in natural samples (expressed as $\delta^{65}\text{Cu}$ (‰) = $[(^{65}\text{Cu}/^{63}\text{Cu})_{\text{sample}} / (^{65}\text{Cu}/^{63}\text{Cu})_{\text{NIST-SRM 976}} - 1] \times 1000$) that ranges from -17‰ to +10‰ with respect to the NIST-SRM 976 standard (e.g., Mathur et al., 2009; Asael et al., 2012a; Mathur and Fantle, 2015).

Cu isotope fractionation is typically very small during high temperature processes. For instance, a homogeneous Cu isotopic composition of non-metasomatized mantle peridotites and produced basalts was observed with $\delta^{65}\text{Cu}$ values similar to the bulk silicate Earth, with an average $\delta^{65}\text{Cu}$ value of $0.06 \pm 0.2\%$ (Liu et al., 2015) and references therein). Moreover, Cu isotope fractionation smaller than 0.7‰ has been observed during Cu partitioning between H₂O-NaCl bearing vapor and liquid, suggesting that the vapor phase is slightly depleted in ^{65}Cu (Li et al., 2010; Rempel et al., 2012).

Oxidation-reduction (redox) process related Cu isotope fractionation induces larger fractionation in comparison to other geological processes, which is frequently observed in various systems and is particularly pronounced at low temperatures. Supergene systems serve as examples, where Cu^0 , Cu^+ , and Cu^{2+} minerals may coexist even within the same hand specimen. Such deposits are important metal sources, which supply over 50% of the Cu production on Earth (Sillitoe, 2005). Natural and experimental findings give clear evidences that changes in oxidation states lead to large fractionations of the stable isotopes for many transition metals such as Cu, Fe as well as Zn, suggesting that transition metal stable isotope signatures could be used as a redox tracer for such systems. In the case of copper the fractionation effect can be described as

$$\Delta^{65}\text{Cu} (\text{‰}) = \delta^{65}\text{Cu}_{\text{product}} - \delta^{65}\text{Cu}_{\text{reactant}} \quad (1)$$

Asael et al. (2007) and Haest et al. (2009) found that $\delta^{65}\text{Cu}$ values of Cu(II) products are 3.5‰ higher than the Cu(I)-precursors after supergene reworking of ore deposits. Ikehata et al. (2011) observed that secondary malachite and native copper have higher $\delta^{65}\text{Cu}$ values than the primary chalcopyrite from the same deposit. Copper isotope data from the modern submarine hydrothermal vent systems support that ^{65}Cu enrichment appears in secondary Cu(II) minerals at low temperature (Zhu et al., 2000; Rouxel et al., 2004), yielding $\Delta^{65}\text{Cu}$ values of 3‰. The natural

Chapter III

redox-related isotopic fractionation has been rendered by experimental investigations. Several research teams (Zhu et al., 2002; Ehrlich et al., 2004; Asael et al., 2006) conducted Cu(II)-Cu(I) reduction experiments and found that the reduced Cu(I) minerals are usually depleted in ^{65}Cu , the $\Delta^{65}\text{Cu}$ values of which are up to 4‰ lower than their source solutions. (Mathur et al., 2005; Fernandez and Borrok, 2009a; Kimball et al., 2009) confirmed a fractionation up to 3‰ during oxidative leaching experiments of Cu(I) minerals with an enrichment of ^{65}Cu in aqueous Cu(II) solution. On the contrary, $\Delta^{65}\text{Cu}$ values smaller than 0.4‰ were observed during precipitation process without changes in the oxidation state (Maréchal and Sheppard, 2002; Ehrlich et al., 2004).

Native Cu is not as common as Cu sulfides, carbonates and sulfates in nature. In most cases native Cu is associated with extrusive and intrusive mafic rocks formed under reducing conditions (e.g. Cooper et al., 2008; Ikehata et al., 2011; Pinto et al., 2011). Other occurrences are reported from porphyry and hydrothermal copper deposits which have been reworked by supergene alteration (Markl et al., 2006; Ikehata et al., 2011; Ikehata and Hirata, 2012; Dekov et al., 2013; Baggio et al., 2017). The overall isotope composition of native copper ranges from -3‰ to 2‰. Larger variations were found for supergene environments (-3‰ - +1.7‰; Maréchal et al., 1999; Larson et al., 2003; Markl et al., 2006; Ikehata et al., 2011) compared to hydrothermal ore deposits and oceanic crust (-1.3‰ - +1.3‰; Zhu et al., 2000; Larson et al., 2003; Rouxel et al., 2004; Dekov et al., 2013).

Increasing interest in understanding the mechanisms of copper deposition from in aqueous solutions comes also from industrial production of electronic device (Kondo et al., 2014). Thin layers of copper metal are often used as ultrascale integrated interconnects. The uniformity and structure of the electroplated layers depend on the deposition kinetics, which may be controlled by reduction processes in the solution and at the substrate surface as well as by nucleation and growth of the metallic phase on the substrate (Mattsson and Bockris, 1959; Bockris and Enyo, 1962; Hurlen et al., 1978; Brande and Winand, 1992; Andersen et al., 1994; Grujicic and Pesic, 2002; Majidi et al., 2009; Nagar et al., 2016). Effects of parameters such as cupric (Cu^{2+}) ion concentration, inorganic and organic additives, pH value of the solution, plating mode and rate, substrate property were systematically investigated (Brande and Winand, 1992; Natter and Hempelmann, 1996; Grujicic and Pesic, 2002; Vincenzo and Cavallotti, 2002; Hu and Wu, 2003; Bozzini et al., 2006; Hai et al., 2012; Nagar et al., 2016). To our knowledge, isotope fractionation during the electrodeposition of copper has not been studied so far. Such data may give some important new views to the mechanisms of electrochemical reduction processes.

Here, we report a series of electrochemical deposition experiments with the aim of exploring the redox effect on Cu isotope fractionation by using the electroplating technique. The purpose of this study was (1) to investigate the isotopic variability of Cu(II) and Cu(0) species, (2) to relate measured copper isotope variations to the possible controlling factors and (3) to interpret the data using theoretical calculations of isotope fractionation between copper species and their relations to possible bonding environments from literature. The results from this study provide new insights into mechanisms of electrochemical processes in aqueous Cu-bearing systems.

2. Experimental setup

An in-house built plating device adjusted to a 500 ml glass beaker was used for copper electrodeposition. A schematic drawing is shown in figure 1. Metallic copper was deposited on a flat gold foil with dimension varying from $5.4 \times 0.5 \text{ cm}^2$ to $5.4 \times 0.8 \text{ cm}^2$. In most of the experiments Au foils of $5.4 \times 0.5 \text{ cm}^2$ were used. A copper foil (purity of 99.99%) with a surface area of $6.3 \times 0.8 \text{ cm}^2$ was used as a counter electrode. The basic working electrolytes were aqueous solutions of 0.01, 0.1, 0.5 and $1.0 \text{ mol kg}^{-1} \text{ CuSO}_4$. The maximum concentration is below the saturation level in the T-range of our study ($1.26 - 3.42 \text{ mol kg}^{-1}$ in the temperature range from 20 to 80°C , (Höffler and Steiger, 2018; Justel et al., 2018)). The plating bath ($\sim 400 \text{ ml}$) was prepared freshly prior to each electroplating experiment by adding definite amounts of copper (II) sulfate (CuSO_4), purchased from VWR with a purity of 99.3%, to deionized water (see Table 1). A Statron power supply was used to control copper deposition. In this study, we applied the controlled current method (galvanostatic technique) to conduct Cu electroplating, i.e. a constant operating current was adjusted at $\leq 0.5 \text{ A}$. The associated voltage displayed by the power supply was $3.3 \pm 0.4 \text{ V}$. A Schott induction hotplate was used for stirring and/or heating. A Teflon coated magnetic stirring bar was placed at the bottom of the beaker to homogenize the solution. The precise temperature of the electrolyte solution was measured by inserting a thermometer in the solution during or after electrodeposition. The pH of the electrolyte solutions was determined by an Inlab microelectrode before and after experiment.

Five sets of experiments were performed which are listed in Table 1. The first three series were performed to find out the optimum conditions for controlled electroplating. In the first set four different electrolyte concentrations were prepared with $\text{CuSO}_{4(\text{aq})}$ ranging from 0.01 to 1 mol kg^{-1} . Next, the effect of stirring speed was tested in the range of 0 - 500 revolutions per minute (rpm). Then, the applied current was varied from 0.1 to 0.5 A. After establishing optimum plating conditions, the stability of the conditions was checked by variation of run duration (35 - 600 s). Finally, the optimized parameters were used to study the temperature effect on copper isotope fractionation in the range of 5 to 80°C . To verify the reproducibility of the isotope compositions, duplicate experiments were performed at selected conditions.

After each run, the cathode electrodes (Au foils) were removed from the plating bath, gently rinsed with deionized water, dried at room temperature, weighed and sent to the ultraclean lab for further treatments. Electrolyte solutions were collected both before and after each run to identify possible changes in copper concentration and isotopic abundance.

3. Analytical methodology

The collected electrolyte solutions were evaporated to dryness at 90°C on a hotplate, and their residuals were dissolved in 1 ml of 3% HNO_3 . The solid samples, deposited Cu on Au foils, were firstly digested by $\sim 15 \text{ ml}$ of 6 mol/l HCl at 120°C overnight. After removal of the Au foil, the solutions were evaporated to dryness, and the residuals were dissolved in 1 ml of 3% HNO_3 for further measurements. The Cu concentration of all solutions was analyzed by inductively coupled plasma optical emission spectrometry (ICP-OES) on a Varian Vista Pro system

Chapter III

(Varian GmbH, Germany), following the procedure of Roebbert et al. (2018). The precision was better than 10% (2SD) for the ICP-OES analyses.

Based on the concentration data, samples were further diluted to ~0.5 µg/g in 3% HNO₃ and doped with 1 µg/g Ni using a Ni NIST SRM 986 standard solution for the solution nebulization MC-ICP-MS (ThermoFinnigan Neptune) measurement. For more details about the MC-ICP-MS measurements see Lazarov and Horn (2015). Standard-sample bracketing and the Ni NIST SRM 986 standard solution were used to correct measured ⁶⁵Cu/⁶³Cu ratios for instrumental mass bias. All results were reported in the delta notation relative to the Cu isotopic standard NIST SRM 976. Measurements of the in-house standard C125-1 were performed along with the sample replicates in order to determine the analytical precision and accuracy. The analyses of the standards are in an excellent agreement with the previously published values (Kusonwiriawong et al., 2016, 2017; Roebbert et al., 2018). The overall uncertainty of the measurement for the isotope data was generally better than 0.06‰ (2SD), with an average value of 0.03‰ (2SD). The daily reproducibility of the standard and samples was also better than 0.06‰ (2SD) (Lazarov and Horn, 2015).

4. Results

After experiment the Au foils show a homogeneous reddish color on both sides due to deposited thin Cu layers, except for the high temperature experiments (>35°C). Here the layers are less homogeneous and contain randomly distributed round pits which are attributed to vapor bubbles generated at electrode surface while heating.

The experimental conditions, measured Cu concentration and isotope fractionation are presented in Table 1 and Fig. 2. Isotopic differences between initial and post electrolyte solution are less than 0.02‰, which is within the analytical precision. Two types of Cu foils with slightly different isotope compositions have been used (Table 1): Cu foil No.1 with a δ⁶⁵Cu value of 0.38 ± 0.05‰ was only used in the concentration series; Cu foil No.2 with a δ⁶⁵Cu value of 0.11 ± 0.01 ‰ was used for the rest runs. In this study, Cu isotope fractionation between the metallic Cu(0) precipitates and the residual bulk electrolyte Cu(II) solutions are expressed as:

$$\Delta^{65}\text{Cu}_{\text{Cu(0)-Cu(II)}} (\text{‰}) = \delta^{65}\text{Cu}_{\text{electroplated Cu}} - \delta^{65}\text{Cu}_{\text{CuSO}_4 \text{ after electrodeposition}} \quad (2)$$

All electroplated samples are isotopically lighter than their stock solutions, yielding negative δ⁶⁵Cu values (Table 1). The measured Δ⁶⁵Cu_{Cu(II)-Cu(0)} values vary from -0.76 ‰ to -2.66 ‰.

Ambient temperatures changed slightly at 24 ± 1°C, but the temperature maintained constant within each series. The measured pH values of 0.01, 0.1, 0.5 and 1.0 mol kg⁻¹ CuSO₄ solutions were 4.69, 4.21, 3.61 and 3.32, respectively, and the pH of the solutions remain constant prior to and after electroplating. The ICP-OES analyses indicate that the Cu concentration of the electrolyte collected before and after each run varies less than 5% except for the run performed at 5°C (CuAu-38). The run CuAu-38 was conducted in such a way that ice crystals were directly added to the electrolyte solution, thus a dilution of electrolyte solution lowered the initial Cu concentration by 14%. Using the concentration of the solution with dissolved copper metal measured by ICP-OES and the

Chapter III

respective volume, the total mass of deposited copper is estimated. Then, the electrodeposition efficiency is the ratio between the measured mass of metallic Cu (m_{real}) and the Faradaic estimation ($m_{theoretical}$):

$$m_{theoretical} = \frac{i \cdot t \cdot M}{F \cdot z} \quad (3)$$

$$\text{Efficiency} = 100 \times \left| \frac{m_{theoretical} - m_{real}}{m_{theoretical}} - 1 \right| \quad (4)$$

where i is the applied current in ampere (A), t is the run duration in second (s), F is the Faraday constant, 96485 C mol⁻¹, M is the molar mass of copper in grams per mol (g mol⁻¹), z is the valence number of dissolved copper ions (+2). An independent measure of the amount of deposited copper is obtained by weighing the gold foil before and after electrodeposition. However, this is an unspecific determination which may be affected by additional components incorporated in the copper layer, i.e. water or electrolyte solution, as well as post-experimental oxidation of copper metal. Nevertheless, in most of the experiments both determinations agree within 20%, see table 1. Low values obtained by ICP-OES are due to some loss of precipitated copper during transfer to the digestion beaker.

Efficiency values are particularly high at high electrolyte concentration and high applied currents, even higher by a factor 2-3 than the predicted values of Eq. (3). We suggest that at such extreme conditions, an additional redox reaction may be initiated by high overpotential at the electrodes, i.e. coupling of the copper redox reaction with the electrolysis of water. These observations reflect the limits of the constant current technique and such extreme conditions are not further considered in our study.

Duplicate runs were conducted at three different temperatures (CuAu-11 and CuAu-14 at 25°C; CuAu-48 and CuAu-44 at 50°C; CuAu-46 and CuAu-64 at 80°C). Both the efficiency estimation and the isotopic data are reproduced within the analytical error by these duplicates (see Table 1). Furthermore, variation of the electrode surface between 2.7 and 3.8 cm² does not affect the efficiency of electrodeposition and the isotopic composition of precipitated copper metal.

Chapter III

Table 1 Experimental conditions and results of Cu electrodeposition

CuSO ₄ mol kg ⁻¹	Stiring speed rpm	Current A	Time s	Temperature °C	Mass gain of cathode ×10 ⁻³ g	Mass * ICP-OES ×10 ⁻³ g	Deposition efficiency ^b ±1σ* %	δ ⁶⁵ Cu ± 2σ (Deposited Cu) %	δ ⁶⁵ Cu ± 2σ (CuSO ₄ after) %	Δ ⁶⁵ Cu ± 2σ (Cu(0)-Cu(II)) %
Initial material										
CuSO ₄ ^a									0.16±0.01	
Cu foil No.1 ^a								0.38±0.05		
Concentration series										
CuAu-5	300	0.3	35	24	0.61	0.91	26±9	-0.62±0.03	0.14±0.03	-0.76±0.04
CuAu-8					2.36	2.66	77±26	-1.29±0.02	0.15±0.02	-1.45±0.03
CuAu-11					6.71	7.85	227±77	-1.77±0.02	0.16±0.02	-1.92±0.03
CuAu-14 ^d					4.08	5.02	145±49	-1.78±0.01	0.16±0.02	-1.94±0.02
CuAu-3					8.54	10.40	301±102	-2.10±0.03	0.16±0.01	-2.26±0.03
Cu foil No.2^a										
CuAu-54 ^R	300	0.3	35	25	3.80	5.03	146±49	0.11±0.01	0.17±0.03	-2.60±0.03
Stiring speed series										
CuAu-60	0			24	3.39	3.75	108±37	-1.08±0.02	0.18±0.05	-1.25±0.05
CuAu-32	100				5.18	3.23	93±32	-1.61±0.06	0.15±0.02	-1.76±0.06
CuAu-36	400				5.44	3.21	93±32	-2.43±0.02	0.19±0.00	-2.60±0.02
CuAu-34	500				3.67	3.06	88±30	-2.40±0.01	0.16±0.03	-2.56±0.03
Current series										
CuAu-24		0.10		24	1.41	1.76	146±49	-2.45±0.05	0.18±0.00	-2.63±0.05
CuAu-30		0.20			4.01	4.95	153±52	-2.20±0.02	0.15±0.00	-2.35±0.02
CuAu-27		0.45			11.53	13.29	215±73	-1.41±0.02	0.15±0.01	-1.55±0.03
CuAu-26		0.50			15.34	17.47	256±87	-0.68±0.01	0.16±0.02	-0.83±0.02
Time series										
CuAu-17				22	7.51	8.77	148±50	-1.98±0.02	0.16±0.01	-2.13±0.02
CuAu-56			120		12.44	12.38	105±35	-2.30±0.00	0.15±0.01	-2.45±0.01
CuAu-19			300		30.55	28.38	96±32	-1.82±0.01	0.15±0.01	-1.97±0.01
CuAu-21			600		59.73	58.71	99±34	-1.56±0.02	0.17±0.02	-1.73±0.03
Temperature series										
CuAu-38				5	4.64	6.45	187±63	-1.05±0.03	0.15±0.01	-1.21±0.03
CuAu-58				35	3.64	3.65	106±36	-2.49±0.01	0.17±0.02	-2.66±0.02

Chapter III

Table 1 continued

CuAu-48	50	4.87	5.72	166±56	-2.27±0.01	0.14±0.02	-2.41±0.02
CuAu-44 ^d	50	3.86	4.54	131±44	-2.37±0.01	0.16±0.03	-2.53±0.04
CuAu-62	65	4.80	5.24	152±51	-2.16±0.01	0.16±0.02	-2.32±0.02
CuAu-46	80	5.69	4.79	139±47	-1.78±0.01	0.15±0.02	-1.93±0.02
CuAu-64 ^d	80	4.61	5.44	157±53	-1.87±0.01	0.16±0.01	-2.03±0.02
Dimension series							
CuAu-54 ^R	Cathode surface area - 0.5×5.4 cm ²	3.80	5.03	146±49	-2.44±0.01	0.17±0.03	-2.60±0.03
CuAu-50	Cathode surface area - 0.7×5.0 cm ²	2.41	3.57	103±35	-2.37±0.03	0.14±0.01	-2.52±0.03
CuAu-52	Cathode surface area - 0.8×5.4 cm ²	9.70	5.88	170±58	-2.45±0.01	0.17±0.03	-2.62±0.03

Notes:

Abbreviations are revolutions per minute (rpm), ampere (A), second (s) and temperature (°C).

Mass gain of the cathode was determined by measuring the weight of the cathode by balance before and after Cu electroplating. Mass* represents the amount of electroplated Cu on cathode which was determined by ICP-OES.

^a represents Cu isotope composition ($\delta^{65}\text{Cu}$) of electrolyte solution (CuSO_4) and Cu foils prior to experiments, all other values are measured after electrodeposition.

Deposition efficiency^b was calculated from the mass determined by ICP-OES, and Eqs. (1, 2). The error of efficiency estimation is calculated by the propagation of several uncertainties, such as the weighing procedure (± 0.00001 g), Cu concentration of ICP-OES analyses (± 0.1) and $m_{\text{theoretical}}$ (± 0.001).

^d denotes duplicate runs.

CuAu-54^R is a reference run performed under standard conditions: 1 mol/kg CuSO_4 , 35 s, 0.3 A, 300 rpm and 25°C. Only parameters deviating from these conditions are reported in the following rows. Data of CuAu-54^R are repeated to enable comparison with respect to the electrode surface dimensions.

Reported errors of $\delta^{65}\text{Cu}$ represent only the two-sigma errors of the triplicate Cu isotope analyses of the same solution. The overall uncertainty of the isotope data was generally better than 0.06‰ (2SD), see text for details.

Chapter III

A positive relationship between electrolyte concentration and the mass of electroplated Cu is visible in Fig.2a. This finding is consistent with Takahashi and Gross (1999) who suggested that the cathodic exchange current increases linearly with copper ion concentration, resulting in an enhancement of the plating rate. Copper isotope fractionation increases with increasing copper concentration in the solution, i.e. $\Delta^{65}\text{Cu}_{\text{Cu(0)-Cu(II)}}$ decreases from -0.76 to -2.26‰ as the $\text{CuSO}_{4(\text{aq})}$ increases from 0.01 to 1 mol kg⁻¹ (Fig. 2b). As noted in previous studies (e.g. Vicenzo and Cavallotti, 2002), high concentrations of CuSO_4 favor formation of homogeneous, well developed copper layers on electrodes and, therefore, we have chosen 1 m $\text{CuSO}_{4(\text{aq})}$ as standard bath solutions.

The stirring rate of the electrolyte solution has insignificant influence on the amount of deposited Cu (Fig.2c), whereas it has a strong effect on Cu isotope fractionation (Fig. 2d). The well stirred run CuAu-54 (300 rpm) yield $\Delta^{65}\text{Cu}_{\text{Cu(0)-Cu(II)}}$ values ~1.40‰ lighter than the run CuAu-60 (non-stirred). The transport of species to the metal surface and away from the metal surface depends on the thickness of the diffusion layer which increases with increasing stirring rate. Higher stirring rates also promote the steady local current at the electrode (Bard and Faulkner, 2001) and support strong isotope fractionation. We choose a stirring speed of 300 rpm as standard conditions to minimize contributions of transport in the diffuse layer to copper isotope fractionation.

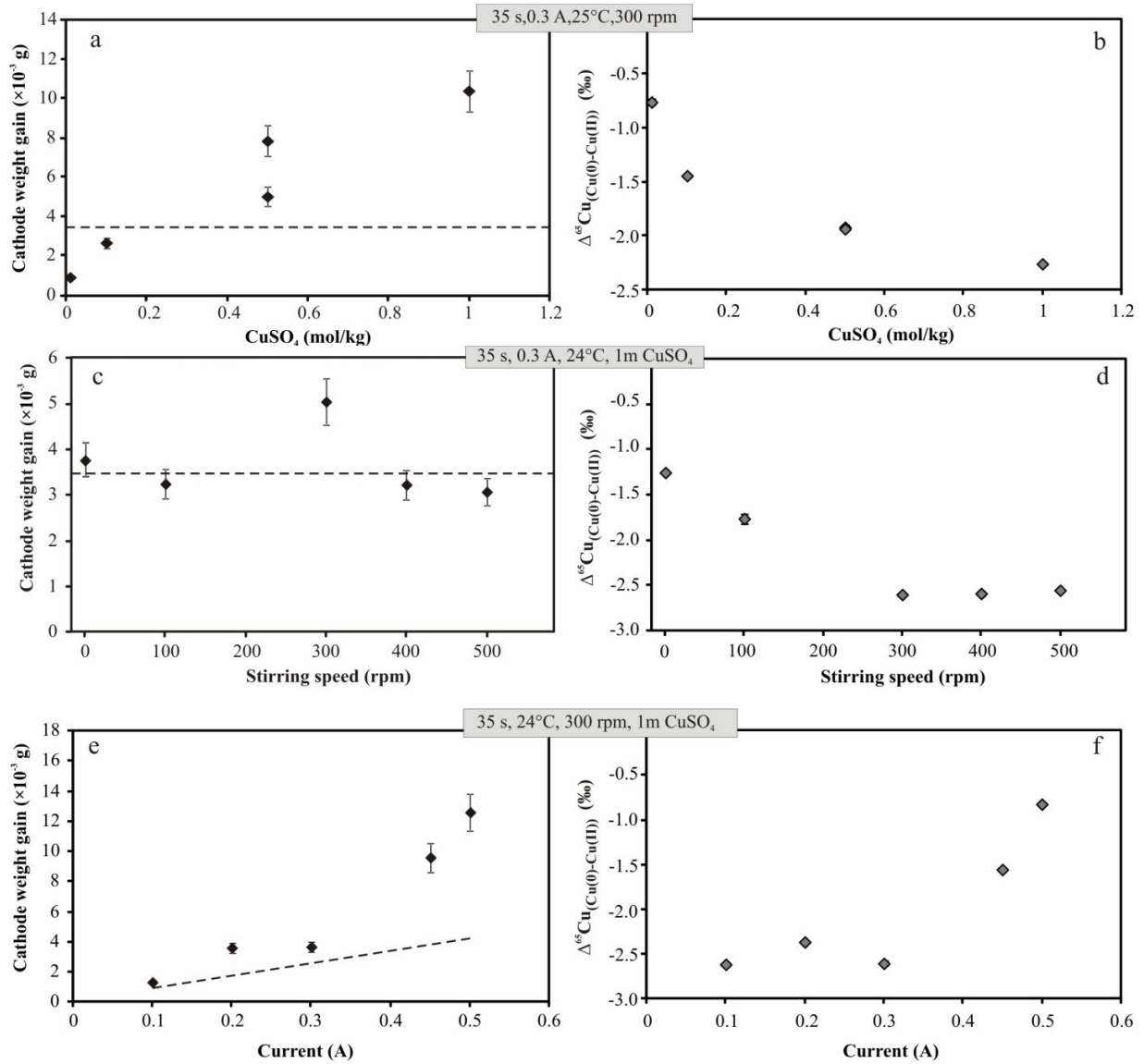
Fig. 2e shows that the mass of deposited Cu strongly increases with increasing current at high current (> 0.3 A). The isotope fractionation remains rather constant at currents up to 0.3 A, while its extent decreases sharply at higher currents (Fig. 2f). This implies that transport in the solution becomes a predominant factor for isotopic fractionation at currents > 0.3 A, and we choose a current of 0.3 A as standard condition for our experiments.

Deposition efficiency at standard conditions (0.3 A, 300 rpm and 1 mol kg⁻¹ $\text{CuSO}_{4(\text{aq})}$) has a positive linear correlation to run duration as shown in Fig. 2g, which is in good agreement with the Faradaic estimation (Eq. (3)). The straight line in Fig. 2g can be extrapolated to the origin, i.e. $m_{(t=0)} = 0$ g, meaning that there is no delay in nucleation in our study. This finding is consistent with literature. Based on microscopic observations, Andersen et al. (1994), Guo and Searson (2010) and Mamme et al. (2017) concluded that nucleation of copper metal from copper sulfate solution occurs within less than 20 seconds and often instantaneously. The copper isotopic data show a trend of increasing $\Delta^{65}\text{Cu}$ values with increasing run duration (Fig. 2h). This trend can be explained by preferential incorporation of ⁶³Cu in the metallic phase and depletion of the adjacent solution in the light copper isotope. With progressing electroplating transport through the diffuse layer becomes increasingly important for the effective isotope fractionation. Since we were particularly interested in the reactions in the double layer, we decided to use a short run duration of 35 s to avoid significant influence of transport in the diffuse layer.

The evolution of the amount of precipitated copper and its isotopic composition with temperature is shown in Figs. 2i, 2j. Both curves have a minimum at 35°C. The minimum is more pronounced in the isotope fractionation, i.e. $\Delta^{65}\text{Cu}_{\text{Cu(0)-Cu(II)}}$ value at 35°C is 1.61‰ lower than that at 5°C. Dilution by ice melting cannot explain this difference. Considering Fig. 2b, lowering of Cu concentration by 15% corresponds to an increase of $\Delta^{65}\text{Cu}_{\text{Cu(0)-Cu(II)}}$ by 0.3‰. The drastic change in isotope fractionation may indicate a change in the controlling mechanisms for electrodeposition. Most likely transport in the diffuse layer becomes important at such conditions. On the one hand,

Chapter III

the thickness of the diffuse layer increases upon cooling due to the increase in viscosity (Hotlos and Jaskuła, 1988). On the other hand, the diffusivity of dissolved species is lowered by a factor of 2 when temperature decreases from 35°C to 5°C (Hinatsu and Foulkes, 1989). Both effects cause the Cu^{2+} ions to take longer to pass through the diffuse layer. Lowering of isotope fractionation is expected when diffusion in the solution becomes the controlling process.



Chapter III

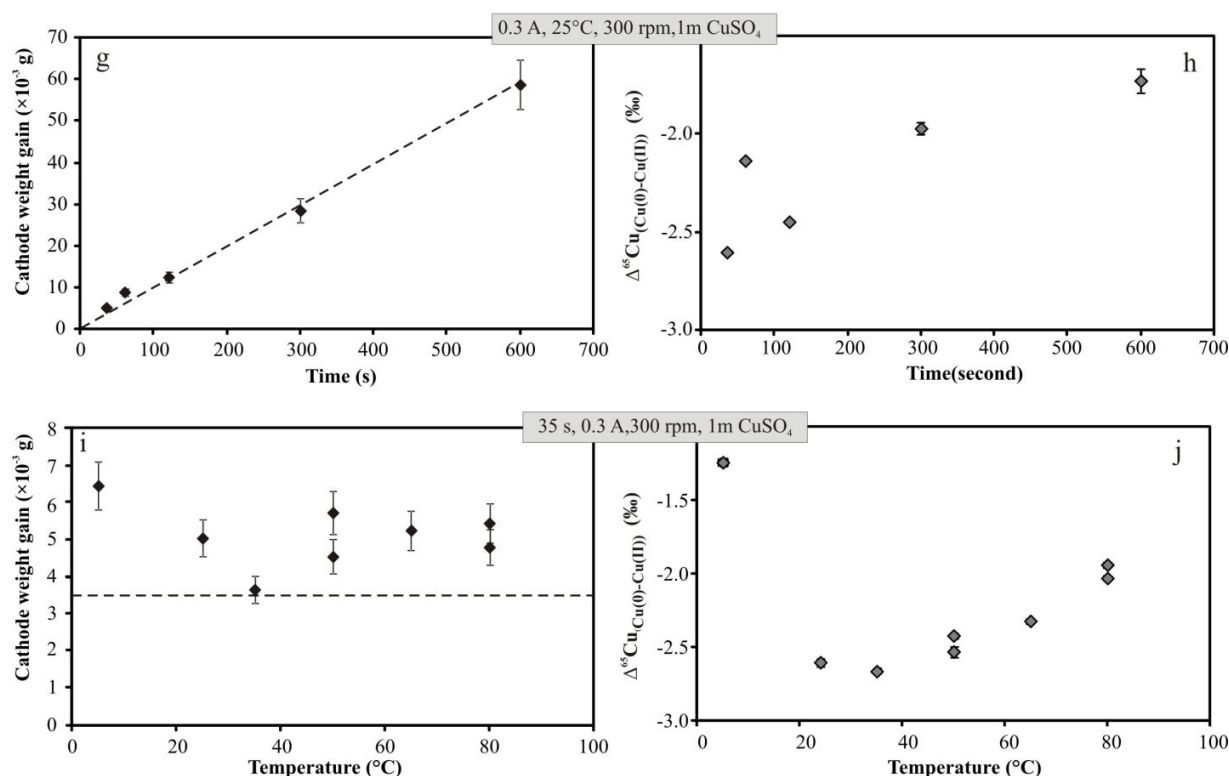


Figure 2 The mass change of electroplated Cu and copper isotope fractionation as a function of experimental variables. Dashed lines are the Faradic estimation of the mass of deposited Cu at given conditions. Cathode mass gain was acquired by the data of ICP-OES analyses. (a, b) variation of CuSO₄ concentration; (c, d) variation of electrolysis time; (e, f) variation of applied current; (g, h) variation of cell temperature; (i, j) variation of solution stirring speed.

5. Discussion

Kavner and co-workers used the electroplating technique to study isotope fractionation during reduction in Fe and Zn solutions (Kavner et al., 2005; Kavner et al., 2008; Kavner et al., 2009; Black et al., 2010b; Black et al., 2014). They applied the constant potential technique which has the advantage to enable measurements of overpotential at the electrodes during operation. The constant current method used in our study, on the other hand, has the advantage to give insights into the material fluxes in the system and is often applied in industrial electroplating. In combination with quantification of the bulk metal deposition rate, information can be obtained on the processes affecting electroplating. However, regardless of whether controlled current or controlled potential is applied, light isotopes are preferentially electroplated, which is consistent with a rule of thumb stating that higher oxidation states tend to favor heavier isotopes (Schauble, 2004).

A key question in isotope fractionation studies is whether the measured fractionation between different phases or different species represents thermodynamic equilibrium or is determined by kinetic effects. Quite often this question could not be answered unequivocally in previous copper isotope fractionation studies (experiments are

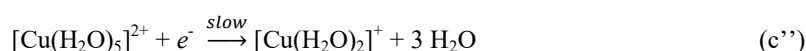
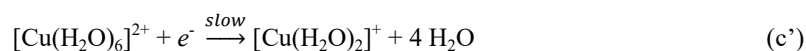
Chapter III

summarized in Moynier et al. (2017)). In the first case, isotopic exchange between coexisting phases/species must be possible at any stage of the experiment, for instance copper isotopes in precipitated minerals must be able to exchange with copper isotopes in solution. This has not been approved in most of the studies. In the second case, one of the steps in the reaction mechanisms is irreversible, for instance there is no possibility of re-mobilization of isotopes which are strongly bonded in newly formed minerals. Diffusion is commonly too slow in minerals at room temperature so that the interior of the minerals is disconnected from the solution. In order to clarify this question, we will have a closer look on the mechanisms of Cu electrodeposition in following.

5.1 Mechanisms of Cu electrodeposition

A simplified illustration of copper electroplating is shown in Fig. 3. Under acidic conditions the dominating copper species in aqueous solutions are aquacomplexes of Cu^{2+} ions. In several papers a sixfold coordination of Cu^{2+} has been proposed with longer Cu^{2+} -O distances along the vertical axis, due to the Jahn-Teller distortion (Musinu et al., 1983; Fulton et al., 2000a; Sherman, 2001). Computational (Amira et al., 2005; Frank et al., 2005) and spectroscopic (Benfatto et al., 2002; de Almeida et al., 2009) studies favor a picture with fivefold coordination of Cu^{2+} , and a rapid interconversion between square pyramidal and trigonal bipyramidal configurations (Pasquarello et al., 2001). In our further considerations we used both the sixfold and the fivefold coordination as extrema to estimate the extent of copper isotope fractionation during electrochemical copper reduction. In addition to the solvated ions, CuSO_4^0 -associates (or ion pairs) are important species in the solutions, i.e. at elevated copper concentrations, low temperature and acidic condition (Casas et al., 2000; Cifuentes et al., 2006). Due to the strong preference of Cu^{2+} to higher coordinations (fourfold-sixfold), it is likely that 2-4 H_2O molecules are bonded in the coordination shell of the copper ions of CuSO_4^0 -associates. In the scheme these water molecules are not shown for clarity. In the bulk solution, $[\text{Cu}(\text{H}_2\text{O})_5]^{2+}$, $[\text{Cu}(\text{H}_2\text{O})_6]^{2+}$ and CuSO_4^0 are rapidly homogenized by stirring and by thermal motion. Thus, five steps need to be discussed as possible rate-controlling during Cu electrodeposition:

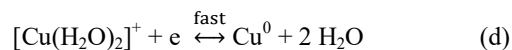
- (a) Near the surface of the electrode the mass transport boundary layer (also called diffuse layer, Bard and Faulkner (2001)) is formed. Its thickness depends on the viscosity of the solution and the stirring rate. In the mass transport boundary layer, diffusion controls the transport of species towards the electrode surface.
- (b) Rapid, reversible interconversion of Cu(II) species occurs in the diffuse layer as well as in bulk solution. Thus, CuSO_4^0 is in dynamic equilibrium with $[\text{Cu}(\text{H}_2\text{O})_5]^{2+}$ and $[\text{Cu}(\text{H}_2\text{O})_6]^{2+}$.
- (c) The surface of the electrodes is covered by adsorbed water molecules and other possible species dissolved in the solution. An electric double layer is formed in response to the charge of the electrode. In this layer hydrated copper (II) complexes are enriched and can react by electron transfer to a monovalent intermediate via



Chapter III

These reactions are shown in the scheme of Fig. 3. In these electrochemical reactions a change in coordination of copper occurs since Cu^+ has strong preference for linear coordination (Fulton et al., 2000a, 2000b).

- (d) Subsequently, the monovalent species is adsorbed and discharged at the electrode surface (Fig. 3).



This reaction is reversible and much faster than step (c) (Mattsson and Bockris, 1959; Bockris and Enyo, 1962). Thus, the first reduction reactions (c', c'') is a bottleneck for the electroplating reaction.

- (e) The final step of the process is the formation of the metallic film. This may include nucleation on the electrode surface as well as the growth of nuclei. This process depends strongly on the overpotential and on the surface structure of the electrode, i.e. suitable sites for hosting copper atoms, (Venables et al., 1984; Brande and Winand, 1992; Budevski et al., 2000; Grujicic and Pesic, 2002; Radisic et al., 2006). Surface diffusion can be rate-controlling when the Cu electrodeposition is conducted at low current densities as well as the electrode surface is specially treated in order to maintain a low number of surface dislocations (Bockris and Enyo, 1962; Bockris and Kita, 1962).

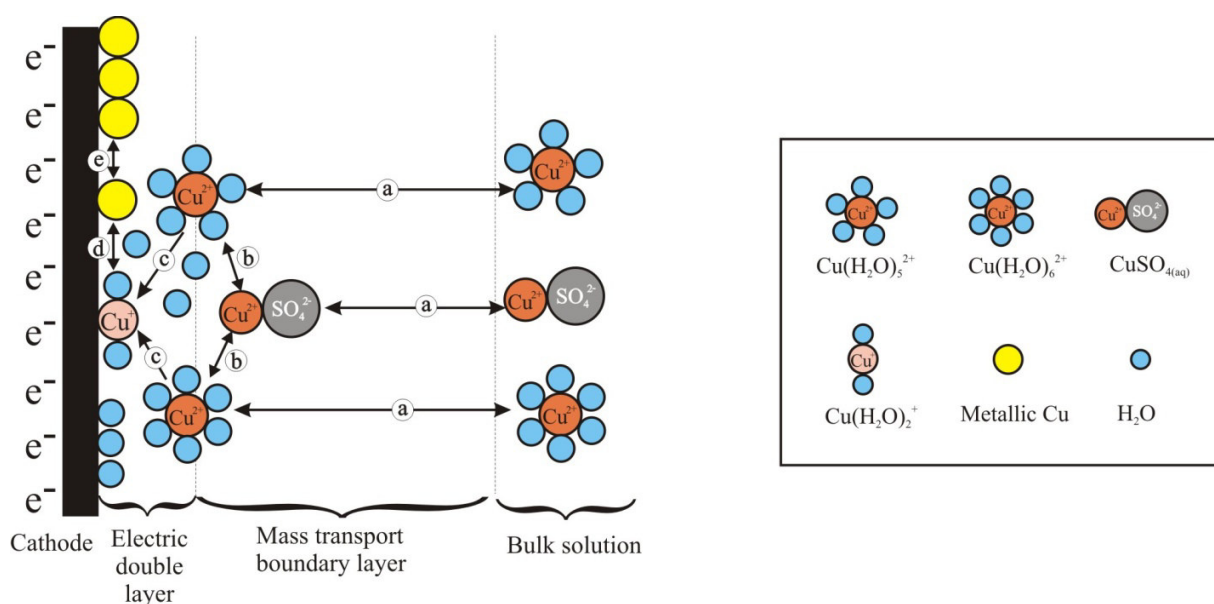


Figure 3. Schematic drawing of copper electroplating (modified from Bard and Faulkner (2001)). The deposition of copper can be controlled by three processes, mass transport in the diffuse layer (step a), kinetics of the electrochemical reaction (step c', c'' and d), and nucleation and growth of metallic phase (step e). See text for more details.

Chapter III

Formation of Cu(I) as an intermediate species during the copper electroplating has been approved by several studies (Mattsson and Bockris, 1959; Brown and Thirsk, 1965; Slaiman and Lorenz, 1974). A cuprous hydroxide has been identified in a pH of ~5 solution by spectroscopic methods (Texier et al., 1998; Velasco-Vélez et al., 2017), consistent with the Eh-pH diagram of the CuSO₄-H₂O system published by (Grujicic and Pesic, 2002). At lower pH as used in our study a [Cu(H₂O)₂]⁺ complex is more likely. If the solution is sufficiently acidic metallic Cu will be formed. On the other hand, at pH ≥ 4.8 the precipitation of Cu₂O instead of metallic Cu was proved by Velasco-Vélez et al. (2017). Since our focus is on the formation of metallic copper and our experiments were performed at pH < 4.7, we will restrict the discussion to acidic conditions. In the following the effects of thermodynamics and kinetics on copper isotope fractionation during electroplating will be discussed from a theoretical point of view.

5.2 Equilibrium effects on isotope fractionation

If the system reaches thermodynamic equilibrium, meaning all processes are reversible, isotope fractionation is a result of different vibration frequencies of isotopes in the coexisting states. When the vibrational frequencies of the isotopomers of all the species are known, the equilibrium isotope fractionations can be easily calculated using their reduced partition function ratios β (Bigeleisen and Mayer, 1947; Urey, 1947; O'Neil, 1986; Criss, 1999; Schauble, 2004; Anbar et al., 2005; Moynier et al., 2017). The β values can easily be converted to $\delta^{65}\text{Cu}$ for two complexes in equilibrium by Eq.(5):

$$\begin{aligned} \Delta^{65}\text{Cu}_{\text{B-C}} (\text{‰}) &= \delta^{65}\text{Cu}_{\text{B}} - \delta^{65}\text{Cu}_{\text{C}} \\ &\approx 1000 \cdot \ln\beta_{\text{Cu(B)}} - 1000 \cdot \ln\beta_{\text{Cu(C)}} \quad (5) \end{aligned}$$

where B and C represents two different copper species.

Fujii et al. (2013) have used this approach to calculate equilibrium fractionation for different copper species in aqueous solutions. As shown in Fig. 3, Cu(II) and Cu (I) species in solution are [Cu(H₂O)₅]²⁺, [Cu(H₂O)₆]²⁺, CuSO₄⁰-associates and [Cu(H₂O)₂]⁺. In the calculation it is assumed that CuSO₄⁰-associates are also complexed by water molecules, i.e. the coordination is [CuSO₄(H₂O)₄]⁰, consistent with Cu-O distances measured by X-ray diffraction (Musinu et al., 1983). The predicted $\Delta^{65}\text{Cu}$ values for the equilibrium between different copper species are included in Fig. 5. Isotope fractionation is more pronounced when a fivefold coordinated Cu²⁺ is involved compared to a sixfold coordinated Cu²⁺. At room temperature, the predicted $\Delta^{65}\text{Cu}$ value at equilibrium is -0.856‰ between [Cu(H₂O)₅]²⁺ and [CuSO₄(H₂O)₄]⁰, and -1.679‰ between [Cu(H₂O)₅]²⁺ and [Cu(H₂O)₂]⁺. With increasing temperature the equilibrium isotope fractionation for these exchange equilibria becomes less pronounced (Fig. 5).

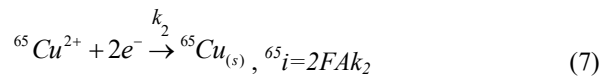
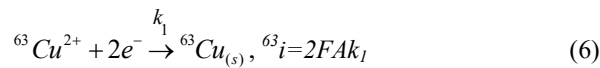
Isotope fractionation during the transformation of dissolved Cu(I) into metallic Cu (reaction (d)) is not predicted by the computational studies. Thus, the contribution of such equilibrium to the overall copper isotope fractionation cannot be estimated. The equilibrium isotope fractionation between the metal precipitates and their hydrated aqua complexes has been calculated for other transitional metals (e.g. Fe, Zn) at 25°C, $\Delta^{56}\text{Fe}_{\text{Fe}^0\text{-Fe}(\text{H}_2\text{O})_6^{2+}} = -0.9\text{‰}$

Chapter III

(Schauble et al., 2001) and $\Delta^{66}\text{Zn}_{\text{Zn}^0\text{-Zn}(\text{H}_2\text{O})_6^{2+}} = -1.6 \text{ ‰}$ (Black et al., 2011). The measured isotope fractionations after electroplating (Black et al., 2010a; Black et al., 2010b; Black et al., 2014) are much larger than the predicted equilibrium fractionation for both isotope systems, implying that kinetics and not thermodynamic equilibrium control the processes.

5.3 Kinetic effects on isotope fractionation

The electrodeposition process is a heterogeneous reaction occurring only at the electrode-electrolyte interface. Its rate depends on mass transport to the electrode and various surface effects, in addition to the usual kinetic variables (Bard and Faulkner, 2001). The rate is typically proportional to the current, expressed as $i=n \cdot F \cdot A \cdot k$ (Bard and Faulkner, 2001), where n is the number of electrons delivered, A is the surface area of an electrode and k is the electrochemical reaction rate ($\text{mol s}^{-1} \text{ cm}^{-2}$). Based on this relation, a mass-dependent current and reaction rate expression has been proposed by Black et al. (2010b) to explain Fe isotope fractionation during electrodeposition experiments. Applying this concept to our experiments yields



where ${}^{63}i$ and ${}^{65}i$ are the partial currents related to both copper isotopes and k_1 and k_2 are the corresponding reaction rates. Following Black et al. (2010b) and using Eqs. (6, 7), the Cu isotope fractionation induced by the different partial currents can be expressed as:

$$\Delta^{65}\text{Cu}_{\text{Cu(0)-Cu(II)}} (\text{‰}) = 1000 \times \left(\frac{{}^{65}i}{{}^{63}i} - 1 \right) - 0.16 \quad (8)$$

where 0.16‰ is the Cu isotope composition of starting electrolyte solution (Table 1). Using Eq.(8), we could theoretically estimate the isotope fractionation controlled by different processes, i.e. mass transport, electrochemical reduction and surface diffusion.

5.3.1 Diffusion related Cu isotopic fractionation

Two steps related to diffusion, i.e. mass transport and surface diffusion, can contribute to isotope fractionation. Theoretical estimations in the following enable us to understand their influence on isotope fractionation.

The mass transport (a) in the diffuse layer to the electrode can be limiting for the reaction rate (Fig. 3). The largest rate of mass transfer of the species occurs when Cu^{2+} is reduced as fast as it is delivered to the electrode surface. The value of the current under these conditions is called the limiting current, $i_{\text{diffusion limited}}$, which can be derived from a semi-empirical treatment of steady state mass transfer, (Bard and Faulkner, 2001):

Chapter III

$$i_{\text{diffusion limited}} = n \cdot F \cdot A \cdot m_o \cdot C_{\text{Cu}^{2+}}^* \quad (9)$$

where $C_{\text{Cu}^{2+}}^*$ is the bulk concentration of Cu^{2+} (mol kg^{-1}), m_o is the mass transfer coefficient (cm s) defined by

$$m_o = \frac{D_{\text{Cu}}}{d} \quad (10)$$

where D_{Cu} is the diffusion coefficient of Cu^{2+} in the solution ($\text{cm}^2 \text{s}^{-1}$), d is the thickness of the diffusion layer (cm) which is in most cases unknown for the specific equipment and conditions of electroplating. However, for calculation of the diffusion-related isotope fractionation, the knowledge of the thickness of the diffusion layer is not required, but only the difference in the diffusion coefficients is relevant. Combining Eqs. (8, 9, 10) yields

$$\Delta^{65}\text{Cu}_{\text{Cu(0)-Cu(II)}} (\text{‰}) = 1000 \times \left(\frac{D_{65\text{Cu}}}{D_{63\text{Cu}}} - 1 \right) - 0.16 \quad (11)$$

The mass dependence of the ratio on the diffusion coefficients can be described as

$$\frac{D_1}{D_2} = \left(\frac{M_2}{M_1} \right)^\gamma \quad (12)$$

where D_1 and D_2 are the isotope-dependent diffusion coefficients of species with molecular mass M_1 and M_2 . In the case of diffusion in ideal gases the exponent γ is experimentally determined as 0.5 (Jähne et al., 1987). Applicability of Eq. (12) has also been verified by experimental data on the isotopic fractionation during diffusion of ions in water (Pikal, 1972; Fritz, 1992; Rodushkin et al., 2004; Richter et al., 2006).

In gases the species are well defined as neutral molecules or atoms with corresponding masses. In aqueous solutions, however, diffusing species are complexes with more or less strongly bond ligands but may be also associates of ions. Hence, effective masses of diffusing species are much larger than the mass of the involved ions and diffusion-induced fractionation is small. Additionally, the γ value of 0.5 seriously overstates the mass dependence of diffusion of ionic species in water. The experimental value of the exponent γ decreases from 0.02 for dissolved Na to 0.002 for dissolved Fe and Zn, respectively, (Pikal, 1972; Rodushkin et al., 2004). As Cu shows similar geochemical behavior as other transitional metals, such as Fe and Zn, we may apply the exponent γ as 0.002 to estimate the extent of fractionation caused by diffusion. Considering $[\text{CuSO}_4(\text{H}_2\text{O})_4]^0$, $[\text{Cu}(\text{H}_2\text{O})_5]^{2+}$ and $[\text{Cu}(\text{H}_2\text{O})_6]^{2+}$ as the Cu diffusing species, the corresponding values of $\frac{D_{65\text{Cu}}}{D_{63\text{Cu}}}$ are 0.9957, 0.9960 and 0.9963, respectively. In all cases, the diffusion-induced $\Delta^{65}\text{Cu}$ values are about -0.2‰. Thus, this calculation confirms that mass transfer in the solution causes only minor Cu isotopic fractionation, consistent with findings of Black et al. (2010a, 2010b) for electrochemical reduction of Fe and Zn isotopes. If the solution is well stirred (e.g. ≥ 300 rpm), currents are kept low (e.g. ≤ 0.3 A) and the concentration of Cu^{2+} is higher than 0.5 mol/kg, the effect of mass transport on copper isotope fractionation is negligible for short electroplating times. However, with progressive precipitation of metallic copper, the solution adjacent to the electrode is depleted in the light copper isotope,

Chapter III

resulting in a decrease of effective fractionation which is determined as the difference between bulk solution and deposited metal.

In addition, surface diffusion on the electrode (step (e)) can be a dominant for the formation of the thin metal film especially at low current. The adsorbed species on the electrode surface can be charged ions (e.g. $[\text{Cu}(\text{H}_2\text{O})_2]^+$) and/or uncharged atoms (Cu^0). A surface diffusion effect on isotope fractionation of these species can be calculated by means of Eqs. (11, 12). When doing so, the estimated isotope fractionation caused by surface diffusion at the electrode is also insignificant, i.e. -0.2‰, when γ is assumed as 0.002.

5.3.2 Isotopic fractionation due to electrochemical kinetics

The previous theoretical estimations of both equilibrium fractionation and diffusion (mass transport, surface diffusion) induced fractionation show much lower values than the experimentally observed fractionation. Thus, the chemical and electron transfer steps governing the precipitation reaction at the electrode must contribute significantly to the isotope fractionations.

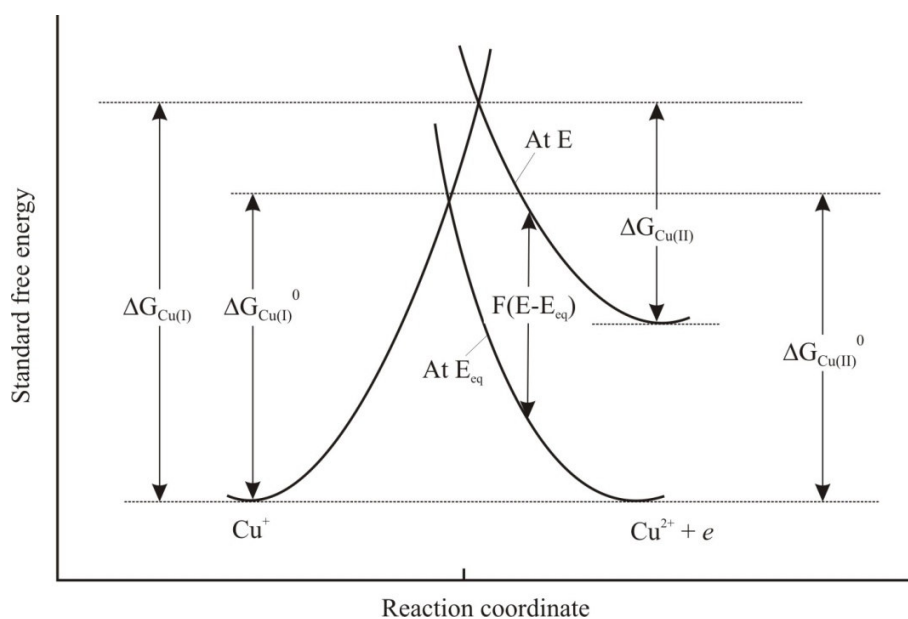


Figure 4. Simplified illustration of standard free energy changes during the first reduction step at the cathode (modified after Bard and Faulkner (2001)). Reaction coordinate represents the changes in bond distances and reorientation of solvent molecules. $\Delta G_{\text{Cu(I)}}^0$ and $\Delta G_{\text{Cu(II)}}^0$ are the activation energies of Cu^{2+} and Cu^+ at equilibrium; $\Delta G_{\text{Cu(II)}}$ and $\Delta G_{\text{Cu(I)}}$ are the activation energies of Cu^{2+} and Cu^+ when the applied potential is more negative than the equilibrium potential. F is Faraday constant. Intersection points of the energy curves correspond to the transition state.

In Figure 4 a simple energy scheme for the rate determining step $\text{Cu}^{2+} + e^- \leftrightarrow \text{Cu}^+$ at the cathode is shown. When no voltage is applied, the forward ($\text{Cu}^{2+} + e^- \rightarrow \text{Cu}^+$) and the backward ($\text{Cu}^+ \rightarrow \text{Cu}^{2+} + e^-$) reaction rates are equal, and the system is at dynamic equilibrium. In that case, the electrode potential (E) is equivalent to the

Chapter III

equilibrium potential of the system (E_{eq}), thus, the overpotential ($\eta = E - E_{eq}$) is zero. The intersection of the energy curves of reactants and products corresponds to the transition state, i.e. a high energetic configuration in the system. The difference in energy between the reactants or the products to the intersection point defines the corresponding activation energy ΔG . In the equilibrium case both values are identical.

When switching on the electrical power, the energy level of the product side (Cu^+) is lowered and a netto flux towards the reduced side occurs. As a consequence, a negative overpotential is generated at the cathode, which modifies the energy landscape. The energy barrier for reduction is lowered and that for oxidation is raised up. The activation energy is determined by two distinct contributions: i) reorganization energy involving changes in bond length and angles prior to electron transfer; ii) the difference in configurational free energy between products and reactants; (Kavner et al., 2005). Hence, difference in vibrational states of the isotopologues result in slightly different activation energies and, subsequently, in an isotopic fractionation.

(Kavner et al., 2005) developed a model for isotope fractionation during electrodeposition by combining stable isotope theory and electron transfer kinetics. For iron electroplating they demonstrated that isotope fractionation can be strongly affected by the applied voltage. However, the effect seems to be highly dependent on the experimental conditions, the specific redox system as well as the ligands available for complexation. For instance, little variation of Zn isotope fractionation with overpotential was observed during zinc electroplating from various solutions (Fig. 5a in Black et al. (2010a)). It is worth noting that the model of Kavner et al. (2005) may not be directly transferable to copper electroplating which is a two-step reaction, and the rate-determining step $Cu^{2+} + e^- \rightarrow Cu^+$ occurs in the solution rather than directly on the electrode surface. Although we cannot exclude that the applied voltage has some effect on isotope fractionation in our experiments as well, we presume that its contribution to the measured fractionation is small, and the key parameter is the vibrational state of the isotopes in the reactants and in the transition state.

5.4 Temperature dependence in comparison to other studies

A linear dependence of $\Delta^{65}Cu$ vs. $1/T^2$ is expected for equilibrium isotope fractionation by stable isotope theory (Bigeleisen and Mayer, 1947; Urey, 1947). In the range from 35 - 80°C our data are well represented by such relationship as shown in Fig. 5. Linear regression yields $\Delta^{65}Cu_{Cu(0)s-Cu(II)aq} = -(0.27 \pm 0.04) \times 10^6 T^{-2} - (0.16 \pm 0.34)$, $R^2=0.93$. However, noticeable deviation from this linear trend is visible towards lower temperature with much smaller fractionation than expected. This implies a change in the controlling mechanisms. Most likely, as discussed in the *Results* chapter, mass transport through the diffuse layer becomes dominating at low temperature for the applied electroplating conditions. The consistency of our high temperature data with the results of Ehrlich et al. (2004) is striking. They conducted anoxic precipitation of covellite ($Cu(I)S$) from an aqueous $CuSO_4$ solution at temperatures from 2°C to 40°C using Na_2S solution as reducing agent. Their experiments were performed at slightly acidic conditions (pH of 4.3 - 4.45). The measured Cu isotope fractionation between $Cu(II)$ and $Cu(I)$ ranged from - 2.7‰ to -3.5‰ and linear regression yields $\Delta^{65}Cu_{Cu(I)s-Cu(II)aq} = -(0.25 \pm 0.03) \times 10^6 T^{-2} - (0.18 \pm 0.30)$, $R^2=0.98$. In the experiments of Ehrlich et al. (2004), the first step is a reduction of Cu^{2+} aquacomplexes by sulfide ions in solution.

Chapter III

Subsequently, covellite is precipitated due to oversaturation of the solution. According to Ehrlich et al (2004) the resulting Cu isotope fractionation is most likely controlled by reaction kinetics and does not represent equilibrium fractionation, since the precipitation is irreversible. Thus, although the experimental conditions are very different in our study and the study of Ehrlich et al. (2004), it appears that in both cases the kinetics of reduction of Cu^{2+} aquacomplexes determine the isotope fractionation. This implies that the specific electron transfer (either from an electrode or from a reducing agent such as sulfide) has minor effect on the fractionation process. Thus, the key parameter is the change in configuration from the reactant to the transition state. Combining both data sets (without our low temperature data) a regression is established over a large temperature range of 2 - 80°C ($\Delta^{65}\text{Cu}_{\text{Cu(I)s} - \text{Cu(II)aq}} = -(0.29 \pm 0.01) \times 10^6 \text{T}^{-2} - (0.31 \pm 0.15)$, $R^2 = 0.98$). This relationship may be used to estimate copper isotope variation also for natural systems or in mining environments when reduction starts from Cu^{2+} aquacomplexes and reaction kinetics control fractionation.

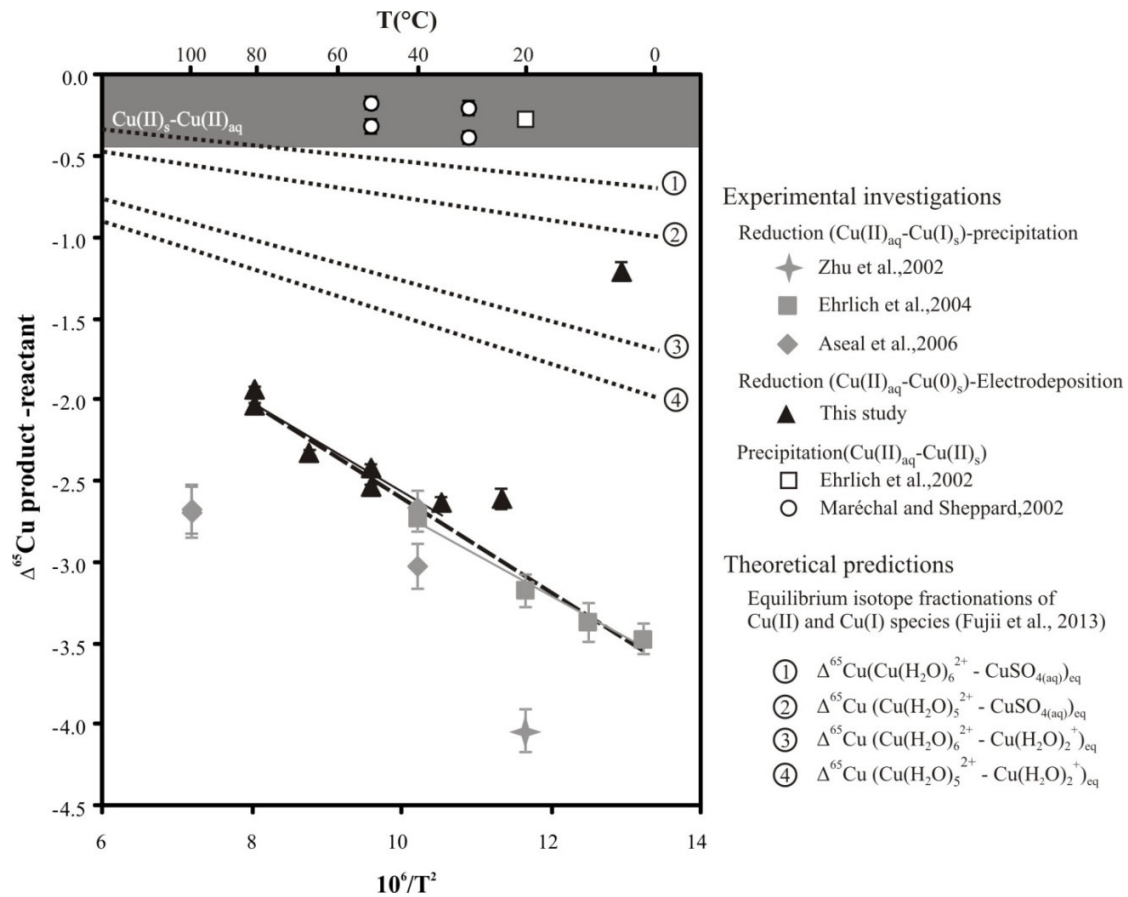


Figure 5. Temperature dependence on Cu isotope fractionation. Solid triangular symbols represent isotope fractionation associated with Cu(0)-Cu(II) reduction process, and data are from this study (T series in Table 1). Gray symbols represent isotope fractionation between Cu(I) minerals and aqueous Cu(II) solutions, data sources and experimental approaches are given in the right side legend. The dark gray field marks the area of precipitation of Cu^{2+} -bearing minerals without redox change. Solid lines are linear regressions to the data of this study (excluding our low temperature data) and Ehrlich et al. (2004). Dashed trend line is the linear-fit regression of both data sets. The dotted lines represent theoretical predictions for species reactions in aqueous solutions (see text for more details).

Chapter III

However, isotope fractionation may be different when copper complexing ligands, i.e. halogens, are present in solution. Zhu et al. (2002) studied reduction of $\text{Cu}(\text{NO}_3)_2$ solution by KI at 20°C. They found a large isotope difference of -4.1‰ between the precipitated CuI and the remaining solution. Furthermore, a different control of the reduction process may occur when solid reduction agents such as pyrite or pyrrhotite are used. Asael et al. (2006) applied this method to precipitate Cu(I) sulfides (i.e., chalcopyrite, covellite and chalcocite) from a CuSO_4 solution at temperature of 40°C and 100°C under anoxic condition and measured fractionation values of ca. -3.0‰ and ca. -2.7‰, respectively.

In any cases, the reduction-induced copper isotope fractionation is much larger than the theoretical predictions for equilibrium fractionation of copper species in aqueous solutions (Fig. 5). Furthermore, chemical reactions without redox state change, e.g., precipitation of malachite or $\text{Cu}(\text{OH})_2$ from Cu(II) solutions, isotope fractionations are generally one order of magnitude lower than those from redox reactions, i.e. -0.2‰ to -0.4‰ (Fig.5; Maréchal and Sheppard, 2002; Ehrlich et al., 2004).

Abiotic oxidative dissolution process can produce substantial variations in Cu isotopes (up to -2.6‰) as shown by Mathur et al. (2005), Fernandez and Borrok (2009a) and Kimball et al. (2009). However, the involved reactions are rather complex and the findings are difficult to interpret in terms of the processes determining copper isotope fractionation. Therefore, these data are not considered in Fig. 5.

6. Conclusions and implications

Cu electrodeposition experiments under constant current condition were performed to reduce Cu(II) to metallic Cu. The results show that the light isotope is preferentially electroplated and large isotope fractionation is induced by the change of the redox state. The Cu isotope fractionation is most strongly affected by the electrolyte concentration, followed by solution stirring speed, electrolysis time, current and temperature. The $\Delta^{65}\text{Cu}_{\text{Cu(0)-Cu(II)}}$ values vary from -2.66‰ at 35°C to -1.93‰ at 80°C, suggesting a negative temperature dependence on the isotope fractionation in this temperature range. However, smaller fractionation observed in the range of 5 - 25°C indicates a change in the controlling mechanism towards lower temperature.

The theoretical estimations indicate that equilibrium fractionation of Cu species in aqueous solution is unlikely responsible for the observed fractionation. Three competing kinetic processes must be considered as rate and fractionation controlling: mass transport to the electrode, electrochemical reaction kinetics and surface diffusion at the surface of the electrode. When the Cu electroplating is carried out at high electrolyte concentration ($> 0.5 \text{ mol kg}^{-1} \text{ CuSO}_{4(\text{aq})}$), short electrolysis time (e.g. 35 s), low current ($\leq 0.3 \text{ A}$), and high temperature ($\geq 35^\circ\text{C}$) in well stirred solutions ($\geq 300 \text{ rpm}$), the effects of mass transport in the solution and surface diffusion are negligible, but the electrochemical kinetics can yield pronounced isotope fractionations. It is the vibrational state of the isotopologues in the reactants and in the transition state that determines the magnitude of isotope fractionation.

The experimental methodology in this study can be considered analogous to the natural galvanic interaction in copper-bearing systems. The galvanic interactions are based on the resting potential difference between two

Chapter III

minerals in direct physical contact. In a galvanic assembly: the mineral with higher resting potential is protected and behaves as a cathode where the reduction reaction occurs; the mineral with the lower resting potential behaves as an anode and preferentially dissolves. In fact, most sulfide minerals are good electronic conductors so that the galvanic process gives rise to metal sulfide anodic oxidization, e.g. Fe(II)-Fe(III), Cu(I)-Cu(II) and S(II)-S(IV), coupling with cathodic reduction, e.g., O^0-O^{-2} , Cu(II)-Cu(I), Cu(II)-Cu(0), (Thornber, 1985; Sikka et al., 1991). Furthermore, galvanic interaction, yet has not been considered in most natural processes, may play a vital role in metal release in various occurrences, such as supergene ore system, black smokers, terrestrial and seafloor sulfide ore deposits, and acid mine drainage (e.g. Sikka et al., 1991; Koski et al., 2008; Webber et al., 2015; Fallon et al., 2017). Dissolution of chalcopyrite (in physical contact with pyrite) by galvanic interaction results in the mobilization of Cu^{2+} and Fe^{2+} in aqueous fluids (e.g. Fallon et al., 2017). Fe^{2+} , one of the most common reducing agents, may promote a subsequent redox reaction with native copper formation (Genovese and Mellini, 2007). Moreover, covellite (Cu(I)S) as one of the most abundant sulfide minerals can be generated by ion-exchange reaction between mobilized Cu^{2+} and FeS/ZnS coupled with a change in oxidations state (Blowes and Jambor, 1990). The results of our study are helpful to understand the processes during cathodic reduction of Cu-bearing galvanic assembly. Most likely the reduction occurs in the electrical double layer in the solution (or between the solution and adsorbed species on the surface), similar as illustrated in Fig. 3. The emphasized transition between high-coordinated Cu^{2+} to low-coordinated Cu^+ may be rate controlling as well. This has to be tested by further experimental investigations.

Acknowledgments

This work was supported by the German Academic Exchange Service (DAAD-57076462) and Graduate School GeoFluxes. We thank Ulrich Kroll for his technical supports.

Chapter III

Nomenclature

A : surface area of an electrode (cm^2)

$C_{\text{Cu}^{2+}}^*$: concentration of Cu(II) in the bulk solution (mol cm^{-3})

d : thickness of the electrode (cm)

$D_{\text{Cu}^{2+}}$: diffusion coefficient of Cu(II) ($\text{cm}^2 \text{s}^{-1}$)

F : Faraday constant ($96485 \text{ Coulombs mol}^{-1}$)

ΔG : activation energy

$i_{\text{diffusion limited}}$: current flowing under diffusion control (Amps)

k : electrochemical reaction rate ($\text{mol s}^{-1} \text{ cm}^{-2}$)

$m_{\text{theoretical}}$: the estimated mass of the substance liberated at an electrode (gram)

m_{real} : the mass of Cu desposits on an electrode (gram)

m_0 : mass transfer coefficient (cm s)

M : is the molar mass of copper in grams per mol (g mol^{-1})

n : stoichiometric number of electrons transferred in reaction

R : gas constant ($8.3145 \text{ J K}^{-1} \text{ mol}^{-1}$)

T : temperature (K)

t : run duration in second (s)

x_i : mole fraction mole fraction of species i in deposits

z : valence number

β : reduced partition function ratios

γ : coefficient to interpret the relation of diffusion coefficients in two isotopologue species

η : overpotential (Volts)

$\delta^{65}\text{Cu}$: Cu isotope composition of certain species (‰)

$\Delta^{65}\text{Cu}$: Cu isotope fractionation between different species (‰)

Chapter III

References

- Amira, S., Spångberg, D. and Hermansson, K. (2005) Distorted five-fold coordination of $\text{Cu}^{2+}(\text{aq})$ from a Car-Parrinello molecular dynamics simulation. *Physical Chemistry Chemical Physics* 7, 2874-2880.
- Anbar, A., Jarzecki, A. and Spiro, T. (2005) Theoretical investigation of iron isotope fractionation between $\text{Fe}(\text{H}_2\text{O})_6^{3+}$ and $\text{Fe}(\text{H}_2\text{O})_6^{2+}$: implications for iron stable isotope geochemistry. *Geochimica et Cosmochimica Acta* 69, 825-837.
- Andersen, J.E., Bech-Nielsen, G. and Møller, P. (1994) Bulk crystalline copper electrodeposited on polycrystalline gold surfaces observed by in-situ scanning tunnelling microscopy. *Surface and Coatings Technology* 70, 87-95.
- Asael, D., Matthews, A., Bar-Matthews, M. and Halicz, L. (2007) Copper isotope fractionation in sedimentary copper mineralization (Timna Valley, Israel). *Chemical Geology* 243, 238-254.
- Asael, D., Matthews, A., Bar-Matthews, M., Harlavan, Y. and Segal, I. (2012a) Tracking redox controls and sources of sedimentary mineralization using copper and lead isotopes. *Chemical Geology* 310, 23-35.
- Asael, D., Matthews, A., Bar-Matthews, M., Harlavan, Y. and Segal, I. (2012b) Tracking redox controls and sources of sedimentary mineralization using copper and lead isotopes. *Chemical Geology* 310-311, 23-35.
- Asael, D., Matthews, A., Butler, I., Rickard, A.D., Bar-Matthews, M. and Halicz, L. (2006) $65\text{Cu}/63\text{Cu}$ fractionation during copper sulphide formation from iron sulphides in aqueous solution. *Geochimica et Cosmochimica Acta* 70.
- Baggio, S.B., Hartmann, L.A., Lazarov, M., Massonne, H.-J., Opitz, J., Theye, T. and Viehhaus, T. (2017) Origin of native copper in the Paraná volcanic province, Brazil, integrating Cu stable isotopes in a multi-analytical approach. *Mineralium Deposita*, 1-18.
- Bard, A.J. and Faulkner, L.R. (2001) *Electrochemical methods: fundamentals and applications*, 2nd ed. Wiley New York.
- Barrat, J.-A., Zanda, B., Moynier, F., Bollinger, C., Liorzou, C. and Bayon, G. (2012) Geochemistry of CI chondrites: Major and trace elements, and Cu and Zn isotopes. *Geochimica et Cosmochimica Acta* 83, 79-92.
- Benfatto, M., d'Angelo, P., Della Longa, S. and Pavel, N. (2002) Evidence of distorted fivefold coordination of the Cu^{2+} aqua ion from an x-ray-absorption spectroscopy quantitative analysis. *Physical Review B* 65, 174205.
- Bigalke, M., Weyer, S., Kobza, J. and Wilcke, W. (2010) Stable Cu and Zn isotope ratios as tracers of sources and transport of Cu and Zn in contaminated soil. *Geochimica et Cosmochimica Acta* 74, 6801-6813.
- Bigeleisen, J. and Mayer, M.G. (1947) Calculation of equilibrium constants for isotopic exchange reactions. *The Journal of Chemical Physics* 15, 261-267.
- Black, J.R., John, S., Young, E.D. and Kavner, A. (2010a) Effect of temperature and mass transport on transition metal isotope fractionation during electroplating. *Geochimica et Cosmochimica Acta* 74, 5187-5201.
- Black, J.R., John, S.G. and Kavner, A. (2014) Coupled effects of temperature and mass transport on the isotope fractionation of zinc during electroplating. *Geochimica et Cosmochimica Acta* 124, 272-282.
- Black, J.R., Kavner, A. and Schauble, E.A. (2011) Calculation of equilibrium stable isotope partition function ratios for aqueous zinc complexes and metallic zinc. *Geochimica et Cosmochimica Acta* 75, 769-783.
- Black, J.R., Young, E.D. and Kavner, A. (2010b) Electrochemically controlled iron isotope fractionation. *Geochimica et Cosmochimica Acta* 74, 809-817.
- Blowes, D.W. and Jambor, J.L. (1990) The pore-water geochemistry and the mineralogy of the vadose zone of sulfide tailings, Waite Amulet, Quebec, Canada. *Applied Geochemistry* 5, 327-346.
- Bockris, J.M. and Enyo, M. (1962) Mechanism of electrodeposition and dissolution processes of copper in aqueous solutions. *Transactions of the Faraday Society* 58, 1187-1202.
- Bockris, J.M. and Kita, H. (1962) The dependence of charge transfer and surface diffusion rates on the structure and stability of an electrode surface: Copper. *Journal of the electrochemical society* 109, 928-939.
- Bozzini, B., Mele, C. and D'urzo, L. (2006) Electrodeposition of Cu from Acidic Sulphate Solutions in the presence of PEG-Part II visible electroreflectance spectroscopy measurements during electrodeposition. *Journal of applied electrochemistry* 36, 87-96.
- Brandt, P.V. and Winand, R. (1992) Nucleation and initial growth of copper electrodeposits under galvanostatic conditions. *Surface and Coatings Technology* 52, 1-7.
- Brown, O. and Thirsk, H. (1965) The rate-determining step in the electro-deposition of copper on copper from aqueous cupric sulphate solutions. *Electrochimica Acta* 10, 383-393.
- Budevski, E., Staikov, G. and Lorenz, W. (2000) Electrocrystallization: nucleation and growth phenomena. *Electrochimica Acta* 45, 2559-2574.
- Casas, J.M., Alvarez, F. and Cifuentes, L. (2000) Aqueous speciation of sulfuric acid-cupric sulfate solutions. *Chemical Engineering Science* 55, 6223-6234.
- Cifuentes, L., Casas, J.M. and Simpson, J. (2006) Temperature Dependence of the Speciation of Copper and Iron in Acidic Electrolytes. *Chemical Engineering Research and Design* 84, 965-969.
- Cooper, H.K., Duke, M.J.M., Simonetti, A. and Chen, G. (2008) Trace element and Pb isotope provenance analyses of native copper in northwestern North America: results of a recent pilot study using INAA, ICP-MS, and LA-MC-ICP-MS. *Journal of Archaeological Science* 35, 1732-1747.
- Criss, R.E. (1999) *Principles of stable isotope distribution*. Oxford University Press on Demand.
- de Almeida, K.J., Murugan, N.A., Rinkevicius, Z., Hugosson, H.W., Vahtras, O., Ågren, H. and Cesar, A. (2009) Conformations, structural transitions and visible near-infrared absorption spectra of four-, five- and six-coordinated Cu (II) aqua complexes. *Physical Chemistry Chemical Physics* 11, 508-519.
- Dekov, V.M., Rouxel, O., Asael, D., Hålenius, U. and Munnik, F. (2013) Native Cu from the oceanic crust: Isotopic insights into native metal origin. *Chemical Geology* 359, 136-149.
- Ehrlich, S., Butler, I., Halicz, L., Rickard, D., Oldroyd, A. and Matthews, A. (2004) Experimental study of the copper isotope fractionation between aqueous Cu (II) and covellite, CuS . *Chemical Geology* 209, 259-269.
- Fallon, E.K., Petersen, S., Brooker, R.A. and Scott, T.B. (2017) Oxidative dissolution of hydrothermal mixed-sulphide ore: An assessment of current knowledge in relation to seafloor massive sulphide mining. *Ore Geology Reviews* 86, 309-337.
- Fernandez, A. and Borrok, D.M. (2009) Fractionation of Cu, Fe, and Zn isotopes during the oxidative weathering of sulfide-rich rocks. *Chemical Geology* 264, 1-12.
- Frank, P., Benfatto, M., Szilagy, R.K., D'Angelo, P., Della Longa, S. and Hodgson, K.O. (2005) The Solution Structure of $[\text{Cu}(\text{aq})]^{2+}$ and Its Implications for Rack-Induced Bonding in Blue Copper Protein Active Sites. *Inorganic Chemistry* 44, 1922-1933.

Chapter III

- Fritz, S.J. (1992) Measuring the ratio of aqueous diffusion coefficients between 6Li^+ Cl^- and 7Li^+ Cr^- by osmometry. *Geochimica et Cosmochimica Acta* 56, 3781-3789.
- Fujii, T., Moynier, F., Abe, M., Nemoto, K. and Albarède, F. (2013) Copper isotope fractionation between aqueous compounds relevant to low temperature geochemistry and biology. *Geochimica et Cosmochimica Acta* 110, 29-44.
- Fulton, J.L., Hoffmann, M.M. and Darab, J.G. (2000a) An X-ray absorption fine structure study of copper (I) chloride coordination structure in water up to 325 C. *Chemical Physics Letters* 330, 300-308.
- Fulton, J.L., Hoffmann, M.M., Darab, J.G., Palmer, B.J. and Stern, E.A. (2000b) Copper (I) and copper (II) coordination structure under hydrothermal conditions at 325 C: an X-ray absorption fine structure and molecular dynamics study. *The Journal of Physical Chemistry A* 104, 11651-11663.
- Genovese, A. and Mellini, M. (2007) Ferrihydrite flocs, native copper nanocrystals and spontaneous remediation in the Fosso dei Noni stream, Tuscany, Italy. *Applied geochemistry* 22, 1439-1450.
- Gregory, M.J. and Mathur, R. (2017) Understanding Copper Isotope Behavior in the High Temperature Magmatic - Hydrothermal Porphyry Environment. *Geochemistry, Geophysics, Geosystems* 18, 4000-4015.
- Grujicic, D. and Pestic, B. (2002) Electrodeposition of copper: the nucleation mechanisms. *Electrochimica Acta* 47, 2901-2912.
- Guo, L. and Seanson, P.C. (2010) Influence of anion on the kinetics of copper island growth. *Nanoscale* 2, 2431-2435.
- Haest, M., Muchez, P., Petit, J.C. and Vanhaecke, F. (2009) Cu isotope ratio variations in the Dikulushi Cu-Ag deposit, DRC: of primary origin or induced by supergene reworking? *Economic Geology* 104, 1055-1064.
- Hai, N.T., Odermatt, J., Grimaudo, V., Krämer, K.W., Fluegel, A., Arnold, M., Mayer, D. and Broekmann, P. (2012) Potential oscillations in galvanostatic Cu electrodeposition: antagonistic and synergistic effects among SPS, chloride, and suppressor additives. *The Journal of Physical Chemistry C* 116, 6913-6924.
- Hinatsu, J.T. and Foulkes, F.R. (1989) Diffusion coefficients for copper (II) in aqueous cupric sulfate - sulfuric acid solutions. *Journal of The Electrochemical Society* 136, 125-132.
- Höfler, F. and Steiger, M. (2018) Thermodynamic properties of CuSO_4 (aq) from 268 K to 377 K and phase equilibria in the $\text{CuSO}_4\text{-H}_2\text{O}$ system. *Monatshefte für Chemie-Chemical Monthly* 149, 369-379.
- Hotlos, J. and Jaskula, M. (1988) Densities and viscosities of $\text{CuSO}_4\text{-H}_2\text{SO}_4\text{-H}_2\text{O}$ solutions. *Hydrometallurgy* 21, 1-7.
- Hu, C.-C. and Wu, C.-M. (2003) Effects of deposition modes on the microstructure of copper deposits from an acidic sulfate bath. *Surface and Coatings Technology* 176, 75-83.
- Hurlen, T., Ottesen, G. and Staurset, A. (1978) Kinetics of copper dissolution and deposition in aqueous sulphate solution. *Electrochimica Acta* 23, 39-44.
- Ikehata, K. and Hirata, T. (2012) Copper isotope characteristics of copper-rich minerals from the Horoman peridotite complex, Hokkaido, northern Japan. *Economic Geology* 107, 1489-1497.
- Ikehata, K., Notsu, K. and Hirata, T. (2011) Copper isotope characteristics of copper-rich minerals from besshi-type volcanogenic massive sulfide deposits, Japan, determined using a femtosecond LA-MC-ICP-MS. *Economic Geology* 106, 307-316.
- Jähne, B., Heinz, G. and Dietrich, W. (1987) Measurement of the diffusion coefficients of sparingly soluble gases in water. *Journal of Geophysical Research: Oceans* 92, 10767-10776.
- Justel, F.J., Taboada, M.E. and Jimenez, Y.P. (2018) Thermodynamic study of the $\text{Cu-Na-H-SO}_4\text{-Cl-HSO}_4\text{-H}_2\text{O}$ system for the solubility of copper sulfate in acid seawater at different temperatures. *Journal of Molecular Liquids* 249, 702-709.
- Kavner, A., Bonet, F., Shahar, A., Simon, J. and Young, E. (2005) The isotopic effects of electron transfer: An explanation for Fe isotope fractionation in nature. *Geochimica et Cosmochimica Acta* 69, 2971-2979.
- Kavner, A., John, S., Sass, S. and Boyle, E. (2008) Redox-driven stable isotope fractionation in transition metals: Application to Zn electroplating. *Geochimica et Cosmochimica Acta* 72, 1731-1741.
- Kavner, A., Shahar, A., Black, J. and Young, E. (2009) Iron isotope electroplating: Diffusion-limited fractionation. *Chemical Geology* 267, 131-138.
- Kimball, B.E., Mathur, R., Dohnalkova, A., Wall, A., Runkel, R. and Brantley, S.L. (2009) Copper isotope fractionation in acid mine drainage. *Geochimica et Cosmochimica Acta* 73, 1247-1263.
- Kondo, K., Akolkar, R.N., Barkey, D.P. and Yokoi, M. (2014) Copper electrodeposition for nanofabrication of electronics devices. Springer.
- Koski, R.A., Munk, L., Foster, A.L., Shanks III, W.C. and Stillings, L.L. (2008) Sulfide oxidation and distribution of metals near abandoned copper mines in coastal environments, Prince William Sound, Alaska, USA. *Applied Geochemistry* 23, 227-254.
- Kusonwiriawong, C., Bigalke, M., Abgottspon, F., Lazarov, M. and Wilcke, W. (2016) Response of Cu partitioning to flooding: A $\delta^{65}\text{Cu}$ approach in a carbonatic alluvial soil. *Chemical geology* 420, 69-76.
- Kusonwiriawong, C., Bigalke, M., Cornu, S., Montagne, D., Fekiacova, Z., Lazarov, M. and Wilcke, W. (2017) Response of copper concentrations and stable isotope ratios to artificial drainage in a French Retisol. *Geoderma* 300, 44-54.
- Larson, P.B., Maher, K., Ramos, F.C., Chang, Z., Gaspar, M. and Meinert, L.D. (2003) Copper isotope ratios in magmatic and hydrothermal ore-forming environments. *Chemical Geology* 201, 337-350.
- Lazarov, M. and Horn, I. (2015) Matrix and energy effects during in-situ determination of Cu isotope ratios by ultraviolet-femtosecond laser ablation multicollector inductively coupled plasma mass spectrometry. *Spectrochimica Acta Part B: Atomic Spectroscopy* 111, 64-73.
- Li, W., Jackson, S.E., Pearson, N.J. and Graham, S. (2010) Copper isotopic zonation in the Northparkes porphyry Cu-Au deposit, SE Australia. *Geochimica et cosmochimica acta* 74, 4078-4096.
- Liu, S.-A., Huang, J., Liu, J., Wörner, G., Yang, W., Tang, Y.-J., Chen, Y., Tang, L., Zheng, J. and Li, S. (2015) Copper isotopic composition of the silicate Earth. *Earth and Planetary Science Letters* 427, 95-103.
- Luck, J.M., Ben Othman, D. and Albarede, F. (2005) Zn and Cu isotopic variations in chondrites and iron meteorites: Early solar nebula reservoirs and parent-body processes. *Geochimica Et Cosmochimica Acta* 69, 5351-5363.
- Majidi, M., Asadpour-Zeynali, K. and Hafezi, B. (2009) Reaction and nucleation mechanisms of copper electrodeposition on disposable pencil graphite electrode. *Electrochimica Acta* 54, 1119-1126.
- Mamme, M.H., Deconinck, J. and Ustarroz, J. (2017) Transition between kinetic and diffusion control during the initial stages of electrochemical growth using numerical modelling. *Electrochimica Acta* 258, 662-668.
- Maréchal, C.N. and Sheppard, S.M.F. (2002) Isotopic fractionation of Cu and Zn between chloride and nitrate solutions and malachite or smithsonite at 30 degrees and 50 degrees C. *Geochim. Cosmochim. Acta* 66.
- Maréchal, C.N., Télouk, P. and Albarède, F. (1999) Precise analysis of copper and zinc isotopic compositions by plasma-source mass spectrometry. *Chemical Geology* 156, 251-273.

Chapter III

- Markl, G., Lahaye, Y. and Schwinn, G. (2006) Copper isotopes as monitors of redox processes in hydrothermal mineralization. *Geochimica et Cosmochimica Acta* 70, 4215-4228.
- Mathur, R. and Fantle, M.S. (2015) Copper Isotopic Perspectives on Supergene Processes: Implications for the Global Cu Cycle. *Elements* 11, 323-329.
- Mathur, R., Ruiz, J., Tittley, S., Liermann, L., Buss, H. and Brantley, S. (2005) Cu isotopic fractionation in the supergene environment with and without bacteria. *Geochimica et Cosmochimica Acta* 69, 5233-5246.
- Mathur, R., Tittley, S., Barra, F., Brantley, S., Wilson, M., Phillips, A., Munizaga, F., Maksaev, V., Vervoort, J. and Hart, G. (2009) Exploration potential of Cu isotope fractionation in porphyry copper deposits. *Journal of Geochemical Exploration* 102, 1-6.
- Mattsson, E. and Bockris, J.M. (1959) Galvanostatic studies of the kinetics of deposition and dissolution in the copper+ copper sulphate system. *Transactions of the Faraday Society* 55, 1586-1601.
- Moynier, F., Vance, D., Fujii, T. and Savage, P. (2017) The isotope geochemistry of zinc and copper. *Reviews in Mineralogy and Geochemistry* 82, 543-600.
- Musinu, A., Paschina, G., Piccaluga, G. and Magini, M. (1983) Coordination of copper (II) in aqueous copper sulfate solution. *Inorganic Chemistry* 22, 1184-1187.
- Nagar, M., Radisic, A., Strubbe, K. and Vereecken, P.M. (2016) The effect of the substrate characteristics on the electrochemical nucleation and growth of copper. *Journal of The Electrochemical Society* 163, D3053-D3061.
- Natter, H. and Hempelmann, R. (1996) Nanocrystalline copper by pulsed electrodeposition: the effects of organic additives, bath temperature, and pH. *The Journal of Physical Chemistry* 100, 19525-19532.
- O'Neil, J.R. (1986) Theoretical and experimental aspects of isotopic fractionation. *Reviews in Mineralogy* 16, 1-40.
- Pasquarello, A., Petri, I., Salmon, P.S., Parisel, O., Car, R., Tóth, É., Powell, D.H., Fischer, H.E., Helm, L. and Merbach, A.E. (2001) First solvation shell of the Cu (II) aqua ion: evidence for fivefold coordination. *Science* 291, 856-859.
- Pikal, M.J. (1972) Isotope effect in tracer diffusion. Comparison of the diffusion coefficients of $^{24}\text{Na}^+$ and $^{22}\text{Na}^+$ in aqueous electrolytes. *The Journal of Physical Chemistry* 76, 3038-3040.
- Pinto, V.M., Hartmann, L.A. and Wildner, W. (2011) Epigenetic hydrothermal origin of native copper and supergene enrichment in the Vista Alegre district, Paraná basaltic province, southernmost Brazil. *International Geology Review* 53, 1163-1179.
- Pokrovski, G.S., Borisova, A.Y. and Harrichoury, J.-C. (2008) The effect of sulfur on vapor-liquid fractionation of metals in hydrothermal systems. *Earth and Planetary Science Letters* 266, 345-362.
- Radisic, A., Vereecken, P.M., Hannon, J.B., Searson, P.C. and Ross, F.M. (2006) Quantifying Electrochemical Nucleation and Growth of Nanoscale Clusters Using Real-Time Kinetic Data. *Nano Letters* 6, 238-242.
- Rempel, K.U., Liebscher, A., Meixner, A., Romer, R.L. and Heinrich, W. (2012) An experimental study of the elemental and isotopic fractionation of copper between aqueous vapour and liquid to 450° C and 400bar in the $\text{CuCl-NaCl-H}_2\text{O}$ and $\text{CuCl-NaHS-NaCl-H}_2\text{O}$ systems. *Geochimica et Cosmochimica Acta* 94, 199-216.
- Richter, F.M., Mendybaev, R.A., Christensen, J.N., Hutcheon, I.D., Williams, R.W., Sturchio, N.C. and Beloso Jr, A.D. (2006) Kinetic isotopic fractionation during diffusion of ionic species in water. *Geochimica et Cosmochimica Acta* 70, 277-289.
- Rodushkin, I., Stenberg, A., Andrén, H., Malinovsky, D. and Baxter, D.C. (2004) Isotopic fractionation during diffusion of transition metal ions in solution. *Analytical Chemistry* 76, 2148-2151.
- Roebbert, Y., Rabe, K., Lazarov, M., Schuth, S., Schippers, A., Dold, B. and Weyer, S. (2018) Fractionation of Fe and Cu isotopes in acid mine tailings: Modification and application of a sequential extraction method. *Chemical Geology*.
- Rouxel, O., Fouquet, Y. and Ludden, J.N. (2004) Copper isotope systematics of the Lucky Strike, Rainbow, and Logatchev sea-floor hydrothermal fields on the Mid-Atlantic Ridge. *economic geology* 99, 585-600.
- Schauble, E., Rossman, G. and Taylor, H. (2001) Theoretical estimates of equilibrium Fe-isotope fractionations from vibrational spectroscopy. *Geochimica et Cosmochimica Acta* 65, 2487-2497.
- Schauble, E.A. (2004) Applying stable isotope fractionation theory to new systems. *Reviews in Mineralogy and Geochemistry* 55, 65-111.
- Sherman, D.M. (2001) Quantum chemistry and classical simulations of metal complexes in aqueous solutions. *Reviews in Mineralogy and Geochemistry* 42, 273-317.
- Sikka, D.B., Petruk, W., Nehru, C.E. and Zhang, Z. (1991) Geochemistry of secondary copper minerals from Proterozoic porphyry copper deposit, Malanjkhanda, India. *Ore Geology Reviews* 6, 257-290.
- Sillitoe, R.H. (2005) Supergene oxidized and enriched porphyry copper and related deposits. *Econ. Geol.* 100, 723-768.
- Slaiman, Q. and Lorenz, W. (1974) Investigations of the kinetics of Cu/Cu^{2+} electrode using the galvanostatic double pulse method. *Electrochimica Acta* 19, 791-798.
- Takahashi, K.M. and Gross, M.E. (1999) Transport phenomena that control electroplated copper filling of submicron vias and trenches. *Journal of The Electrochemical Society* 146, 4499-4503.
- Texier, F., Servant, L., Bruneel, J.L. and Argoul, F. (1998) In situ probing of interfacial processes in the electrodeposition of copper by confocal Raman microspectroscopy. *Journal of Electroanalytical Chemistry* 446, 189-203.
- Thornber, M. (1985) Supergene alteration of sulphides: VII. Distribution of elements during the gossan-forming process. *Chemical Geology* 53, 279-301.
- Urey, H.C. (1947) The thermodynamic properties of isotopic substances. *Journal of the Chemical Society (Resumed)*, 562-581.
- Velasco-Vélez, J.-J., Skorupska, K., Frei, E., Huang, Y.-C., Dong, C.-L., Su, B.-J., Hsu, C.-J., Chou, H.-Y., Chen, J.-M. and Strasser, P. (2017) The Electro-Deposition/Dissolution of CuSO_4 Aqueous Electrolyte Investigated by In Situ Soft X-ray Absorption Spectroscopy. *The Journal of Physical Chemistry B* 122, 780-787.
- Venables, J., Spiller, G. and Hanbucken, M. (1984) Nucleation and growth of thin films. *Reports on Progress in Physics* 47, 399.
- Vicenzo, A. and Cavallotti, P. (2002) Copper electrodeposition from a pH 3 sulfate electrolyte. *Journal of applied electrochemistry* 32, 743-753.
- Webber, A.P., Roberts, S., Murton, B.J. and Hodgkinson, M.R.S. (2015) Geology, sulfide geochemistry and supercritical venting at the Beebe Hydrothermal Vent Field, Cayman Trough. *Geochemistry, Geophysics, Geosystems* 16, 2661-2678.
- Zhu, X., Guo, Y., Williams, R., O'niions, R., Matthews, A., Belshaw, N., Canters, G., De Waal, E., Weser, U. and Burgess, B. (2002) Mass fractionation processes of transition metal isotopes. *Earth and Planetary Science Letters* 200, 47-62.
- Zhu, X., O'niions, R., Guo, Y., Belshaw, N. and Rickard, D. (2000) Determination of natural Cu-isotope variation by plasma-source mass spectrometry: implications for use as geochemical tracers. *Chemical Geology* 163, 139-149

Summary and conclusions

The transport of Cu in the liquid phase of NaCl/KCl-HCl-HAc/KAc-H₂O systems has been experimentally investigated at both high P-T (800°C and 200 MPa) and low P-T ranges (100-250°C, 5-30 MPa). The total chloride concentration varies from 0 to 4.3 m. It is worth noting that copper content increases with temperature increment, e.g., there are 0.35 wt% and 0.86 wt% Cu dissolved in 0.9 m NaCl solution at 250°C and 800°C, respectively. In addition, Cu content is positively in proportion to the increasing salinity, e.g., 0.5 wt% and 4.3 wt% Cu in 0.17 m and 4.3 m NaCl solutions at 800°C, respectively. Cu was found to dissolve primarily as Cu⁺, likely CuCl₂⁻.

1. Conclusion remarks from high P-T experiments (800°C, 200 MPa)

Experiments, which were conducted with Cu/Cu₂O/CuCl and NaCl/HCl/H₂O at magmatic-hydrothermal conditions (800°C, 200 MPa), revealed that chloride-bearing aqueous fluids have the potential to increase Cu content appreciably, e.g., 1.5 wt% and 5.4 wt% of Cu dissolved in 1.5 m NaCl and 1.5 m HCl solutions, respectively. In native Cu-NaCl_{aq} systems, two types of inclusions were formed, namely fluid inclusions and Na-bearing silicate melt inclusion, indicating that hydrothermal brine and silicate melt phase can coexist at run condition. Note that Na-bearing silicate melt inclusion was formed exclusively in native Cu-NaCl_{aq} systems. Cuprite trapped in fluid inclusions and Na-bearing silicate melt inclusions is precipitated as quench product due to different cooling rates. In HCl-bearing systems, nantokite has been a common daughter mineral throughout all experiments. Quench fluids of native Cu + NaCl systems are basic whereas the fluids of the runs with native Cu ± Cu₂O + HCl + CuCl and Cu₂O+NaCl are generally acidic. A linear correlation between Cu content and initial chloride content has been derived, with Cu/Cl molal ratios of 1:7 in native Cu-NaCl_{aq} system and nearly 1:1 in native Cu-HCl systems. It is evident that not only chloride concentration but also fluid acidity has strongly effects on Cu enrichment. However, a Cu/Cl molal ratio of 1:3 has been found in native Cu-CuCl-H₂O and Cu₂O-NaCl_{aq} systems, which is caused by a back reaction with the production of native Cu (i.e., Cu⁺ + H₂ = Cu + H⁺). Thus, the stability of Cu-bearing species is strongly affected by systems oxygen fugacities and the Cu⁺ content.

These experiments also shed some lights about the inclusion properties. Firstly, regarding to the fluid inclusion synthesis technique, few inclusions can be formed in the intact quartz cylinder prior to intermediate quench but this will have minor effect on Cu content in this quartz cylinder. In addition, using two types of quartz cylinders, i.e. prefractured and in situ fractured quartz, is a reliable technique to acquire information of hydrothermal fluids. Secondly, the addition of silica gel is of great importance not only for crack healing but also for improvement of fluid inclusion quality. Thirdly, well isolated and isomeric inclusions are properly sealed whereas necking down and irregular inclusions tend to lose or gain H₂O and/or metals. Finally, rapid quench is an optimum quench technique to rule out fluid inclusions formed at late stage, which can be applied to NaCl-bearing system. Caution should be taken

Summary and conclusions

when using Rb and Cs contents to standardize LA-ICP-MS data in native Cu-NaCl_{aq} system due to the coexistence of two phases (fluid as well as melt phases), which will lead to trace elements partitioning between both phases.

2. Conclusion remarks from moderate P-T experiments (100-250°C, 5-20 MPa)

The partitioning of Cu between cuprite and hydrothermal fluids (K(Na)Cl / HAc-K(Na)Ac / H₂O, where Ac refers to acetate) is investigated elementally and isotopically at 100-250°C and 50-300 bar. The experiments were carried out for periods of up to 72 hours in a Parr autoclave allowing for in-situ sampling of fluid phase. Native copper and tenorite are the dominant experimental products. At 250°C, native Cu has been found to precipitate in pure H₂O, KCl-bearing solutions and in acetate-bearing runs (\leq 24 hours). Tenorite is observed in 150°C and 250°C long-termed (72 hours) acetate-bearing runs.

The decomposition of cuprite in hydrothermal fluids was found to be controlled by several types of reactions: (1) simple cuprite dissolution and production of Cu(I) in hydrothermal fluids at the early stage (\leq 6 hours); (2) Cu(I) disproportionation into Cu(II) and native Cu (likely 6-24 hours); (3) decarboxylation reaction and production of equimolar methane and carbon dioxide; (4) oxidation of Cu(I)/Cu(0) to Cu(II). Processes (1-3) are dominant in KCl-bearing systems, and processes (1-4) predominate in H₂O-acetate-bearing systems. Cu was found to dissolve primarily as Cu⁺, however, Cu²⁺ produced by Cu(I) disproportionation reaction may account for \leq 15% in bulk solution.

During the early stage (<24 hours) cuprite dissolution process, constant Cu content can be achieved within 24 hours at 100°C - 250°C. Dissolved Cu in pure solutions (KCl_{aq} and H₂O) is \sim 20 times lower than that in pH buffered solutions (KCl/H₂O + pH buffer). Without the presence of pH buffer (0.2 m HAc/KAc), Cu content in KCl-bearing solutions is ca. 2 log units higher than that in pure water, i.e., 160 μ g/g and 3 μ g/g, respectively. In the presence of pH buffer: (1) the temperature increment positively correlates to Cu content in KCl-bearing solutions but negatively correlates to dissolved Cu in acetate-bearing solutions; (2) pressure has almost insignificant effect on cuprite solubility; (3) increasing chloride concentration strongly enhances Cu content.

The most significant isotope fractionation is induced by oxidation reaction of Cu(I) to Cu(II), i.e., $\Delta^{65}\text{Cu}_{[\text{Cu(II)O-Cu(I)}}$ values are up to $0.35\pm 0.05\%$. To a lesser extent, isotope fractionation can be caused by the Cu(I) disproportionation reaction, i.e., $\Delta^{65}\text{Cu}_{[\text{Cu(0)-Cu(I)}}$ values are up to $0.10\pm 0.10\%$.

The gas phase determination indicates that equimolar methane and carbon dioxide are produced by acetate/acetic acid decarboxylation. It is likely that the decarboxylation results in significant reduction of dissolved Cu at 250°C after 6 hours. Furthermore, the produced gas phase (e.g., carbon dioxide) can act as oxidant, which later help to oxidize the Cu(I) into tenorite.

This study indicates that acetate plays a dual role in copper transport and deposition. On the one hand, the presence of acetate appreciably enhances Cu content by an order of magnitude, suggesting that acetate as a complexation ligand can be responsible for metal transportation in hydrothermal fluids. On the other hand,

Summary and conclusions

decarboxylation of acetate substantially decreases the dissolved Cu and aids the precipitation of Cu-bearing minerals (e.g., native Cu and tenorite). These findings may elucidate the enrichment of copper in sediment-hosted Cu ore deposit.

3. Conclusion remarks from low P-T experiments (5-80°C, 0.1 MPa)

Cu electrodeposition experiments under constant current condition were performed to reduce Cu(II) to metallic Cu. The results show that the light isotope is preferentially electroplated and large isotope fractionation is induced by the change of the redox state. The Cu isotope fractionation is most strongly affected by the electrolyte concentration, followed by solution stirring speed, electrolysis time, current and temperature. The $\Delta^{65}\text{Cu}_{\text{Cu(0)-Cu(II)}}$ values vary from -2.66‰ at 35°C to -1.93‰ at 80°C, suggesting a negative temperature dependence on the isotope fractionation in this temperature range. However, smaller fractionation observed in the range of 5 - 25°C indicates a change in the controlling mechanism towards lower temperature.

The theoretical estimations indicate that equilibrium fractionation of Cu species in aqueous solution is unlikely responsible for the observed fractionation. Three competing kinetic processes must be considered as rate and fractionation controlling: mass transport to the electrode, electrochemical reaction kinetics and surface diffusion at the surface of the electrode. When the Cu electroplating is carried out at high electrolyte concentration ($> 0.5 \text{ mol kg}^{-1} \text{ CuSO}_{4(\text{aq})}$), short electrolysis time (e.g. 35 s), low current ($\leq 0.3 \text{ A}$), and high temperature ($\geq 35^\circ\text{C}$) in well stirred solutions ($\geq 300 \text{ rpm}$), the effects of mass transport in the solution and surface diffusion are negligible, but the electrochemical kinetics can yield pronounced isotope fractionations. It is the vibrational state of the isotopologues in the reactants and in the transition state that determines the magnitude of isotope fractionation.

Two consecutive reduction processes are related to Cu(II)-Cu(0) reduction, i.e., Cu(II) to Cu(I) and Cu(I) to metallic Cu reduction steps. Based on the findings of Cu(I) disproportionation reaction (previous part), isotope fractionation induced by second step ($\text{Cu}^+ + \text{e} \rightarrow \text{Cu}^0$) is limited to the range of $\sim 0\%$ to $\sim 0.2\%$ ($\Delta^{65}\text{Cu}_{\text{Cu(0)-Cu(I)}}$). It is evident that the transformation of fivefold to sixfold coordinated aquacomplexes of Cu^{2+} to linear Cu^+ complexes is a key step during reduction of copper in aqueous solutions, inducing large negative copper isotope fractionation.

Curriculum Vitae

Personal details

Name:	Dongmei Qi	Tel:	+49(0)17682567233
Address:	Wilhelmshavener Strasse 16, 30167 Hannover Germany	Gender:	Female
		Nationality:	Chinese
		Date of birth:	Dec.29th, 1987
E-mail:	d.qi@mineralogie.uni-hannover.de	Family status:	unmarried

Education

Since 06, 2014	PhD student at the Institute of Mineralogy, LUH
02, 2014-06, 2014	German language training
09, 2013-01, 2014	PhD student at Chinese Academy of Science
09, 2010 - 07, 2013	Master of Science, major in Geology. China University of Geosciences (Wuhan) Thesis: <i>Hydrothermal alteration processes in the NO.4 breccia pipe of the Qiyugou gold deposit, Henan Province— Implications from altered fragments and the matrix</i>
09, 2006-07, 2010	Bachelor of Science, major in Geology China University of Geosciences (Wuhan) Thesis: <i>Hydrothermal system of the Qiyugou Gold Deposit, Henan Province</i>

Research interests

- Experimental petrology and geochemistry
 - Synthetic fluid inclusions
 - Cu isotope fractionation during fluid-mineral interaction at ore forming condition as well as the electrochemical reduction process
 - Transport of metal in hydrothermal fluids (e.g. metal solubility, partition and enrichment)
-

Awards/Grants

since 02, 2014	PhD fellow of the German Academic Exchange Service
09, 2010 - 06, 2013	National Scholarship for Graduate Students
10, 2012	Hengshun Mining Scholarship

Curriculum Vitae

06, 2010	Excellent Graduates, China University of Geosciences (Wuhan)
10, 2009	President Scholarship for Elite of China University of Geosciences

Academic experience

10, 2017-01, 2018	Teaching assistant of both <i>Mineralogy</i> and <i>Experimental Petrology</i> courses at the Institute of Mineralogy, LU Hannover
10, 2015-01, 2016	Teaching assistant of <i>Mineralogy</i> at the Institute of Mineralogy, Leibniz Universität (LU) Hannover
Since 06,2014-	PhD student at the Institute of Mineralogy, LUH
02, 2014-06, 2014	German language training (funded by DAAD)
09, 2013-01, 2014	PhD student at Chinese Academy of Science
09, 2011-06, 2013	Research assistant in the projects of “ <i>The magmatism and ore deposit during the destruction of craton: evidence from Xiaolinling - Xiong’ershan region</i> ” and “ <i>Metallogenic regularity of gold deposit in Xiaolinling area</i> ” at the Faculty of Earth Sciences, China University of Geosciences (Wuhan)
03, 2011-07, 2012	Teaching assistant of <i>Petrology and Mineralogy</i> at the Faculty of Earth Sciences, China University of Geosciences (Wuhan)
09, 2011-04, 2012	Teacher of Wuhan Finance & Trade School, Hubei Province, China

Additional skills:

- Analytical methods (a selection): LA-ICP-MS (*Spectra Physics, Element XR*), MC-ICP-MS (*Neptune*), ICP-OES (Varian), fluid inclusion microthermometry (Linkam THMSG 600 heating and freezing stge), Raman spectroscopy and Fourier transform infrared spectroscopy (*Bruker*)
 - Languages: Chinese (native); English (excellent); German (fluent)
-

References:

Prof. Harald Behrens, Leibniz Universität Hannover, Germany
Phone: +49 511 762 8054; Email: h.behrens@mineralogie.uni-hannover.de

Prof. Francois Holtz, Leibniz Universität Hannover, Germany
Phone: +49 511 762 5281; Email: f.holtz@mineralogie.uni-hannover.de

Prof. Stefan Weyer, Leibniz Universität Hannover, Germany
Phone: +49 511 762 2933; Email: s.weyer@mineralogie.uni-hannover.de

Prof. Roman Botcharnikov, Johannes Gutenberg Universität Mainz, Germany
Phone: +49 6131 39 22295; Email: rbotchar@uni-mainz.de

List of publications

Qi D, Behrens H, Lazarov M, Weyer S. (----) Cu isotope fractionation during reduction processes in aqueous systems: evidences from electrochemical deposition. *Contributions to Mineralogy and Petrology*, (under review).

Qi D, Behrens H, Botcharnikov R, Derrey I, Holtz F, Zhang C, Li X and Horn I. (----) Reaction between Cu-bearing minerals and hydrothermal fluids at 800°C and 200 MPa: constraints from synthetic fluid inclusions. *Geochimica et Cosmochimica Acta*, (under review).

Qi D, Zhou H, Gong Y, *et al.* 2015. Element mobility during the fluid-rock hydrothermal alteration: Evidence from altered porphyritic granite in NO.4 pipe of the Qiyugou gold deposit, Henan Province. *Acta Petrologica Sinica*, 31(09):2655-2673 (in Chinese with English Abstract).

Abstracts

Qi D, Behrens H, Botcharnikov R, Derrey I and Holtz F. 2015. A synthetic fluid inclusion study of copper solubility in NaCl-H₂O fluids at 800°C and 200 MPa. GeoBerlin, Berlin, *Poster*

Qi D, Behrens H, Botcharnikov R, Derrey I and Holtz F. 2016. Experimental study of the behavior of copper in single phase at elevated hydrothermal condition: a fluid inclusion study using LA-ICP-MS microanalysis. Deutsche Mineralogische Gesellschaft Meeting, Bremen. *Poster*

Qi D, Behrens H, Botcharnikov R, Derrey I and Holtz F. 2016. Quenching effect on synthetic fluid inclusions: implications for study of Cu solubility. EMPG XV, Zurich. *Talk*

Qi D, Behrens H, Botcharnikov R, Derrey I and Holtz F. 2017. Experimental study of the behavior of copper in single phase at elevated hydrothermal condition: a fluid inclusion study using LA-ICP-MS microanalysis. 2nd GOOD Meeting, Hannover. *Poster*

Qi D, Behrens H, Holtz F, Botcharnikov R and Weyer S. 2015. Mobility of metals in fluids: Implications for the formation of ore deposits. Deutsche Mineralogische Gesellschaft Meeting, Potsdam. *Talk*

Qi D, Behrens H, Lazarov M, Botcharnikov R, Holtz F. 2017. Experimental investigation of copper transport in fluids: Cu solubility and isotopic fractionation. Goldschmidt, Paris. *Poster*